NONLINEAR DYNAMIC BEHAVIOUR OF FULLY COUPLED SPAR PLATFORM

A.B.M. SAIFUL ISLAM

THESIS SUBMITTED TO THE DEPARTMENT OF CIVIL ENGINEERING IN FULFILLMENT OF THE REQUIREMENTS FOR THE DEGREE OF DOCTOR OF PHILOSOPHY

2013

ORIGINAL LITERATURE DECLARATION

Name of the Candidature: A.B.M. Saiful Islam
Registration /Metric No: **KHA 100037**
Name of the degree: **Doctor of Philosophy**

Title of the thesis: **NONLINEAR DYNAMIC BEHAVIOUR OF FULLY COUPLED SPAR PLATFORM**

Field of study: **Structural Engineering**

I do solemnly and sincerely declare that:

1. I am the sole author/writer of this work
2. This work is original
3. Any use of any work in which copy exists was done way of fair dealing and for permitted purpose and any extract 1from, or reference to or reproduction of any copyright work has been disclosed expressly and sufficiently and the title of the work and its authorship have been acknowledged.
4. I do not have any actual knowledge nor ought reasonably to know that the making of this work constitutes an infringement of any copyright work.
5. I hereby assign that the all and very rights in the copy right to this work to the University of Malaya (UM), who henceforth shall be owner of the copy right of this work and that any reproduction or use any form or by any means whatsoever is prohibited without the written consent of UM having been first had and obtained.
6. I am fully aware that if in the course of making this work I have infringed any copy right whether intentionally or otherwise, I may subject to legal action or any other action as may be determined by UM.

Candidature's Signature Date
Subscribed and solemnly declare before,

Witness's Signature Date
Name:
Designation:

ABSTRACT

The offshore industry has moved towards deep water regions due to continuous depletion of oil and gas reserves at shallow to intermediate water depths. Conventional fixed jacket and bottom supported compliant platforms are inefficient for deep water exploration. Attention has therefore shifted to floating production systems. Floating Spar is one of the concepts amongst the floating structure categories. Spar platform is an assemblage of mooring, riser and Spar hull responding in a complex way to aerodynamic and hydrodynamic forces. At deep water, mooring lines/risers contribute significant inertia and damping. Associated nonlinearities compound the problem further. Precise motion investigation of platform is required for integrity and associated costs of Spar hull and mooring lines/risers. Proper dynamics cannot be assessed by conventionally used decoupled quasi-static methods which ignore all or part of the mooring/riser-platform interaction effects. Coupled analysis can capture all the complexities in reliable fashion. Hence, coupled behaviour of Spar Platform under wave, current and wind loading is of great interest. Suitability of Spar platform in Malaysian deep sea and coupled effect of riser deserve essential concern.

In the present study, fully coupled integrated Spar-mooring system (NONLIN-COUPLE6D) has been modelled. Using a nonlinear finite element approach, the deep draft Spar (DDS) hull and each catenary mooring line (CML) are simulated in a single assemblage. Spar hull is treated as rigid beam element and CML as hybrid beam element. The mooring lines as an integral part of the system support the spar hull at fairlead and pinned at the far end on the seabed. They partly hang and partly lying on the sea bed. Sea bed is modelled as a large flat surface with a provision to simulate mooring contact behaviour. Mooring line dynamics considers the instantaneous tension fluctuation and damping forces with time-dependent variance of other properties. Essential nonlinearities involved in the system are properly captured. As all the forces on Spar and CMLs act simultaneously, coupled action is achieved. Hence, there is no need of iteratively matching the force, displacement, velocity and acceleration at the fairlead position. The commercial finite element code ABAQUS/ AQUA is found to be suitable for the present study. The selected configuration of coupled Spar platform is analysed under regular wave, severe wave, current force, wind loading as well as Malaysian environment. For moderate wave, Stroke's 5^{th} order wave theory is chosen, whereas for other cases wave kinematics are computed by Airy's wave theory. The API RP 2A and Emil Simiu spectrum have been considered for wind forces. Wave and wind characteristics of Malaysian sea are simulated for 100-year storm condition. Effect of sea bed friction is evaluated under Malaysian environment. Stable response analysis is performed by bifurcation technique and Mathieu instability. Integrated Spar-mooring-

riser system is modelled. Rigid riser is considered as hybrid beam element and the effect of riser inclusion with Spar-mooring system is evaluated.

Static, free vibration and dynamic responses obtained from the developed Spar platform model have been compared with the published experimental results of Ocean Technology Research Centre (OTRC). The results are found in good agreement. The responses are evaluated by time histories, power spectra and statistical analysis. Six DOF (degree of freedom) responses are compared for non-quartering sea and quartering sea wave for 12000 sec. of loading. Surge response at platform level is deeply influenced by the coupled pitch. CML may experience significant tension even after long duration of wave. Hence, a wide range of loading duration with respective probabilities of occurrences should be considered. The responses of platform under wave at $\pi/4$ radian are equally divided for surge & sway, roll & pitch and top tension in CML 1 & 2. The yaw response of platform is also activated. It confirms that coupled Spar platform has been appropriately modelled in six DOF. Spar motions in surge, heave and pitch experience substantial change in behaviour under severe sea states. With decreasing wave intensity, Spar motions and CML tension decreases.

Current force causes major static offset of Spar in severe sea states and significantly reduces heave and pitch. Diminishing of dynamic fluctuation due to current force shows firmness of moored Spar with controlled oscillations around its new mean position. Aerodynamic loading induces larger lateral shift of platform. Constant wind causes static offset, reduces heave and pitch similar to current force. However, turbulent wind induces significant fluctuations. The extent of tension fluctuations under wind loading is not high because of high pretension in CML, but the force magnitude is higher. As wind speed decreases, the maximum values of surge and mooring tension reduces nonlinearly. The API RP 2A spectrum estimates higher platform motions and mooring tension than Emil Simiu spectrum. Both spectra can be advantageously used for the coupled Spar platform. Malaysian deep water fields can play a vital role to meet the nation's energy demand. Except Kebabangan field, all the offshore hydrocarbon reserves are located at its deeper water around 1000 m. Coupled responses are evaluated under simulated 100 year return period wave and wind characteristics of Sarawak, Malaysia. Sea bed friction induces additional damping to the floating system which suppresses heave and pitch. Stabilized platform motions and consistent closed trajectory in phase plots at long duration shows no bifurcations. The Spar doesn't show Mathieu instability for selected loading case. Riser induces further damping to the coupled system and reduces platform motions and CML tension.

ABSTRAK

Industri luar pesisir kini telah bergerak ke arah kawasan laut dalam akibat penggunaan berterusan rizab minyak dan gas di kawasan laut yang cetek dan laut yang sederhana dalam. Jaket tetap konvensional dan platform bawah bersokong sedia ada tidak cekap untuk proses cari gali di laut dalam. Oleh itu, perhatian kini beralih kepada sistem pengeluaran terapung. Spar Terapung adalah salah satu konsep di kalangan kategori struktur terapung. Platform spar adalah himpunan mooring, riser dan Spar hull yang bertindak dengan kompleks terhadap daya aerodinamik dan hidrodinamik. Di kawasan laut dalam, mooring garis/ riser menyumbang kepada daya tekun dan redaman yang ketara. Sifat-sifat "nonlinear" yang berkaitan meyulitkan lagi masalah ini. Siasatan gerakan tepat platform diperlukan untuk meyelidik integriti dan kos Spar hull dan mooring/riser. Dinamik yang betul tidak boleh dinilai oleh kaedah konvensional decoupled kuasi-statik yang mengabaikan semua atau sebahagian daripada kesan interaksi mooring/riser-platform. Analisis coupled boleh menangkap semua kerumitan dalam fesyen dipercayai. Oleh itu, tingkah Spar platform di bawah gelombang, loading semasa dan angin adalah sangat menarik. Kesesuaian Spar platform di kawasan laut dalam Malaysia dan kesan coupled riser perlu diberi perhatian.

Dalam kajian ini, sistem bersepadu penuh Spar-mooring (NONLIN-COUPLE6D) telah dimodelkan. Menggunakan pendekatan nonlinear unsur terhingga, draf yang mendalam Spar (DDS) hull dan setiap baris mooring katenari (CML) telah disimulasikan sebagai satu sistem bersepadu. Spar hull dianggap sebagai unsur rasuk tegar dan CML sebagai elemen hibrid rasuk. Garis mooring dianggap sebagai sebahagian daripada sistem yang menyokong hull kapal spar di fairlead dan disematkan di hujung di dasar laut. Sebahagian daripada garis mooring tersebut tergantung dan sebahagiannya terletak di dasar laut. Dasar laut dimodelkan sebagai permukaan rata yang besar dengan peruntukan untuk simulasi tingkah laku hubungan mooring. Dinamik yang digunakan untuk baris mooring menganggap perubahan serta-merta daripada tension dan daya redaman dengan perbezaan masa yang bergantung kepada sifat-sifat yang lain. Sifat-sifat nonlinear yang terlibat dalam sistem ini direkodkan dengan terpat. Disebabkan semua kuasa-kuasa pada Spar dan CML bertindak serentak, tindakan coupled dicapai. Oleh itu, iterasi yang sepadan dengan kekerasan, anjakan, halaju dan pecutan pada kedudukan fairlead tidak diperlukan. Kod komersial untuk finite elemen ABAQUS / AQUA didapati sesuai untuk kajian ini. Konfigurasi yang dipilih daripada coupled Spar platform dianalisis di bawah ombak tetap, ombak bergelora, aliran semasa, beban angin serta persekitaran Malaysia. Untuk ombak sederhana, teori kelima gelombang Strok telah digunakan, manakala bagi kes-kes lain kinematik ombak dikira dengan teori ombak Airy. API RP 2A dan Emil Simiu spektrum telah dipertimbangkan untuk kuasa angin. Gelombang dan angin ciri-ciri laut Malaysia telah disimulasi untuk keadaan ribut 100 tahun. Kesan geseran dasar laut adalah dinilai di bawah persekitaran Malaysia. Analisis sambutan stabil dilakukan menggunakan teknik bifurcation dan Mathieu instability. Sistem bersepadu Spar-mooring-riser telah dimodelkan. Riser tegar dianggap

sebagai hibrid elemen rasuk dan kesan daripada kemasukan riser dengan sistem Spar-mooring telah dinilai.

Statik, getaran bebas dan tindak balas dinamik yang diperolehi daripada model Spar platform telah dibandingkan dengan keputusan eksperimen yang diterbitkan daripada OTRC. Keputusan telah didapati agak serupa. Keputusan daripada model telah dinilai dari segi sejarah masa, spektrum kuasa dan analisis statistik. Keputusan untuk enam DOF (darjah kebebasan) dibandingkan dengan ombak bukan condong dan condong sehingga 12000 sec. beban. Keputusan Surge di peringkat platform yang amat dipengaruhi oleh coupled pitch. CML mungkin mengalami tension yang ketara walaupun selepas tempoh ombak yang panjang. Oleh kerana itu, julat panjang memuatkan tempoh dengan kebarangkalian masing-masing kejadian yang perlu dipertimbangkan. Tindak balas platform di bawah gelombang di π / 4 radian sama-sama dibahagikan untuk lonjakan & bergoyang, roll & padang dan ketegangan teratas dalam CML 1 & 2. Sambutan rewang platform juga diaktifkan. Ini mengesahkan bahawa Spar platform sesuai dimodelkan dalam enam DOF. Gerakan Spar dalam keadaan melonjak, menarik dan padang pengalaman perubahan besar dalam tingkah laku di bawah negeri laut yang teruk. Dengan mengurangkan intensiti gelombang, gerakan Spar dan tension CML telah berkurangan.

Kuasa daripada ombak menyebabkan static offset yang tinggi dalam keadaan laut yang bergelora dan meyebabkan pengurangan tarikan dan penolakan yang ketara. Pengurangan dinamik oscillation menunjukkan ketegasan daripada moored Spar dengan ayunan dikawal oleh kedudukan mean baru. Beban aerodinamik mendorong anjakan sisi yang lebih besar daripada platform. Angin yang malar menyebabkan statik offset, mengurangkan tarikan dan tolakan sama dengan kuasa semasa. Walau bagaimanapun, angin yang bergelora mendorong fluctuation penting. Tahap turun naik ketegangan di bawah beban angin tidak tinggi kerana pretension yang tinggi dalam CML, tetapi magnitud kuasanya lebih tinggi. Apabila kelajuan angin berkurangan, nilai-nilai maksimum daripada surge dan tension mooring mengurangkan nonlinear. API RP 2A spektrum menganggarkan usul platform yang lebih tinggi dan ketegangan mooring daripada spektrum Emil Simiu. Kedua-dua spektrum boleh digunakan untuk coupled Spar platform dengan baik. Bidang air dalam Malaysia boleh memainkan peranan yang penting untuk memenuhi keperluan tenaga negara. Kecuali di kawasan Kebabangan, semua rizab hidrokarbon luar pesisir yang terletak di laut dalam sekitar 1000 m. Keputusan coupled dinilai di bawah simulasi 100 tahun tempoh pulangan gelombang dan ciri-ciri angin daripada Sarawak, Malaysia. Geseran di dasar laut mendorong tambahan redaman kepada sistem terapung, yang mengurangkan heave dan pitch. Gerakan platform yang stabil dan trajektori tertutup konsisten dalam plot fasa pada tempoh yang panjang tidak menunjukkan bifurcations. Spar tidak menunjukkan Mathieu ketidakstabilan untuk kes beban yang dipilih. Riser membantu mendorong pengurangan beban pada sistem coupled dan mengurangkan gerakan daripada platform dan mooring tension.

ACKNOWLEDGEMENTS

With a lot of pleasure I wish to express my deepest gratitude to the Almighty Allah for His unlimited blessings to bring out this work a success. I am also thankful to my parents for their encouragement in every step of getting education.

I would like to express profound gratitude and sincere appreciation to my supervisors, Dr. Mohammed Jameel, Department of Civil Engineering, University of Malaya, and Prof. Ir. Dr. Mohd Zamin Jumaat, Department of Civil Engineering, University of Malaya, whose encouragement, guidance and support from the beginning to the final level enabled me to develop an understanding of my research. I was remarkably motivated by their dynamic supervision, continuous guidance, important directions, helpful criticism, invaluable suggestion, enthusiastic encouragement, strong support and persistent simulation. Their fervent guidance in every aspect of this work was the most valuable experience of my life and also would remain so forever.

I am indebted to thank all the researchers, lab assistants, lab technicians, all the members linking to CICT (Centre for Innovative Construction Technology). This research was supported by the university research grants: UMRG 140-12AET, UMRG 093-10AET, HIRG-16001-00-D000036 and PV052-2011B provided by University of Malaya, Kuala Lumpur, Malaysia.

Computing resources were made available by the Department of Civil Engineering, University of Malaya. Special credits to Computer Aided Design & Computer Aided Manufacturing (CAD/CAM) lab personnel for arranging me to use ABAQUS licensed software.

Finally, I gratefully acknowledge the help, encouragement, cooperation received from my friends and associates.

A.B.M. Saiful Islam

University of Malaya, Malaysia

June, 2013

TABLE OF CONTENTS

LIST OF FIGURES

LIST OF TABLES

LIST OF ABBREVIATIONS

CML	Catenary Mooring Line
DDS	Deep Draft Spar
RR	Rigid Riser
OTRC	Ocean Technology Research Centre
FPS	Floating production systems
TLP	Tension-leg platform
FPSO	Floating Production Storage & Offloading (FPSO) systems

LIST OF NOTATIONS

a	Wave amplitude
Ai	Inner cross-section area of the mooring line
Am	Outer cross-sectional area of the mooring line
A_p	Projected area of spar and topside above mean sea level
A_s	Cross-sectional area of the spar hull
At	Structural cross-section area of the mooring line
b vector	Unit vector in mooring bi-normal direction at Cartesian coordinate
c	Speed of the wave traveling through the fluid
C	Shape parameter
[C]	Damping matrix
C_D	Drag coefficient
C_{Dn}	Normal drag coefficient
C_{Dt}	Tangential drag coefficient
C_L	Lifting coefficient
C_M	Inertia coefficient
C_{Mn}	Normal inertia coefficient
C_{Mt}	Tangential inertia coefficient
$C_p(x,z)$	Wind drag coefficient at elevation z and horizontal coordinate x
d	Water depth
D	Diameter of the member
D_m	Diameter of mooring line
D_s	Diameter of the Spar hull
e_1	Torsional strain due to Torsional moment M_3
e_x	Unit vector in X-axis
e_y	Unit vector in Y-axis
e_z	Unit vector in Z-axis
$\vec{e}_t$	Unit vectors in the axial direction
$\vec{e}_c$	Unit vectors in the current direction
f	Frequency in cycles/sec.
f_p	Peak frequency
F_B	Buoyancy force per unit length of mooring line

F_m	Force per unit length of mooring line
F_s	Force per unit length of Spar platform
$F_{wind}(x,z,t)$	Aerodynamic force on the moored spar
$F(X,Z,t)$	Force per unit length
{F}	Static load vector
$\{F(t)\}$	Total force on the spar-mooring system
$G(t,z)$	Gust factor
H	Wave height
H_s	Significant wave height
I_{xx}, I_{yy}, I_{zz}	Moment of inertia about X,Y &Z axis respectively
$I(z)$	Turbulence intensity
k	Wave number
[K]	Stiffness matrix
$[K_E]$	Elastic stiffness matrix for the structure
$[K_G]$	Geometrical stiffness matrix
L	Wave length
m_i	Generalized mass
M_1	Bending moment employed on CML
M_2	Warping moment employed on CML
M_3	Twisting moment employed on CML
M_a	Added mass per unit length of the structure
[M]	Mass matrix
N	Transfer matrix between Cartesian and global coordinates
N	Axial force variable acting on CML
N_k	Keulegan-Carpenter number
N_R	Reynolds number
n vector	Unit vector in mooring normal direction at Cartesian coordinate
P	Wave period
P_i	Internal pressure related to well head pressure.
P_{res}	Force due to hydrostatic pressure on catenary mooring
P_m	Hydrostatic external pressure around the mooring line

P_W	Pressure of the sea water
$S(f)$	Spectral energy density
t	Instantaneous time
T	Transfer matrix between Cartesian and global coordinates
t vector	Unit vector in mooring tangential direction at Cartesian coordinate
u	Wind velocity
u_c	Current velocity
$\dot{u}$	Water particle velocity
$\dot{u}(x,t)$	Along wave horizontal velocity
$\ddot{u}$	Water particle acceleration
u_c	Current velocity normal to the Spar hull and the mooring lines
$\dot{u}_m$	Maximum water particle velocity
u′	Virtual displacement
$U_w(z)$	Mean wind velocity
$U_w{}'(x,z,t)$	Fluctuating wind velocity
$U_{W_G}(t,z)$	Gust wind speed
$U_{W_G}(t,z_R)$	Gust wind speed at the reference level above MWL
U_{50W}	Wind speed with 50–year return period
U_{100W}	Wind speed with 100–year return period
$U_w(1h,z_R)$	1-h mean wind speed at the reference elevation
$\dot{v}(x,t)$	Vertical velocity
W_L	Wave length
W_P	Wave period
X	Point of evaluation of water particle kinematics from the origin
{X}	Structural displacement vector
$\{\dot{X}\}$	Structural velocity vector
$\{\ddot{X}\}$	Structural acceleration vector
z	Elevation of the wind centre of pressure above MWL
z_R	Reference elevation
z_s	Thickness of surface layer

$\breve{A}_{ij}$, $\breve{B}_{ij}$, $\breve{C}_i$	Constants depending on the ratio of sea depth to wave length.
$\breve{c}$	Wave celerity
$\delta W_1^{\ I}$	Internal virtual work done
$\delta W_1^{\ E}$	External virtual work done
α_i	Coefficients of quadratic nonlinear terms
β_i	Coefficients of cubic nonlinear terms
ω	Angular velocity of wave
ω_i	Natural frequency
$\sigma_w(z)$	Wind speed's standard deviation
θ	Phase angle
θ_1	Beam curvature measures due to M_1
θ_2	Beam curvature measures due to M_2
Δt	Time interval of data sampling
μ	Viscosity of the water
$\Phi(\ )$	Cumulative distribution function
$\varphi(\ )$	Cumulative density function
ρ	Ratio of combining internal virtual works
ρ_a	Density of air
ρ_w	Mass density of the sea water
ρ_m	Mass per unit mooring line
ρi	Mass density of the inside fluid
ρt	Mass density of the mooring's tube
ρ_s	Mass density of the spar
$\phi(1)$	First-order potential of incident waves
$\phi(5)$	Fifth-order potential of incident waves
ξ	Structural damping ratio
Φ	Modal matrix
ε	Axial strain
η	Periodic motion of the nonlinear damped Mathieu equation

CHAPTER 1: INTRODUCTION

1.1 Background

Continuous depletion of oil and gas reserves in shallow waters has moved the exploration of these resources in deeper waters. At deep sea environments, traditional fixed types of offshore energy exploration structures are expensive and uneconomical. This has necessitated the design of structures with new configurations compatible with deep water conditions. Attention has therefore turned to compliant/ floating production systems (FPS). Several floating platform concepts have been developed for deep-water applications such as Compliant piled tower, Semi-submersibles, Tension-leg platform (TLP), SPAR and the Floating Production Storage & Offloading (FPSO) systems. The interest of present study is Spar platform. A number of operational Spar platforms such as Shell's ESSCO Brent Spar, Oryx Neptune Spar, Chevron Genesis Spar, Exxon's Diana Spar etc. in the Gulf of Mexico and North Sea prove the effectiveness, economy, and success of such deep water platforms. This floating system is an integrated dynamic system of mooring, riser and hull. Major complexities in the design of floating Spar are prediction of hydrodynamic and aerodynamic loads as well as induced structural responses. Nonlinearities in the system add more complication in analysis. Moreover, design of mooring/riser system connected to floating platforms is primarily influenced by the platform motions. Therefore, accurate prediction of platform motions is very important for the integrity and associated costs of the structural systems.

Coupled action of spar-mooring system changes the behaviour of floating structure significantly. Several studies have assessed coupling effect of different offshore floating production systems such as TLP (Kim et al., 2001; Ma and Patel, 2001; Yang and Kim, 2010), Spar buoy (Chen et al., 2001; Colby et al., 2000; Culla and Carcaterra, 2007;

Gupta et al., 2000b; Ran and Kim, 1997; Ran et al., 1996), Truss Spar (Montasir and Kurian, 2011), Cell Spar (Zhai et al., 2008), Cell-Truss Spar (Zhang et al., 2008). Ran et al. (1999) studied coupled dynamic analysis of a moored spar in random waves and currents adopting time-domain and frequency-domain analysis. Chen et al. (1999) presented Spar response constrained by slack mooring lines with steep ocean waves by quasi-static approach (SMACOS) and coupled dynamic approach (COUPLE) to reveal coupling effects between Spar and mooring system. The motion and dynamic equations for spar and mooring lines are solved simultaneously by matching displacements and forces of moorings to spar at fair leads. Chen et al. (2001) conducted parametric studies on Spar and TLP for different depths in deep water. A mathematical model considering coupled action in nonlinear dynamic Spar response under regular sea waves was presented by Agarwal and Jain (2003). Tahar and Kim (2008) developed numerical tool for coupled analysis of deep water platform with polyester mooring lines.

When riser is added in the Spar-mooring system, the analysis of Spar platform becomes more complex. In deep water, mooring lines and riser in coupled Spar platform system contribute significant damping and inertia. Therefore, precise prediction of such action in Spar platform motions is imperative. Full dynamic equilibrium of platform, mooring lines and risers was suggested by Chaudhury and Ho (2000) for accurate dynamic motion. Zhang and Zou (2002) showed that for coupling of supporting guide frames and moorings/risers upon the Spar, lower heave and pitch/roll responses decreases hull draft which influenced size and weight of hull, moorings and risers substantially. Koo et al. (2004a) examined nonlinear multi-contact coupling between vertical riser and guide frame. Garrett (2005) performed coupled analysis of a large semi-submersible associated with 16 moorings and 20 risers. Low and Langley (2008) described a hybrid coupled analysis approach in time/frequency domain of vessel/mooring/riser suitable in shallow water. The lines had been discretized as lumped masses associated with linear rotational and extensional springs. Yang and Kim (2010) performed hull-tendon-riser coupled dynamic analysis of a TLP where riser/tendon act as elastic rod. Yang et al. (2012) carried out coupled dynamic analysis for wave interaction with truss spar and mooring line/riser system in time domain. Present study deals with fully coupled behaviour of integrated Spar-mooring and Spar-mooring-riser system.

Effect of wind on an offshore structure becomes important when the superstructure i.e. portion above the MWL is significant. The exposed portion of the Spar platform is subjected to drag force caused by the wind velocity normal to the platform. Ahmad et al. (1997) investigated wind-induced response of a tension leg platform. Random wind and waves were modelled by Monte-Carlo simulation. Ahmad and Ahmad (1999) described an active control strategy to check the non-linearly coupled response of a tension leg platform (TLP). A deep water semi-submersible type compliant offshore structure was moored by vertical taut cables called tendons or tethers. Zaheer and Islam (2008a, b) dealt with the wind induced response characteristics of double hinged articulated loading platform. Articulated loading platforms (ALP) were found as sensitive to the dynamic effects of wind, waves and currents. Islam et al. (2009a, b) evaluated double hinged articulated tower interaction with wind and waves. The displacement response of such towers was mainly governed by rigid body mode of vibration which has a very low frequency. It is of great interest to incorporate wind loading on coupled Spar platform and evaluate its behaviour.

The effect of mooring line-seabed contact is an interesting issue of on-going research (Zeitoun et al., 2008). Palmer et al. (1988) studied considerable lateral resistance to movement of marine pipelines simulating on the seabed. A simple approach to configure mooring-sea bed contact is the basic Coulomb friction model. Wagner et al. (1989) dealt with typical coulomb friction estimation by including soil strength information and pipe displacement history in the resistance prediction. Yu and Tan (2006) evaluated the effect of friction between mooring cable and elastic as well as elasto-plastic sea bed. Zeitoun et al. (2009) evaluated the effect of seabed on mooring line. As the mooring line movement and soil resistance are interrelated, the sea bed friction effect should be captured properly.

The stable response analysis of platform motion is of utmost importance to seek the stable behaviour of offshore structure. Stability analysis of various offshore platforms have been conducted such as: TLP by Siddiqui and Ahmed (1996), Simos and Pesce (1997), Chandrasekaran et al. (2006); marine cable-body systems by Huang (1999); articulated tower joint by Islam and Ahmad (2007). Esmailzadeh and Goodarzi (2001) performed stability analysis of a catenary anchor leg mooring (CALM) floating structure. Umar and Datta (2003) and Umar et al. (2004) have shown that different kinds of instability phenomena like nT sub harmonic oscillations, symmetry breaking bifurcation and aperiodic responses might occur in moored Spar.

Haslum and Faltinsen (1999) investigated Mathieu instability in pitch motion combined with extreme amplitude heave resonance. They showed a stability diagram for Mathieu’s equation without considering pitch damping effects. Zhang et al. (2002) included pitch damping effects and developed a damped Mathieu’s stability diagram. However, the effects of time-varying displacement were ignored. Koo et al. (2004b) revealed that if heave resonance occurs at heave natural period equal to half of pitch natural period, Mathieu instability, a kind of lock-in phenomenon, arises in classic Spar. Chandrasekaran et al. (2006) have conducted Mathieu instability analysis of TLPs for different water depths and shapes. Munipalli et al. (2007) and Chillamcharla et al. (2009) assessed weathervaning instabilities of a FPSO under regular wave and bi-directional sea states respectively using similar model. Arnoult et al. (2011) introduced modal stability procedure for linear and dynamic finite element analysis subjected to random parameters. Further interest looks for response stability analysis of fully coupled Spar platform.

In the conventional approaches of analysis, force and displacement of mooring heads and vessel fairleads are iteratively matched at every instant of time marching scheme to solve the equilibrium equations. Furthermore, the continuity of vessel and mooring/riser is missing. Major mooring/riser contributions in terms of drag, inertia and damping due to their longer lengths, larger sizes and heavier weights in deep water are not fully incorporated. Hence, in the present study, the Spar-mooring and Spar-mooring-riser integrated system have been idealized as fully/strongly coupled systems. Large spar cylinder is kept in position with mooring lines linked at fairleads and hinged at sea bed. Instantaneous mooring tension fluctuation, damping forces with time-wise variation, drag and inertia on Spar due to sea states have been properly considered. Simulated Spar platform model is analysed under selected hydrodynamic (wave, current), aerodynamic (wind) loading and proper sea bed contact. Its structural response behaviour is studied together with the stability analysis.

1.2 Spar Platform

Rather than shallow water of depth 0-305 m (Chakrabarti, 2005; Rapp, 2008), for deep (305-1524 m) and ultra-deep (>1524 m) water (Chakrabarti, 2005; Montasir et al., 2008; Rapp, 2008), the compliant floating Spar platform has been in popular use for a number of years. The idea of Spar as a stable floating platform was to design a simple structure with a natural frequency far below the typical dominant ocean wave frequency-range in order to reduce the resulting dynamic effects. Therefore, appreciable reductions of wave-induced forced vibrations in the range of frequencies of waves are achieved. Structurally, the spar platform is a rigid cylinder with 6 DOF, anchored to the sea-bottom by vertical or catenary cables (Figure 1.1).

This deep-draft floating caisson is a hollow cylindrical structure similar to a very large buoy. Its four major systems are hull, moorings, topsides, and risers. The spar relies on a traditional anchor-spread mooring system to maintain its position. About ninety per cent of the structure is underwater. Its deep-draft hull produces very favourable motion characteristics compared to other floating concepts. Low motions and a protected centre-well also provide an excellent configuration for deep-water operations. In the classic or full cylinder hull forms, upper section is compartmentalized around a flooded centre-well containing risers. This section provides buoyancy for the spar. Middle section is also flooded but can be economically configured for oil storage. The bottom section (keel) is organised to provide buoyancy during transport and to contain any field-installed, fixed ballast.

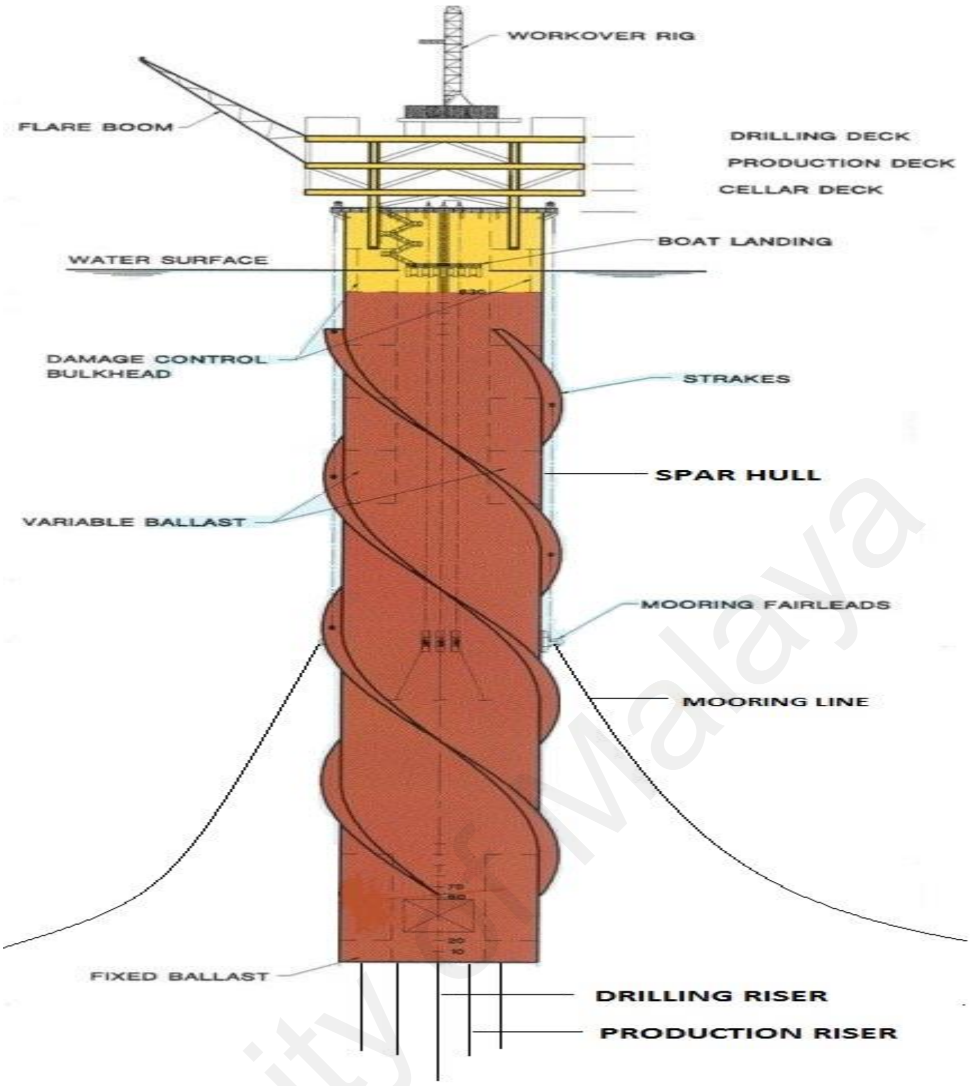

Figure 1.1: Drilling and Production Spar Platform (RSI, 2012)

1.3 Spar platform in Malaysian scenario

1.3.1. Oil and gas status in Malaysia

Rapidly rising fuel consumption may potentially lead to an enormous crisis of global energy in the near future. Following the trend, Malaysia’s fuel feed has been mounting by an annual rate of 7.2% since 1990, touched 44.9 Mtoe at 2008 and is forecasted to be 207.3 Mtoe by 2030. Substantial reduction of oil and natural gas from the energy mix in Malaysia has created an urgent need for deeper exploration of these resources. Seven sedimentary basins of Malaysia in the South China Sea are being looked at as having huge energy reserves. According to the 2008 statistics, the Malaysian demand for energy was being primarily met by natural gas at 43.4%, crude oil at 38.2%, coal at 15.3% and hydropower at 3.1%. Around 70 % of the oil and 85% of the natural gas come from offshore fields. Malaysia's first oil well was discovered on Canada Hill in Miri, Sarawak in 1910. Not long after, the exploration and production activity stepped up and covered the entire Sarawak land mass, followed by the Sabah and Terengganu waters. To date, oil and later the discoveries of gas fields have propelled and fuelled the socio-economic development of the country and its people for about 100 years, with contribution to the Government totalling RM 403.3 bil between 1974 and 2008. Nearly all of Malaysia's oil and gas comes from offshore fields. Partly driven by the ever increasing demands for energy worldwide, the industry requires new fields and technology as well as faster production with improved energy recovery.

1.3.2. Sedimentary Basins

Sedimentary basins are major area for potential oil and gas reservoirs as they contain many faults and natural traps, which collect and accumulate hydrocarbons under its impermeable layer. As shown in Figure 1.2, the continental shelf offshore of Malaysian waters is divided into 7 sedimentary basins (Petronas, 2010), out of which 3 basins have major on-going oil and gas exploration and production activity, namely the Malay basin in West Malaysia off Terengganu and the Sarawak and Sabah basins off the two East Malaysian states of Sabah and Sarawak. Most of the country’s oil reserves are located in the Malay basin and tend to be of high quality.

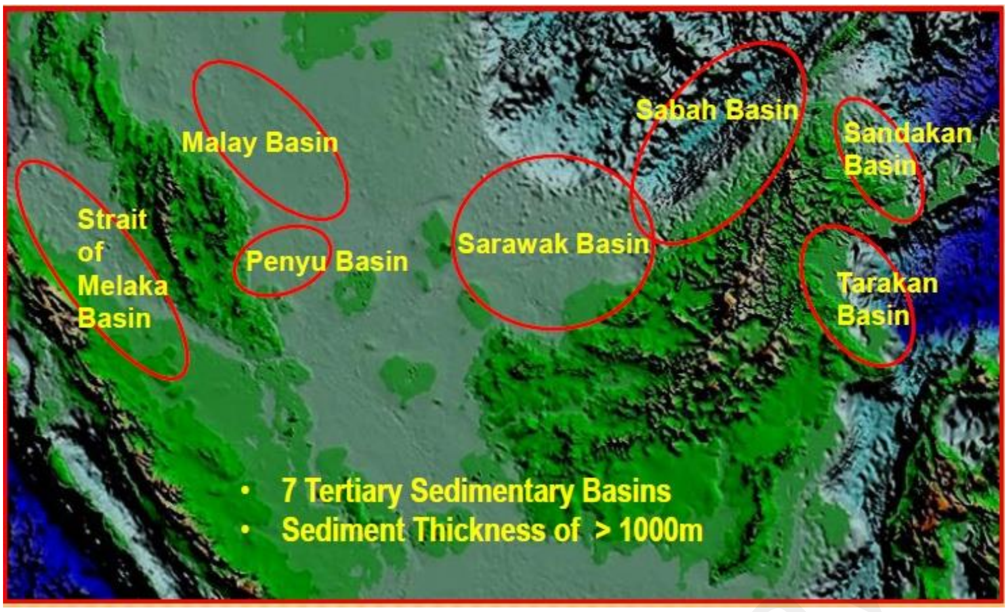

Figure 1.2: Sedimentary Basins of Malaysia (Petronas, 2010)

Since 2002, the focus has been on deep-water fields on the eastern continental shelf that pose high operating costs and require substantial technical expertise. New oil production projects in the planning or construction phase include: Gumusut/Kakap project, located offshore Sabah in 1220 m of deep water which includes the regions' first deep-water floating production system with 150,000 bbl/d processing capacity. As the oil and gas industry looks further into newer ways and locations to recover hydrocarbons, exploration and production activity has seen itself heading towards greater frontiers. Table 1.1 shows the timeline of operation for the deep-water projects in Malaysia, and it can be seen that Malaysia is already priming itself to be a deep-water operations regional hub.

Table 1.1: List of Deep-water Fields that are in Appraisal / Operation

Field Name	Recoverable	Water Depth	On-stream Date	Operator
Kikeh	536 mmboe	1,300 m	Q2/Q3 2007	Murphy Oil
Gumusut/Kakap	620 mmboe	1,220 m	Q4 2010 / Q1 2011	Shell
Kebabangan	2.2 tscf	>200 m	Q3 2011	Conoco P.
Jangas	81 mmboe	>1000 m	Q4 2011	Murphy Oil
Ubah Crest	215 mmboe	>1000 m	Q2 2012	Shell
Pisangan	56 mmboe	>1000 m	Q3 2012	Shell
Kamunsu	2.2 tscf	>1000 m	Q2 2013	Shell

1.3.3. Spar in Malaysian deep sea

To accomplish deep-ocean exploration, traditional fixed offshore structures have become expensive. Therefore, Spar platforms are compliant floating structures relevant for the exploration of deep water deposits from Malaysian deep sea bed. The first floating spar in Malysia was installed in 2007. This truss Spar was located at Kikeh field which is 1330m deep. The first spar and overall deep water conditions seem promising for the floating Spar platform in most of the Malaysian continental shelf regions. Furthermore, deep and deeper wells are being drilled; this in turn results in greater challenges for designing and setting up of offshore production facilities showing possibility of floating Spar in this region.

1.4 Present State of the problem

Though the technology of oil and gas exploration is blooming for deep water ocean deposits, only a few configurations of the Spar platform have been reported. There are several issues that are yet to be explored and investigated. Following are the important aspects required to be addressed.

- For precise behaviour of Spar platform, consideration of structural idealization comprising the platform and other components as an integrated, strongly coupled, incorporating appropriate boundary conditions in one system is essential.
- Fluctuating and mean wind components act on the superstructure of Spar platform. It is a source of wave generation in substructure region. Hence it is important to model the bluff configuration of superstructure and obtain the wind induced forces on the same while the substructure experiences the hydrodynamic loading.
- To evaluate the Spar platform behaviour in six DOF for long duration of wave

loading is of important concern.

- To evaluate the responses under wind, current and wave induced vibration of the Spar platform is essential
- There is an ample scope to improve the solution technique of nonlinear system of dynamic equations. Accuracy and faster convergence may be achieved if an improved algorithm is adopted.
- Spar platform may be a good alternative to conduct the exploration from Malaysian deep sea. As most of the offshore fields of Malaysia are under deep water, suitability of floating Spar platform for its deep sea exploration is to be assessed.
- Effect of frictional sea bed on mooring line is to be properly evaluated which may influence the structural responses of the Spar system.
- Stable response of Spar platform requires to be analysed for long duration of loading.
- Coupled effect of riser inclusion on platform responses and mooring tension is essential.

1.5 Objectives of Research Work

In view of the literature reviewed some important areas of further research with their future scope of applications are identified. The focus of the present study is, therefore, on the following objectives.

1. To develop a fully coupled three-dimensional numerical model (NONLIN-COUPLE6D) of Spar platform using finite element idealization.

2. To validate the fully coupled Spar platform model with published experimental results and carry out nonlinear coupled dynamic analysis of Spar platform for long duration of wave loading.
3. To study coupled dynamic responses under quartering sea wave loading and assess the six degrees of freedom motions of Spar platform.
4. To evaluate the effect of severe sea waves as well as effect of current on nonlinear coupled dynamic responses of moored Spar.
5. To study the effect of aerodynamic loading on coupled Spar.
6. To appraise the suitability of Spar platform in Malaysian deep water regions.
7. To evaluate the coupled effect of riser on Spar-mooring system in deep water conditions.

1.6 Scope of the work

The research seeks to develop Spar-mooring system and Spar-mooring-riser system in complete integrated models. The nonlinear coupled integrated Spar platform used in the present study is bound by the following constraints:

1. The deep draft Spar (DDS) hull is a rigid cylinder which connects catenary mooring system. Proper linkage characteristics provided by six nonlinear springs are ensured in a finite element software ABAQUS. It is characterized as strong coupling.
2. Each catenary mooring line (CML) supports the Spar at fairlead and is pinned at the far end on the sea-bed. These integral components are partly hanging like a catenary and partly lying on the sea bed.

3. The sea bed is modelled with two configurations with provision to simulate mooring-sea bed contact. One is as a frictionless surface and another simulates frictional sea bed to evaluate proper friction effect to the structural system.
4. Mooring line dynamics envisages the instantaneous tension fluctuations and damping forces with time-wise variation of other properties. Coupling effect of top tensioned risers in the model is ignored and it is treated as massless element.
5. Drag, inertia and damping forces due to waves, current and wind force on mooring lines act simultaneously on Spar cylinder. Hence, the force, displacement, velocity and acceleration are automatically attained.
6. Wind loading was considered on the superstructure portion of the Spar system which includes topside and a portion of cylindrical hull.
7. Malaysian sea environment considers the ocean loading of offshore Sarawak.
8. Stable response analysis has been performed by phase plot of spar responses along with the Mathieu instability formulation.
9. The rigid riser has been considered as linked at Spar keel and coupled behaviour of platform-mooring-riser integrated system is assessed.

1.7 Organization of the thesis

The thesis comprises of five chapters dealing with various aspects of dynamic response and probabilistic analysis. A brief outline follows:

Chapter 1 Introduction

Chapter 1 gives general introduction of deep water Spar platform. A brief research background on recent advancement of coupled Spar platform and oil and gas exploration in Malaysian scenario is presented. Accordingly the problem statement, research objectives and scope of work are discussed. The chapter is concluded with an outline of the thesis.

Chapter 2 Literature review

The basic aim of this chapter is to critically review various aspects of the current state-of-the-art on floating Spar platform and its structural analysis. Detail review of the existing literature on wind loading, sea bed friction and stability analysis has been described. Furthermore, oil and gas energy status in Malaysia, wave data of Malaysia waters and the suitability of Spar platform in Malaysian region has been reviewed. In order to establish the scope of the present study and salient objectives, a comprehensive literature review is carried out with the main focus on mathematical idealization and dynamic response of Spar-mooring system and Spar-mooring-riser system associated with crucial nonlinearities.

Chapter 3 Methodology

In this chapter, methodology for the present research work has been described. The approach for developing fully coupled integrated Spar-mooring system as a single model in finite element simulation is described. Selected loading conditions, nonlinearities, analyses techniques for the response evaluation are discussed. Incorporation of aerodynamic loading has been deliberated. The simulation of sea wave data for Malaysian sedimentary basins has been discussed. Capturing the sea bed friction and the procedure to carry out stable response analysis of coupled Spar platform is elaborated. Moreover, description of modelling Spar-mooring-riser in integrated system has been outlined.

Chapter 4 Results and Discussion

Chapter four discusses the obtained results and their critical evaluations. The validation of the developed model has been shown. Influence of various sea environments comprising severe wave, current and wind on coupled Spar platform has been evaluated. Assessment of suitability of present Spar platform in Malaysian deep water has been discussed. The effect of sea bed friction is shown compared to frictionless sea bed case. Stable response analysis has been presented for the moored Spar. Finally, the effect of riser in the coupled Spar-mooring-riser system has been shown.

Chapter 5 Conclusion

Chapter five ends the study with a discussion of results followed by salient conclusions. The final conclusion has been outlined point to point to generalize the characteristic of the Spar-mooring system and Spar-mooring-riser system under various hydrodynamic and aerodynamic loading environments. Concluding remark on the suitability of moored Spar installation at Malaysia Sea is given. Furthermore, several important research aspects beyond the scope of the present study are recommended for future work.

CHAPTER 2:LITERATURE REVIEW

2.1 Introduction

Spar platform is an offshore floating structure ideal for deep water explorations of oil and natural gas; especially drilling wells, extracting and producing, processing and storing, as well as the eventual off-loading of these ocean deposits. Unlike onshore and shallow water platforms, in deeper water, Spar platform is characterized by the presence of mooring lines/risers which contribute substantial inertia along with damping because of their larger sizes, extensive lengths and significant weights. At recent years, there has been a growing interest in employing Spar technology as deep water production platforms. In this chapter a detailed literature survey is carried out to review various approaches adopted by the past investigators for dynamic analysis of Spar platform. Incorporation of wind loading in the frontal area of offshore platform is investigated. Sea bed friction effect and stability analysis have also been reviewed.

2.2 Floating platform for energy exploration

Oil and gas exploration from offshore region is technologically further complicated than that from land area. Extensive theoretical studies, model testing and hands-on experience in the scientific disciplines are essential for the design and operation of offshore structures leading to hydrocarbon exploration underneath the sea bed. Several alternatives for fixing the platform deck comprising its equipment to the seabed are described. Fixed offshore structures are widespread offshore structures for drilling and production of oil and gas in ocean environment. It is appropriate in shallow water which is fixed at seabed. Usually fixed offshore structure poses high stiffness and relatively small displacement. Several types of fixed platform are existent viz. Jacket platforms, gravity platforms, hybrid platforms and Jack-up platforms. Bottom supported compliant structures can change its position by wave, current and wind forces to a limited extent. Such platforms are attached to the seabed through tension legs, guy lines, flexible members or articulated joints. Some examples of such structures are Guyed tower, Buoyant tower, Compliant piled tower, Flexible tower, Articulated tower, Tension buoyant tower, Tension leg platform and Hybrid compliant platform.

To conduct the operation in deeper water, fixed platform as well as bottom supported complaint platform become uneconomical and incompatible. Floating offshore structures are most suitable for oil and gas exploration in increased water depth. Several floating platform concepts e.g. drill ships, semi-submersibles, Spar platforms, floating towers, floating jacket, deep draft caisson vessel are suggested. Such platforms are efficient and economical for deep water installation owing to less structural weight than other kinds of conventional platforms. These structures are customarily anchored to sea-bed through wires, chains or cables to facilitate the anchoring system providing necessary restoring forces. Floating platforms resist loads experiencing large excursion by environmental conditions and thereby the forces on the structures reduces. The platform is movable and can be used repeatedly particularly for reservoirs with marginal reserves. The structure can be swiftly detached allowing path for extreme conditions, large ice bergs. Moreover, the design of such floating platform may not be affected considerably by earthquakes and even the depth of water.

2.3 Spar as a floating platform

Spar platform is regarded as the latest and new generation, floating structure ideal for offshore oil and gas exploration from deep water (Montasir and Kurian, 2011). The feasibility of floating Spar such as a stable ocean platform is acknowledged for a few years. Prospective practice and application of floating Spar were seen in off-shore industry in 1970s following the construction of Royal Dutch Shell’s Brent Spar which was designed specifically for oil storage and off-loading at the North Sea. Investigation on vessel was dealt by a few oil companies in mid-1970s, even though the use and potential of Spar concept is realized later on. Floating Spar has been suggested and recommended to serve as a low cost production facility for remote, sub-sea well sites (Jameel and Ahmad, 2011). Several operational Spar platforms in Gulf of Mexico and North Sea viz. Oryx Neptune Spar, Exxon's Diana Spar, Chevron Genesis Spar etc. show the efficacy, economy as well as accomplishment of such floating platforms for deep water applications.

2.3.1. Advantages of Spar Platform

Spar is the most suited offshore system for deep water exploration and production. Its popularity is attributed to the following merits.

1. The Spar platform is highly stable relative to its weight. It can be installed up to 3000 m water depth.
2. It contains sea keeping features which are superior to other practically moveable drilling platforms and units.
3. Its installation, operation and relocation of mooring system are easier. It can function like a transportable drilling rig and demobilization cost is fairly low.
4. It is cost insensitive to water depth, as only the cost of cable system and its installation increases as the water depth increases.
5. The full cylinder Spar has the additional characteristics that it can be configured for oil storage at a relatively low/marginal cost. Typical classic Spar design can store five to ten times the platform's daily oil production.
6. Separate buoyancy cans support the production risers in the centre well. It has the ability to accommodate a variety of riser configurations.

7. It attracts lesser impact of the wave loading due to its compliant nature and hence, can be operated even in rough sea.
8. The natural periods in the horizontal modes of motion are controlled by the pretension in the cable system.
9. The installation of such platform is comparatively easy. Moreover, it can conveniently be transferred to other fields of sufficient depth of water. In the event of major topside retrofit or foremost maintenance and repair, such platform can conveniently be towed to a shielded deep-water location.
10. The structure is simple, round and slender and an accurate evaluation of the forces acting on it becomes possible.
11. The spar platform is now regarded as the next generation of deep water off-shore structure. A number of new Spar platforms with successful operations have proven the technology well established and more efficient.

2.4 Analysis techniques of Spar platform

Several advancements on analysis techniques of Spar platform is seen in literature. The most common approach for solving the dynamics of Spar platform is to employ a decoupled quasi-static method, which ignores all or part of the interaction effects between the platform and mooring lines. Coupled dynamic analysis of Spar platform was carried out first where the mooring line mass and damping was neglected. Coupling of the stiffness matrix from the mooring line to dynamic behavior of Spar platform was considered. This technique dealt with one degree of freedom response. The coupled analysis approach was extended later on to three degrees of freedom responses and six degrees of freedom responses by some researchers. However, they have solved the equation of motion of mooring line/riser and Spar separately and then matched together. Coupled action of the mooring line/riser with platform in a single model is complicated which is to be accomplished in actual manner. Following sections discuss existing works dealt by several investigators.

2.4.1. Spar-mooring system

The system of Spar-mooring lines is a slacky moored floating platform experiencing very low natural frequency in translational motion. Such configuration of classic spar contains full hull cylinder kept in station through mooring lines. As the system floats at deep water, the action of wave forces on its surface is dampened by counter balance effect of the structure's net buoyancy. Several studies have been conducted on the Spar-mooring system. Ran et al. (1996) and Ran and Kim (1997) analysed the response characteristics of a large slack-moored spar under regular and irregular waves. The influence of mooring inertia and damping was found as important to consider for better estimation of the moored platform responses. The Spar models in Ran and Kim (1997) were relatively smaller than that in study of Ran et al. (1996). Numerous experiments with a 1:55 scale model have been conducted in the deep-water model basin of Ocean Technology Research Centre (OTRC) in presence or absence of currents and wind. Small Spar was supported by a vertical tether and six spread moorings. Tether/Hull coupling effects were considered together as an integrated system. A time-domain coupled non-linear analysis computer program was developed to solve both static and dynamic behaviours of a moored compliant platform. The results were obtained from the program and compared with uncoupled analysis results to see the effects of tethers and mooring lines on hull motions and vice-versa.

Ran et al. (1999) performed non-linear coupled analysis for a moored spar under random waves. The Spar platform was positioned through four groups of taut catenary moorings containing three mooring lines in every single group. Mooring lines were attached with the platform through linear and rotational springs along with dampers.

Collinear currents reduced low frequency surge and pitch appreciably because of increased viscous damping. Jha et al. (1997) dealt with the wave tank experiment of floating Spar buoy platform motions considering damping in reliable manner. Mooring lines were treated as a set of mass-less linear springs. The initial model test included non-linear diffraction loads and a linear stiffness and damping characteristics of Spar mooring system. Refined models added the effect of wave-drift damping, and viscous forces as well. Consistent choices of damping and wave input were considered in detail.

Chen et al. (1999) assessed the responses of a slack moored spar platform aimed at showing the coupling phenomenon among the Spar and mooring system. A computer code COUPLE was used to get the responses and those were compared to respective laboratory results. COUPLE was shown to be a proper tool for numerical simulation to recover laboratory experiments particularly in deep water. The dynamic tensions of a truncated mooring system were found very different than the tensions for a full- depth (undistorted) mooring system (Chen et al., 2000). Chen et al. (2001) carried out the evaluation of Spar platform response constrained by slack mooring lines. Cable dynamics and couple dynamic analysis were focused in the study. Developed coupled dynamic analysis program, COUPLE was applicable for both Spars and TLPs. The lessening of slow drift surge because of mooring line damping touched around 10% at 1018m water depth. Mooring tension at wave frequency range was eight times greater than that in quasi static method. The results were shown to be important to estimate the fatigue strength and life span of mooring system in deeper water.

A hybrid method was proposed by Ormberg et al. (1999) to generalize a truncated mooring model test on the respective full–depth mooring system through numerical simulations using coupled dynamic study. Coupled dynamic analysis was shown as advantageous tool to deal with a truncated mooring system. Hydrodynamic characteristics of Spar platform was evaluated by Ma and Patel (2001) under ocean waves along with the quantification of those non-linear wave components. Centrifugal and axial divergence force components were shown as significant, matched with those of non-linear forces. Agarwal and Jain (2003) conducted coupled dynamic analysis of Spar platform under regular wave where mooring line dynamics was ignored. The hull was configured as a rigid body of six dof linked with sea bed by multi-component mooring lines which are linked with Spar hull at fairlead position. Coupling of stiffness matrix was shown to play a significant role on platform's dynamic behaviour.

Dynamic behaviour of spar-mooring system were performed in both time domain and frequency domain by (Anam, 2000; Anam et al., 2003). It was difficult to suppress transient effects in cases when the wave excitation was at one of the natural frequencies. Linearization in frequency domain could give a reasonable approximation to the nonlinear drag damping in the time domain, but can miss out on higher order drag forces. Higher order effects may be important near natural frequencies, but they are unlikely to be significant otherwise. To represent the static and dynamic response of nonlinear structures properly, an appropriate combination of secant and tangent modulus is preferred to a gross 'linearized' representation. Tao et al. (2004) investigated heave responses of Classic Spar with variable geometry. Platform with cylindrical shape and fixed cross-section might practice resonant heave under ocean environments with longer peak periods. This was excessive in riser integrity because of its low damping and comparatively low natural heave period. The heave resonant response was proved to be noticeably reduced with alternative hull shapes by means of improved damping mechanism keeping natural heave period beyond wave energy range.

Mazaheri and Downie (2005) suggested a generalized Artificial Neural Networks (ANN) based approach to predict platform response and mooring forces of floating offshore structures under long-term met-ocean data. Chernetsov and Karlinsky (2006) proposed three floating sub-structures viz. Spar-Classic, Spar-Ring and TLP-Ring for Stockman gas field in North West Russia. Due to ice pressure Spar and Semi-submersible were unsuitable because of their intolerable flexibility. SPAR-Ring was treated as most suitable floating structure at North West Russian region. Jameel (2008) evaluated coupled Spar-mooring line system where the large spar cylinder was attached with mooring lines at fairleads. Mooring lines as an integral part of the system are pinned at the far end on the seabed. The Spar-mooring structure was analysed under wave and current conditions. Diffraction theory and reliability analysis were included to obtain behaviour of Spar platform.

Tahar and Kim (2008) presented a numerical tool for deep water floating platforms with polyester mooring lines. Large elongations along with nonlinear stress-strain relationships were considered for polyester fibres. Mooring-line dynamics considered the rod theory. Static and dynamic analysis of a classic Spar comprising a tensioned buoy and polyester mooring lines had been performed. The motions, mean offset and tension in polyester mooring lines were completely different from the original rod theory results allowing linear elastic lines.

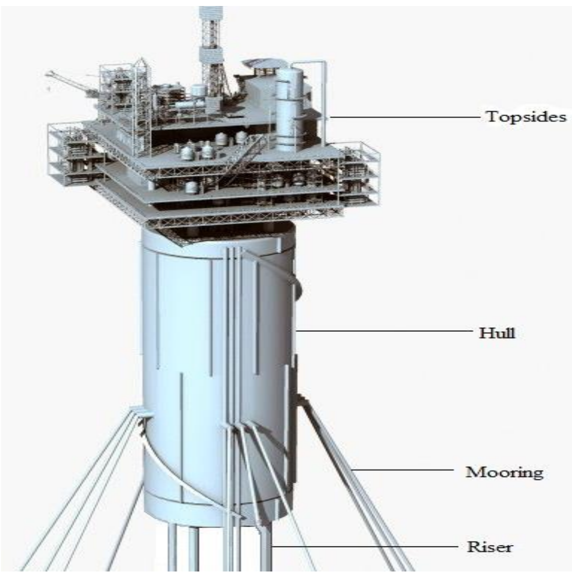

Figure 2.1: Assemblage of classic Spar Platform (QLEE, 2011)

Kim et al. (2013) compared dynamic coupled behaviour of floating structure and mooring system in time domain using two numerical methods for the mooring lines: linear spring method and nonlinear Finite Element Method (FEM). In linear spring method, hydrodynamic coefficients and forces on the floating body were calculated using BEM (Boundary Element Method) and equation in time domain is derived using convolution. The coupled solution was acquired by simply adding the pre-determined spring constants of the mooring lines into the floating body equation. In FEM, the minimum energy principle was applied to formulate the mooring system nonlinear dynamic equation with a discrete numerical model. The coupled solution was attained iteratively solving the floating body equation and the FEM equation of the mooring system. Two example structures such as weathervane ship and semi-submersible structure were analysed and the difference of those two methods were presented. The effect of coupling stiffness of the mooring system was discussed by analysing the cases with or without surge-pitch or sway-roll coupling stiffness of mooring lines.

2.4.2. Spar-mooring-riser system

The analysis of Spar platform becomes more complex when riser is added with mooing lines. In deep water, mooring lines and riser contribute substantial damping and inertia. Moreover, the design of risers and mooring system are governed by platform motion. An under-prediction of responses may lead to insufficient design and probably catastrophic failure. Again, an over-prediction necessitates exorbitant risers and mooring lines. Therefore, precise prediction of Spar platform motions is imperative for both the integrity and related expenses of the mooring lines and risers. Through study has been performed to evaluate different concepts employed by several investigators to analyse Spar-mooring-riser system.

Ormberg and Larsen (1998) suggested an approach to conduct coupled dynamic analysis of floater, mooring and riser system operating 150 m, 330 m and 2000 m water depth. Turret forces, turret motions and line tensions obtained from experiments, separate analysis coupled analysis were compared. The correspondence between the experiments and the coupled analysis results was generally good with respect to turret motions, turret forces and line tensions. The turret motions estimated by a separated analysis also compared well with both coupled analysis and experiments if mean current loads and low frequency (LF) damping from moorings and risers were included in an accurate manner. Otherwise, the use of separate analysis would severely under predict the mean off-set and over predict LF motions especially for deep water. Both, line tension and turret forces were under-predicted by using a coupled approach compared to coupled analysis. In deep water, a coupled analysis approach was, therefore, highly recommended for checks of important design cases.

Irani et al. (2000) performed wave basin model tests on Spar platform with risers. Riser-Spar keel plate interaction and buoyancy can-Spar hull interaction was evaluated for total damping contributions from risers to Spar heave. Damping from the buoyancy can/Spar hull interaction was much more compare to the damping from riser/keel plate interactions. Assessment of a generic Spar platform under 100 year extreme hurricane condition was dealt by Cobly et al. (2000). In coupled analysis the vessel forces including the wave frequency and low frequency hydrodynamic forces were generated in the time domain, using the computer code SIMO. In the decoupled analysis the vessel equations of motions were solved in time domain similar to that described above using the program SIMO. It was shown that the response characteristics of a Spar were fairly complex due to the interaction of wave frequency and low frequency surge, pitch and heave motions. About 10 to 30 per cent reductions for coupling of mooring/riser with the vessel in extremes than de-coupled condition were obtained. The amount of lessening increased with water depth. For such reductions, the design of mooring and riser system results in significant cost savings.

Gupta et al. (2000a) developed computation tool ABASIM combining ABAQUS and MLTSIM for studying the involvement of mooring lines and risers in dynamic behaviours of platform. The heave of classic Spar was found low like that of a truss spar if damping caused by mooring lines and risers was considered. Chaudhury and Ho (2000) simulated an integrated system of platform, mooring lines and risers in ABAQUS considering nonlinear soil-mooring line interaction. A non-linear integrated coupled dynamic analysis of floater (NICDAF) was developed, which was shown to predict vessel motion accurately in less time compared to ABAQUS. The difference in vessel motions through NICDAF and ABAQUS were mostly satisfactory for standard deviation of dynamic motion and negligible in case of static offset. For accurate dynamic motion prediction, full dynamic equilibrium of platform/moorings/risers was suggested. Similar work was extended to develop a new approach of coupled analysis by Chaudhary (2001) which can estimate six rigid body motions with considerable saving in computational cost. For deep water platforms, restoring force involvements of mooring lines/risers was imperative showing importance of coupled analysis.

Astrup et al. (2001) described the prominence of risers/mooring coupling with floating production systems. Coupling effects from riser and mooring systems reduced low frequency platform motion than the de-coupled approach. This low frequency motion of Spar offered smaller and economic riser/mooring system confirming lighter and hence cost-effective Spar platform. Kim et al. (2001) provided an assessment of the existing industrial capability to predict the responses of several categories of deep water floating production systems (TLPs, and SPAR). Low frequency and high frequency responses were mostly higher than wave frequency motions. Damping from risers and mooring lines increased with depth of water and influenced more on low frequency motions.

Ma et al. (2000) presented a method based on Deep-water Non-linear Coupled Analysis Tool (DeepCAT) to attain nonlinear coupled behaviours among platform, risers and tendons/moorings. The analysis tool comprises two numerical algorithms: 1) time domain platform motion simulation code (COUNAT) and 2) time domain cable dynamic analysis code (CABLE3D). Large changes in mean offsets for uncoupled and coupled analyses were seen under a 100 year loop current environment. RMS values of Spar motions and mooring tensions in coupled analysis were smaller than those of uncoupled case. Zhang and Zou (2002) checked the coupling results of supporting guide frames and risers upon the spar motion together with mooring line dynamics. The resisting moment caused by contact forces at keel joints and support guides influenced considerable on pitch/roll response and mooring tension. Lower heave and pitch/roll responses decreased hull draft and solid ballast at keel tank. Such reductions influence the size and weight of hull, mooring lines along with risers substantially.

Tahar et al. (2002) carried out nonlinear coupled dynamic analyses of a classic Spar comprising hull/mooring/riser. A 100-yr Hurricane condition with non-parallel wind, wave, and current was chosen for the numerical study considering various riser models. The first riser model considered elastic rod extending to the keel while free to slide vertically and constrained horizontally. Neglecting the riser portion inside the spar hull ensued over-estimation of pitch motion. Second model comprised buoyancy-can that reduced the maximum roll/pitch significantly. Ding et al. (2003) extended original code CABLE3D for large elongation in moorings. Potential wave load on moored platform was computed by diffraction wave theory using commercial code WAMIT. The code was used for moored classic Spars as well as mini TLP. Comparing to the corresponding model tests the code and was found to be consistent to assess dynamic response of floating platform-mooring/riser system.

Koo et al. (2004a) examined nonlinear multi-contact coupling between vertical riser and guide frame. Truncated riser model assumed riser as an elastic rod which is truncated at keel position. Alternate configuration allowed the risers to slide vertically with constant tension keeping constraint in horizontal direction. Truncated riser model ignored riser portion inside moon-pool which caused overestimation of pitch motion. Multi-contact guide frame-riser coupling forces showed minimal influence on Spar surge and mooring tension. Yung et al. (2004) performed a model experiment for vortex induced vibration (VIV) of Spar hull at David Taylor model basin (DTMB) set in Carderock division, United States Naval Surface Warfare Centre. The model was validated with Hoover's Deep draft caisson vessel (DDCV) and found to be reliable for VIV evaluation.

Kim et al. (2005) carried out vessel/mooring/riser coupled analysis considering a turret-moored tanker based FPSO in water depth 1830 m. The vessel motions and mooring tension were examined at the OTRC wave basin under non-parallel wind–wave–current, 100-year hurricane condition in the Gulf of Mexico. Evaluation with the OTRC 1:60 model-testing results concluded that the dynamic mooring tension might be underrated when truncated mooring system was considered. Garrett (2005) performed fully coupled investigation for floating vessel-mooring-riser system. The accuracy and efficiency of the procedures were explained by a large semi-submersible associated with 16 moorings and 20 risers. The approach was shown as precise and efficient. Rodrigues et al. (2007) offered enhanced numerical tools for coupled analysis of floating platforms. Two types of domain disintegration along with decomposition methods were described. The sub-cycling approach allowed the partition between hull and the lines. Another technique measured the internal disintegration and decomposition of the network of finite elements to represent mooring lines and risers. The approaches were developed emphasizing their computer application with parallel architecture.

Low and Langley (2007), Low and Langley (2008), Langley (2008) evaluated different procedures for analysing vessel/mooring/riser structures with fully coupled analysis in time domain as a benchmark for the accuracy. Two innovative approaches were described in their studies. The first was an improvement of frequency domain technique by a linearization of geometric nonlinearities. This approach enhances prediction of low frequency vessel motion with minimal computational cost. However, still discrepancies in time domain results were seen due to certain limits. Hybrid method simulated low frequency responses of coupled system in time domain and frequency domain. Such technique was found reliable as fully coupled analysis but required only one-tenth computational time for highly nonlinear system. For relatively shallow water depths, a good agreement of suggested technique was found.

Yang and Kim (2010) performed coupled dynamic analysis of hull-tendon-riser considering a TLP. Modelling was done choosing the mooring line/riser/tendon as an elastic rod. They were attached to the hull by means of rotational and linear springs. Equilibrium equations of mooring line/risers/tendon system and the hull had been solved concurrently. Hasan et al. (2011) investigated the response of a multi-hinged articulated offshore tower subjected to various seismic activities in the presence of random waves. The influence and impact of the vertical component, to the overall seismic behaviour of the articulated tower were examined. Dynamic responses were evaluated by spectral densities and time histories of hinge shear, axial force at the articulation, rotational angle and bending moment at peak ground acceleration in various seismic sea environments. Sun et al. (2011) performed coupled dynamic analysis of the Deep Draft Multi-Spar (DDMS) platform and mooring system under waves and current in time domain. By means of a geometrically nonlinear finite element method, the mooring-line dynamics are simulated based on total Lagrangian formulation. The results indicate that the wave groups have a substantial effect on the mooring line tensions and platform motion responses.

Seebai and Sundaravadivelu (2012) conducted the analysis of Spar platform responses supporting a 5MW wind turbine, with taut mooring and with bottom keel plate in regular and random waves with experiment and numerically. The accelerations in heave and surge at top of the platform were measured and used to compute the responses. Geometric modelling of the Spar was done by MULTISURF and directly exported to WAMIT for succeeding hydrodynamic and mooring system analysis.

Davison and Miles (2013) carried out a case study into the Availability, Reliability and Maintainability (AR&M) modelling activity undertaken for the Skynet 5 Beyond Line Of Sight (BLOS) service programme between January 2006 and July 2011. The modelling activity was completed using the Monte Carlo simulation tool SPAR, produced by Clockwork Solutions. The development of this end-to-end type approach has provided a number of benefits, including: highlighting potential areas of weakness in the support solution; understanding the impact on global AR&M performance; and validation of consolidated spares recommendations and identification of areas with insufficient spares, at multiple levels of support.

Liqin Liu and Zhang (2013) analysed the response in heave of Spar platform hull considering the moonpool water motion. The wave loading of platform hull was calculated by potential flow theory and the coupled motion of hull heave and moonpool water was analysed. The hull heave motion decreased when the moonpool water motion was considered. The hull heave RAO appeared two peaks for the large opening area of guide plate, and the higher heave was exhibited when the wave period was near the natural period of moonpool water vertical vibration.

2.4.3. Truss Spar

Kim et al. (2001) carried out nonlinear hull/mooring coupled analysis of a truss spar platform in time domain under wave loading including collinear steady wind together with currents. Mooring/hull dynamics was interpreted employing a time-domain FEM based analysis code, WINPOST. Motion spectra and tension in uncoupled analysis with a non-linear mass-less spring had been compared with the fully coupled study. Large dynamic tension indicated the requirement of dynamic or fatigue analyses for deep water platforms with taut-leg mooring. Minor discrepancy between the uncoupled and coupled analyses in low frequency motions and tension was observed.

Figure 2.2: Floating Truss Spar at Tahiti field, USA (Offshore technology, 2012b)

Montasir and Kurian (2011) studied the effect on motion behaviour of truss Spar platforms, of slowly varying drift forces. An efficient methodology to compute the slow motion responses of slender floating offshore structures subjected to wave forces were presented. Subsequently a MATLAB program termed as 'TRSPAR' was developed to predict the time domain dynamic responses. The truss spar was attached to the sea floor using 09 taut moorings simulated as nonlinear springs. Static offset simulation was conducted to obtain their stiffness. The TRSPAR code was validated with results obtained from a typical truss spar model test. Influence of different sources of second order difference frequency forces were compared for drag forces and inertia in terms of response spectra.

Coupled dynamic analysis was carried out by Yang et al. (2012) for wave interaction with a truss spar and its riser system/ mooring line in time domain. A time domain second order method was developed for the hydrodynamic loads. Taylor series expansions are applied to the free-surface boundary conditions and body surface, and then the Stokes perturbation procedure is used to establish the corresponding boundary value problems with time-independent boundaries. They also developed a higher-order boundary element method (HOBEM) to calculate the velocity potential, at each time step, of the resulting flow field. Dynamic equations for tendons/mooring-lines/risers and the motion equation for the hull, in the coupled dynamic analysis, are solved simultaneously. Numerical results of Spar motions and tensions at risers/ mooring-line's top are described with some important conclusions.

Yiu et al. (2013) conducted field measurements of motions of a truss spar subjected to multiple high current events in the Gulf of Mexico between the years 2006 and 2011. The motion data were studied to see if VIM lock-in occurred during any of these periods of high current events. Assumptions and procedures for estimating the reduced velocity (UR) and A/D ratio using field observations had been summarized. They also presented the comparison between the design guide based on the model tests and the field measurements.

2.4.4. Cell Spar

Zhai et al. (2008) dealt with the structural forms of a Cell Spar. The optimized selection of cell Spar platforms is studied under South China Sea as well as the operational necessities of a platform. Finite element analysis of the Cell Spar platform employing ANSYS is carried out. Analysis of structural strength of the platform subjected to survival and operation conditions has been carried out. The level of stress and demand of strength of overall system as well as key positions are obtained. The approaches for overall structural strength analysis of cell Spar platform have been implemented.

Lim et al. (2005) performed an experimental investigation on motion behaviour of cell Spar platform. Free-decay tests are carried out in a wave tank with a scaled model to obtain the natural period and damping coefficient in heave and pitch. Platform motions in regular waves are measured to derive the transfer function. During the experiments, it was witnessed that pitch motions become unstable at a certain time range. It is revealed that kinetic energy is transferred from heave mode to pitch mode due to nonlinearity. The experimental results agree well with the numerical results except for the time range of unstable pitch motion. Mooring effect was found to be insignificant on the motion response.

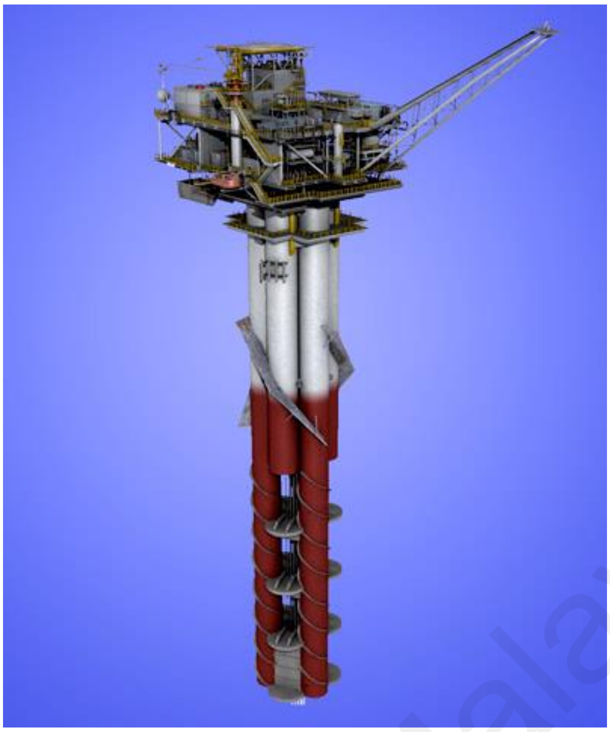

Figure 2.3: Floating Cell Spar assembly for oil and gas exploration (NDCo, 2012)

2.4.5. Cell-Truss Spar

To make more cost-effective, the cell and truss element are added together for the same Spar platform by several investigators. Zhang et al. (2007a; 2007c) have accomplished a numerical analysis on the hydrodynamic performances of a newly adopted cell Spar motion. In their study, cell-truss Spar combination was considered as an offshore floating platform. Experimental investigation in addition to numerical study on the global performances of cell-truss Spar platform have been conducted by Zhang et al. (2007b). Zhang et al. (2008) further examined the coupling influence of cell-truss Spar platform. They modelled the Spar riser/mooring by three methods viz. quasi-static coupled, semi-coupled and coupled approach. The response behaviour observed in time-domain along with frequency-domain analyses have then been assessed with experimental results.

2.5 Aerodynamic loading incorporation

One of the big complexities in design of floating production systems is prediction of proper loading and responses of the structure due to combined action of all applicable forces. The dynamic force acting on the platform is due to hydrodynamic and aerodynamic forces. Although the design of offshore structures is dominated by hydrodynamic loads, aerodynamic wind loading is very vital in design consideration as it may alter the response behaviour of the floating structure. Hydrodynamic load comprises forces from wave and current. The wind force that acts upon the exposed part of the platform is composed of fluctuating and mean wind components. API-RP2A (2000) requires that the dynamic effects of the wind be taken into account and the flow induced cyclic wind loads due to vortex shedding be investigated when the ratio of height to the least horizontal dimension of structure is greater than five. Though the wind forces contribute only a small percentage of the total forces acting on the structure, it is an important parameter in the loading estimation of the structural design process.

Wind force generally has two effects - one caused by the mean speed and the other caused by the fluctuation about this mean value (Chakrabarti, 2005). Mean speed is taken as a steady load on the offshore structure. Only the mean speed is considered for a fixed structure as the effect of the fluctuation of wind about the mean value has negligible effect on it. This, however, is not the case for a floating structure. Here, the dynamic wind effect may be quite significant and cannot be overlooked. Ahmad et al. (1997) investigated wind-induced response of a tension leg platform. Dynamic analysis in time domain were investigated performed considering influence of nonlinearities due to variable submergence, variable cable tension, hydrodynamic drag force, long excursions and fluctuating wind, along with the effect of coupling. Fluctuating wind has been estimated using the Emil Simiu's wind spectrum (Simiu and Leigh, 1984), ideal for compliant offshore structures; and the sea state is characterised by the Pierson

Moskovitz spectrum. The Monte-Carlo simulation is used to model random wind and waves. The wind-induced dynamic responses of the structure are highlighted by power spectral density functions (PSDF). Ahmad and Ahmad (1999) described an active control strategy of a Tension leg platform. The TLP is a deep water semi-submersible type compliant offshore structure that is moored by vertical taut cables called tethers or tendons. Random sea and fluctuating wind characteristics were incorporated.

The exposed portion of the Spar platform (Li and Kareem, 1990), due to wind velocity acting normally upon the platform, is subjected to drag force. The simple expression for such wind-induced loading is: the drag force per unit area projected on plane normal to the wind velocity. The computation of wind force acting on the floating structures at deep waters is based on the empirical formula recommended by API -RP2A (2000). Fluctuating wind component may be based on single point simulation as estimated by the Fourier synthesis of wind spectrum which was first developed by Emil Simiu. There are a number of wind spectra: Emil Simiu, API-RP2A, Kareem, Davenport spectrum etc. Irregular and mean wind forces play a significant role in the incidence of wave-induced loading. Sometimes, a severe wind caused by hurricanes may result in more damage than the normal hydrodynamic loading.

Zaheer and Islam (2008a), stated that wave and wind loadings play a major role in the design of offshore structures in general, and the design of articulated towers to ensure successful service and survival during both normal and extreme environmental conditions. The dynamic interaction of these towers with the respective environmental loads (waves, wind and currents) acts in such a way as to impart a lesser overall shear and overturning moment. Geometric nonlinearity due to large displacements becomes an important consideration in the analysis. Zaheer and Islam (2008b) dealt with the fluctuating wind induced response characteristics of double hinged articulated loading platform. Wave and wind loadings play a vital role in the design of articulated loading platforms (ALP) to ensure their successful service and survival. For comparative studies of the ALP, responses under different wind spectra suggested by Emil Simiu, Kareem, Davenport and API-RP2A are employed. The analysis of the same structure under wind along with buoyancy as a restoring force is also investigated. Response time histories of deck displacement, hinge rotation and hinge shear as well as power spectral density functions (PSDFs) are presented. Statistical analysis under various parametric combinations was also conducted. Contribution of wind force to the platform responses was mainly governed by the size of the wind generated waves.

Islam et al. (2009a) evaluated double hinged articulated tower interaction with waves and wind. Single and double hinged articulated offshore towers are designed in such a way that they derive their stability from inherently large buoyancy forces and are highly flexible against rotation at the hinges. Wind induces significant dynamic response since the fluctuating wind velocity spectrum has high energy content in low frequency region. Stochastic response is characterized by statistical quantities and power spectral density functions (PSDF) for various parametric combinations. The studies of wind effects were deemed to be imperative. Islam et al. (2009b) assessed response behaviour to wind forces of double hinged articulated tower platforms. Emil Simiu's spectrum is used to model the fluctuating wind. Nonlinearities form drag force, added mass, instantaneous tower orientation are considered. Power spectra obtained from random response time histories show the significance of low frequency responses.

2.6 Spar platform in Malaysia water

Recently Malaysia has installed her first spar which is positioned at 1330m water depth, in Kikeh field, Sabah on the year 2007. This floating assemblage is the first Spar ever employed outside the Gulf of Mexico. The structural configuration for this deep water fits with the kind of truss Spar. Among the Malaysian continental shelf offshores, deep basins are well-matched to mount floating platforms. Particularly the Sarawak basin off the East Malaysian state Sarawak as well as the Sabah basins off the East Malaysian state Sabah are located at deeper water. Exploring deep-water hydrocarbons from the eastern continental shelf is a challenging job. Newly embraced oil production project under planning and construction stage is the Gumusut/Kakap project located at offshore Sabah at water depth 1200 m. Offshore Sarawak basin is also located at deeper water. Only the Kebabangan field is located in shallow water depth of almost 200 m. The other six sedimentary basins are located in deep sea at water depths more than 1000 m (Table 2.1). High functioning expenses and extensive technical expertise signpost the suitability of floating platforms like Spar in such deep sedimentary basins.

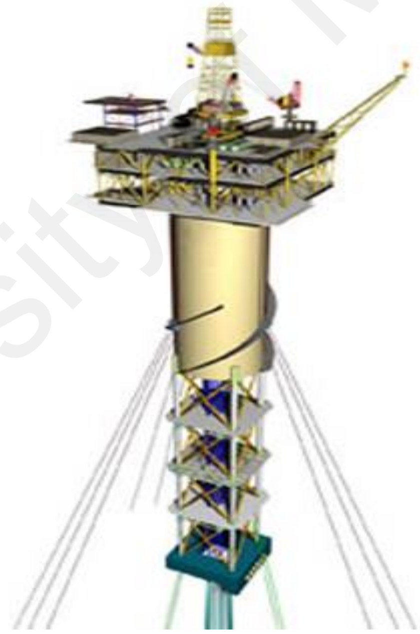

Figure 2.4: Kikeh Floating Spar in Malaysia (Offshore technology, 2012a)

Table 2.1: Offshore fields in Malaysia at different water depths

Name of Field	Depth of Water
Kikeh	1,300 m
Gumusut/Kakap	1,220 m
Jangas	>1000 m
Ubah Crest	>1000 m
Pisangan	>1000 m
Kamunsu	>1000 m
Kebabangan	>200 m

2.6.1. Wave data simulation in Malaysian water

Wave data are important during the design of floating ocean structures. It is needed for the calculation and prediction of the motion characteristics, performance and operability of vessel in waves as well as in determining the suitability of the structure to withstand rough/extreme weather conditions. Very important input for these calculations is the accurate and reliable wave data in the form of its probability of occurrences of wave heights and wave periods. Presently, only two main sources of published data for Malaysian waves are available. One is based on Global Wave Statistics (GWS) derived by British Maritime Technology Ltd., Unwin, London (Deo, 2012) and another is Malaysian Meteorological Service (MMS) conducted by Marine Meteorological Observations at Kuala Lumpur, Malaysia (MMS, 2010). Both the data from GWS and MMS are based on voluntary observation from ships. Wave data simulation is required to analyse the moored Spar in Malaysian sea conditions and predict return periods.

Several approaches to obtain sea wave parameters have been addressed by various researchers. Yaakob et al.(2004) presented a reliable and comprehensive wave database for Malaysian seas using satellite altimetry. Saleh et al.(2010) identified and compared the wave characteristics of five crucial places in Sabah waters, so as to accomplish the upshots of Northeast Monsoon (NEM) for Sandakan and Tawau together with Southwest Monsoon (SWM) for Labuan and Kota Kinabalu beside the state's east and west coasts. They collected month-wise wave period and wave height records for 8 years. The range of wave heights surrounding Sabah coastal water was found as 0.5-2 m. The wave height has been observed as higher than 1 m at west coast in the time of NEM and around 0.5 m in the east coast in both monsoons. Marghany and Hashim (Marghany and Hashim, 2010) introduced Doppler spectra model incorporating two-dimensional Fourier transform (2DFFT) and obtained a linear equation for sea radial component. Horizontal surface current has been estimated relying on Doppler spectra's maximum peak at the seas offshore of Terengganu, Malaysia. Furthermore Biswas and Kara (2011) introduced conservation laws of regularized long wave equation.

For simulating ocean wave characteristics, frequency distribution is an outstanding tool. Frequency distribution studies and return period estimations of sea waves have been covered by few investigators (Van den Brink and Konnen, 2008, 2011; Van den Brink et al., 2005). Caires and Sterl (2005) presented global estimates, based on the ERA-40 reanalysis data, of 100-year return period of significant wave heights. They used peaks-over-threshold method to calculate return values, with a threshold on the 93% level of entire 6-hourly records. Onni Suhaiza et al. (2007) studied the suitability of determining magnitude and frequency of floods for Sarawak using Gumbel distribution based on a limited period of data. Nineteen stations were selected for the study based on the criteria stated in Hydrological Procedure No. 4 (HP4). The probability plot and flood-frequency curves by Gumbel distribution of each individual station were prepared. Muzathik et al. (2011) presented wave measurement and wave climate prediction within East Coast Peninsular Malaysia by in-situ measurements from 1998 to 2009. Rayleigh and Weibull density functions were used to predict wave heights. Extreme significant wave heights ranging 2.6 to 3.4 m obtained from Gumbel Distribution showed a marked increase compared to the values from Weibull or Generalized Pareto Distributions (GPD).

2.7 Sea bed friction

The effect of sea bed friction on mooring line is still an issue and area of on-going research (Zeitoun et al., 2008). A modest approach to configure CML-sea bed soil contact is the basic Coulomb friction model. The Coulomb friction strategy considers pure constant plastic friction between the CML and the seabed. The friction approach does not reflect any passive resistance or loading history because of embedment. In the model represented by Zeitoun et al. (2009), it is assumed that the effect of seabed on the mooring line is the foremost concern. Mooring line-soil interaction is modelled in the ABAQUS FE model using a rigid element. The seabed model serves two purposes:

• Providing “vertical/normal” support to the mooring line.

• Providing “lateral/tangential” resistance to the mooring line through a frictional mechanism (Coulomb friction).

When a mooring line is subject to oscillatory wave action, it is very likely for it to develop a complex interaction with the soil on the sea bed. If such movements are small in nature, the mooring line may be caused to penetrate into the soil. On the other hand, if the movements are large in nature, they are likely to cause the mooring line to break out laterally (Brennodden et al., 1989). Thus, for small cyclic lateral movements, the mooring line tends to get embedded into the soil whereby it penetrates the soil by pushing it aside, making a berm or a mound formation, and eventually bringing about an escalation in passive soil resistance. Palmer et al. (1988) conducted a geotechnical investigation of the lateral resistance to movement within a wider research investigation of the lateral stability of marine pipelines. The investigation covered extensive full scale tests on a nominal 10 inch pipe on sand, subject to a host of loading conditions designed intentionally to simulate the loading scenario and history of a pipeline on the seabed. It was observed that the resistance is actually much higher than what is generally assumed. The outcome is particularly significant when the loading is cyclic with increasing amplitude, and also when the pipe is partially embedded in the seabed.

Wagner et al. (1989) developed a model through The PIPESTAB Pipe-Soil Interaction Project, which predicts soil resistance to lateral motions of entrenched submarine pipelines. The model includes pipe displacement history and pipe displacement history in the resistance prediction, thereby significantly improving upon typical coulomb friction estimation. Unlike simple friction, pipe-soil resistance is dramatically more complex. Test data reveal significant dependence of lateral resistance on soil strength and pipe penetration. For large movements, the mooring line instead breaks out from embedment. Even so a finite penetration or embedment is still retained. Thus, besides Coulomb friction, there is an additional residual lateral resistance caused by a mound of soil being pushed ahead of the mooring line following the break-out. Mooring line movement, mooring line penetration, and soil resistance were shown as interrelated.

Liu et al. (2001) studied how seabed properties affect acoustic wave fields in a seismo-acoustic ocean waveguide. This analysis considers acoustic wave fields in an ocean waveguide, with a sediment layer having continuously varying density, and sound speed overlying an elastic sub bottom to investigate the effects of such seabed acoustic properties on the characteristics of wave fields. Kamarudin et al. (2007) investigated combined influence of piggyback on the hydrodynamic forces on offshore pipeline bundles under both wave and current environments employing Computational Fluid Dynamics (CFD). The orientation of smaller pipe relating to main pipeline plus flow conditions i.e. different Keulegan-Carpenter numbers was the key concern. Presence of the piggyback substantially influenced the hydrodynamic features of the main pipe. Kiu et al. (2011) dealt with the upshots of uniform surface roughness on the vortex-induced vibration (VIV) of cylindrical offshore structures like Spars in strong currents. An elastically mounted rigid vertical cylinder with no end plates, towed along the length of a water tank has been assembled in experiment. Maximum response amplitude and maximum mean drag coefficient decreased with increase of cylinder roughness. Rough cylinders required lower dynamic mean drag than smooth cylinder case. As the friction effect on ocean structures has not widely covered, the effect of sea bed friction on mooring line and hence on coupled Spar platform is of great interest.

2.8 Stability analysis of Spar platform

The stability of Spar is one of the most essential design topics which should be keenly analysed for the floating platform. It is likely for the designer to opt for sophisticated methods to check stable responses where mooring line is allowed for displacement under extreme ocean environments. It is necessary and useful to explore the instability with a range of physical parameters and for the prediction of the cylinder motion under various ocean loadings. A few studies have been conducted on stability analyses of different structures. Huang and Leonard (1990) have evaluated lateral stability of a submarine flexible hose line in a slowly varying current. The hose segment is assumed to slide on the sea bottom without twisting if the current force overcomes the sea bottom resistance. Hose tensions, lateral deflections, and anchor loads were considered the evaluation of stability. Most critical parameters for a practical hose line included: the axial rigidity of hose, segment length-to-span ratio, current velocity and hose size.

Stability analysis of the TLP was presented by Siddiqui and Ahmed (1996). Measured nonlinearities due to large displacements, and coupled stiffness matrix, etc. were used to analyse the structure under random and regular sea states. Monte Carlo stimulation was utilized to calculate the reliability of tethers. Tether pretension was one of the key parameters responsible for hydrodynamic response, hydrostatic stability, and instantaneous tether tension. Optimising the tether pretension for its natural frequency was very essential to avoid unexpected response. Mathieu stability in the dynamics of

TLP tethers was investigated by Simos and Pesce (1997) considering variable tension along the tether length. A linear cable equation for tethers modelling submitted to tension which varies linearly along its length was considered by the modal analysis. Amplitudes of tether vibrations were obtained via Mathieu stability analyses. Tension variation played a vital role and its consideration is indeed indispensable as high value of pretension is greatly reduced by increase in water depth.

Huang (1999) dealt with dynamic stability analysis of heave motion of marine cable-body systems operating in alternating taut–slack conditions, based on a single-degree-of-freedom model. The cable is replaced by a spring of bi-linear stiffness and the fluid damping is linearized in this model. Jacobian matrix is analysed to assess stability and the period-one Poincare map is derived. Transition from a periodic response to a chaotic one, through period doubling was shown through various numerical simulations. Esmailzadeh and Goodarzi (2001) performed stability analysis of a CALM floating offshore structure. Necessary and sufficient condition for the existence of stable periodic response, for a type of catenary anchor leg mooring system (CALM) was observed. From mathematical model, the governing equation of motion for the system was seen as non-linear parametric second-order ordinary differential equation.

Umar and Datta (2003) performed nonlinear dynamic analysis of a multipoint slack moored buoy subjected to first and second order wave forces. Various types of dynamic instability phenomena that tend to arise due to the nonlinearity of the system are investigated by analysing the nonlinear responses to the system. They utilize a hollow cylindrical buoy anchored to sea bed by means of six slack mooring lines. The system's responses are obtained and analysed across three regular waves, specifically, 5 m/5 s, 12 m/10 s and 18 m/15 s. The results of the study indicate that various types of instability phenomena such as symmetry breaking bifurcation, nT sub harmonic oscillations, and aperiodic responses might occur in slack mooring systems. The dynamic stability of such systems might be significantly influenced by a second order wave force.

Umar et al. (2004) carried out stability analysis of a moored vessel. Using a two term harmonic balance method (HBM) to find approximate response, the authors have presented a procedure for the stability analysis of a slack mooring system for periodic wave excitation. Floquet's theory and Hill's variational approach have been utilized to establish the conditions for determining both, the local and global stability of the approximate solutions. With respect to the mooring system for certain frequencies of excitations that fall outside the acceptable range of frequencies that have been obtained from the analytically derived stability boundaries, the study identifies a number of instability phenomena. Such phenomena include sub harmonics, symmetry breaking bifurcation, 3T and 5T solutions, etc. In some cases even chaotic motion is exhibited.

Haslum and Faltinsen (1999), using simplified calculations and a model test of floating Spar, investigated the Mathieu instability in pitch motion combined with extreme amplitude heave resonance. They presented a stability diagram for Mathieu’s equation, without taking into consideration pitch damping effects. Rho et al. (2002) adopted conducted model tests for a Spar platform with helical strakes, a moon-pool, and damping plates. Additional damping due to helical strake and heave plates reduced heave motion. They experimentally confirmed pitch/heave coupled nonlinear motion for Spar platforms. Zhang et al. (2002) extended their works including pitch damping effects, and developed a damped Mathieu’s stability diagram from Mathieu’s equation. Haslum and Faltinsen (1999), Zhang et al. (2002), and Rho et al.’s (2002) studies, however, did not consider the effects of time-varying displacement. Moreover, the mooring/hull/riser coupling effects are not considered in Haslum's and Rho's studies.

Koo et al. (2004b) have shown that when there is a harmonic variation in the pitch of a Spar platform restoring coefficients caused by large heave motion, and when the period of the heave motion is half of the natural pitch period, then the resulting lock-in phenomenon that arises is known as Mathieu instability. This pitch/heave coupling can be represented using Mathieu's equation. They explored Mathieu's instability of a classical Spar for the typical (i.e. West Africa and North Sea) swell conditions as well as a regular wave environment as well. The ratio between wave frequency heave motion and pitch natural period motion, in such a situation, is in the range of the principal unstable zone of the Mathieu instability.

Chandrasekaran et al. (2006) have performed stability analysis of TLP tethers. Pretension cables are used to connect them to the sea bed. The effect of variable tension in the tether dynamics is made more significant as a result of the increasing use of TLPs in deep waters as well as the necessity of reduction of usually high value of pretension. Mathieu stability analysis is performed for TLPs of different water depths, viz. 527.8, 872, and 1200 m, and different shapes to obtain precise amplitudes of tether vibrations. Increased tether tension leads not only to a stable platform but also significantly improves the stability by increased hydrodynamic loading contributing positively to the added mass. Triangular configuration TLPs characterized with increased initial pretension are far more stable compared to four leg TLPs in the first mode of vibration.

Munipalli et al. (2007) explore the weathervaning instabilities of a FPSO under the regular wave conditions and the effect on RAO. Several experimental tests have been carried out in regular sea states incorporating a1:60 scaled model of a standard FPSO. Four instrumented mooring lines were linked with an internal turret. Hull responses to swell conditions are assessed along with the weathervaning characteristics of the turret assemblage. Possible reasons of yaw instabilities comprising the consequence of moorings and test duration were discussed. Similarities and variances with RAOs for selected sea headings were pointed out through RAO with SESAM comparison. Analysis of a weathervaning FPSO subjected to bi-directional sea states have been performed by Chillamcharla et al. (2009) using similar model like Munipalli et al. (2007) at Institute for Ocean Technology, Canada, in collaboration with the University of Western Australia (UWA). Mooring tensions were noted as relatively immune to yaw instabilities and upshots of bi-directional sea states were described. Numerical simulations in time domain were compared with model tests at 45, 60 and 90 deg separation between the seas together with the swell showing reasonable agreement.

Tørnes et al. (2009) addressed pipeline hydrodynamic stability as fundamental design topics. They discussed the numerous different design approaches and the acceptance and suitability criteria typically implemented in pipeline stability design. An alternative stability design rationale based on a detailed deliberation of Limit States relating to pipeline stability was proposed. This method is based on the application of advanced dynamic stability analysis for assessing the pipeline response. Arnoult et al. (2011) introduced the modal stability procedure for linear and dynamic finite element analysis subjected to variability. They presented modal stability procedure (MSP), utilized for the calculation of natural frequencies and frequency response functions (FRFs) of finite element systems with random parameters. A systematic comparison between the Monte Carlo simulation approach and MSP has been conducted, are reported and commented about. The MSP, from a computational perspective was found very efficient.

From the literature review it is observed that precise motion investigation of platform is very essential for integrity and associated costs of Spar hull and mooring lines/risers. Proper dynamics cannot be assessed by conventionally used decoupled quasi-static methods which ignore all or part of the mooring/riser-platform interaction effects. Coupled analysis can capture all the complexities in reliable fashion. Again, coupled behaviour of Spar Platform under wave, current and wind loading is of pronounced interest. Suitability of Spar platform in Malaysian deep sea and coupled effect of riser deserve essential concern. In the present study, fully coupled integrated Spar-mooring system has been modelled. Using a nonlinear finite element approach, the deep draft Spar hull and each catenary mooring line as well as rigid riser are simulated in a single assemblage. Along with the hydrodynamic loading effect the aerodynamic (wind) loading has also been incorporated along with the sea bed friction to investigate the actual structural behaviour. Furthermore, the stability analysis of coupled Spar platform has been carried out.

CHAPTER 3: METHODOLOGY

3.1 Introduction

Nonlinear coupled integrated Spar platform has been modelled as a finite element assemblage in unique system. Nonlinearities arising due to long flexible mooring geometry, variable submergence, added mass, damping and mooring line-sea bed contact are duly considered. Effect of integrated coupling embraces the significance of drag damping of mooring systems in deep-sea conditions. A surface to surface contact interaction is selected with circumferential surface of catenary mooring and non-deformable surface of sea-bed. The Spar-mooring model is presented to be tested in several sea conditions. The influence of aerodynamic loading is incorporated on the frontal area of coupled Spar. Compatible wave data has been simulated for Malaysian water to analyse Spar platform in its deep sea. Sea bed friction effect on the mooring system is captured with friction penalty in Coulomb friction model. Techniques of stable response analysis of coupled Spar platform are described. Moreover, modelling of integrated Spar-mooring-riser system and coupled analysis have been discussed.

3.2 Configuration of Spar Platform

The Spar platform has been modelled as a nonlinear coupled (NONLIN-COUPLE 6D) system which ensures the actual characteristics of compliant floating platform. A rigid cylinder has been modelled to shape the Spar hull with six degrees-of-freedom (DOF). Among the six DOF, three are displacement viz. Surge, Sway and Heave about X, Y and Z axes. Other three DOF designate the rotations Roll, Pitch and Yaw along X, Y and Z axes respectively. Discrete rigid element is selected to simulate cylindrical Spar hull in ABAQUS/AQUA environment. As the cylindrical hull is considered a rigid member, the displacements and rotations occur around the centre of gravity, CG. The radii of gyration and the cylinder mass are defined at CG. The stability and stiffness of Spar hull is maintained by a number of CML made of steel rope. The mooring lines are connected at fair leads close to the platform centre of gravity and spread out horizontally. The stiffness of translation springs is very high, whereas the stiffness of rotational springs is very low, simulating a hinge connection. Figure 3.1 shows the detailed elemental view of the Spar platform system.

Four catenary mooring lines have been modelled as hybrid beam element in the FEM model. The line configuration is hybrid since it employs a mixed formulation comprising movement in six DOF, with six displacements along with axial tension as nodal degrees of freedom. As the steel rope formed cable experiences axial tension, the catenary shape of these mooring lines is a useful feature. Sea bed has been modelled as rigid surface and maintained as non-deformable. The mooring line anchors with its bottom end at sea bed. For avoiding complexity of the dynamic solution, the connection is treated as hinge. The mooring line slides on the sea bed to an extent for attaining stable configuration of the entire Spar-mooring system.

3.3 Solution approach of Spar Platform

Most usual technique for solution of Spar platform dynamics in existing literature is decoupled quasi-static method. This quasi-static approach overlooks the entire or part of the interaction effects amongst the platform and mooring lines. Moreover, the mooring lines are configured as mass-less linear or non-linear springs. The spar motion for the prescribed loading is obtained from only the platform modelling. Separate finite element model of mooring line is built where the motions of platform are induced as external loading by means of forced boundary conditions. Mooring line responses are estimated from this separate model. Hence, the dynamic interaction among platform and mooring lines are not properly incorporated in the traditional uncoupled analysis. In case of deep water platforms, mooring lines usually pay substantial inertia and damping because of their longer lengths, larger sizes, and heavier weights. This damping action should be precisely employed for perfect motion analysis of deep water platforms.

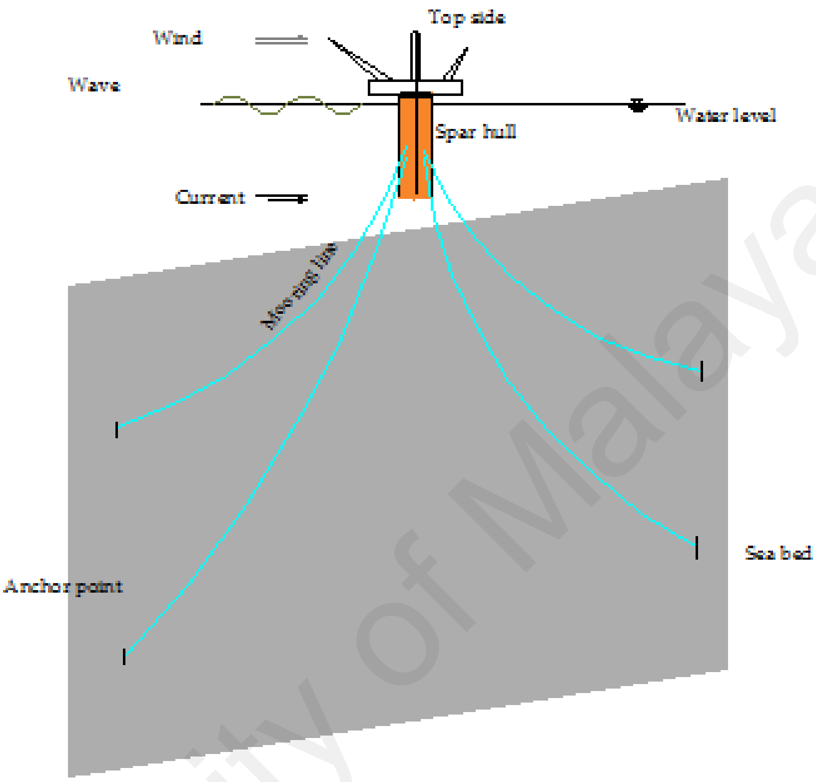

Figure 3.1: Outlook of offshore Spar Platform

Present nonlinear coupled analysis includes the CML and DDS hull in a unique model. This technique is realistic to capture the damping due to mooring lines in a consistent manner. Dynamic equilibrium is suitably achieved among the forces acting on the DDS and CML at each time instant. The ability of more accurate prediction of platform motions by coupled analysis approach may consequently contribute to a smaller and less expensive station keeping system and hence a lighter Spar platform through a lessening in payload necessities. Spar hull and mooring line coupled action is captured with required structural and environmental nonlinearities. Water particle kinematics estimates the drag and inertia for all the six degrees of freedom. The static coupled problem is solved by Newton's method. In order to incorporate high degrees of non-linearities, an iterative time domain Newmark-beta time integration scheme has been adopted for solving the coupled dynamic model.

3.4 Involved nonlinearities

The idealization and analysis of Spar platform in deep waters turns out to be a complex procedure largely because of the uncertainties associated with the environmental loadings and the system configuration. In an extensive study, this problem is further compounded by the nonlinearities in the structural system, occasionally contributing to resonant slow drift and large amplitude responses. Projected nonlinearities in the Spar–mooring assemblage are discussed in brief.

3.4.1. Variable submergence

The linear wave theory is valid only for constant depth of water corresponding to the mean still water level. The fluctuations in the depth of structural submergence with the passage of waves might be significant except for waves with small heights and therefore cannot be neglected. This is so because the variable submergence effects generate harmonics of wave loading at frequencies equal to multiples of the wave frequency and at zero frequency (static component), which in turn may cause significant effects on structural response due to resonance excitation of higher modes of the structure. Several approaches explain how the linear wave theory can be extended to consider free surface effect. Chakrabarti (1987) considered instantaneous elevation of sea surface as the mean still water level considering a time varying water depth. Wheeler (1970) suggested the modification on the vertical co-ordinate making use of a time varying scale factor equal to the ratio of the normal water depth and the instantaneous depth of water. In the present work, Airy's linear wave theory for most of the cases and Stokes nonlinear wave theory for special case are assumed to be valid up to the tangible level of structural submergence due to the passage of waves by incorporating the modification suggested by Wheeler (1970).

3.4.2. Added mass

The added mass arises because of the tendency of submerged platform components moving with acceleration relative to the surrounding sea water to induce fluid accelerations. These sea water accelerations require forces exerted by the Spar through a pressure distribution of sea water on the Spar. As the submerged Spar operationally imparts acceleration to some of the surrounding sea water, this phenomenon can be equated to the Spar platform having an added mass of deep water involving its own physical mass. The added mass force produced by the water surrounding the Spar platform components is mathematically calculated by the modified Morison’s equation (Sarpkaya, 1986). It varies with time nonlinearly. The effect of the structure accelerating in the water is equivalent to increasing the mass of structure by the amount known as added mass per unit length of the structure.

3.4.3. Damping

Damping is customarily anticipated to be viscous or proportional to the velocity. Capturing the damping properties is a suitable way of counting the important energy absorption without modelling the effects in detail. The different sources of damping for Spar platform can be recognized as structural damping, radiation damping, wave-drift damping and mooring line damping. The structural damping is assumed as constant and its computation is based on the initial values of [K] and [M] only. In the present study, the integrated nonlinear coupled system offers damping through long stretched and hanging mooring lines. Mooring line damping is very important for deep water platform which arises due to time varying stiffness and drag force on moorings. The heave damping arises due to vertical drag force component of Morison's equation and vertical mooring stiffness. A significant contribution is made by the drag force acting on the Spar as per Morison's equation.

3.4.4. Geometric non-linearity

Geometric nonlinearity arises when the deformation of mooring lines being analysed modifies the response of the whole structure to additional loading. The techniques are commonly implemented in computer programs as a large deformation, small strain formulation, rather than in terms of large strains. Long flexible mooring lines deform significantly under the loading conditions. The large change in the profile introduces geometric non-linearity. The initial stresses or load stiffening also contribute to the non-linear geometry. The Spar platform mooring lines undergo large deformations and are pre-tensioned to achieve initial equilibrium position. The geometric non-linearity is incorporated by considering the updated stiffness matrix at every time step.

3.4.5. Non-linearity due to boundary condition

The mooring line hangs in catenary shape, partially lying on the sea bed. The hanging part of mooring line is connected to the Spar platform in the present model. Due to the action of environmental forces the profiles of all the mooring lines change with time. Therefore, the portion of mooring line up to the touch down point also changes with time. This change of boundary condition (at touch down point) with time introduces non-linearity. If the sea bed is considered as frictional, it further adds to the degree of non-linearity. Non-linearity due to mooring line interaction with sea bed is highly discontinuous; it causes serious difficulties in numerical stability of solving the equation of motion. This change at each and every time instant is fully incorporated by up-dated stiffness matrix.

3.4.6. Forces acting on the Spar platform

One of the complexities in the design of Spar platform is the prediction of environmental loads. Forces experienced by the structure due to the environment are difficult to predict because they are the functions of the platform motions, while the motions are basically responses to the forces. For slender bodies with D/L (diameter/wavelength) ratio less than 0.2, Morison's equation is considered to be adequate in calculating hydrodynamic forces. Furthermore, when the ratio of height to the smallest horizontal dimension of the structure is larger than 5 (five), the dynamic effects of the wind needs to be taken into account (API-RP2A, 2000). These aerodynamic forces contributing a small percentage of the total forces are important parameters for loading estimation in structural design process.

3.5 Mathematical Formulation

In this section the dynamic equations for catenary mooring lines and Spar hull have been derived. Combined equations of motion of spar-mooring system have been generated accordingly. Then the Virtual work approach has been implemented to formulate the dynamic equations, resulting in a set of nonlinear differential equations in time domain. Three dimensional models of spar-mooring line system (Figure 3.2) have been considered here. The static coupled problem is solved by Newton's method. With the intention of incorporating high degrees of nonlinearities, an iterative time domain numerical integration is required to solve the equation of motion and to obtain the response time histories. The Newmark-β time integration scheme with iterative convergence has been adopted for solving the coupled dynamic model.

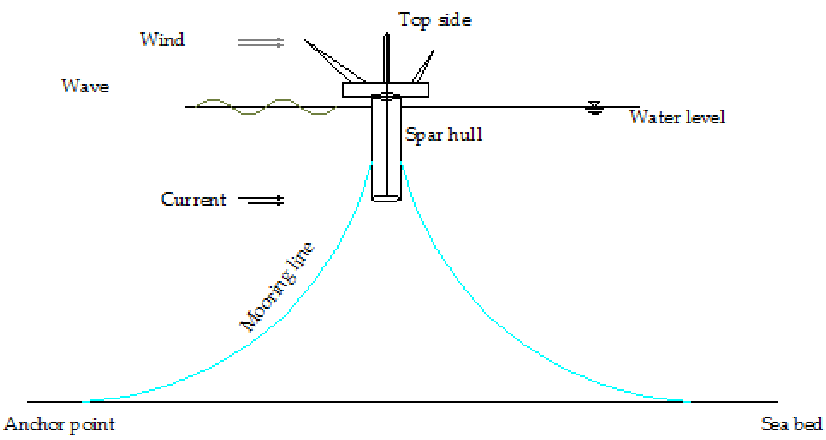

Figure 3.2: Sketch of Spar-mooring system

3.5.1. Assumptions

- The mooring line is modelled as a hybrid beam element.
- The spar hull is a rigid cylinder.
- Mooring line is attached by springs at fairlead of the spar hull with hinge connection. The other end of the mooring is anchored to the sea bed.
- Airy's wave theory and Stokes wave theory are adopted to calculate the water particle kinematics.
- Morison's equation is suitable for calculating the wave exiting forces.
- The distortion of waves by spar and mooring lines is insignificant.
- The cylindrical spar hull is considered as rigid beam element. Its mass and rotary inertia are specified at the centre of gravity.
- The platform and mooring lines are connected through hinge connections.
- The wave field is virtually undisturbed by the floating moored Spar.
- Mooring line behaves as an elastic rod. The initial pretensions in all the mooring lines are treated as equal.
- Sea bed is modelled as rigid plate, allowing no penetration of the mooring line.

- The contact between mooring line and sea bed is modelled as surface to surface. There is no friction between mooring line and sea bed. Circumferential surface of mooring line and surface of sea bed is selected for contact interaction.
- Wave forces have been projected at the instantaneous equilibrium position of the moored Spar incorporating the Morison's equation with stretching modifications suggested by Wheeler for factoring in the influence of variable submergence.
- Directionality of waves approaching the Spar platform is ignored in the analysis and only the unidirectional wave train has been considered.
- Four mooring lines have been placed in line with surge and sway direction.

3.5.2. Equation of motion

The formation of a non-linear deterministic model for coupled dynamic analysis includes the formulation of a non-linear stiffness matrix allowing for mooring line and Spar hull-mooring coupling under variable buoyancy as well as structural and environmental nonlinearities. The model involves selection and solution of wave theory which realistically represents the water particle kinematics to estimate drag and inertia for all the six degrees of freedom. The equation of motion describing the Spar-mooring system equilibrium amongst inertia, damping, restoring and exciting forces is assembled as:

$$[M]\{\ddot{X}\}+[C]\{\dot{X}\}+[K]\{X\}=\{F(t)\} \tag{3.1}$$

Where

$\{X\}$ = 6 DOF structural displacements at each node

[M] =Total mass matrix= $[M]^{\text{Structural component}}+[M]^{\text{Added mass}}$

[C] = Damping Matrix= $[C]^{\text{Structural damping}}+[C]^{\text{Hydrodynamic damping}}$

[K] =Stiffness matrix=$[K]^{\text{Elastic}}+[K]^{\text{Geometric}}$

Total force on the spar-mooring system is denoted by $\{F(t)\}$. The dot symbolizes differentiation based on time. Total Spar-mooring mass matrix of the system comprises structural mass and added mass components. The structural mass of moored Spar is made up of elemental consistent mass matrices of the moorings and lumped mass properties of the rigid Spar hull. The lumped mass properties are assumed to be concentrated at the CG of Spar hull. The added mass of the structure occurs due to the water surrounding the entire structure. Considering the oscillation of the free surface, this effect of variable submergence is simulated as per Wheeler's approach.

Total stiffness matrix [K] of mooring lines/risers consists of two parts, the elastic stiffness matrix [K_E] as well as the geometrical stiffness matrix [K_G]. The major damping is induced due to the hydrodynamic effects. It may be obtained if the structure velocity term in Morison equation is transferred from the force vector on right hand side to the damping term on the left hand side in the governing equation of motion. The structural damping is simulated by Rayleigh damping. It follows equation (3.2) in which ξ is the structural damping ratio, Φ is modal matrix, ω_i is natural frequency and m_i is generalized mass.

$$\Phi^T [C]^{Structural} \Phi = [2\xi\omega_i m_i] \tag{3.2}$$

Morison's equation is considered to be adequate in calculating hydrodynamic forces. The wave loads on the Spar-mooring system are calculated by integrating forces along the free surface centreline at instantaneous sea water surface at the displaced position. As the diameter of the mooring line is small in comparison to the length of the wave encountered, the distortion of the waves by the structure is negligible.

3.5.2.1. Idealization for mooring line nonlinear motion equations

A complete non-linear deterministic equation for catenary mooring lines encompasses the formulation of a non-linear stiffness matrix allowing mooring line tension fluctuations due to variable buoyancy and other essential nonlinearities. Development of equations of motion of mooring line/riser considering as slender rod is summarized mainly following the work by Nordgren (1974), Garrett (1982), Paulling and Webster (1986), Ma and Webster (1994) and Chen (2002). In a 3-D Cartesian coordinate system, the instantaneous configuration of a mooring line is expressed in terms of a vector, X_r (s,t), which is a function of s, the deformed arc length along the mooring line, and time t (Figure 3.3). The vector terms t, n and b are unit vectors in tangential, normal and bi-normal directions respectively; and e_x, e_y and e_z are unit vectors in the x-, y- and z-axis respectively. The unit vectors are also termed as e_1, e_2 and e_3 for corresponding directions. If we assume that the mooring line is inextensible, the arc length s is the same in both deformed and un-deformed states. The internal state of stress at a mooring line point is described fully by resultant force and the resultant moment acting at the centreline of the mooring line.

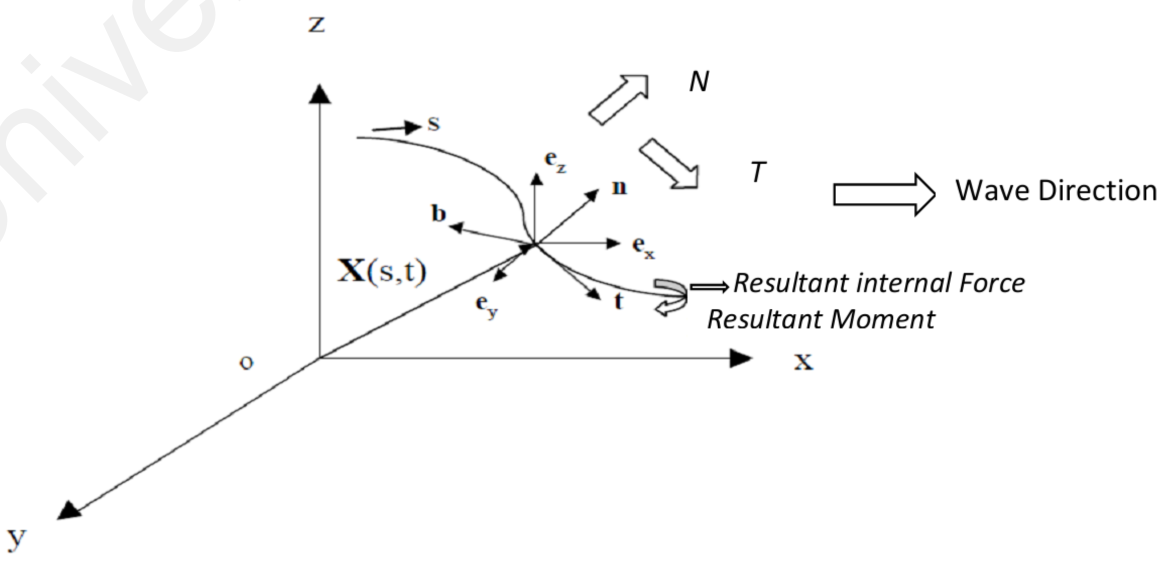

Figure 3.3: Coordinate System of mooring line

The external forces applied on a mooring line consist of hydrostatic force including gravity forces, and hydrodynamic forces. The gravity force on the mooring line leads to a distributed load given by:

$$F_{Gravity} = -\rho_t g A_t e_z \tag{3.3}$$

The hydrostatic force per unit length working on the mooring line can be written as

$$F_{Hydrostatic} = F_B + (P_{res} X_r')' \tag{3.4}$$

F_B is the buoyancy force per unit length of mooring line. P_{res} is presenting the force due to hydrostatic pressure on catenary mooring/riser (Arcandra, 2001) and can be denoted as

$$P_{res} = A_m P_m - A_i P_i \tag{3.5}$$

The hydrostatic external pressure which exists around the mooring line is P_m. In addition, P_i the internal pressure related to well head pressure. Therefore, the hydrostatic force relation for mooring line/riser comes up as following Equation (3.6). For solid cross section of mooring line, the internal pressure P_i is to be null.

$$F_{Hydrostatic} = \rho_w g A_m + ((A_m P_m - A_i P_i) X_r')' \tag{3.6}$$

The hydrodynamic forces acting on the mooring line consist of Inertia/added-mass force, drag force, and Froude-Krylov force. The Morison equation is used to predict the inertia and drag forces. The inertia force can be derived as

$$F_{Inertia} = \rho_w A_m C_{Mn} \mathbf{N} (\ddot{u} - \ddot{X}_r) + \rho_w A_m C_{Mt} \mathbf{T} (\ddot{u} - \ddot{X}_r) \tag{3.7}$$

When the motion of the structure is considered, the inertia force is reduced by a factor proportional to the structural acceleration. The terms **N** and **T** refer to the transfer matrices between the Cartesian and global coordinate systems. The drag force is reduced by the relative motion and the appropriate form of the inertia terms per unit length acting on a mooring line element, can be obtained by substituting $|\dot{u}-\dot{X}_r|(\dot{u}-\dot{X}_r)$ for $|\dot{u}|\dot{u}$, $(\ddot{u}-\ddot{X}_r)$ for $(\ddot{u})$.

$$F_{Drag} = \frac{1}{2}\rho_w D_m C_{Dn} \mathbf{N}(\dot{u}-\dot{X}_r)\left|\mathbf{N}(\dot{u}-\dot{X}_r)\right| + \frac{1}{2}\rho_w D_m C_{Dt} \mathbf{T}(\dot{u}-\dot{X}_r)\left|\mathbf{T}(\dot{u}-\dot{X}_r)\right| \quad (3.8)$$

Where, ρ_w denotes water density, C_{Mn} and C_{Mt} denote normal inertia coefficient and tangential inertia coefficient respectively. C_{Dn} and C_{Dt} symbolize normal drag coefficient and tangential drag coefficient correspondingly. $\dot{u}$ is the horizontal velocity and $\ddot{u}$ denotes the acceleration of water particle respectively associated with the wave.

Froude - Krylov force due to sea water outside the mooring line is:

$$F_w^{\,F-K} = \rho_w (g e_z + \ddot{u}) A_m + (P_w A_m X_r')' \quad (3.9)$$

Froude-Krylov force (pressure forces) caused by the fluid inside the mooring line/riser is:

$$F_i^{\,F-K} = -\rho_i g A_i e_z + (P_i A_i X_r')' \quad (3.10)$$

In the above equations, prime indicates that the derivative is being done with respect to the arc length *s* of mooring line. Associated symbols are noted as follows:

$\rho_m = \rho_t A_t + \rho_i A_i$, the mass per unit mooring line including internal fluid

N, T = transfer matrices of normal and tangential forces,

I = identity matrix

Where, the subscripts w, *i* and *t* denote the sea water, the fluid inside the tube and the tube itself. **T** and **N** are defined by:

$$\mathbf{T} = X_r'^{\,T} X_r' \quad (3.11)$$

$$\mathbf{N} = \mathbf{I} - \mathbf{T} \quad (3.12)$$

Summing up all the applied forces, the wave force F(X,Z,t) per unit length of mooring line imparting on a single mooring line of diameter D can be derived as follows:

$$F(X,Z,t) = F_{Gravity} + F_{Hydrostatic} + F_{Inertia} + F_{Drag} + F^{F-K}{}_{Sea\,water} + F^{F-K}{}_{Inside\,fluid} \qquad (3.13)$$

This implies that

$$\begin{aligned} F = & -\rho_t g A_t e_z + \rho_w A_m C_{Mn} \mathbf{N}(\ddot{u} - \ddot{X}_r) + \rho_w A_m C_{Mt} \mathbf{T}(\ddot{u} - \ddot{X}_r) \\ & + \frac{1}{2}\rho_w D_m C_{Dn} \mathbf{N}(\dot{u} - \dot{X}_r) \left| \mathbf{N}(\dot{u} - \dot{X}_r) \right| + \frac{1}{2}\rho_w D_m C_{Dt} \mathbf{T}(\dot{u} - \dot{X}_r) \left| \mathbf{T}(\dot{u} - \dot{X}_r) \right| \\ & + \rho_w (g e_z + \ddot{u}) A_m + (P_w A_m X_r')' - \rho_i g A_i e_z + (P_i A_i X_r')' \end{aligned} \qquad (3.14)$$

The Equation (3.14) can be rearranged as the succeeding relation by Equation (3.15) as well.

$$\begin{aligned} F = & (\rho_w A_m - \rho_i A_i - \rho_t A_t) g e_z + \rho_w A_m (I + C_{Mn} \mathbf{N} + C_{Mt} \mathbf{T})(\ddot{u} - \ddot{X}_r) \\ & + \frac{1}{2}\rho_w D_m C_{Dn} \mathbf{N}(\dot{u} - \dot{X}_r) \left| \mathbf{N}(\dot{u} - \dot{X}_r) \right| + \frac{1}{2}\rho_w D_m C_{Dt} \mathbf{T}(\dot{u} - \dot{X}_r) \left| \mathbf{T}(\dot{u} - \dot{X}_r) \right| \end{aligned} \qquad (3.15)$$

The values of the drag and inertia coefficients can generally be expected from dimensional reasoning to vary with the maximum water velocity $\dot{u}_{wm}$ of the wave motion and with the wave period, P through the dimensionless numbers

$$N_R = \frac{\rho_w \dot{u}_{wm} D_m}{\mu}, \qquad N_k = \frac{\dot{u}_{wm} P}{D_m} \qquad (3.16)$$

Where, ρ_w and μ denote the density and viscosity of the sea water respectively. The first term of Equation (3.16) is the Reynolds number which is representative of the effect of viscosity. The second term is the Keulegan-Carpenter number, representative of the effect of the wave period. Only limited experimental data exists on the variation of drag and inertia coefficients with both these numbers, and they are assumed as constant in usual engineering practice. The values of the drag coefficient are chosen within the range 0.6 to 1.0 and the inertia coefficient within the range of 1.5 to 2.0. The velocity $\dot{u}$ and acceleration $\ddot{u}$ in Equation (3.14) are calculated from an appropriate wave theory for the appropriate drag and inertia coefficients. As the motion of the structure is considered, there will be addition of some force exerted per unit length acting due to structural acceleration of a mooring line element equivalent to $\rho_w A_m \ddot{X}$. Hence the relation of added mass force on mooring line comes to be

$$Fm_{Added\ mass} = \rho_w A_m \ddot{X} \tag{3.17}$$

Therefore the total force acting on mooring line is

$$F(X,Z,t) = F_{Gravity} + F_{Hydrostatic} + F_{Inertia} + F_{Drag} + Fm_{Added\ mass} + F^{F-K}{}_{Sea\ water} + F^{F-K}{}_{Inside\ fluid} \tag{3.18}$$

This implies to the succeeding expression in Equation (3.19).

$$\begin{aligned} F = {} & (\rho_w A_m - \rho_i A_i - \rho_t A_t) g e_z + \rho_w A_m (I + C_{Mn}\mathbf{N} + C_{Mt}\mathbf{T})(\ddot{u} - \ddot{X}_r) \\ & + \frac{1}{2}\rho_w D_m C_{Dn} \mathbf{N}(\dot{u} - \dot{X}_r) \left| \mathbf{N}(\dot{u} - \dot{X}_r) \right| + \frac{1}{2}\rho_w D_m C_{Dt} \mathbf{T}(\dot{u} - \dot{X}_r) \left| \mathbf{T}(\dot{u} - \dot{X}_r) \right| + \rho_w A_m \ddot{X}_r \end{aligned} \tag{3.19}$$

Equation (3.19) can be re-written as

$$\begin{aligned} F = {} & (\rho_w A_m - \rho_i A_i - \rho_t A_t) g e_z + \rho_w A_m (I + C_{Mn}\mathbf{N} + C_{Mt}\mathbf{T})\ddot{u} - \rho_w (C_M - 1) A_m \ddot{X}_r \\ & + \frac{1}{2}\rho_w D_m C_{Dn} \mathbf{N}(\dot{u} - \dot{X}_r) \left| \mathbf{N}(\dot{u} - \dot{X}_r) \right| + \frac{1}{2}\rho_w D_m C_{Dt} \mathbf{T}(\dot{u} - \dot{X}_r) \left| \mathbf{T}(\dot{u} - \dot{X}_r) \right| \end{aligned} \tag{3.20}$$

The effect of the structural acceleration in the water is equivalent to increasing the mass of the structure (or unit length) by the amount, $M_a m$. This mass $M_a m$ is known as the added mass per unit length and the total mass $(M + M_a)_m$ is known as the virtual mass per unit length of the structure.

$$M_a m = \rho_w (C_M - 1) A_m \ddot{X}_r \tag{3.21}$$

In actual field, the structure experiences some sort of current in ocean environment. Considering the current velocity, u_c along with wave velocity the Equation (3.20) can be modified to become

$$\{F_m(t)\} = (\rho_w A_m - \rho_i A_i - \rho_t A_t) g e_z + \rho_w A_m (I + C_{Mn}\mathbf{N} + C_{Mt}\mathbf{T})\ddot{u} - \rho_w (C_M - 1) A_m \ddot{X}_r$$
$$+ \frac{1}{2}\rho_w D_m C_{Dn}\mathbf{N}(\dot{u} + u_c - \dot{X}_r)\left|\mathbf{N}(\dot{u} + u_c - \dot{X}_r)\right| + \frac{1}{2}\rho_w D_m C_{Dt}\mathbf{T}(\dot{u} + u_c - \dot{X}_r)\left|\mathbf{T}(\dot{u} + u_c - \dot{X}_r)\right| \tag{3.22}$$

The virtual mass matrix is simplified as:

$$[M]^{Mooring} = (\rho_t A_t + \rho_i A_i) I + \rho_w A_m C_{Mn}\mathbf{N} + \rho_w A_m C_{Mt}\mathbf{T} \tag{3.23}$$

The equation of motion for mooring line/riser can be written through the conservation of linear momentum as

$$[M]\{\ddot{X}\} = \{F_m(t)\} + \tilde{F}' \tag{3.24}$$

Here, the force $\{F_m(t)\}$ is applied force and $\tilde{F}$ is the resultant internal force per unit length of mooring line.

The conservation of moment of momentum leads to

$$\tilde{M}' + X_r' \times \tilde{F} + \hat{M} = 0 \tag{3.25}$$

Here, the force $\hat{M}$ is external/applied moment and $\tilde{M}$ is the resultant moment per unit length of mooring line. Effects of shear deformations and rotary inertia have been neglected for the above relations.

According to classical Euler-Bernoulli theory of elastic rods with equal principal stiffness, the bending component of the stress couple is proportional to the curvature κ and is directed along the binormal. Furthermore the torsional component of the stress couple is proportional to the angle of twist per unit length and is directed along the tangent.

Thus, the resultant moment $\tilde{M}$ can be written as

$$\tilde{M} = X'_r \times (EIX''_r) + HX'_r \tag{3.26}$$

And so

$$\tilde{M}' = X'_r \times (EIX''_r)' + HX'_r + HX''_r \tag{3.27}$$

The term H is the torque and EI is bending rigidity. Assuming the torque and external moment as zero, plugging the $\tilde{M}'$, the expression of moment of momentum comes to

$$X'_r \times (EIX''_r)' + X'_r \times \tilde{F} = 0 \tag{3.28}$$

That is

$$\tilde{F} = -(EIX''_r)' \tag{3.29}$$

Introducing a scalar function $\lambda(s,t)$ called Lagrangian multiplier and taking its product with X'_r to the above equation, following formula is obtained:

$$\tilde{F} = -(EIX''_r)' + \lambda X'_r \tag{3.30}$$

As the catenary mooring line is considered as inextensible, the succeeding condition is to be satisfied

$$X'_r . X'_r = 1 \tag{3.31}$$

The Lagrange multiplier λ is considered as $T - EI\kappa^2$ where EI is bending rigidity, κ is local curvature of the mooring line T is the local tension equals to $X'_r.\tilde{F}$.

Then the equation of motion becomes as

$$[M]\{\ddot{X}\} + (EIX''_r)'' - (\lambda X'_r)' = \{F_m(t)\} \tag{3.32}$$

While load is applied in mooring line, the total stiffness [K] of its own results from the summation of elastic stiffness and geometric stiffness. Elastic stiffness matrix [K_E] comes from the material characteristics of mooring line. Furthermore, damping is induced on the structural element when it is subjected to environmental loading. Hence the equation of motion is given by:

$$
\begin{aligned}
&[M]^{Mooring}\{\ddot{X}\} + (EIX_r'')'' - (\lambda X_r')' + \left(\frac{[2\xi\omega_{im}m_{im}]}{\Phi^T\Phi} + [C]^{hydrodynamic}\right)\{\dot{X}\} \\
&+ \left([K]_E^{\;Mooring} + [K]_G^{\;Mooring}\right)\{X\} \\
&= (\rho_w A_m - \rho_i A_i - \rho_t A_t) g e_z + \rho_w A_m (I + C_{Mn}\mathbf{N} + C_{Mt}\mathbf{T})\dot{u} - \rho_w (C_M - 1) A_m \ddot{X}_r \\
&\quad + \frac{1}{2}\rho_w D_m C_{Dn}\mathbf{N}(\dot{u} + u_c - \dot{X}_r)\left|\mathbf{N}(\dot{u} + u_c - \dot{X}_r)\right| + \frac{1}{2}\rho_w D_m C_{Dt}\mathbf{T}(\dot{u} + u_c - \dot{X}_r)\left|\mathbf{T}(\dot{u} + u_c - \dot{X}_r)\right|
\end{aligned}
\tag{3.35}
$$

3.5.2.2. Idealization for 6-DOF rigid Spar hull nonlinear motion equations

The rigid body motion equations with respect to the centre of gravity (CG) were derived earlier in Paulling and Webster (1986); Lee (1995) and the addition with modification is stated in subsequent write up. Two coordinate systems are employed in the derivation of motion equations of a floating rigid body. Coordinate system *oˆxˆyˆzˆ* is a space-fixed coordinate system, while *oxyz* is the platform-fixed coordinate system moving with the Spar. The origin *o* can be the centre of gravity (*g*) or any point fixed on the body. The platform-fixed coordinate *oxyz* coincides with *oˆxˆyˆzˆ* when the body is at its initial position (Figure 3.4). A third set of coordinates *OXYZ* which is a spaced-fixed coordinate system with the *OXY* plan lying on the free surface and *Z*-axis positive upward is also introduced as a reference coordinate system. Incoming waves are given in this space-fixed reference coordinate system.

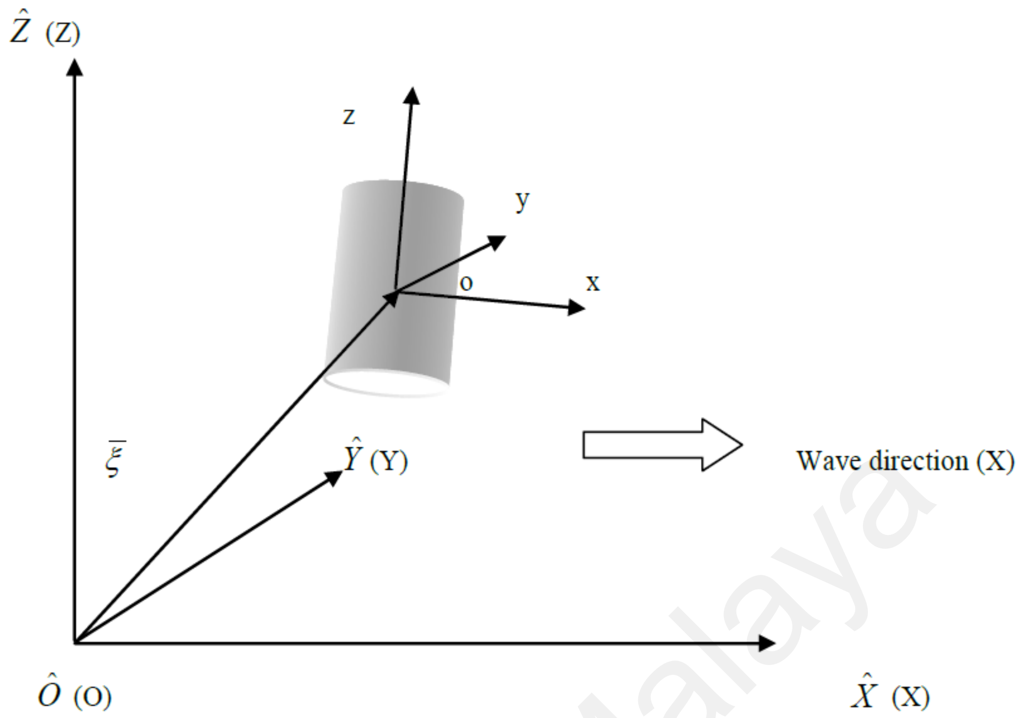

Figure 3.4: Coordinate system for rigid spar hull

The external forces applied on a spar hull involve the hydrostatic forces comprising gravity forces, and hydrodynamic forces.

The nonlinear hydrostatic restoring force on the spar hull (Chen, 2002) leads to a distributed load given by:

$$F_{Hydrostatic_n} = -\rho_w g A_W e_{zs} + \rho_w g A_W d_{CG} \frac{\theta^2}{2} + K x_s \tag{3.36}$$

In the above equation e_{zs}, θ, d_{CG}, A_W, K and x_s denotes the heave motion, pitch angle, depth from mean sea level to CG of Spar, water plane area, hydrostatic stiffness matrix and surge motion respectively. Total ocean environmental loads on an offshore structure can be divided into three major parts according to their origins which are denoted by the subscripts. The forces are exerted from wave, current and wind loads. The hydrodynamic forces acting on the spar hull consist of Inertia/added-mass force and drag force. The hull of a classical spar is virtually a cylinder. In using the Morison equation to compute wave and current loads, the normal force per unit length on a cylinder of uniform diameter D_s can be estimated. Morison equation is used to predict the inertia and drag force. When the motion of the structure is considered, the inertia force is reduced by a factor proportional to the platform acceleration and so the inertia force comes to

$$Fs_{Inertia} = \rho_w A_s C_M (\ddot{u} - \ddot{X}_s) \tag{3.37}$$

The form of this last term for added mass is derived from fluid mechanics and represents the force associated with water acceleration from the structure motion. It is especially important in the dynamic analysis of off-shore structures, where the inertia of the members is considered.

The drag force acting on a spar hull element, can be obtained by substituting $|\dot{u} - \dot{X}_s|(\dot{u} - \dot{X}_s)$ for $|\dot{u}|\dot{u}$, $(\ddot{u} - \ddot{X}_s)$ for $(\ddot{u})$.

$$Fs_{Drag} = \frac{1}{2}\rho_w D_s C_D (\dot{u} - \dot{X}_s)\left|(\dot{u} - \dot{X}_s)\right| \tag{3.38}$$

Where, C_M is inertia coefficient and C_D symbolizes drag coefficient. The force is considered with the related vector in the direction normal to the cylinder axis. Water particle velocity and acceleration are the superposition of those of currents and waves.

In order to account for Vortex Induced Motion (VIM) of a spar in the presence of strong currents, such as loop currents in the Gulf of Mexico, an additional term representing the lifting force (or transverse force) applied on per unit length on the cylinder is added into the Morison equation.

$$F_l = \frac{1}{2}\rho_w C_L D_s v_c^{\,2} \cos(2\pi\, f.t)\vec{e}_t \times \vec{e}_c \tag{3.39}$$

Where $\vec{e}_t$ and $\vec{e}_c$ are the unit vectors in the axial direction and the current direction correspondingly, C_L the lifting coefficient, and f the vortex shedding frequency. It is related to the Strouhal Number, S_o, defined by

$$S_o = \frac{fD_s}{v_n} \tag{3.40}$$

The Strouhal number and lifting coefficients in the context of a spar equipped with helical strakes on its surface and constrained by its mooring/riser systems are not well documented. In the computation, they are calibrated by fitting the mean, and the average 1/3rd and 1/5th amplitude and period of the simulated LF sway of a spar model. The selected values of these coefficients are fitted as S_o= 0.25 and C_L= 0.45.

3.5.2.3. Wave force deterministic description

The information on wave motion like water particles kinematics and wave speed, using the input information of wave height, its period and depth of water at the sea condition are designated by wave theories. Several wave theories exist to define water particle kinematics have different degrees of complexity and altitudes of acceptance in offshore structural community (Chakrabarti, 2005). However, a few of the wave theories are commonly used such as linear or Airy wave theory, Stokes second and other higher order theories, Stream-Function and Cnoidal wave theories (Dean and Dalrymple, 1991). All the described wave theories involve several common assumptions:

- The waves have regular profiles.
- The flow is two-dimensional.
- The wave propagation is unidirectional.
- The fluid is ideal i.e. inviscid, incompressible and irrotational.
- The sea bed is impermeable and horizontal.

In this study, Airy's linear wave theory (Sarpkaya and Isaacson, 1981) and Stokes fifth order wave theory (Nishimura et al., 1977) have been incorporated.

3.5.2.3.1. Airy's wave theory

In Airy's sinusoidal wave train, it is considered that the velocity potential is dependent on the wave particle position and time. The approach is a linearized wave theory based on irrotational flow of an inviscid incompressible fluid. In the wave train, the linearization is attained considering the wave height as small compared to the wavelength as well as the mean still water depth. It is also assumed that the fluid is of uniform depth (that is, the bottom is smooth). The wave height, H is selected as the vertical distance from trough to crest. Accordingly the wave amplitude, a is half of the wave height H. Additionally, the wave length, L is the distance between successive crests, the wave period P is the time interval between successive crests passing a particular point and the wave speed or celerity, $\breve{c}$ is the speed of the wave travelling through the fluid ($\breve{c}$ = L/P). Two serious difficulties arise in the attempt to obtain an exact solution for a two-dimensional wave train. The first is that the free surface boundary conditions are non-linear, and the second is that these conditions are prescribed at the free surface Z=(z+d) which is initially unidentified. The simplest and most fundamental approach is to seek a linear solution of the problem by taking the wave height H to be much smaller than both the wave length, L and the mean still water depth, d; that is H << L, d.

The velocity potential for Airy wave is given by

$$\phi = \frac{\omega \mathrm{H}}{2}\frac{\cosh(\mathrm{k}(z+d))}{\sinh(\mathrm{kd})}\cos(\mathrm{k}X - \omega \mathrm{t}) \tag{3.41}$$

The surface elevation of an Airy wave of amplitude a=H/2, at any time instant t and horizontal location x along the wave direction, $\breve{\eta}(x,t)$ is represented by:

$$\breve{\eta}(x,t) = \frac{H}{2}\cos(kX - \omega t) \tag{3.42}$$

The wave angular frequency ω = 2π/P and the wave number k = 2π/L. Thus the celerity, or speed, of the wave, $\breve{c} = \frac{L}{P} = \frac{\omega}{k} = \frac{gP}{2\pi}\tanh(kd)$.

The along wave horizontal, $\dot{\mathrm{u}}(x,t)$ and vertical water particle velocity, $\dot{\mathrm{v}}(x,t)$ at position *z* measured from the MWL in water depth d are given as:

$$\dot{\mathrm{u}} = \frac{\omega \mathrm{H}}{2}\frac{\cosh(\mathrm{k}(z+d))}{\sinh(\mathrm{kd})}\cos(\mathrm{k}\,X - \omega\,\mathrm{t}) \tag{3.43}$$

$$\dot{\mathrm{v}} = \frac{\omega \mathrm{H}}{2}\frac{\sinh(\mathrm{k}(z+d))}{\sinh(\mathrm{kd})}\sin(\mathrm{k}\,X - \omega\,\mathrm{t}) \tag{3.44}$$

Where,

X	=	point of evaluation of water particle kinematics from the origin in the horizontal direction
t	=	time instant in sec at which water particle kinematics is evaluated

The dispersion expression relates wave number k to circular frequency ω (as these are not independent), via:

$$\omega^2 = gk\tanh(kd) \tag{3.45}$$

As the wave amplitude is considered quite small in comparison to water depth h, for the deep water conditions, kh >π, the modified velocity potential can be approximated to:

$$\phi^{(1)} = \frac{\omega \mathrm{H}}{2}e^{kz}\cos(\mathrm{k}\,X - \omega\,\mathrm{t}) \tag{3.46}$$

Hence, the velocities and accelerations are computed as:

$$\dot{u} = \frac{\omega H}{2} e^{kz} \cos(kX - \omega t) \tag{3.47}$$

$$\dot{v} = \frac{\omega H}{2} e^{kz} \sin(kX - \omega t) \tag{3.48}$$

$$\omega^2 = gk \tag{3.49}$$

$$\ddot{u} = \frac{\omega^2 H}{2} e^{z} \sin(kX - \omega t) \tag{3.50}$$

$$\ddot{v} = -\frac{\omega^2 H}{2} e^{z} \cos(kX - \omega t) \tag{3.51}$$

The above relationships indicate that the elliptical orbits of the water particles produced by the general Airy wave through Equations (3.43) and (3.44), would reduce to circular orbits in deep water environments defined at Equations (3.47) and (3.48).

3.5.2.3.2. Stoke’s Fifth order Wave theory

Nonlinear Stokes wave train assumes that an infinite series of plane, uniform waves travels through the fluid in the positive X-direction. The z-coordinate is chosen to be positive in the vertical direction, so the gravity potential is G=g(d+z) where z is the distance above mean MWL. The fluid is treated as inviscid and incompressible. The pressure at the surface is assumed to be negligible. The flow potential has been approximated by perturbation parameters which increase with the wave amplitude. After substituting the high order perturbation expansions into the governing relations and manipulating the equations, the desired solution is yielded. Fenton (1985) derived a contemporary presentation of Stokes theory, recalling terms to fifth order. As such, the fifth order Stokes theory is popular due to its better prediction of the actual water particle kinematics. The progression followed in the fifth order theory to attain the values of particle kinematics gives the flow potential as below:

$$\phi^{(5)} = \frac{\bar{c}}{k}\sum_{n=1}^{5}\breve{D}_n \cosh(nk(d+z))\sin(n\theta) \tag{3.52}$$

For uniform waves of wavelength L and period P, the solution as a function of X and t duly appears in terms of a phase angle θ as:

$$\theta = 2\pi(\frac{X}{L} - \frac{t}{P} + \frac{\alpha}{360}) = \frac{2\pi}{L}(X - \bar{c}t + \frac{L\alpha}{360}) \tag{3.53}$$

Where $\bar{c} = \frac{L}{P}$ is the wave celerity and can be re-written as:

$$\bar{c} = \frac{g}{k}\tanh(kd)[1 + \breve{C}_1\breve{\lambda}^2 + \breve{C}_2\breve{\lambda}^4] \tag{3.54}$$

Where,

$$\tanh(kd)[1 + \breve{C}_1\breve{\lambda}^2 + \breve{C}_2\breve{\lambda}^4] = \frac{4\pi^2}{gkP^2} \tag{3.55}$$

The terms $\breve{D}_1$ ~ $\breve{D}_5$ can be obtained through empirical relations. The along wave horizontal velocity, $\dot{u}(x,t)$ and vertical velocity, $\dot{v}(x,t)$ at the position *z* elevated MWL in the water depth d are given as:

$$\dot{u} = \bar{c}\sum_{n=1}^{5} n\breve{D}_n \cosh(nk(d+z))\cos(n\theta) \tag{3.56}$$

$$\dot{v} = \bar{c}\sum_{n=1}^{5} n\breve{D}_n \sinh(nk(d+z))\sin(n\theta) \tag{3.57}$$

The fluid particle accelerations of the Stokes fifth order wave field can be approximated as:

$$\ddot{u} = \bar{c}\omega\sum_{n=1}^{5} n^2 \breve{D}_n \cosh(nk(d+z))\sin(n\theta) \tag{3.58}$$

$$\ddot{v} = \bar{c}\omega\sum_{n=1}^{5} n^2 \breve{D}_n \sinh(nk(d+z))\cos(n\theta) \tag{3.59}$$

In addition, the surface elevation of a Stokes fifth order wave of amplitude a=H/2, at horizontal position x in the direction of travel of the wave for any instant of time t, $\breve{\eta}(x,t)$ is signified by:

$$\breve{\eta} = \frac{1}{k}\sum_{n=1}^{5} \breve{E}_n \cos(n\theta) \tag{3.60}$$

The parameters $\breve{E}_{1\sim5}$ are computed from empirical relations. In the Stokes wave train the velocity, acceleration, and dynamic pressure at spatial locations for each time extent are defined by the wave field. The wave parameters and dynamic pressure are determined by using the instantaneous (for geometrically nonlinear analysis) or reference (for geometrically linear analysis) position of the structure at current time in the proper equations. Furthermore, the time incorporated in the wave field equations is the entire time for solution, which accumulates over all static and dynamic steps in the analysis.

Forces applied on the truncated bottom of a cylinder in the axial direction include the integration of wave pressure over the bottom, S_B and drag and added-mass forces which are equivalent to one half of a thin circular disk of the same diameter of the cylinder in heave motion (Sarpkaya and Isaacson, 1981).

The force acting on the Spar hull bottom is

$$F_a = \rho_w \iint_{S_B} \left(\frac{\partial(\phi^{(n)})}{\partial t}\right) n_t \, ds + C_{mt}\rho_w \frac{4}{3}\left(\frac{D_s}{2}\right)^3 \left[\ddot{u}_t - \ddot{X}_t\right] + \frac{1}{2}\rho_w C_{Dt} A_s (\dot{u}_t - \dot{X}_t)\left[(\dot{u}_t - \dot{X}_t)\right] \tag{3.61}$$

Where $\phi^{(n)}$ is the velocity potential of incident waves, C_{mt} and C_{Dt} are added-mass and drag coefficients of the truncated cylinder bottom, respectively. $(\dot{u}_t - \dot{X}_t)$ and $\left[\ddot{u}_t - \ddot{X}_t\right]$ are the relative velocity and acceleration of the cylinder bottom to ambient fluid in the axial direction, respectively.

The basic model in the present study is based on the Airy's wave theory and hence the velocity potential $\phi^{(n)}$ is $\phi^{(1)}$. For the special case where the Stokes fifth order wave theory has been used, the velocity potential takes the parameter $\phi^{(5)}$.

Considering that the diameter of a spar, the velocities of currents and waves may change along its axis, the total wave and current loads on the spar are computed through the numerical integration of the corresponding loads over a number of segments along its longitudinal axis. Obviously, the force F(X,Z,t) per unit length of spar hull cylinder of diameter D_s can be derived as follows:

$$F(X,Z,t) = F_{Hydrostatic_n} + Fs_{Inertia} + Fs_{Drag} + F_{Axial} + F_{Lifting} \tag{3.62}$$

However, the spar-mooring system contains a significant portion of superstructure such as the top side which caters to offloading, operation and maintenance activities. This superstructure portion is subjected to the aerodynamic loading namely wind force. Such wind-induced forces can alter the nonlinear response behaviour of floating moored spar. Therefore, it is imperative that the wind loading action be precisely interpreted. The succeeding section discusses the formulation of wind loading on the spar platform.

3.5.2.4. Formulation of Aerodynamic force

The dynamic force working on floating moored spar platform is caused by aerodynamic and hydrodynamic loading. Though the environmental loads are from Wind load, Wave load and Earthquake load, usually the design of ocean structures is dominantly affected by hydrodynamic wave loads. However, the aerodynamic wind loading is a vital design consideration as it may alter the response behaviour of floating structure. Hydrodynamic load comprises Inertia, Drag, Froude - Krylov force, Axial force as well as Lifting force from wave and current which was derived earlier. The wind loading acts on the exposed part of the platform facing the wind that supports the topside. The force consists of mean and fluctuating wind components. In addition to the wave loads, codes indicate the critical two portions of wind loadings: 1) One minute sustained wind speeds combined with extreme waves and 2) Three seconds gust wind speeds. While the ratio of elevation to the smallest horizontal dimension of structure is larger than 5 (five), the dynamic effects of the wind are to be taken into account according to API -RP2A (2000).

In deep water environment, wind is an important source of dynamic loading. On top of wave –induced loading, the mean and fluctuating wind forces may alter the structural responses in substantial fashion. In reality, severe wind in ocean may occasionally cause significant damage than the customary hydrodynamic loading. In the present study, suitable mean wind speed acting on the moored spar is considered. Besides, API RP 2A (API-RP2A, 2000) and Emil Simiu (Simiu and Leigh, 1984) sea-site fluctuating wind spectra have been employed, which are exclusively generated for compliant offshore structure installations. Exposed portion of the platform (Li and Kareem, 1990) is imperilled to the drag force due to wind velocity normal to the floating platform. Henceforth, the basic relation for wind-induced loading on the moored spar is specified as the drag force per unit projected area in the plane normal to the wind force. Such computation of wind force acting on the floating structures at deep ocean is based on the following empirical formula recommended by API -RP2A (2000).

$$f(x,z,t) = 0.5\rho_a C_p(x,z)[U_w(z) + U_{W_G}(t,z) - \dot{x}(t)]^2 \quad (3.63)$$

The term C_p is sea drag coefficient. It is quantified in terms of roughness length and Karman constant as well as shape effect. Fluctuating wind velocity component $U_{W_G}(t,z)$ is specified through single point simulation anticipated by wind spectrum. The wind spectrum has maximum ordinate at low frequencies (Simiu and Leigh, 1984). In several studies, formulation along with aerodynamic force response computation have been described (Ahmad and Ahmad, 1999; Kareem, 1985; Li and Kareem, 1990; Vickery, 1982) for different structures. Estimated total aerodynamic force on the moored spar $F_{wind}(x,z,t)$ is thus arranged as the subsequent expression. Total force is computed as per the projected area of its wind action. A_p is the projected area of spar and topside above sea level.

$$F_{wind}(x,z,t) = \int_{A_p} f(x,z,t)\,dxdz \quad (3.64)$$

3.5.2.4.1. Wind speed and Wind Spectrum

On the offshore structure, the mean speed is generally treated as a steady load (Chakrabarti, 2005). In case of a fixed platform, only the mean speed is considered as the effect of the fluctuation of wind about the mean value has little effect on the structure. Conversely, for a floating structure, the wind effect may be noteworthy and should not be overlooked. Even the mean wind flowing over a changing free surface produces a fluctuating load caused by the variation of the exposed structural portion with the wave. For a linear wave, this fluctuation may be determined by a simple straightforward fashion if the exposed surface is supposed to vary sinusoidally. Subsequent section discusses the mean wind speed and the fluctuations about this mean value along with its possible impact on a floating Spar-mooring system.

3.5.2.4.2. Wind Speed

To analyse the moored Spar, the presumed steady wind speeds are estimated as the average velocity occurring at a period of 1-h extent. A reference height as customarily 10 m above the MWL is chosen for quantifying the mean wind speed. Based on the marginal distribution of the occurring wind velocities at the exact location, design progression uses a mean wind speed obtained for a 100-year return period. In the evaluation of structural excursions, the directionality of the wind is of utmost importance in several applications.

In addition, a portion of aerodynamic loading with a time-varying wind component named as the gust wind speed is computed, which produces low-frequency motion to the moored Spar. This fluctuating wind component is defined by a wind gust spectrum. Values of sustained wind speeds and gust wind speeds are obtained from meteorological records or from recommendations made by certifying authorities in the offshore area of interest. The main concern in calculating wind loads is the estimation of extreme wind speed with 50–year or 100–year return period, denoted as U_{50W} or U_{100W}. The estimation procedure is same as estimation for extreme significant wave height except for the extrapolation. The extrapolation is made to the probability corresponding to a given return period for wind duration of 1–hour, giving:

$$[P(U_W)]_{T_r} = 1 - \frac{1}{24 \times 365 \times T_r} \tag{3.65}$$

3.5.2.4.3. Wind Spectrum

Similar to the random waves, the wind blowing on the superstructure over mean still sea level is also random formulating a mean speed overlaid on it. There are a number of wind spectrum models available in literature. In the present study, the derivation of the wind frequency spectrum have been adopted according to the guiding principle of API-RP2A (2000). However, the technique implemented here is supposed to be functional for any practical frequency spectrum of wind (Ochi and Shin, 1988). The estimation simplified in Equation (3.64) is referred to a standard height above mean still water level (MWL). However, the mean profile for the wind speed average over 1–hour at elevation z can be approximated by API-RP2A (1993). The variation of wind speed with the superstructure elevation is estimated following the subsequent expression:

$$U_w(1h, z) = U_w(1h, z_R).\left(\frac{z}{z_R}\right)^{0.125} \tag{3.66}$$

In accordance with the API-RP2A (2000), the wind frequency spectrum for 1-h mean value is given in the succeeding equation.

$$S(f) = \frac{(\sigma_w(z))^2}{f_p[1 + 1.5 f / f_p]^{5/3}} \tag{3.67}$$

It is pertinent to mention that several ideals of peak frequency of the spectrum may be considered. The recommended range of f_p is indicated as in Equation (3.68). Generally, $f_p coeff$ in the expression is taken as 0.025.

$$0.01 \leq f_p coeff = \frac{f_p.z}{U_w(1h, z)} \leq 0.10 \tag{3.68}$$

The fluctuating wind velocity named as gust wind speed is quantified as the average speed of wind over a time interval of 3 seconds measured at the reference elevation above MWL. The same 50–year or 100–year return period gust wind speed can be stipulated for the design of individual structural elements. Adjustments for elevation above MWL are given by the following relation (Patel, 1989).

$$U_{W_G}(t,z) = U_{W_G}(t,z_R)(\frac{z}{z_R})^{0.100} \tag{3.69}$$

The gust wind speed, denoted as $U_{W_G}(t,z)$ which depends on gust factor, $G(t,z)$ can be defined as API-RP2A (1993):

$$G(t,z) \equiv \frac{U_{W_G}(t,z)}{U_W(1h,z)} = 1 + g(t)\, I(z) \tag{3.70}$$

To determine the gust wind speed, above relationship can be simplified as

$$U_{W_G}(t,z) = U_W(1h,z)(1 + g(t)\, I(z)) \tag{3.71}$$

Where, $I(z)$ is the turbulence intensity described below and t is gust duration with units of seconds. The factor $g(t)$ can be calculated from API-RP2A (1993):

$$g(t) = 3.0 + \ln\{(3/t)^{0.6}\} \quad \text{for} \quad t \le 60 \text{ seconds} \tag{3.72}$$

The standard deviation of the projected wind speed is specified by

$$\sigma_w(z) = \left| \begin{array}{l} U_w(1h,z) \times 0.15(\frac{z}{z_s})^{-0.125} \quad if \;\; z \le z_s \\ U_w(1h,z) \times 0.15(\frac{z}{z_s})^{-0.275} \quad if \;\; z > z_s \end{array} \right. \tag{3.73}$$

Where, z_s is the thickness of the "surface layer" and is taken as 20 m.

The turbulence intensity can be approximated by API-RP2A (1993):

$$I(z) = \frac{\sigma_w(z)}{U_w(1h,z)} = \left| \begin{array}{l} 0.15(\frac{z}{z_s})^{-0.125} \quad if \;\; z \le z_s \\ 0.15(\frac{z}{z_s})^{-0.275} \quad if \;\; z > z_s \end{array} \right. \tag{3.74}$$

Following the aforementioned expressions, a wind spectrum model is revealed. The density spectrum of wind speed is incorporated to be consistent with the one shown in Chakrabarti (2005) and Tahar & Kim (2003). On the other hand the Simu spectrum has been incorporated following the considerations by Simiu & Leigh (1984) and Islam et al. (2009a). In contrast with the wave spectrum, estimated wind spectrum is very wide-banded. The high frequency part of the spectrum is trivial for floating platform analysis.

Nevertheless, floating structures are susceptible to low frequency part of the wind spectrum for which the moored spar experiences a slow drift oscillation.

3.5.2.4.4. Spar dynamic response induced by wind

The Spar platform system requires the consideration of service-ability and survivability in deep sea under inconsistent wind environment. The response failure in extreme conditions and the provision of adequate fatigue life of mooring system necessitate a realistic prediction (Ahmad, 1996) of the stresses, displacements and rotational excursions under fluctuating wind field induced loading. As in the present study all the major nonlinearities are taken care of, statistical characteristics get modified. Evaluation of structural characteristics can be achieved by extensive simulation studies where the response time histories are generated for accurate consideration of fluctuating wind spectrum. The wave behaviour is dependent on the occurring wind loading in the offshore environment. According to the range of wind speed, wave height and wave period the sea state can be classified as shown in Table 3.1.

Table 3.1: Classification of Sea states (Chakrabarti, 2005)

Description of sea	**Wind speed range (m/sec)**		**Significant wave height range (m)**		**Wave period range**	
Small Wavelets	2.57	5.14	0.1	0.43	0.5	5
Large wavelets	5.14	7.2	0.43	0.91	1	7.5
Small waves	7.2	9.25	0.91	1.83	1.4	8.8
Small to moderate waves	9.25	9.77	1.83	2.13	2.5	10.6
Moderate waves	9.77	12.34	2.13	3.96	2.8	13.5
Large waves	12.34	15.42	3.96	6.71	3.8	15.5
Moderate gale	15.42	20.56	6.71	13.72	4.7	21
Strong gale	20.56	28.27	13.72	21.34	6.5	25
Hurricane type storm	28.27	35.98	21.34	35.06	10	30

3.5.2.5. Comprehensive dynamic force on Spar

Including the effect of aerodynamic wind loading, the total force F(X,Z,t) per unit length of spar hull cylinder of diameter D_s can be derived as follows.

$$F(X,Z,t) = F_{Hydrostatic_n} + Fs_{Inertia} + Fs_{Drag} + F_{Axial} + F_{Lifting} + F_{wind} \quad (3.75)$$

Which denotes the relation as

$$\begin{aligned}
F &= -\rho_w g A_W e_{zs} + \rho_w g A_W d_{CG}\frac{\theta^2}{2} + Kx + \rho_w A_s C_M(\ddot{u} - \ddot{X}_s) \\
&+ \rho_w A_s \ddot{X}_s + \frac{1}{2}\rho_w D_s C_D(\dot{u} - \dot{X}_s)\left|(\dot{u} - \dot{X}_s)\right| \\
&+ \frac{1}{2}\rho_w C_L D_s v_c^{\ 2}\cos(2\pi\ f.t)\vec{e}_t \times \vec{e}_c \\
&+ \rho_w \iint_{S_B}\left(\frac{\partial(\phi^{(n)})}{\partial t}\right)n_t ds + C_{mt}\rho_w\frac{4}{3}\left(\frac{D_s}{2}\right)^3\left[\ddot{u}_t - \ddot{X}_t\right] + \frac{1}{2}\rho_w C_{Dt} A_s(\dot{u}_t - \dot{X}_t)\left[(\dot{u}_t - \dot{X}_t)\right] \\
&+ 0.5\rho_a C_p(x,z)[U_w(z) + U_{W_G}(t,z) - \dot{x}(t)]^2
\end{aligned} \quad (3.76)$$

As the motion of the structure is considered, there will be addition of some force exerted per unit to length acting due to structural acceleration of a spar hull element equivalent to $\rho_w A_s \ddot{X}_s$. Such relation of added mass force on the Spar hull is

$$F_{Added\,mas} = \rho_w A_s \ddot{X}_s \quad (3.77)$$

Taking into account the foregoing modification by adding this term, the Equation (3.75) modifies to the total force acting on the spar hull as

$$F(X,Z,t) = F_{Hydrostatic_n} + Fs_{Inertia} + Fs_{Drag} + Fs_{Added\,mass} + F_{Axial} + F_{Lifting} + F_{wind} \quad (3.78)$$

This implies that

$$
\begin{aligned}
F &= -\rho_w g A_W e_{zs} + \rho_w g A_W d_{CG} \frac{\theta^2}{2} + Kx + \rho_w A_s C_M (\ddot{u} - \ddot{X}_s) \\
&+ \rho_w A_s \ddot{X}_s + \frac{1}{2}\rho_w D_s C_D (\dot{u} - \dot{X}_s)\left|(\dot{u} - \dot{X}_s)\right| \\
&+ \frac{1}{2}\rho_w C_L D_s v_c{}^2 \cos(2\pi\, f.t)\vec{e}_t \times \vec{e}_c \\
&+ \rho_w \iint_{S_B} (\frac{\partial(\phi^{(n)})}{\partial t}) n_t ds + C_{mt}\rho_w \frac{4}{3}\left(\frac{D_s}{2}\right)^3 \left[\ddot{u}_t - \ddot{X}_t\right] + \frac{1}{2}\rho_w C_{Dt} A_s (\dot{u}_t - \dot{X}_t)\left[(\dot{u}_t - \dot{X}_t)\right] \\
&+ 0.5\rho_a C_p (x,z)[U_w(z) + U_{W_G}(t,z) - \dot{x}(t)]^2
\end{aligned}
\tag{3.79}
$$

The effect of the structural acceleration in the water is equivalent to increasing the mass of the structure (or unit length) by the amount M_as which signifies added mass for unit length of the floating platform. Furthermore, the total mass, $(M + M_a)_s$ is known as the virtual mass per unit length.

$$
\mathrm{M_a s} = \rho_w (C_M - 1) A_s \ddot{X}_s \tag{3.80}
$$

It is worth noting that the structure experiences current motion in the actual ocean environment. Considering the current velocity, u_c along with wave velocity, the equation for spar hull becomes:

$$
\begin{aligned}
&[Ms + M_a s]\{\ddot{X}\} + (\frac{[2\xi\omega_{is} m_{is}]}{\Phi^T \Phi} + [C]^{hydrodynamic})\{\dot{X}\} \\
&= -\rho_w g A_W e_{zs} + \rho_w g A_W d_{CG} \frac{\theta^2}{2} + \rho_w A_s C_M (\ddot{u} - \ddot{X}_s) \\
&+ \rho_w A_s \ddot{X}_s + \frac{1}{2}\rho_w D_s C_D (\dot{u} + u_c - \dot{X}_s)\left|(\dot{u} + u_c - \dot{X}_s)\right| \\
&+ \frac{1}{2}\rho_w C_L D_s v_c{}^2 \cos(2\pi\, f.t)\vec{e}_t \times \vec{e}_c \\
&+ \rho_w \iint_{S_B} (\frac{\partial(\phi^{(n)})}{\partial t}) n_t ds + C_{mt}\rho_w \frac{4}{3}\left(\frac{D_s}{2}\right)^3 \left[\ddot{u}_t - \ddot{X}_t\right] \\
&+ \frac{1}{2}\rho_w C_{Dt} A_s (\dot{u}_t + u_c - \dot{X}_t)\left[(\dot{u}_t + u_c - \dot{X}_t)\right] \\
&+ 0.5\rho_a C_p (x,z)[U_w(z) + U_{W_G}(t,z) - \dot{x}(t)]^2
\end{aligned}
\tag{3.81}
$$

3.5.3. Discretization of equations of motion

For a deformable body, the shape and dimensions of the body are changeable. This criterion has been followed for mooring line formulation. The element is characterized as hybrid beam element. The hybrid beam elements used in this study are designed to handle very slender situations, where the axial stiffness of the beam is very large in comparison to the bending stiffness; and so a mixed method, where axial force is treated as an independent unknown, is considered. For such hybrid elements, in which the axial (and transverse) forces are treated as independent degrees of freedom, can be beneficial. Distributed pressure loads applied to beams (for example, due to wind or current) will rotate with the beam, leading to follower force effects.

The large-strain formulation in these elements allows axial strains of arbitrary magnitude; but quadratic terms in the nominal torsional strain are neglected compared to unity, and the axial strain is assumed to be small in the calculation of the torsional shear strain. The radius of curvature of the beam θ is assumed as large in comparison to the distances in the cross-section: the beam cannot fold into a tight hinge. The response of open sections is strongly affected by warping, when material particles move out of the plane of the section along lines parallel to the beam axis so as to minimize the shearing between lines along the wall of the section and along the beam axis. The beam element formulation includes provision for such effects. Moreover, basically a rigid body can only translate and rotate. Therefore, the Spar hull is treated as rigid beam element. Virtual work principal is incorporated to discretise the equations of motion.

3.5.4. Virtual work principal for discretization

Virtual work on a practical system is the mechanical work occasioning from either virtual forces inducing via a real displacement or the real forces imparting through a virtual displacement. The virtual displacements are infinitesimal alteration in the location coordinates of a structural system in such a way that the constraints remain undisturbed. The term displacement may refer to a translation or a rotation. and the term force refers to either a force or a moment. While the virtual measures are independent variables, they are also arbitrary. The arbitrary quantity is an essential characteristic which enables to draw imperative suppositions from mathematical relations.

- The virtual work principle states that at equilibrium the strain energy change due to a small virtual displacement is equal to the work done by the forces in moving through the virtual displacement.
- A virtual displacement is a small imaginary change in configuration that is also an admissible displacement.
- An admissible displacement satisfies kinematic boundary conditions.
- Neither loads nor stresses are altered by the virtual displacement.

The principle of virtual Work is derived from the potential energy function by assuming that a virtual displacement, u′, is applied to an existing equilibrium state of displacement, u. According to this notion, the sum of works of the internal (stored strain energy) and external forces (applied force) done by virtual displacements is zero. In equation form this is written as

$$\delta W^{I} + \delta W^{E} = 0 \tag{3.82}$$

The principle is extremely useful in discretising finite element equations (Reddy, 2002). The equilibrium equations are not used. Only the strain energy and work for the system need to be calculated. The stiffness matrix will come from the expression in strain energy and the applied force vectors from the expression for the work done.

3.5.4.1. Virtual work approach for applied forces in static equilibrium

A system of particles, i, is considered in static equilibrium. In the system, the total force on each particle, $F_i^{(T)}$, equals to zero. Summing the works applied by the force on each particle through an arbitrary virtual displacement, δr_i, of the system leads to the expression for the virtual work by Equation (3.83). Since the forces are zero, the summation of work done must be zero:

$$\delta W = \int_L (F_i^{(T)}.\delta r_i) dL = 0 \tag{3.83}$$

The imaginative vector equation might be improved by identifying that the work expression essentially holds for arbitrary virtual displacements. Sorting out the forces into applied forces, F_i, and constraint forces, C_i, (Bruce, 1984), the above expression yields a modified relation as below.

$$\delta W = \int_L (F_i.\delta r_i + C_i.\delta r_i) dL = 0 \tag{3.84}$$

If the arbitrary virtual displacements are considered in orthogonal direction to the constraint forces, the constraint forces do no work. These types of displacements are treated to be consistent with the constraints. Hence, the formulation of the principle of virtual work is yielded for applied forces stating evidently that forces functioning to a static system do no virtual work (Bruce, 1984) as in Equation (3.85). A corresponding principle for accelerating systems called D'Alembert's principle has a similar foundation, which forms a theoretical basis for Lagrangian mechanics.

$$\delta W = \int_L (F_i.\delta r_i) dL = 0 \tag{3.85}$$

3.5.4.2. Virtual work principle for deformable CML

The free body diagram of a deformable catenary mooring line is considered, which is composed of a number of differential cubes. Two unrelated states for the deformable body are defined as:

- σ-State: This shows external surface forces Q, body forces f, and internal stresses σ in equilibrium.
- ε-State: This shows continuous displacements u^* and consistent strains ε^*.

The superscript * highlights that the two states are disparate. If it is assumed that forces and stresses in the σ-State cause the displacements and deformations in the ε -State, total virtual (imaginary) work done by all forces acting on the faces can be expected as:

$$\int_S u^{*T} Q dS + \int_V u^{*T} f dV = \int_V \varepsilon^{*T} \sigma dV \tag{3.86}$$

The right-hand-side of the differential equation (3.86) is habitually called the internal virtual work. The above expression establishes the principle of virtual work: "External virtual work is equal to internal virtual work when equilibrated forces and stresses undergo unrelated but consistent displacements and strains". The statement comprises the principle of virtual work for rigid bodies as an exceptional case in which the internal virtual work is zero. The expression can be shown from the above derivation that

$$\int_S u\,.\,Q dS + \int_V u\,.\, f dV = \int_V \varepsilon\,.\,\sigma dV \tag{3.87}$$

3.5.4.2.1. External virtual work done

The external virtual work of deformable mooring line, CML considering hybrid beam element can be written as

$$\delta W^E = \int_L \{F(t)\}\delta u dL = \int_L \{F_{Gravity} + F_{Hydrostatic} + F_{Inertia} + F_{Drag} + Fm_{Added\ mass} + F^{F-K}{}_{Sea\ water} + F^{F-K}{}_{Inside\ fluid}\}\delta u dL$$

$$= \int_L \left\{ \begin{aligned} &(\rho_w A_m - \rho_i A_i - \rho_t A_t) g e_z + \rho_w A_m (I + C_{Mn} N + C_{Mt} T)\ddot{u} - \rho_w (C_M - 1) A_m \ddot{X}_r \\ &+ \frac{1}{2}\rho_w D C_{Dn} N(\dot{u} + u_c - \dot{X}_r)\left|N(\dot{u} + u_c - \dot{X}_r)\right| + \frac{1}{2}\rho_w D C_{Dt} T(\dot{u} + u_c - \dot{X}_r)\left|T(\dot{u} + u_c - \dot{X}_r)\right| \end{aligned} \right\} \delta u dL \tag{3.88}$$

Let introduce in dW^E the interpolation-based approximation,

$$u(x) \approx \tilde{u}(x) = \langle n(x) \rangle \{D\} \tag{3.89}$$

For a *n*-elements & *n+1*-node mesh

$$\langle D\rangle=\langle U_1 \quad U_2 \quad U_3 \quad \ldots \quad U_n \quad U_{n+1}\rangle$$
$$\langle n(x)\rangle=\langle n_1(x) \quad n_2(x) \quad n_3(x) \quad \ldots \quad n_n(x) \quad n_{n+1}(x)\rangle$$

At this point, choosing $du = n_i(x)$ $(i=1, 2, 3, \ldots, n, n+1)$

$$\delta W^E = \int_L \begin{Bmatrix} \{(\rho_w A_m - \rho_i A_i - \rho_t A_t)ge_z + \rho_w A_m (I + C_{Mn}\mathbf{N} + C_{Mt}\mathbf{T})\ddot{u} - \rho_w (C_m - 1)A_m \ddot{X}_r \\ +\frac{1}{2}\rho_w DC_{Dn}\mathbf{N}(\dot{u}+u_c-\dot{X}_r)\left|\mathbf{N}(\dot{u}+u_c-\dot{X}_r)\right| + \frac{1}{2}\rho_w DC_{Dt}\mathbf{T}(\dot{u}+u_c-\dot{X}_r)\left|\mathbf{T}(\dot{u}+u_c-\dot{X}_r)\right| \end{Bmatrix} n_i(x)dL \tag{3.90}$$

3.5.4.2.2. Internal virtual work done

In the sea environment the flexible mooring line linking at spar fairlead and sea bed poses the internal virtual work as Equation (3.104). δW_1^I is the internal virtual work done due to axial and bending behaviour. N is the axial force variable acting on mooring line. *M1*, *M2*, *M3* are bending moment, warping moment and twisting moment respectively employed on catenary mooring line.

$$\delta W_1^I = \int_L (N\delta\varepsilon + M_1\delta\theta_1 + M_2\delta\theta_2 + M_3\delta e_1)dL \tag{3.91}$$

ε denotes axial strain. This can also be called Green's strain of beam axis. θ_1, θ_2 are describing beam curvature measures due to M_1 and M_2 respectively. Torsional strain due to Torsional moment M_3 is expressed in term of e_1.

Alternatively, an independent axial force variable $\tilde{N}$ can be introduced.

$$\delta W_2^I = \int_L (\tilde{N}\varepsilon + M_1\delta\theta_1 + M_2\delta\theta_2 + M_3\delta e_1 + \delta\lambda(N - \tilde{N})dL \tag{3.92}$$

Where $\delta\lambda$ is a Lagrange multiplier introduced to impose the constraint $N=\tilde{N}$. A linear combination of these expressions is

$$\delta W^I{}_C = \rho\delta W_1^I + (1-\rho)\delta W_2^I \tag{3.93}$$

ρ is a parameter that denotes the ratio of combining internal virtual works. Substituting the terrms of Equations (3.91) and (3.92) in Equation(3.93), the new form of Equation (3.94) comes to

$$\delta W^{I}{}_{C} = \int_L \left[(\rho N + (1-\rho)\tilde{N})\delta\varepsilon + M_1 \delta\theta_1 + M_2 \delta\theta_2 + M_3 \delta e_1 + (1-\rho)\delta\lambda (N - \tilde{N}) \right] dL \quad (3.94)$$

So the equation of virtual work approach from Equation (3.82) leads to

$$\int_L \left[(\rho N + (1-\rho)\tilde{N})\delta\varepsilon + M_1 \delta\theta_1 + M_2 \delta\theta_2 + M_3 \delta e_1 + (1-\rho)\delta\lambda (N - \tilde{N}) \right] dL$$
$$+ \int_L \begin{matrix} \{(\rho_w A_m - \rho_i A_i - \rho_t A_t) g e_z + \rho_w A_m (I + C_{Mn} N + C_{Mt} T)\ddot{u} - \rho_w (C_m - 1) A_m \ddot{X} \\ + \frac{1}{2}\rho_w D C_{Dn} N(\dot{u} + u_c - \dot{X}) \left| N(\dot{u} + u_c - \dot{X}) \right| + \frac{1}{2}\rho_w D C_{Dt} T(\dot{u} + u_c - \dot{X}) \left| T(\dot{u} + u_c - \dot{X}) \right| \end{matrix} \} dL = 0$$

(3.95)

The contribution of the left side term to the Newton scheme is computed as

$$\int_L \left[(\rho N + (1-\rho)\tilde{N})\delta\varepsilon + dM_1 \delta\theta_1 + dM_2 \delta\theta_2 + dM_3 \delta e_1 + (1-\rho)\delta\lambda (dN - d\tilde{N}) + \bar{N}\delta\varepsilon + M_1 d\delta\theta_1 + M_2 d\delta\theta_2 + M_3 d\delta e_1 \right] dL$$
$$= -\int_L \left[\bar{N}\delta\varepsilon + M_1 \delta\theta_1 + M_2 \delta\theta_2 + M_3 \delta e_1 + (1-\rho)\delta\lambda (N - \tilde{N}) \right] dL$$

(3.96)

where

$$\bar{N} = \rho N + (1-\rho)\tilde{N} \quad (3.97)$$

The tangent stiffness of the section behaviour gives

$$\begin{Bmatrix} d\tilde{N} \\ dM_1 \\ dM_2 \\ dM_3 \end{Bmatrix} = \begin{bmatrix} A_{00} & A_{01} & A_{02} & A_{03} \\ & A_{11} & A_{12} & A_{13} \\ sym & & A_{22} & A_{23} \\ & & & A_{33} \end{bmatrix} \begin{Bmatrix} d\varepsilon \\ d\theta_1 \\ d\theta_2 \\ de_1 \end{Bmatrix} \quad (3.98)$$

It is assumed that an inverse of the first relation of Equation (3.98) defines $d\varepsilon$ from $d\tilde{N}$:

$$d\varepsilon = \frac{1}{A_{00}} (d\tilde{N} - A_{01} d\theta_1 - A_{02} d\theta_2 - A_{03} de_1) \quad (3.99)$$

and so

$$dM_1 = (A_{11} - \frac{A^2{}_{01}}{A_{00}}) d\theta_1 + (A_{12} - \frac{A_{01}A_{02}}{A_{00}}) d\theta_2 + (A_{13} - \frac{A_{01}A_{03}}{A_{00}}) de_1 + \frac{A_{01}}{A_{00}} d\tilde{N} \quad (3.100)$$

$$dM_2 = (A_{12} - \frac{A_{01}A_{02}}{A_{00}}) d\theta_1 + (A_{22} - \frac{A_{02}A_{02}}{A_{00}}) d\theta_2 + (A_{23} - \frac{A_{02}A_{03}}{A_{00}}) de_1 + \frac{A_{02}}{A_{00}} d\tilde{N} \quad (3.101)$$

$$dM_3 = (A_{13} - \frac{A_{01}A_{03}}{A_{00}})d\theta_1 + (A_{23} - \frac{A_{02}A_{03}}{A_{00}})d\theta_2 + (A_{33} - \frac{A_{03}A_{03}}{A_{00}})de_1 + \frac{A_{03}}{A_{00}}d\tilde{N} \qquad (3.102)$$

Now using the first tangent section stiffness multiplied by ρ and the second multiplied by *1-ρ*, the Newton contribution of the element becomes

$$\int_L \lfloor \delta\varepsilon\delta\theta_1\delta\theta_2\delta e_1 A_{00}\delta\lambda \rfloor [\bar{A}] \begin{Bmatrix} d\varepsilon \\ d\theta_1 \\ d\theta_2 \\ de_1 \\ d\tilde{N} \end{Bmatrix} dL + \int_L (\tilde{N}d\delta\varepsilon + M_1 d\delta\theta_1 + M_2 d\delta\theta_2 + M_3 d\delta e_1)dL \qquad (3.103)$$

$$= \int_L \left[\tilde{N}d\varepsilon + M_1\delta\theta_1 + M_2\delta\theta_2 + M_3\delta e_1 + A_{00}\delta\lambda(1-\rho)(\frac{N-\tilde{N}}{A_{00}}) \right] dL$$

Where

$$[\bar{A}] = \begin{bmatrix} \rho A_{00} & \rho A_{01} & \rho A_{02} & \rho A_{03} & 1-\rho \\ & A_{11} - (1-\rho)\frac{A^2{}_{00}}{A_{00}} & A_{12} - (1-\rho)\frac{A_{01}A_{02}}{A_{00}} & A_{13} - (1-\rho)\frac{A_{01}A_{03}}{A_{00}} & (1-\rho)\frac{A_{01}}{A_{00}} \\ & & A_{22} - (1-\rho)\frac{A^2{}_{02}}{A_{00}} & A_{23} - (1-\rho)\frac{A_{02}A_{03}}{A_{00}} & (1-\rho)\frac{A_{02}}{A_{00}} \\ & symm & & A_{33} - (1-\rho)\frac{A^2{}_{03}}{A_{00}} & (1-\rho)\frac{A_{03}}{A_{00}} \\ & & & & -(1-\rho)\frac{1}{A_{00}} \end{bmatrix} \qquad (3.104)$$

The variable $\tilde{N}$ is taken as an independent value at each integration point in the element. We choose ρ as $\tilde{\rho}/A_{00}$, where $\tilde{\rho}$ is a small value. With this choice, by ensuring that the variables $\tilde{N}$ are eliminated after the displacement variables of each element, the Gaussian elimination scheme has no difficulty in solving the equations. In the mixed elements that allow transverse shear, the transverse shear constraints are imposed by treating the shear forces as independent variables. But since the catenary mooring line is itself a cable, the effect of transverse shear is insignificant. Likewise, the internal virtual work associated with transverse shear is treated as negligible.

3.5.4.3. Virtual work principle for rigid spar hull

The spar hull in the present study is treated as a rigid body which obviously follows the basic concept of virtual work approach for a rigid body. For applied forces acting on individual particles of the cylindrical hull, the principle can be generalized. If the rigid hull exists in equilibrium state inducing virtual compatible displacements, the total virtual work of all external forces is zero. This is in conformity with the fact that for a rigid body there is no internal virtual work.

3.5.4.3.1. External virtual work done

The external virtual work of the rigid beam element 'Spar hull" subjected to the external forces induced by sea environment can be written as

$$\delta W^{E} = \int_{L} \{F(t)\} dL = \int_{L} \{F_{Hydrostatic\,n} + Fn_{Inertia} + Fn_{Drag} + Fs_{Added\,mass} + F_{Axial} + F_{Lifting} + F_{wind}\} \delta u dL$$

$$= \int_{L} \left\{ \begin{array}{l} -\rho_w g A_W e_{zs} + \rho_w g A_W d_{CG} \dfrac{\theta^2}{2} + \rho_w A_s C_M (\ddot{u} - \ddot{X}_s) \\ + \rho_w A_s \ddot{X}_s + \dfrac{1}{2} \rho_w D_s C_D (\dot{u} + u_c - \dot{X}_s) \left| (\dot{u} + u_c - \dot{X}_s) \right| \\ + \dfrac{1}{2} \rho_w C_L D_s v_c{}^2 \cos(2\pi\, f.t) \vec{e}_t \times \vec{e}_c \\ + \rho_w \iint\limits_{S_B} \left(\dfrac{\partial(\phi^{(n)})}{\partial t}\right) n_t ds + C_{mt} \rho_w \dfrac{4}{3} \left(\dfrac{D_s}{2}\right)^3 \left[\ddot{u}_t - \ddot{X}_t\right] \\ + \dfrac{1}{2} \rho_w C_{Dt} A_s (\dot{u}_t + u_c - \dot{X}_t) \left[(\dot{u}_t + u_c - \dot{X}_t) \right] \\ + \dfrac{1}{2} C_s \rho_a V_a{}^2 A_p \end{array} \right\} n_i(x) dL \qquad (3.105)$$

3.5.4.3.2. Internal virtual work done

In reality, the Spar hull is totally rigid internally as the structural component is triggered. Consequently, inside this rigid member no internal forces will be endangered. Hence, the internal virtual work of the cylindrical spar hull is transcribed as:

$$\delta W^{I} = 0 \qquad (3.106)$$

3.5.4.4. Boundary conditions

The deformable mooring line is linked at rigid spar fairlead at the topmost end and anchored with sea bed at the remote end. Detail contributions of applied boundary conditions on the system by means of these connections are discretised in the subsequent section.

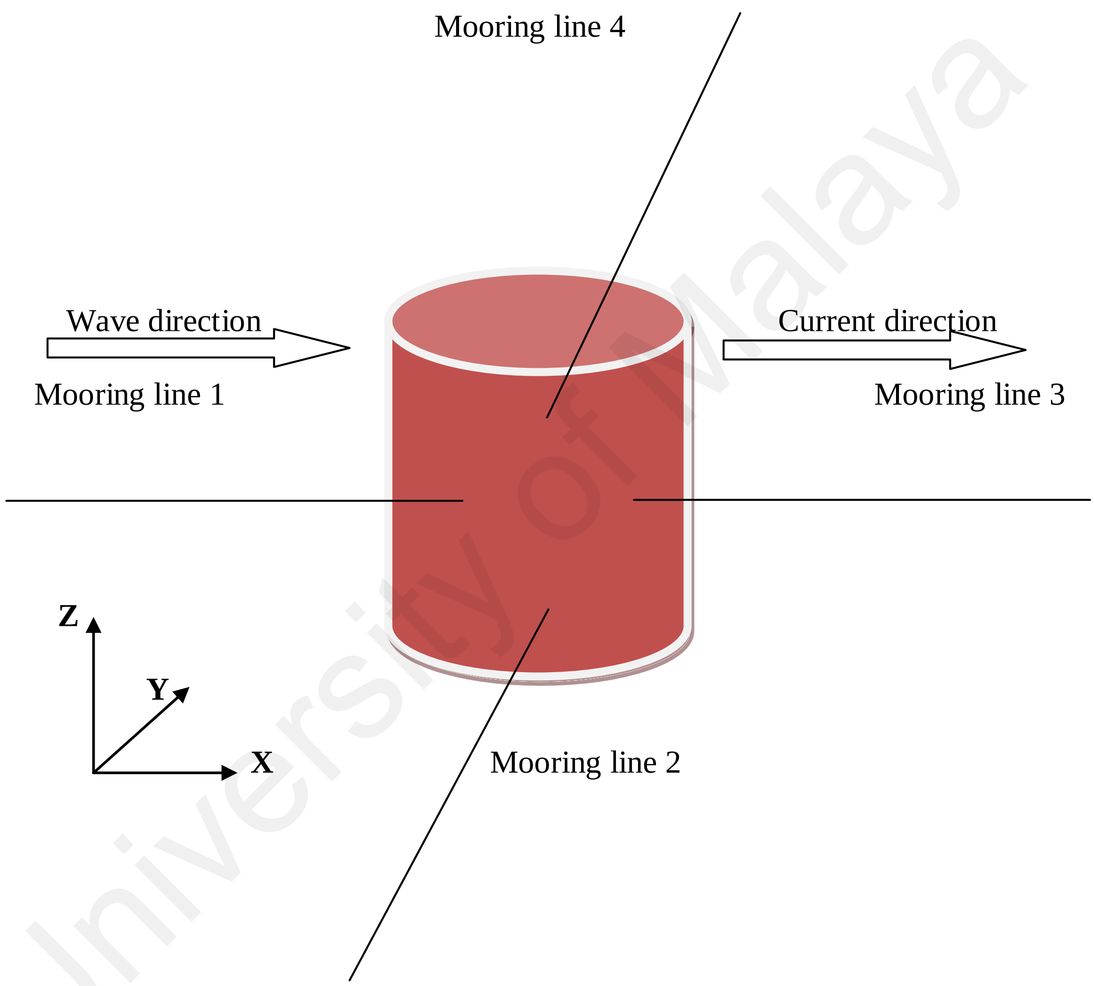

Figure 3.5: Mooring system arrangement

3.5.4.4.1. Spar hull –mooring line connection

The catenary mooring line is associated to the spar hull fairlead by means of spring. This linking allows the spar-mooring hinge connection. The boundary conditions between two adjacent elements as per the connection assemblage can be expressed as the relation in Equation (3.107).

$$^{(n)}u_{3n} = {}^{(n+1)}u_n$$

$$^{(n)}u_{4n} / L^{(n)} = {}^{(n+1)}u_{2n} / L^{(n+1)}$$

$$^{(n)}\tilde{\lambda}_3 \neq {}^{(n+1)}\tilde{\lambda}_1 \qquad (3.107)$$

In the above expressions $L^{(n)}$ and $L^{(n+1)}$ are the corresponding length of (n) and (n+1)-th elements. In identical fashion, f_n is force of respective n-th element. Henceforward the connection gives the following constraints as in Equation (3.108).

$$^{(n)}f_3 + {}^{(n+1)}f_1 = 0$$

$$^{(n)}f_4 = 0 \qquad (3.108)$$

$$^{(n+1)}f_2 = 0$$

3.5.4.4.2. Sea bed –mooring line connection and friction

The sea bed has been modelled as rigid surface to allow surface to surface contact with catenary mooring line. The Surface-to-surface contact discretization contemplates the shape of both the slave (mooring line) and master surface (sea bed) in the expanse of contact constraints. The direction of contact is based on an average normal of the slave surface around a slave node. For the sea bed-CML contact, the sliding and frictional interaction behaviours are important aspects in computing the projected contact forces and shears. This category of contact collaborations can be defined through the principle of virtual work by the succeeding equilibrium equation:

$$\int_{\Omega} \sigma.\delta\varepsilon dv + \oint_{S} \tau.\delta\|u\| ds = \int_{\Omega} f.\delta u dv + \oint_{\partial\Omega} \tau.\delta u ds \qquad (3.109)$$

Above equation incorporates $\|u\|$ as displacement jump surrounded by the surfaces. The sea bed surface normal direction n satisfy the restraints as $\|u\|.n \geq 0$. The virtual work concomitant with the surface interaction is described by $\oint_{S} \tau.\delta\|u\| ds$. The terminology of surface interaction $\delta\Gamma_{con}$ is customarily labelled in the local coordinate system through front tangential and surface normal at front. This can be expressed as:

$$\delta\Gamma_{con} = \oint_{\bar{S}} \tilde{\tau}.\delta\Delta d\bar{s} \tag{3.110}$$

At the above relation, $\delta\Delta$ is the opening translation along the normal and two sliding directions. The symbol $\tilde{\tau}$ is the surface traction in the local coordinate system. Application of the Gauss quadrature to the Equation (3.110) brings out below expression.

$$\delta\Gamma_{con} = \sum_{l} s_l d\tau_l \delta\Delta_l \tag{3.111}$$

The symbol s_l describes surface area accompanying with the contact integration point *l*. The traction force τ_l is related to the displacement jumps Δ_l which comprise mutually the contact reaction force as well as the frictional force. This relation is derived by:

$$\tau_l = \begin{bmatrix} -\breve{K}_1 & 0 & 0 \\ \mu\breve{K}_1 & \breve{K}_2 & 0 \\ \mu\breve{K}_1 & 0 & \breve{K}_3 \end{bmatrix} \begin{bmatrix} \Delta_{l,1} \\ \Delta_{l,2} \\ \Delta_{l,3} \end{bmatrix} \tag{3.112}$$

Where the penalty stiffness K_1 reaches to zero when $\Delta_{l,1}$ greater than or equals critical penetration translation around the surface. Moreover, K_2 *or* K_3 values down to zero if $\Delta_{l,2}$ or $\Delta_{l,3} \geq$ the critical elastic slip Δ_{cr} after which the contact surfaces commences sliding. The coefficient μ denotes itself as Coulomb friction parameter. For smooth surface friction resistance is ignored and $\mu\breve{K}_1$ comes to null. Hence, for a zero friction coefficient, no shear forces will grow and the contact surfaces are unrestricted to slide.

In the Coulomb friction model, frictional resistance is defined as a function of contact pressure and equivalent slip rate. Elementary idea of Coulomb friction model is to relate the maximum allowable frictional (shear) force surrounding an interface to contact pressure between sea bed and mooring line. Here, two contacting surfaces are able to transmit shear stresses up to an assured extent before they start sliding each other. This shear transmitting state is recognized as sticking. The critical shear stress is τ_{cr}, at which the sliding of two adjacent surfaces begins as a fraction of contact pressure, $\breve{P}$, between them and its value is proportional to contact pressure as $\tau_{cr} = \mu\breve{P}$. The transition time of a point from sticking to slipping or from slipping to sticking is determined by stick/slip calculations. As mooring line is a node-based slave surface, contact pressure equals to normal contact force divided by cross-sectional area at contact node.

3.5.4.5. Numerical Application

The integrated action of Spar hull and the mooring line induces the coupled behaviour of the system in proper fashion. The coupling phenomena treated in static and dynamic problem have been described meticulously in the following section.

3.5.4.5.1. Static coupling solution

The static problem of the coupled spar-mooring system is solved using Newton's method. The static equation for the moored Spar hull is:

$$K_{Hydrostatic}\, x(t) = F_{Steady} + F_{Hydrostatic_n} + F_{Mooring} \tag{3.113}$$

$K_{Hydrostatic}$ is the hydrostatic stiffness and $F_{Hydrostatic_n}$ is the hydrostatic nonlinear force. The terminology F_{Steady} is the steady forces functioning on the rigid hull comprising the inertia and drag force through Morison equation including added mass. The force on mooring line $F_{Mooring}$ is captured in the coupled action in consistent manner. Incorporating Newton's method, the expressions lead to:

$$x = x^0 + \delta x \tag{3.114}$$

$$(K_{Hydrostatic} + \frac{\partial F_{Hydrostatic_n}}{\partial x} + \frac{\partial F_{Mooring}}{\partial x})\delta x = F_{Steady} + F^{0}{}_{Hydrostatic_n} + F^{0}{}_{Mooring} - K_{Hydrostatic} x^{0} \tag{3.115}$$

Sequential procedure for the coupled dynamic solution is given as:

Step 1: The static problem of mooring line system is solved at initial position of the Spar fairlead, pretension or anchor point. Then $\frac{\partial F_{Mooring}}{\partial x}$ is computed in initial location.

Step 2: The terms $\frac{\partial F_{Hydrostatic_n}}{\partial x}$, $F^{0}{}_{Hydrostatic_n}$ an $F^{0}{}_{Mooring}$, is computed at x^{0} position solving the Equation (3.115) where the x is updated by Equation (3.116).

Step 3: The increment is checked. When δx is contains a reasonable increment next step is employed. But for small δx value Step 2 it to be followed again.

Step 4: $\frac{\partial F_{Mooring}}{\partial x}$ is updated at the static equilibrium position of the coupled Spar. It is usable for solution of dynamic coupling problem.

3.5.4.5.2. Dynamic coupling solution

The dynamic problem of the coupled spar-mooring system is solved using Newton's method. The motion equation for the moored Spar hull is:

$$\begin{aligned}&[M + M_a]\{\ddot{X}\} + (\frac{[2\xi\omega_i m_i]}{\Phi^T\Phi} + [C]^{hydrodynamic})\{\dot{X}\} + ([K]_E{}^{Mooring} + [K]_G{}^{Mooring})\{X\} \\ &= F_{Hydrostatic_n} + Fs_{Inertia} + Fs_{Drag} + F_{Added\ mass} + F_{Axial} + F_{Lifting} + F_{wind} + F_{Mooring}\end{aligned} \tag{3.116}$$

This 6-DOF nonlinear equation of coupled platform is supposed to be expressed in the forms as:

$$\hat{M}\ddot{x}(t) + \hat{C}\dot{x}(t) + Kx(t) = \hat{F}(t) + F_M(t) \tag{3.117}$$

Where $F_M(t)$ signify mooring system forces and $\hat{F}(t)$ represent all other forces. If k is the time step as $t = k\Delta t$. Hence, the equation of motion can be re- written by

$$\hat{M}^{(k)}\ddot{x}^{(k)} + \hat{C}^{(k)}\dot{x}^{(k)} + K^{(k)}x^{(k)} = \hat{F}^{(k)} + F_M^{(k)} \tag{3.118}$$

For each individual element, the mooring line dynamic equation is given by

$$\gamma_{ikm}M_{njm}^{(k)}\ddot{u}_{kj}^{(k)} + \alpha_{ikm}B_m u_{kn}^{(k)} + \beta_{ikm}\hat{\lambda}_m^{(k)}u_{kn}^{(k)} = \mu_{im}^{(k)}\hat{f}_{mn}^{(k)} + f_{in}^{(k)} \tag{3.119}$$

It is to be mentioned that $F_M^{(k)}$ in Equation (3.118) and $f_{in}^{(k)}$ in Equation (3.119) are related through the boundary conditions shown earlier. In a coupled dynamic analysis the motion equations for the hull and dynamic equations for mooring lines are solved simultaneously using Newmark-β method which is stated as following.

Step 1: At t=0 (or time step k=0), given a coupled system of the mooring system and the hull, $u^{(0)}$, $\lambda^{(0)}$ and $x^{(0)}$ are solved in the corresponding static problem. Given initial conditions $\dot{u}^{(0)}$ and $\dot{x}^{(0)}$, $\ddot{u}^{(0)}$ for the mooring lines is solved from Equation (3.90). When a dynamic analysis starts from a static equilibrium position, $\ddot{u}^{(0)} = 0$. For the Spar hull at t=0 given initial conditions $\dot{x}^{(0)} = \dot{x}_0$, $x^{(0)} = x_0$, $\ddot{x}^{(0)}$ are solved using Equation (3.118), in which the forces given by the mooring system are calculated after solving equation (3.119).

Step 2: At time step K (>0), the predictor, $x^{(k)}$, $\dot{x}^{(k)}$ and $\ddot{x}^{(k)}$ for motions of the hull are specified as:

$$\begin{aligned}
\ddot{x}^{(k)} &= \ddot{x}^{(k-1)} \\
x^{(k)} &= x^{(k-1)} + \Delta t\dot{x}^{(k-1)} + \Delta t^2(\frac{1}{2} - \beta)\ddot{x}^{(k-1)} + \Delta t^2\beta\ddot{x}^{(k)} \\
\dot{x}^{(k)} &= \dot{x}^{(k-1)} + \Delta t(1-\gamma)\ddot{x}^{(k-1)} + \Delta t^2\gamma\ddot{x}^{(k)}
\end{aligned} \tag{3.120}$$

And in identical manner, the predictors $u^{(k)}, \dot{u}^{(k)}$, $\ddot{u}^{(k)}$ and $\hat{\lambda}^{(k)}$ for CML can be described as:

$$
\begin{aligned}
&\ddot{u}^{(k)} = \ddot{u}^{(k-1)} \\
&u^{(k)} = u^{(k-1)} + \Delta t \dot{u}^{(k-1)} + \Delta t^2 (\frac{1}{2} - \beta)\ddot{u}^{(k-1)} + \Delta t^2 \beta \ddot{u}^{(k)} \\
&\dot{u}^{(k)} = \dot{u}^{(k-1)} + \Delta t (1-\gamma)\ddot{u}^{(k-1)} + \Delta t^2 \gamma \ddot{u}^{(k)} \\
&\hat{\lambda}^{(k)} = \hat{\lambda}^{(k-1)}
\end{aligned}
\tag{3.121}
$$

Step 3: At time step k, the coefficients at both sides of Equation (3.122) for the hull are computed using $x^{(k)}, \dot{x}^{(k)}$, $\ddot{x}^{(k)}$ and the coefficients of Equation for the mooring lines are computed using $u^{(k)}, \dot{u}^{(k)}$ and $\ddot{u}^{(k)}$. The subsequent equations for the hull and mooring lines are needed to solve $\delta x^{(k)}$, $\delta u^{(k)}$ and $\delta\hat{\lambda}^{(k)}$ for the rigid spar:

$$
\left[-\frac{\partial F}{\partial x} - \frac{\partial F_M}{\partial x} + \frac{1}{\Delta t^2 \beta}\hat{M} + \frac{\gamma}{\Delta t \beta}\hat{C} + K \right] \delta x^{(k)} = \hat{F}^{(k)} + F_M^{(k)} - \hat{M}\ddot{x}^{(k)} - \hat{C}\dot{x}^{(k)} - Kx^{(k)} \tag{3.122}
$$

For catenary mooring lines of small elongation:

$$
\begin{aligned}
&\frac{\gamma_{ikm}}{\Delta t^2 \beta} M_{njm}{}^{(k)} \delta u_{kj}{}^{(k)} + (\alpha_{ikm} B_m + \beta_{ikm} \hat{\lambda}_m{}^{(k)}) \delta u_{kn}{}^{(k)} + \beta_{ikm} u_{kn}{}^{(k)} \delta \hat{\lambda}_m{}^{(k)} \\
&= \mu_{im}{}^{(k)} \hat{f}_{mn}{}^{(k)} + f_{in}{}^{(k)} - \gamma_{ikm} M_{njm}{}^{(k)} \ddot{u}_{kj}{}^{(k)} - \alpha_{ikm} B_m u_{kn}{}^{(k)} - \beta_{ikm} \hat{\lambda}_m{}^{(k)} u_{kn}{}^{(k)}
\end{aligned}
\tag{3.123}
$$

$$
\begin{aligned}
&\beta_{ikm} u_{in}{}^{(k)} \delta u_{kn}{}^{(k)} - (\eta_{lm} + \tilde{\gamma}_{jlm} \varepsilon_j{}^{(k)}) \left\{ \frac{\delta \hat{\lambda}^{(k)}}{EA} + (\rho_m A_m - \rho_i A_i) \frac{\delta y^{(k)}}{EA} \right\} \Bigg|_l \\
&= \frac{1}{2} (\tau_m + 2\eta_{lm} \varepsilon_l{}^{(k)} + \tilde{\gamma}_{jlm} \varepsilon_j{}^{(k)} \varepsilon_l{}^{(k)} - \beta_{ikm} u_{in}{}^{(k)} u_{kn}{}^{(k)})
\end{aligned}
\tag{3.124}
$$

The equations for elements are grouped into global equations for each mooring line. $F_M^{(k)}$ and $f_{in}{}^{(k)}$ are related through the boundary conditions as mentioned earlier. To solve the above equations, it is assumed that $\delta x^{(k)} = 0$. The dynamic equations for each mooring line are solved applying the boundary conditions to obtain $\delta u^{(k)}$, $\delta\hat{\lambda}^{(k)}$ and $f_{in}{}^{(k)}$ at Spar fairlead. After attaining $F_M^{(k)}$ based on $f_{in}{}^{(k)}$ at each fairlead, the Equation (3.122) is solved for $\delta x^{(k)}$. Up to the state where the difference of $\delta x^{(k)}$ in two successive iterations is small, further iteration is required within this step.

Step 4: The correctors of $x^{(k)}, \dot{x}^{(k)}$ and $\ddot{x}^{(k)}$ are estimated as

$$
\begin{aligned}
x^{(k)} &= x^{(k)} + \delta x^{(k)} \\
\dot{x}^{(k)} &= \dot{x}^{(k)} + \frac{\gamma}{\Delta t \beta}\delta x^{(k)} \\
\ddot{x}^{(k)} &= \ddot{x}^{(k)} + \frac{1}{\Delta t^2 \beta}\delta x^{(k)}
\end{aligned}
\tag{3.125}
$$

And the expressions for $u^{(k)}, \dot{u}^{(k)}$, $\ddot{u}^{(k)}$ and $\hat{\lambda}^{(k)}$ are as

$$
\begin{aligned}
u^{(k)} &= u^{(k)} + \delta u^{(k)} \\
\dot{u}^{(k)} &= \dot{u}^{(k)} + \frac{\gamma}{\Delta t \beta}\delta u^{(k)} \\
\ddot{u}^{(k)} &= \ddot{u}^{(k)} + \frac{1}{\Delta t^2 \beta}\delta u^{(k)} \\
\hat{\lambda}^{(k)} &= \hat{\lambda}^{(k)} + \delta\hat{\lambda}^{(k)}
\end{aligned}
\tag{3.126}
$$

Up to the parameters $\delta x^{(k)}$, $\delta u^{(k)}$ and $\delta\hat{\lambda}^{(k)}$ are small enough, iteration is to be done through Step 3 and then follow again for $k+1$ the Step 2 onward.

3.6 Finite element model

The analysis of Spar platform considering actual physical coupling between the rigid vertical floating cylinder and mooring lines is possible using finite element method. In actual field problems hydrodynamic loads due to wave and currents act simultaneously on Spar platform and mooring lines. In FE model, the entire structure acts as a continuum. This model can handle all nonlinearities, loading and boundary conditions. Commercial finite element code ABAQUS/ AQUA is found to be suitable for the present study. Its module AQUA appropriately models an off-shore environment. It is capable of simulating the hydrodynamic and aerodynamic loading appropriately. The equations of motion are solved using the FE code. The FE code has the capability of modelling slender and rigid bodies with accurate boundary conditions, counting fluid inertia and viscous drag. Figure 3.5 shows the arrangement of CMLs with Spar hull. Hybrid beam element is used to model the mooring lines. The element is designated in

FE code as B31H. It is hybrid because it employs two shape functions, one for simulating elastic behaviour and another to model the axial tension to maintain the catenary shape of mooring. Target catenary shape of an individual mooring line is displayed in Figure 3.6. Hybrid beam element is selected for easy convergence, but other elements such as linear or nonlinear truss elements can also be considered.

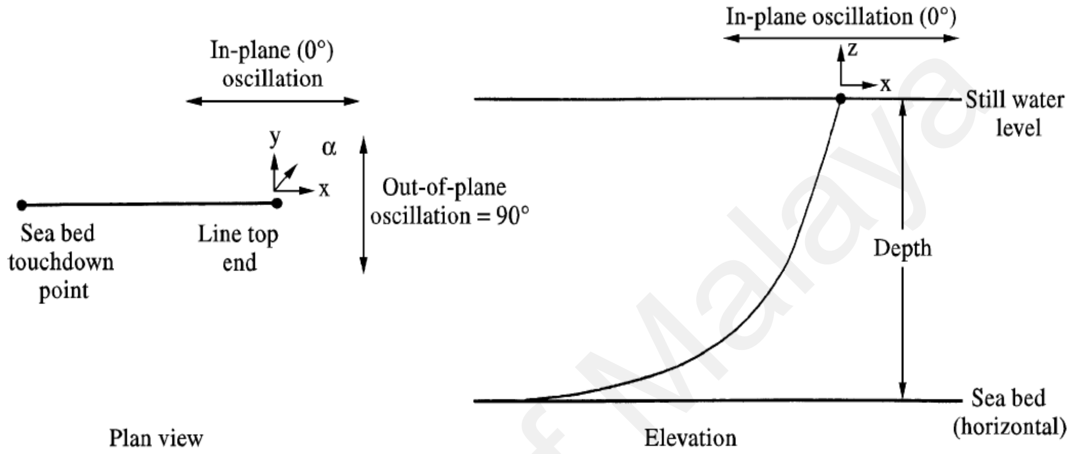

Figure 3.6: Catenary mooring line outline at operational state

The Spar cylinder is simulated by rigid beam element connecting its centre of gravity, riser reaction points and mooring line fair leads. The component in the FEM model is named as RB3D2 element. Rigid Spar platform is connected to the elastic mooring lines by six springs (Three for translation and three for rotation). The stiffness of translation springs is very high, whereas the stiffness of rotational springs is very low, simulating a hinge connection. Seabed is modelled as a rigid plate. The contact between CMLs and seabed is such that the mooring lines do not penetrate the seabed. The contact is modelled as surface to surface and friction-less. Furthermore, to evaluate the sea bed friction, Coulomb friction model is chosen. Circumferential surface of mooring line and surface of seabed are selected for contact interaction.

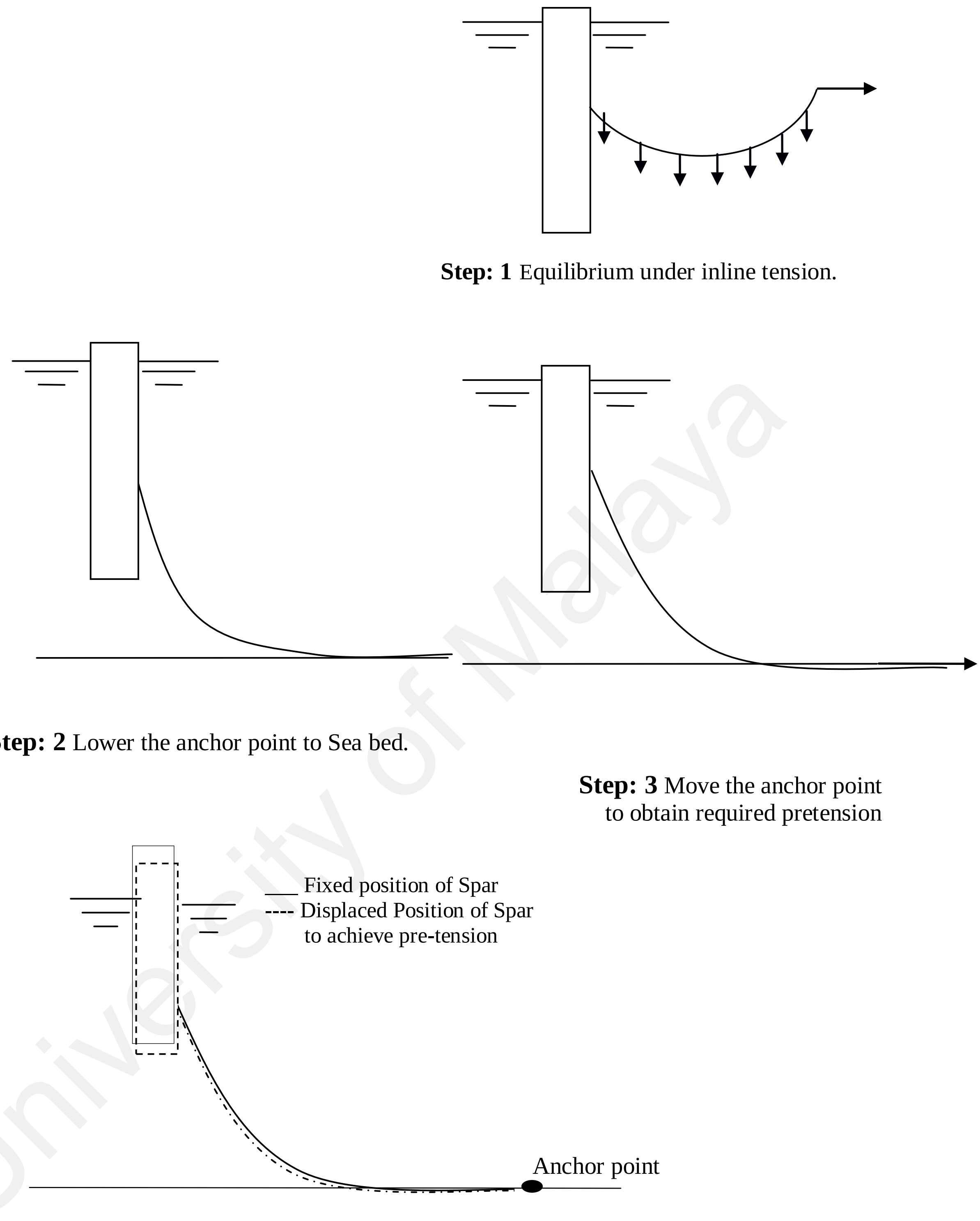

Step: 1 Equilibrium under inline tension.

Step: 2 Lower the anchor point to Sea bed.

Step: 3 Move the anchor point to obtain required pretension

Step: 4 Stable configurations

Figure 3.7: Analysis Steps involved in achieving stable configuration

The static analysis is carried out in four steps (Figure 3.7). The basic aim is to obtain the proper catenary shape of mooring line with actual stresses and stiffness associated with its mean curvature. For defining a catenary shape of mooring line, the location of two end points is required. But instead of second point location, the tension at the top of mooring line (connect to Spar cylinder at fair lead) is known here. In the first step of static analysis, the mooring lines are horizontally stretched out in their individual orientation at fairlead level by incorporating inline tension, which maintains the cylindrical hull fixed. In the second step, the anchor ends of the CMLs are lowered to the seabed providing hinge connection with sea bed. In the third step, the mooring lines are moved on the seabed in such a way that the desired pretension is achieved at the fairlead end. Therefore, in the first three steps, Spar is kept fixed and by stretching the anchor point at the seabed, required tension at the mooring top is achieved and matched.

In the fourth step, Spar is released free and equilibrium is achieved due to self-weight of Spar, self-weight of mooring lines, buoyancy of Spar, buoyancy of mooring lines and tension at the top ends of all the four mooring lines. In the fourth step, the tension at the top of all the four mooring lines is matched again, after matching the position of CG. Static as well as dynamic loads have then been induced as needed. This technique is more precise as the stress and stiffness associated with the mean curvature are automatically incorporated in the NONLIN-COUPLE6D model. Wave, current and wind loadings on the structural system are computed at each time step. In the fifth step, dynamic analysis is carried out. The wave elevation and wave period are specified in the numerical data from the published literature. The cylinder of Spar is very large; therefore, the wave force computed will also be of large value. To overcome the instability of Spar due to sudden large force, the wave force is applied in the form of ramp. After 200 seconds, the wave force acts fully on Spar.

3.6.1. Solution with time Integration

The nonlinear dynamic analysis has been carried out using the time domain numerical integration technique. In the system with time dependent nonlinearities, the stiffness coefficient is dependent on the change of the mooring tension with time and added mass from Morison's equation. Wave loading organizes the primary loading on the moored Spar. Since the dynamic response prevails, the structural behaviour becomes nonlinear because of the drag component of the wave load as it varies with the square of the velocity of the water particle relative to the structure and at each time step. The force vector is updated to consider the change in the top tension of mooring line. The equation of motion is solved by an iterative procedure using entirely stable Newmark's Beta method (Argyris and Mlejnek, 1991). The algorithm is based on Newmark's method for solving the equation of motion

The equation of motion involves time dependent mass, stiffness and damping matrices whose effect is balanced by a force vector. The force vector is exclusively a function of structural displacement, velocity, acceleration and time. Because of the nonlinear coupled nature of the equation of motion, an implicit analysis in time domain is essential for achieving the response time histories. This methodology essentially involves the integration of velocity and acceleration in time domain. The Newmark- β method is used to obtain precise response time histories in an iterative fashion.

In the implicit iterative solution scheme involving Newmark- β method at a time station T_n , structural velocity, displacement and acceleration are initialized and [K], [M] and [C] matrices and vector {F} are determined. Automatic time interval (Δt) incremental solution scheme is selected. The scheme uses half– step residual control to ensure an accurate dynamic solution. The half-step residual is basically the equilibrium residual error (out-of-balance forces) in the middle of a time increment. For a continuum solution the equilibrium residual should be moderately smaller than the significant forces in the problem. This half-step residual check is the basis of the employed time interval incremental scheme. Smaller value of the half-step residual indicates higher accuracy of the solution. Furthermore, it recommends increasing the time step safely. Otherwise, the time step used in the solution has to be lessened.

The ABAQUS package increments and iterates as necessary to analyse a step, depending on the severity of nonlinearity. In transient cases with a physical time scale, parameters to indicate a level of accuracy can be provided in time integration, and the program chooses time increments to achieve this accuracy. Upper limit to the number of increments is defined in an ABAQUS/Standard analysis. In direct cyclic analysis procedure, this upper limit is set to the maximum number of increments in a single loading cycle. The analysis stops if this maximum is exceeded before complete solution of respective step. To arrive at a solution, it is allowed to increase number of increments when necessary to allowed by defining a new upper limit. The tolerance limit of convergence is satisfied at every time station. Effective stiffness and effective load vector are then accomplished. The equations are then solved and at each time step the following parameters are determined.

1) Six components of the structural motion at each node viz. surge, sway, heave, roll, pitch and yaw together with respective velocities and acceleration.
2) Total wave induced forces and moments incorporating structural motion.
3) Stiffness Mass and Damping matrices.
4) Mooring line tension, nodal displacements and rotations.
5) Sea surface elevation to incorporate variable submergence.

Convergence criteria regulate the number of iterations over the above process and the final values are ascertained at n^{th} time station. The values of the required parameters at n^{th} time station are used to determine the same at $n+1^{th}$ time station and so on. The time histories for all the above responses at all the nodes and mooring tensions are obtained.

3.7 Validation of the model

Integrated coupled analysis of modelled Spar mooring system has been performed for 1018 m water depth. The characteristics of Spar platform and environmental loading are exposed in Table 4.1. Hydrodynamic properties are illustrated in Table 4.2. The results for static analysis, natural frequencies and dynamic analysis are obtained. The static analysis results and natural frequencies obtained by the present study are compared with the work of Chen et al. (2001). The results obtained from dynamic analysis are compared with the study performed by Ran et al. (1996).

3.7.1. Validation of static behaviour

Static profile of mooring lines and their resultant tensions for different cases are reported in the literature. Mathematical models differ in different approaches. However, the models do not significantly influence the reported static results. Chen et al. (2001) reported the variation of net tension in four mooring lines at fairlead position varying against various static off-sets in surge direction. The variation of tension versus Spar offsets has been evaluated with the results using the present model. The boundary conditions are appropriately implemented for required state of equilibrium. The comparison of mooring tension is shown in Figure 4.1. The present study takes into account the actual integrated coupling of entire structure by FE assembly considering all major nonlinearities, which differs from the approach taken by Chen et al. (2001).

3.7.2. Validation of natural time periods

Free vibration analysis of Spar platform has been carried out. Lanczos method is employed to acquire the natural frequencies and corresponding mode shapes. Table 4.3 shows the comparison of natural time periods between Chen et al. (2001) and the present study. The natural periods in surge, heave and pitch obtained by the present simulation are compared with the experimentally measured values by Chen et al. (2001) as shown in Table 4.3. The difference is marginal in surge but significant in heave and pitch. It may be due to difference in basic models. However, both values seem to be of similar nature.

3.7.3. Validation of Spar response

Ran et al. (1996) carried out experimental studies on Spar platform. As per the published results the Spar was subjected to regular wave of W_H= 6 m and W_P=14 sec for water depth of 1018 m. The results obtained for the actual integrated Spar mooring line coupling as employed in the present study are compared. The surge and pitch responses obtained in the present study are for the same Spar and wave loading as modelled by Ran et al. (1996). The numerical data is the same as shown in aforementioned values. The Spar data is the same as adopted by Chen et al. (2001).

3.8 Static Equilibrium of coupled system

The static analysis has been carried out in first four major steps as mentioned in Figure 3.7. In the case of Spar a pretension value is specified in the mooring line at the fairlead end. The bottom point is then iteratively fixed to achieve the catenary shape and the required tension at the top. This process is completed for all the four mooring lines simultaneously by systematically following the sequential four steps. In the first step the Spar cylinder is kept fixed and CMLs are horizontally stretched out in their corresponding orientations at the fairlead level. In the second step, anchor ends of the mooring lines are lowered to seabed. In the third step, mooring lines are iteratively moved and adjusted horizontally at sea bed in their respective orientations so that the required tension is achieved at fair lead level. The bottom points are then temporarily hinged at seabed. In the fourth step, the Spar is released and the entire structure consisting of Spar cylinder and mooring system slowly attains an equilibrium position. The equilibrium is attained under self-weight, buoyancy forces and pretension at fairleads. In this process the pretension and the position of the CG of cylinder may be altered and differ from required value. To achieve the requisite pretension and the draft of the cylinder the hinged location at seabed are further moved iteratively. After a few trials, all the design requirements are achieved with the equilibrium position.

In this state of equilibrium of integrated coupled system all the boundary conditions are explicitly defined in ABAQUS/AQUA environment. The mooring lines are modelled maintaining the continuity with the Spar cylinder at fairlead. This modelling of mooring line is more realistic as it also incorporates the changed stiffness due to the curvature of catenary shaped mooring line. The resulting stiffness matrix consists of two parts, namely $K_{E,}$ elastic stiffness matrix and $K_{G,}$ geometric stiffness matrix. The inclusion of large deformation makes the model more accurate and realistic.

3.9 Response evaluation in various sea environments

A number of sea states have been selected to investigate the nonlinear coupled behaviour of the present Spar-mooring system. Subsequent sections discuss the various loading environment combinations which are adopted in the dynamic analysis process for the NONLIN-COUPLE6D model of moored Spar.

3.9.1. Long duration regular wave

The responses of Spar hull and catenary mooring lines in deep sea conditions under the assigned wave in nonlinear finite element analysis have been analysed for 1 and 3 hours duration. The wave height is chosen as 6 m and the wave period is 14 sec. The results are weighed up at both the time states 3000 to 4000 sec. and 11000 to 12000 sec.

Comparative evaluation for surge, heave and pitch motion responses has been carried out in terms of time history and power spectral density (PSD).

3.9.2. Quartering sea wave

Similar large wave with wave height 6m and wave period 14 sec has been applied to the moored Spar at $\pi/4$ radian angle with the horizontal direction. Platform responses and top tension in catenary mooring lines has then been evaluated for 12000 seconds of wave loading. The results are compared with the large wave at 0 radian incidence. Statistical evaluation has been carried out for though study of six degrees of freedom responses of Spar along with tension characteristics of catenary mooring lines in both orthogonal direction.

3.9.3. Severe sea states

The sea states shown as critical in the study of Jameel and Ahmad (2011) has been considered as severe while applying on the coupled Spar-mooring system in deep water environment. Table 3.2 outlines the sea states in their study with respective wave height, wave period and probability of occurrences.

Table 3.2: Severe dynamic stresses (Jameel and Ahmad, 2011)

Sea State	W_H (m)	W_P (sec)	RMS stress (MPa)	Probability of occurrence
S1	17.15	13.26	123.81	0.0000003
S2	15.65	12.66	122.74	0.0000023
S3	14.15	12.04	122.34	0.0000143
S4	12.65	11.39	121.88	0.0000798
S5	11.15	10.69	121.38	0.0004057
S6	9.65	9.94	120.09	0.0018712
S7	8.15	9.14	119.67	0.0077382
S8	6.65	8.26	118.98	0.0282212
S9	5.15	7.26	117.89	0.0885110
S10	3.65	6.12	117.46	0.2283116
S11	2.15	4.69	116.82	0.4354235
S12	0.65	2.58	115.93	0.2094203

3.9.3.1. Strong gale

Sea-state having "W_H" (wave height) and "W_P" (wave period) of 17.15 m and 13.26s (sea states S1) has been considered. These sea states have been defined as they are extremely critical, as pointed out by Jameel and Ahmad (2011). Among all the sea states of their study (Table 3.2), sea state S1 (17.15 m wave height and 13.26 sec wave period) is large in loading magnitude but lowest in probability of occurrence. According to Chakrabarti (2005) the sea state is treated as strong gale (SG-W).

3.9.3.2. Moderate gale

The integrated coupled spar-mooring system has also been analysed under the ocean wave comprising a strong combination of wave period and wave height. The sea state is also critical, as stated by Jameel and Ahmad (2011), ensuring a rational occurrence of probability (Table 3.2) in deep water. In the sea-states represented by two parameters W_H and W_P, value of W_H is chosen as 11.15m and the W_P as 10.69 s. The wave loading of this sea state S5 is treated as moderate gale (MG-W) as per recommendation in Chakrabarti (2005). This sea-state adequately covers the conditions of significant dynamic excitation for a steady load.

3.9.3.3. Moderate wave

Modelled spar platform has been chosen allowing coupling of spar-mooring system subjected to ocean waves in 1018 m deep water. The critical sea state has been selected as S11 (2.15 m wave height and 4.69 sec wave period) according to Jameel and Ahmad (2011). This sea loading is the lowest in loading magnitude but its probability of occurrence is the highest (Table 3.2). Therefore, in the study sea state S11 is considered for the assessment of the structural behaviours under extreme mild but critical wave loading. Consistent with Chakrabarti (2005) the sea wave is named as moderate wave

(MW-W). Detailed evaluation clearly explains the Spar-mooring system responses due to coupled analysis for extreme wave conditions.

3.9.4. Severe waves with current

In reality, for every sea state, considering only the regular wave case is impractical even though it represents the response characteristics for a floating platform. It is expected that the current loading is a relevant component in addition to the wave action which is experienced by the ocean structures. Thus the current loadings compatible to every individual wave condition have been added as the input loading in the FE model and respective solutions are obtained. For all the selected severe sea states, current loading are considered to analyse the coupled behaviour of Spar platform.

The competent current velocity for this strong gale (SG-WC), moderate gale (MG-WC) and moderate wave (MW-WC) are selected as 1.0 m/s, 0.80 m/s and 0.40 m/s respectively at MWL of the sea environment. Effect of current in severe sea wave has been evaluated by time histories, power spectra and statistical analyses.

3.9.5. Wind loading

Former discussion revealed that the aerodynamic loading effect on floating Spar is required to be incorporated as it significantly induces additional dynamic excitation on the top side of the entire system. In this study these wind induced forces have been included for each and every aforementioned case. In the coupled model of spar platform, the top side is incorporated as 16.77m height (OTRC, 1995) over the DDS hull. Therefore, the Spar-mooring system captures the wind loading together with wave and current forces for every individual sea state in the deep water. All the selected sea states along with wind characteristics are illustrated in Table 4.4 in the next chapter.

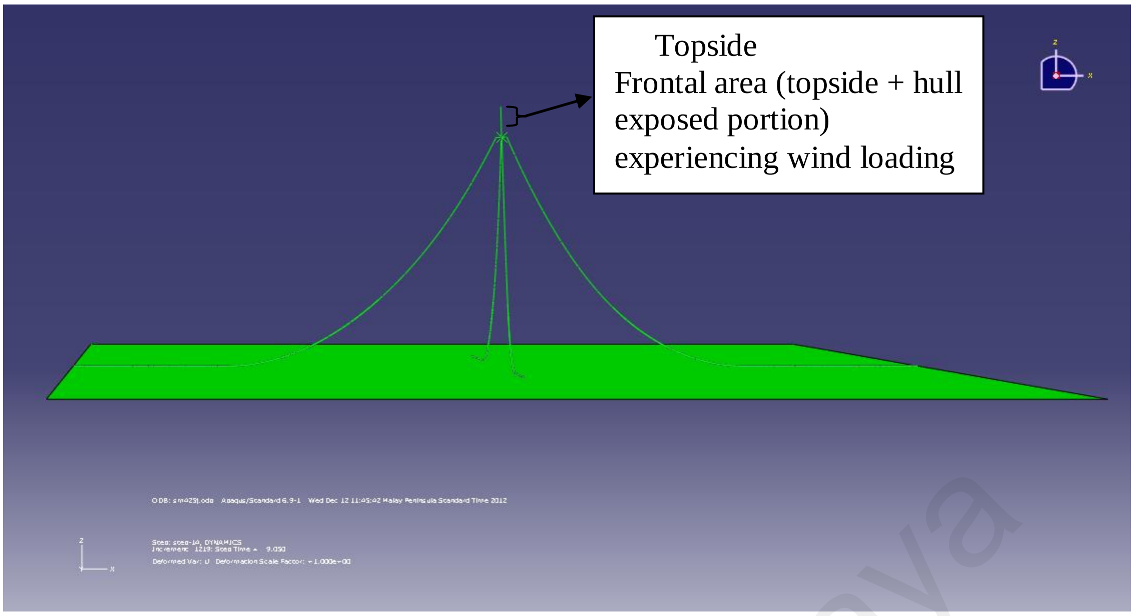

Figure 3.8: Sketch of Spar-mooring system showing frontal area

Mean wind speeds for strong gale (SG-WCW), moderate gale (MG-WCW) and moderate wave (MW-WCW) environments are considered as 26.28 m/s, 20 m/s and 10 m/s respectively (Table 3.1) at a 10m height above MWL. This wind loading is added with corresponding current velocity to study individual total loading effect. Turbulent wind is considered as per the turbulent wind spectrum API-RP2A (2000). Furthermore, comparison API-RP2A spectrum and Emil Simiu spectrum has been done for each case. Response variation has been analysed with variation of wind speed. All the responses are evaluated by time histories, power spectra and statistical analyses.

3.10 Suitability study of spar platform in Malaysian sea

Since the Malay basin of the projected offshore for installing the Spar-mooring system is also of present concern, detailed study of nonlinear coupled Spar platform subjected to the Malaysian sea state has been conducted. The sea wave data along with current and wind loading have been simulated to begin with. In the early phase the moored spar has been analysed in nonlinear dynamic solver for regular wave + current + wind case of Malaysian deep water condition. Later on the effect of sea bed interaction and stability analyses have been carried out under selected Malaysian sea environments along with other ocean loading states.

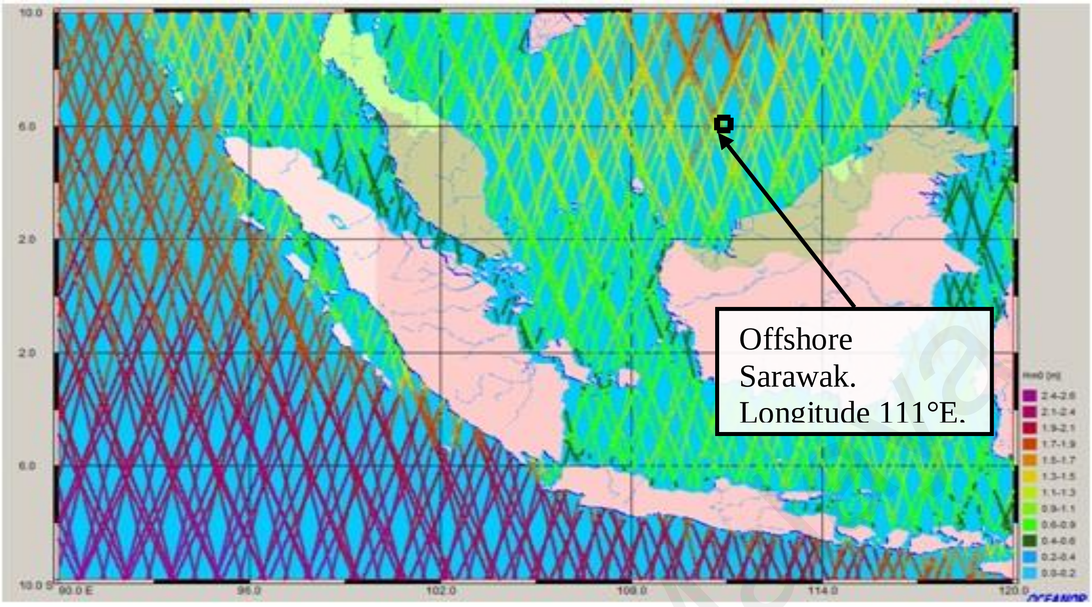

Figure 3.9: Mean seasonal wave heights at Malaysian water (WorldWaves, 2010).

3.10.1. Simulating wave data in Malaysian deep water

It is worth mentioning that wave height data needs precise consideration of the possible sea conditions that could be encountered for any offshore structure during its intended operating lifespan. From the existing literature, it is found that readily available wave data for Malaysia is scarce and of questionable reliability. Presently, there are only 2 such data sources, both of which are obtained from observations from volunteer ships. This situation resulted in the wave data being confined to when and where these ships set sail. Consequently, there are certain periods of time and certain locations for which there is no data at all. The particulars of offshore local to Malaysian region or South China sea have been shown in Figures 3.10~3.12. Offshore Sarawak has been considered to obtain the wave data as representative of Malaysian deep water region. The raw data has been collected from WorldWaves (2010).

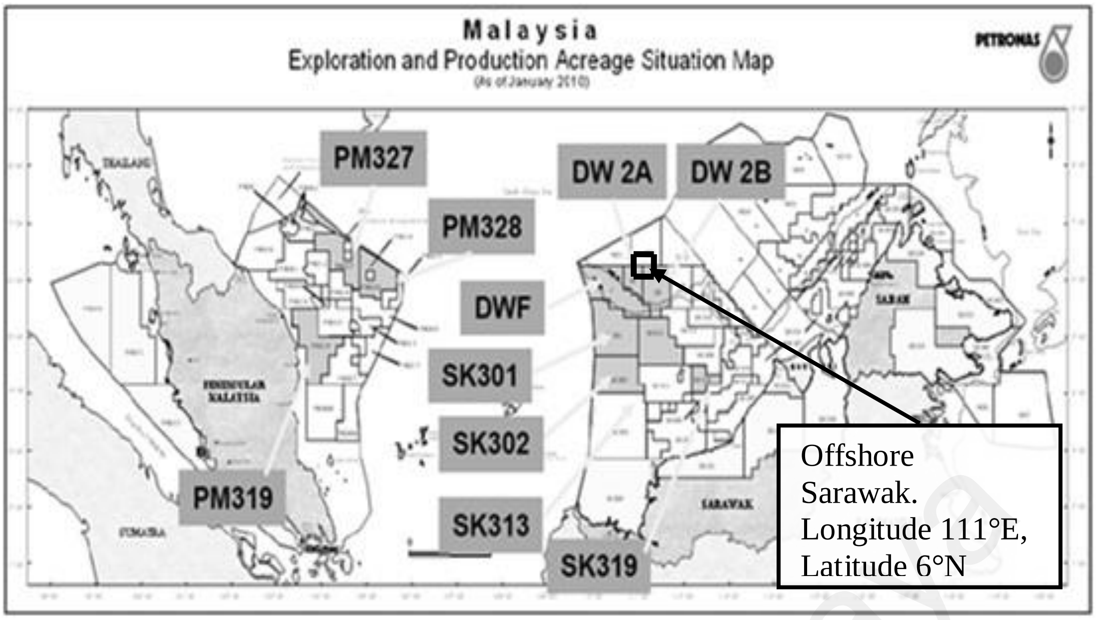

Figure 3.10: Location of Malaysian deep water oil and gas blocks (Petronas, 2010).

The instruments were checked and calibrated to ensure the quality of data collected. To give a better perspective on the representative wave conditions in the offshore region Malaysia, data based on in situ measurements have been generated. However, recent researches have shown that satellite altimetry data may be interpreted and calibrated to provide reliable and accurate sea wave parameters for any location in the world. The following wave data was obtained from two independent sources that have based their findings on satellite altimetry:

- WorldWaves (2010) data on a 0.5° x 0.5° grid offshore of the state of Sarawak, from the European Centre for Medium-Range Weather Forecasts (ECMWF) WAM model archive. (Calibrated and corrected by Fugro OCEANOR, 2010).

Based on the locations of known oil and gas reserves as well as possible future exploration and production activities, the location for the satellite wave data was chosen for offshore Sarawak, longitude 111°E, latitude 6°N. The locations of targeted data are illustrated in Figures 3.10~3.12, for comparison with the locations of wave height distributions, Malaysian oil and gas blocks and also sea depth ranges.

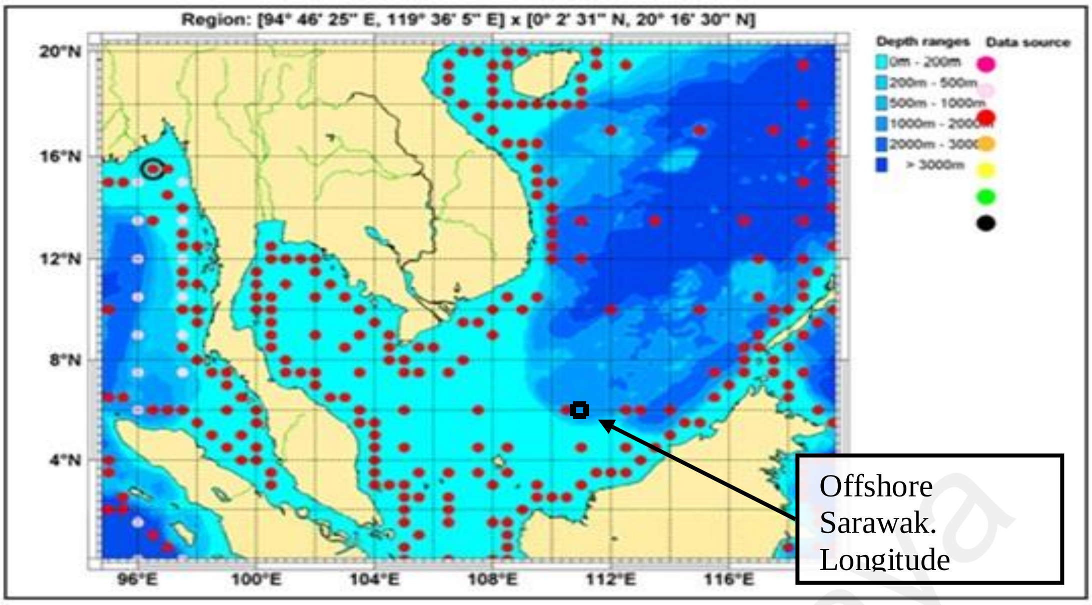

Figure 3.11: South East Asian water depth contours (WorldWaves, 2010)

Tables 3.2~3.3 show the corresponding summary of wave data obtained. Wherever the sea is idealized as regular, wave height and wave periods are considered as wave heights and wave periods of sine waves. The altimetry data from Table 3.3 was exhibited based on repeat cycle of the T/P satellite within this area from the year 1997. For a particular known wave height, *H*, wave period, *T* and the mean wind velocity, U_w can be attained assuming the same occurrence probability (Siddiqui and Ahmad, 2000). *H* & *T* yield a correlation as per the empirical relation in Equations (3.127) and (3.128).

$$T = \sqrt{\frac{32\pi H_s}{g}} \tag{3.127}$$

$$U_w = \sqrt{\frac{gH_s}{0.283}} \tag{3.128}$$

Table 3.3: Raw wave data for offshore Sarawak, 6°N, 111°E (WorldWaves, 2010).

Wave height, H_s (m)	Midpoint (m)	Frequency of Occurrence
5-6	5.5	2
4-5	4.5	12
3-4	3.5	53
2-3	2.5	138
1-2	1.5	593
0-1	0.5	662
		Total: 1460

Nine sea states have been considered, namely $S_a \sim S_b$. The matching wave periods, T and wind velocity, u are calculated based on these relations. Because offshore engineering design requirements specify that loadings on a structure be based on at least 100-year return periods, the raw data obtained was insufficient for a direct estimation.

For $X \geq 0$,

$$F = e^{e^{-(0.9413 * X^{1.46} - 0.65)}} \tag{3.129}$$

The cumulative frequency distribution model in equation (3.129) is for shallow water. In the present study, equations (3.130) and (3.131) have been adopted to obtain the cumulative frequency distribution for deep water. The 100 years occurrence probabilities for different sea states have been determined to be related to wave periods and wind velocities. The predicted sea states will contribute significantly to the precise offshore structure design and implementation.

For $X < 1.06$,

$$F = e^{e^{-(2.44 * X - 2.224)}} \tag{3.130}$$

For $X > 1.06$,

$$F = e^{e^{-(1.5 * X - 1.1873)}} \tag{3.131}$$

3.10.2. Response evaluation for spar platform in Malaysian sea

A thorough study of wave data of Malaysian deep water region, Sarawak was found for 100 year return period wave loading as 8.72 m wave height and 9.45 s wave period. This determination of forecasting Malaysian deep sea state has been shown in the next chapter. The anticipated wave environment falls on the condition of “moderate gale”. Present NONLIN-COUPLE6D model of Spar-mooring system has again been analysed under this wave condition of Malay basin. Coupled responses of the nonlinear dynamic

Spar model have been induced with more excitation including current loading along with the wave forces forecasted for Malay basin. For the 8.72m/9.45s sea state the supplementary current loading is chosen as 0.70 m/s speed (Table 3.1). Inclusion of wind force along with the wave and current condition of Malaysian sea is an additional interest. Estimated wind field (discussed in Chapter 4) gives the mean wind speed as 17.25 m/s at the 10m height above MWL which is assimilated to conduct the nonlinear coupled analysis. The turbulent wind is considered following the API-RP 2A spectrum.

3.11 Seabed friction

The interaction of sea bed with mooring line has a considerable effect on the mooring behaviour and so on the total Spar-mooring system. A number of cases for the categories of modelled sea beds mentioned below have been selected for detailed assessment which is described in the next Chapter. In the present study, the seabed is considered as a non-deformable element. Modelling of sea bed includes two forms

1) Frictionless seabed
2) Frictional sea bed

These two modelling techniques assume that the seabed deformations during a catenary mooring to seabed interaction are ignored. However, the resistance to mooring movement delivered by the seabed is accounted for through the contact interaction properties that are well-defined for the mooring line and the seabed.

3.11.1. Frictionless sea bed

The main constraint of counting a deformable seabed/soil model is the computational cost involved. If a large area of seabed is included in a typical dynamic stability analysis, the size of the FE model will increase which could render this approach impractical. In addition, the other restrictions include the difficulty of analysis convergence due to the occurrence of excessive localised deformation in the underlying soil elements, and the difficulty of capturing the behaviour properly or identifying an appropriate material constitutive model for it.

The present frictionless seabed is considered as “analytic rigid surface” in the modelling. The surface is absolutely rigid and doesn’t face deformation while contacting with hybrid beam element catenary mooring line. Proper contact behaviour in between the catenary mooring line and sea bed is incorporated. To avoid the analysis complexities, the characteristic is maintained that the hybrid mooring line will slide on the analytic rigid sea bed. Furthermore, the system stability of the Spar platform through the station keeping system is maintained.

3.11.2. Frictional sea bed

The frictional seabed is modelled as “discrete rigid surface” elements. In ABAQUS/AQUA, its element type is R3D4. Interactions in the normal direction between CML and underlying seabed element are defined by a “softened contact with linear contact pressure and over-closure relationship” algorithm employed in the FEM model. A softened contact algorithm has been incorporated as it is applicable for modelling soft layers on a contact sea bed surface. In the tangential directions (mooring line axial and lateral directions) the frictional constraint has been assigned by standard ABAQUS Coulomb friction reinforced by penalty method. The frictional restraint change under the combined mooring line submerged weight and lifting forces, depending on the mooring to undulated seabed contact force and contact over closure/clearance.

Since the seabed is modelled with non-deformable rigid surfaces/elements, during mooring line landing and impacting the seabed, kinetic energy is not dissipated through soil plastic deformation and/or other possible mechanisms. Instead it is conserved in the system and causes the mooring to seabed contact to behave essentially as a “mass-spring” system. For simulating the energy dissipation mechanism, and attenuate the possibly excessive contact impact oscillation, appropriate damping (critical damping definition) has been introduced to dissipate part or all of the kinetic energy associated with the contact. Damping is effectuated in the normal direction for the particular contact definition after contact occurs.

3.12 Procedures of stable response analysis

The structural stability of moored Spar subjected to hydrodynamic and aerodynamic forces is an essential aspect that deserves careful investigation for the floating system in deep water. In order to check the stability of floating platform with the station keeping system evaluation of stable and unstable platform motion responses are conducted in the present study. Subsequent sections discuss the approaches relating to the present Spar-mooring system.

3.12.1. Bifurcation technique

From nonlinear coupled analysis of Spar-mooring system, platform motion histories and respective velocity histories of Spar hull are obtained. For similar time duration, velocity response and displacement/rotation responses are plotted. These portraits, called Phase plots, give a description of stable and unstable characteristics of platform responses (Rand, 2005). Three numbers of phase plots of surge, heave and pitch show different kinds of instability phenomena in pattern of symmetry breaking bifurcations caused by mT sub harmonic/super harmonic oscillations and aperiodic responses of the Spar platform.

The bifurcation concept is a mathematical study of changes in qualitative or topological behaviour of structure (Figure 3.12). Without occurrence of bifurcation, the system seems to be quite stable. Figure 3.12a shows structural behaviour through phase plot when no bifurcation is observed and hence the system is quite stable. In reality bifurcations may occur in both continuous systems (described by ODEs, DDEs or PDEs) and discrete systems (described by maps). In a dynamical system, a bifurcation occurs when a small smooth change made to the bifurcation parameters causes a sudden qualitative or topological alteration (Figure 3.12b) in the structural behaviour. When the symmetry of phase plot is disturbed, the bifurcation is termed as symmetry breaking bifurcation. Sub harmonic oscillations occur when the time period of subsequent cycle lessens by 1/n times than the previous time period. When the time period of subsequent cycle increases n times of previous time period, the oscillation is super harmonic.

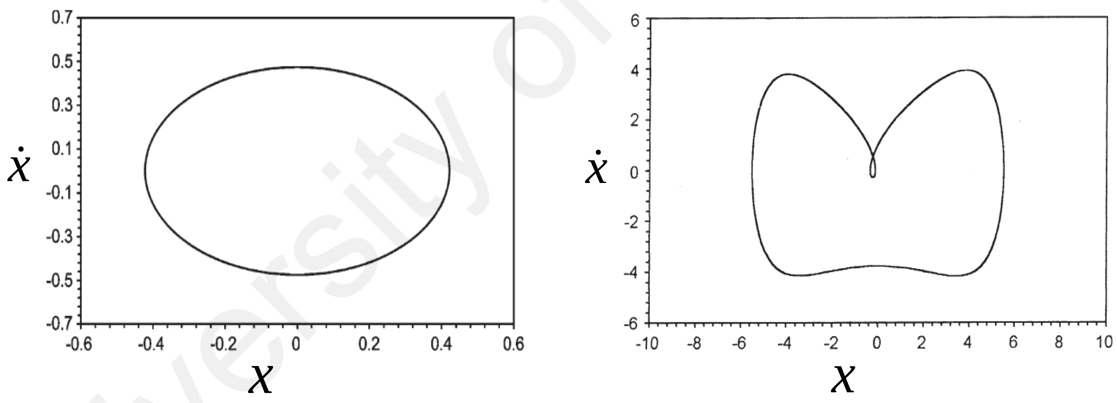

a) No bifurcation and system stability b) Bifurcation and system instability

Figure 3.12: Typical phase plot showing stability, bifurcation and instability (Umar and Datta, 2003)

In a dynamic system, a limit cycle on a two-dimensional manifold can be anticipated as a closed trajectory by means of phase plot. A trajectory is closed if and only if it corresponds to a periodic solution of the system. When a system approaches periodic behaviour and a closed curve in phase plane is appeared, the closed path is called a limit cycle. A close trajectory of a dynamic system which has nearby open trajectories spiralling towards it both from inside and outside is called stable limit cycle (Figure

3.13a). If nearby open trajectories spiral away from closed path on both sides, the close trajectory is unstable limit cycle (Figure 3.13b). Figure 3.13 shows the limit cycles where the thick line closed trajectory is limit cycle and other paths are neighbouring open trajectories.

When the neighbouring trajectories spiral towards the limit cycle from one side and spiral out from the other side, it is semi-stable limit cycle (Figure 3.13c). If nearby trajectories neither approach nor recede from closed trajectory, it is neutrally-stable limit cycle (Figure 3.13d). A stable limit cycle attracts all neighbouring trajectories. In reality, the stable limit cycles indicate self-sustained oscillations. It is agreed that the trajectories for various initial states of this structural system converge to the limit cycle as described for Van der Pol oscillator. Therefore, self-sustained oscillations are attained by the system.

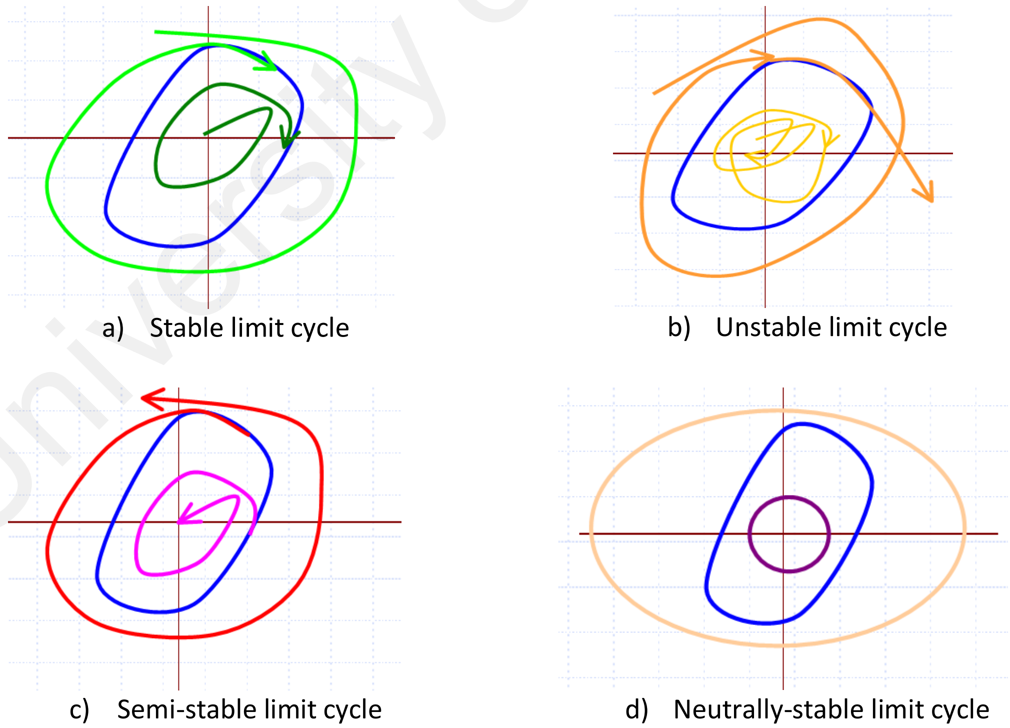

Figure 3.13: Characteristics of limit cycle

According to the bifurcations concept, a Hopf or Poincaré–Andronov–Hopf bifurcation is a local bifurcation where a fixed point of a dynamic assembly loses stability as a pair of complex conjugate eigenvalues of the linearization around the fixed point cross the imaginary axis of the complex plane. This local bifurcation occurs when a parameter change causes the stability of an equilibrium or fixed point to change. Satisfying realistic generic assumptions about the dynamical system, a small-amplitude limit cycle branching from the fixed point is seen. The topological changes in phase portrait of the structural system can be confined to arbitrarily small neighbourhoods of the bifurcating fixed points by moving the bifurcation parameter close to the bifurcation point. To deliberate limit cycle of platform motions in the three dimensional structural system, generalized form of van der Pol's equation can be written as:

$$\ddot{\forall} + \forall = c\dot{\forall} + \alpha_1 \forall^2 + \alpha_2 \forall\dot{\forall} + \alpha_3 \dot{\forall}^2 + \beta_1 \forall^3 + \beta_2 \forall^2 \dot{\forall} + \beta_3 \forall \dot{\forall}^2 + \beta_4 \dot{\forall}^3 \tag{3.132}$$

When Spar platform is considered, in the above relation, c is the coefficient of damping, α_i s are coefficients of quadratic nonlinear terms, and β_i s are coefficients of cubic nonlinear terms in the Spar-mooring system. Equation (3.132) may reveal a limit cycle for some sensitive values of these parameters. The dot symbols indicate derivatives with respect to time t. The born of periodic solution for varying parameters can be investigated using Lindstedt's method. Assuming $\forall = \in \mathrm{X}$ into Equation (3.132) gives the succeeding expression:

$$\text{`}\ \ddot{\mathrm{X}} + \mathrm{X} = c\dot{\mathrm{X}} + \in \left[\alpha_1 \mathrm{X}^2 + \alpha_2 \mathrm{X}\dot{\mathrm{X}} + \alpha_3 \dot{\mathrm{X}}^2\right] + \in^2 \left[\beta_1 \mathrm{X}^3 + \beta_2 \mathrm{X}^2 \dot{\mathrm{X}} + \beta_3 \mathrm{X}\dot{\mathrm{X}}^2 + \beta_4 \dot{\mathrm{X}}^3\right] \tag{3.133}$$

The term X is the displacement/rotation of the platform where its derivatives are velocity and accelerations sequentially. To scale the coefficient of damping, the parameter c is expanded in a power series incorporating the small parameter $\in$:

$$c = c_0 + c_1 \in + c_2 \in^2 + \cdots\cdots\cdots\cdots \tag{3.134}$$

Initial damping coefficient c_0 is taken as zero where the next value of damping is considered as c_1. Although the quadratic terms are of $f(\in)$, their first contribution to resonance terms in Lindstedt's method occurs at $f(\in^2)$. Consequently, if c_1 is non-zero, the scheme may fail to achieve a limit cycle irrespective of the values of α_i and β_i coefficients. In fact, damping would be too strong relative to the nonlinearities for a limit cycle to exist. Therefore, the coefficient c is scaled to be $f(\in^2)$, and it is set as $c = \in^2 \wp$:

$$\ddot{X} + X = \in\left[\alpha_1 X^2 + \alpha_2 X\dot{X} + \alpha_3 \dot{X}^2\right] + \in^2 \left[\wp\dot{X} + \beta_1 X^3 + \beta_2 X^2 \dot{X} + \beta_3 X\dot{X}^2 + \beta_4 \dot{X}^3\right] \quad (3.135)$$

For adopting the Lindstedt's method to Equation (3.135), a relation is set as τ = ωt. Expanding the expression gives the following equations:

$$\omega = 1 + \kappa_1 \in + \kappa_2 \in^2 + \cdots\cdots\cdots \quad (3.136)$$

$$X(\tau) = X_0(\tau) + \in X_1(\tau) + \in^2 X_2(\tau) + \cdots\cdots\cdots \quad (3.137)$$

Substituting Equations (3.136) and (3.137) into Equation (3.135) and collecting terms gives:

$$X_0'' + X_0 = 0 \quad (3.138)$$

$$X_1'' + X_1 = -2\kappa_1 X_0'' + \alpha_1 X_0^2 + \alpha_2 X_0 X_0' + \alpha_3 (X_0')^2 \quad (3.139)$$

The prime (') symbols indicate derivatives with respect to time τ. The solution then can be taken to Equation (3.138) as

$$X_0(\tau) = \Lambda \cos\tau \quad (3.140)$$

Placing Equation (3.140) into Equation (3.139) and simplifying the trig terms requires that κ_1 be taken as 0 so as to be left with no resonance terms. The technique yields the following expression for $X_1(\tau)$:

$$X_1(\tau) = \frac{\Lambda^2}{6}(3(\alpha_1 + \alpha_3) + (\alpha_3 - \alpha_1)\cos 2\tau + \alpha_2 \sin 2\tau) \quad (3.141)$$

Incorporating these results into the successive equation for $X_2(\tau)$ and freeing the coefficients of both the $\sin\tau$ and $\cos\tau$ of resonance terms, the following is obtained:

$$\begin{aligned}\Lambda &= 2\sqrt{\frac{-\wp}{\alpha_2(\alpha_1+\alpha_3)+\beta_2+3\beta_4}} \\ &= 2\sqrt{\frac{-\wp}{\Diamond}}\end{aligned} \tag{3.142}$$

Consistent with this approximate study, a limit cycle will exist if the expression (3.142) for the amplitude Λ is real. To satisfy the phenomenon the damping coefficient $\wp$ should have the opposite sign to the lower part of the function in between the square root. If this quantity is defined by $\Diamond$, its value comes from the following expression:

$$\Diamond = \alpha_2(\alpha_1+\alpha_3)+\beta_2+3\beta_4 \tag{3.143}$$

In addition, the succeeding relation gives the value of κ_2:

$$\kappa_2 = \frac{\wp(10\alpha_1{}^2+\alpha_2{}^2+10\alpha_1\alpha_3+4\alpha_3{}^2+9\beta_1+3\beta_3)}{6\alpha_1\alpha_2+6\alpha_2\alpha_3+6\beta_2+18\beta_4} \tag{3.144}$$

If for certain circumstances $\Diamond$ is fixed and $\wp$ is allowed to vary quasi-statically, a limit cycle is either created or destroyed, as $\wp$ goes through the value zero. This situation is called a Hopf bifurcation. Two cases which exist are: supercritical ($\Diamond < 0$) and subcritical ($\Diamond > 0$). The stability of the equilibrium point at the phase plane origin in either case is influenced only by the sign of $\wp$, and not by the value of α_i's or β_i's. Identical verdicts may be seen by rewriting Equation (3.135) in the practice

$$\ddot{X} + X - \in^2 \wp\dot{X} = \in\left[\alpha_1 X^2 + \alpha_2 X\dot{X} + \alpha_3\dot{X}^2\right] + \in^2\left[\beta_1 X^3 + \beta_2 X^2\dot{X} + \beta_3 X\dot{X}^2 + \beta_4\dot{X}^3\right] \tag{3.145}$$

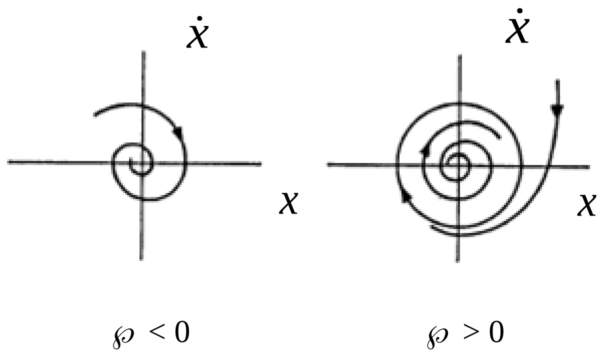

Figure 3.14: Supercritical Hopf Bifurcations (Rand, 2005)

The right hand side terms of the Equation (3.145) are entirely nonlinear. In the case $\Diamond < 0$, the limit cycle exists only when $\wp > 0$, where the limit cycle is stable. The bifurcation is a supercritical Hopf (Figure 3.14). Conversely, when $\Diamond > 0$ and the limit cycle is unstable, the bifurcation is a subcritical Hopf (Figure 3.15). For both cases, the amplitude of the newly born limit cycle grows like $\sqrt{|\wp|}$, a function having infinite slope at $\wp = 0$, to facilitate the size of the limit cycle growing radically for parameters neighbouring the bifurcation value of $\wp = 0$. The limit cycle is orbitally stable when a specific measure termed as the first Lyapunov coefficient is negative and the bifurcation is supercritical. Or else the structural system is unstable and the bifurcation is subcritical.

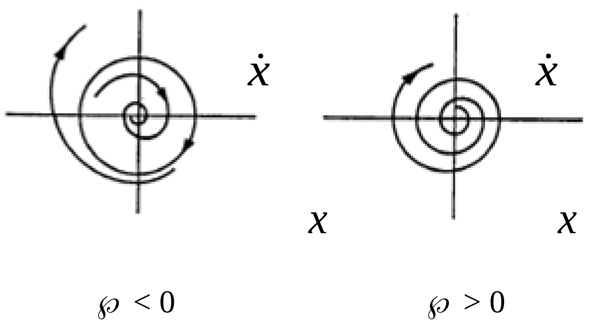

Figure 3.15: Subcritical Hopf Bifurcations (Rand, 2005)

Furthermore, a homo-clinic bifurcation is a global bifurcation which often occurs when a periodic orbit collides with a saddle point. At the bifurcation point the period of the periodic orbit is matured to infinity contributing a homo-clinic orbit. After the bifurcation there is no longer a periodic orbit. In homoclinic bifurcation, a limit cycle collides with a saddle point. If the limit cycle collides with two or more saddle points, the phenomenon is heteroclinic bifurcation. Furthermore, for infinite-period bifurcation, a stable node and saddle point simultaneously occur on a limit cycle. In this study, these types of global bifurcations are not interpreted.

3.12.2. Nonlinear damped Mathieu instability approach

Mathieu instability for a classical spar platform is supposed to arise when the period of the heave motion is half of the pitch natural period. The heave and pitch responses under dynamic loading have been obtained considering damping and hull/mooring coupled effects in the system. The Mathieu instability of the coupled Spar platform is checked. The Mathieu equation is an exceptional case of Hill's equation that is a linear expression with a periodic coefficient. When periodic loading is induced, the standard form of Hill's equation becomes:

$$\ddot{X} + (\lambda + \hbar \cos t)X = 0 \tag{3.146}$$

Where, the periodic force is $\hbar \cos t$. Above equation is Mathieu's expression comprising a linear differential equation with variable coefficients which commonly occurs in nonlinear vibration problems in two different ways: (i) in systems where there is periodic forcing, and (ii) in stability studies of periodic motions in nonlinear autonomous systems. The Equation (3.146) is relevant to the un-damped situation. When the damping is incorporated, the damped Mathieu equation is quantified by the succeeding Equation (3.147).

$$\ddot{X} + c\dot{X} + (\lambda + \hbar \cos t)X = 0 \tag{3.147}$$

For the instance of (i), the case of a pendulum is chosen whose support is periodically forced in a vertical direction. The governing differential equation is

$$\ddot{\mathrm{X}} + c\dot{\mathrm{X}} + \left(\frac{g}{L} - \frac{\widehat{A}\omega^2}{L}\cos\omega t\right)\sin \mathrm{X} = 0 \tag{3.148}$$

As a case in point of (ii), a system is considered known as “the particle in the plane”. This consists of a particle of unit mass which is constrained to move in the *x*-*y* plane, and is restrained by two linear springs, each with spring constant of 1/2. Anchor points of the two springs are positioned on the *x* axis at X = 1 and X = −1. Each of the two springs has unstretched length *L*. An exact solution is attained from the autonomous system corresponding to a mode of vibration in which the particle moves along the *x* axis as: $\mathrm{X} = \widehat{A}\cos t$, $y = 0$. For obtaining the stability of this motion, initially derived equations of motion are to be substituted by $x = A\cos t + u$, $y = 0 + v$, where *u* and *v* are small deviations from the motion. By linearizing *u* and *v*, the result yields two linear differential equations on *u* and *v*.

Foremost concern regarding Mathieu’s equation (3.147) is whether or not all solutions are bounded for the selected values of λ and $\hbar$. When all solutions are bounded, the corresponding point in the λ-$\hbar$ parameter plane is supposed to be stable. Conversely, a point is called unstable if an unbounded solution occurs. These unbounded solutions may result from resonances between the forcing frequency and the oscillator’s unforced natural frequency. Since the resonance causes the amplitude of the motion to increase, the relation between period and amplitude causes the resonance to detune, decreasing its tendency to produce large motions. This is a characteristic effect of nonlinearity and a more realistic model can be obtained comprising nonlinear terms in the Mathieu equation. For this purpose, in the Equation (3.148), if sin *x* is expanded in a Taylor series, the approximation comes as:

$$\ddot{X} + c\dot{X} + (\frac{g}{L} - \frac{\widehat{A}\omega^2}{L}\cos\omega t)(X - \frac{X^3}{6} + \cdots\cdots) = 0 \tag{3.149}$$

For simplification, the term can be scaled as $\tau = \omega t$, $\lambda = \frac{g}{\omega^2 L}$ and $\hbar = \frac{\widehat{A}}{L}$. Hence the relation is approximated as

$$X'' + cX' + (\lambda - \hbar\cos\tau)(X - \frac{X^3}{6} + \cdots\cdots) = 0 \tag{3.150}$$

By further scaling X to $X = \sqrt{\hbar}\Im$, the subsequent expression can be obtained as

$$\Im'' + c\Im' + (\lambda - \hbar\cos\tau)\Im - \frac{\lambda}{6}\Im^3 + f(\hbar^2) = 0 \tag{3.151}$$

Neglecting the terms of $f(\hbar^2)$, the equation appears as

$$\Im'' + c\Im' + (\lambda - \hbar\cos\tau)\Im - \frac{\lambda}{6}\Im^3) = 0 \tag{3.152}$$

Motivated by this relation, the modified expression can be approximated as the following nonlinear damped Mathieu equation:

$$\ddot{X} + c\dot{X} + (\lambda + \hbar\cos t)X + \hbar\widehat{\alpha}X^3 = 0 \tag{3.153}$$

Diagram of Nonlinear damped Mathieu instability has been shown in Figure 3.16. Two-variable expansion approach is incorporated to explain this equation for small $\hbar$. For facilitating the approach, the damping co-efficient c is scaled as $c = \hbar\wp$. Supposing $\xi = t$ and $\eta = \hbar t$, the Equation (3.153) is derived as :

$$\frac{\partial^2 X}{\partial\xi^2} + 2\hbar\frac{\partial^2 X}{\partial\xi\partial\eta} + \hbar^2\frac{\partial^2 X}{\partial\eta^2} + \hbar\wp(\frac{\partial X}{\partial\xi} + \hbar\frac{\partial X}{\partial\eta}) + (\lambda + \hbar\cos\xi)X + \hbar\widehat{\alpha}X^3 = 0 \tag{3.154}$$

The term X and λ can be expanded (Rand, 2005) in power series as

$$X(\xi,\eta) = X_0(\xi,\eta) + \hbar X_1(\xi,\eta) + \cdots\cdots \tag{3.155}$$

$$\lambda = \frac{1}{4} + \lambda_1\hbar + \lambda_2\hbar^2 + \cdots\cdots \tag{3.156}$$

Therefore, solution of the Equation (3.154) is projected as:

$$\frac{\partial^2 X_0}{\partial \xi^2} + \bar{\lambda} X_0 = 0 \tag{3.157}$$

$$\frac{\partial^2 X_1}{\partial \xi^2} + \frac{1}{4} X_1 = -2\frac{\partial^2 X_0}{\partial \xi \partial \eta} - \wp \frac{\partial X_0}{\partial \xi} - X_0 xos\,\xi - \bar{\lambda}_1 X_0 - \hat{\alpha} X_0{}^3 \tag{3.158}$$

Where X_0 comprises the form:

$$X_0(\xi,\eta) = \bar{A}(\eta)\cos\frac{\xi}{2} + \bar{B}(\eta)\sin\frac{\xi}{2} \tag{3.159}$$

Exclusion of resonant terms in Equation (3.158) results in the appearance of certain supplementary cubic terms in the slow flow as:

$$\frac{d\bar{A}}{d\eta} = (\bar{\lambda}_1 - \frac{1}{2})\bar{B} + \frac{3\hat{\alpha}}{4}\bar{B}(\bar{A}^2 + \bar{B}^2) \tag{3.160}$$

$$\frac{d\bar{B}}{d\eta} = -(\bar{\lambda}_1 + \frac{1}{2})\bar{A} - \frac{3\hat{\alpha}}{4}\bar{A}(\bar{A}^2 + \bar{B}^2) \tag{3.161}$$

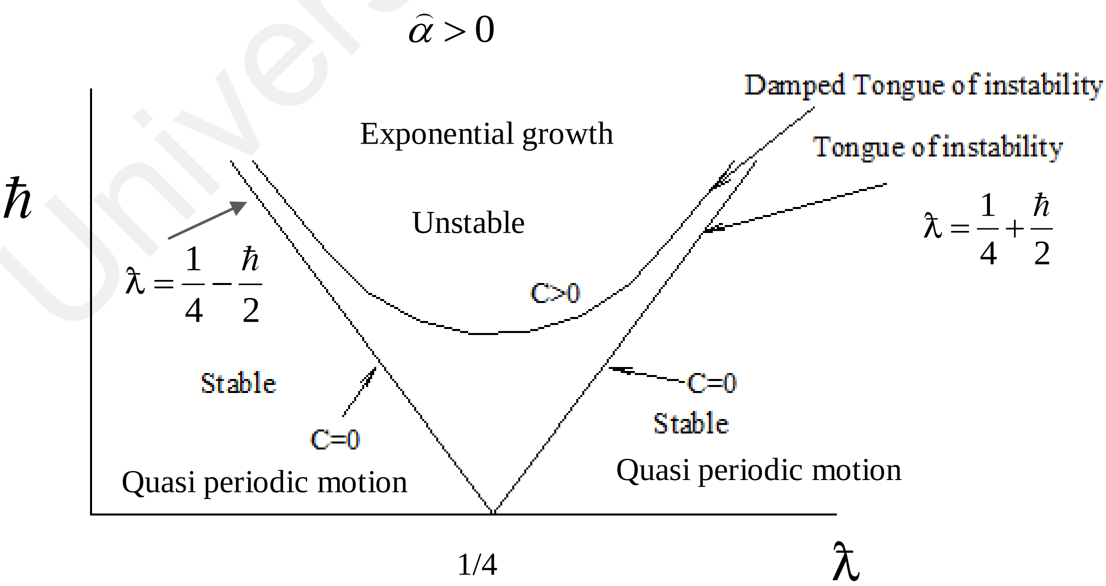

Figure 3.16: Diagram of Nonlinear damped Mathieu instability

For significant real solution considering $\hat{\alpha}$ =0, it is observed that $\hat{\lambda}_1 = \pm 0.5$ agrees to transition curves for the stability. Hence, the analysis predicts that divergences arise as the transition curves are crossed in the $\hat{\lambda}$ - $\hbar$ plane. This requires quasi-statically decreasing the parameter $\hat{\lambda}$ while $\hbar$ is kept fixed, and moving through the n = 1 tongue of instability emanating from the point $\hat{\lambda} = 0.25$ on the $\hat{\lambda}$ axis. As $\hat{\lambda}$ decreases across the right transition curve, the trivial solution X= 0 becomes unstable and simultaneously a stable 2:1 sub harmonic motion is born. As such the motion rises in amplitude as $\hat{\lambda}$ continues to decrease. While the left transition curve is crossed, the trivial solution becomes stable again, and an unstable 2:1 sub harmonic is initiated. This scenario is visualized as involving two pitchfork bifurcations. For the nonlinearity parameter $\hat{\alpha}$ < 0, a similar sequence of divergences occurs, except that the sub harmonic motions are born as $\hat{\lambda}$ increases quasi-statically through the aforementioned region of instability.

3.13 Effect of riser in integrated Spar-mooring-riser system

As risers are integral parts of drilling and production activity, proper investigation for the effect of risers on coupled dynamics of Spar is of great importance. Therefore, fully coupled integrated Spar-mooring-riser system (Figure 3.17) has been simulated to evaluate the physical behaviour of nonlinear responses. The response of coupled Spar in platform motions and top tension in mooring lines are obtained in presence of risers in the integrated system.

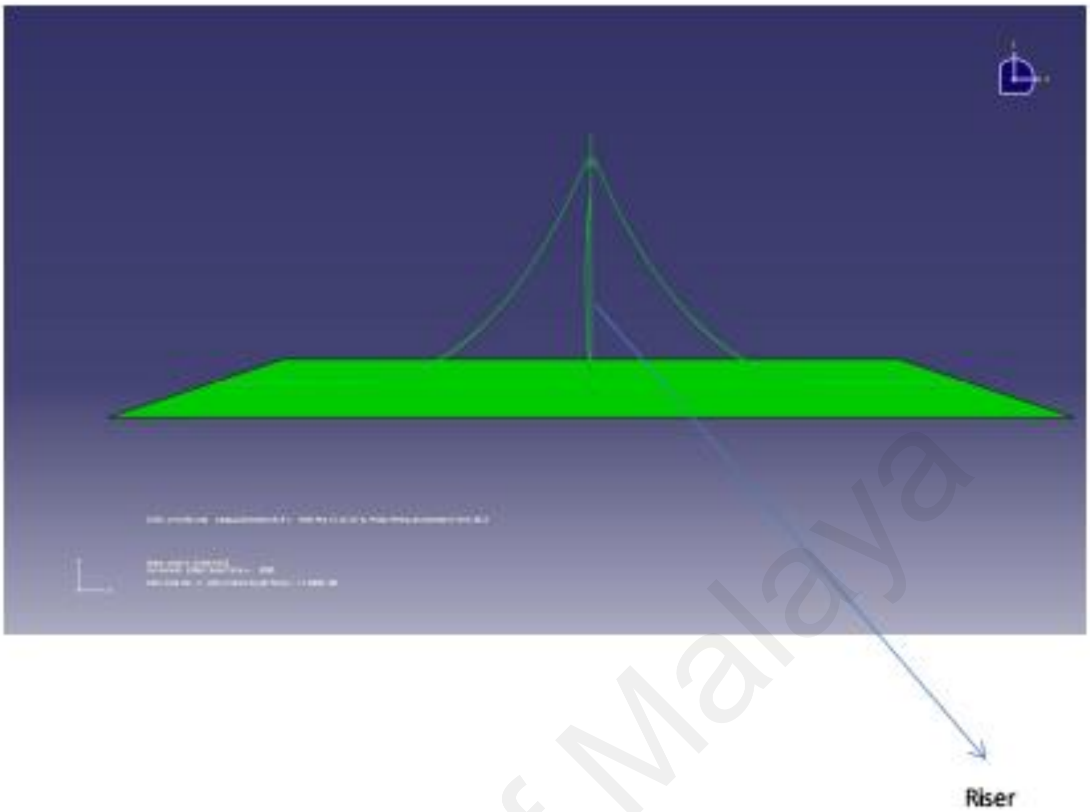

Figure 3.17: Sketch of the Spar-mooring-topside-riser system

The riser component has been modelled allowing coupled analysis of the whole integrated Spar-mooring-topside-riser system. The riser is modelled as hybrid beam element with six degrees of freedom at every single node (three translation and three rotations). The riser model in ABAQUS (ABAQUS, 2006) finite element program is configured with proper boundary conditions. The bottom end of the rigid riser is hinged and considered as restrained in horizontal and vertical directions. Moreover, the top end of the riser is restrained in the horizontal direction. The analysis comprises nonlinearities caused by large deformation, time-varying variation of submergence, added mass, buoyancy and drag force.

The equation of riser is similar to mooring equation except that outer diameter and inner diameter of riser pipe are to be considered instead of solid mooring diameter. The problems of static and dynamic behaviour of marine riser, formulated by equations of motion can be solved by the finite element method. The marine riser comprises string of beam finite elements having appropriate mass and stiffness characteristics. The elastic deformation of riser subjected to steady sea current and tension forces is mathematically modelled by the equation of static equilibrium.

3.13.1. Coupled effect of riser

Coupled dynamic of integrated Spar-mooring-riser system has been performed under critical hydrodynamic loading considering riser. The results are then compared with the without riser case. A severe sea environment may sometimes cause more damage than the normal hydrodynamic loading. Hence, critical sea state, strong gale (SG-W) has been selected for comparative evaluation of extreme responses of the coupled Spar. Comparative time histories, power spectrum have been evaluated along with the statistical analysis.

CHAPTER 4: RESULTS AND DISCUSSIONS

4.1 Introduction

The nonlinear coupled dynamic approach addresses all the interactions amongst the floating platform and station keeping system, mooring lines as an integrated system. Adopting this fully coupled analysis can adequately include proper damping, stiffness as well as inertial impacts of mooring lines in the study of platform nonlinear motions. Therefore, a realistic structural assemblage of Spar-mooring system is achieved. Offshore exploration progressively requires incorporating platform–mooring coupled-dynamic-analysis tools for deep water and ultra-deep water applications. The coupled dynamic technique in this study ensures dynamic equilibrium between the forces acting on the floating spar and the mooring line at every time instant. The present NONLIN-COUPLE6D model has been well validated with experimental published results considering identical input data with good agreement. Nonlinear coupled dynamic analyses in time domain have been performed under several sea states under hydrodynamic and aerodynamic loading. Responses of moored Spar platform under severe sea states incorporating wave and current in deep-water conditions are evaluated. Aerodynamic loading on coupled spar has been incorporated for nonlinear response assessment of spar hull and mooring lines. The influence of sea bed friction on the Spar-mooring system has been studied. Sea wave data for Malaysian deep water at Sarawak basin are simulated. Subsequently, analysis of coupled Spar platform for deep-water oil exploration in Malaysia is performed. Stable response analyses of the coupled Spar platform in deep water have been carried out. Last of all, coupled analysis of integrated Spar-mooring-riser system has been performed and the effect of riser is evaluated.

4.2 Spar-mooring simulation

The preceding chapter discussed the adopted methodology for nonlinear coupled dynamic analysis of floating Spar platform in deep water. In this chapter, the coupled behaviour of Spar-mooring system under numerous sea environments and realistic geometric configurations have been studied. The geometric characteristics of spar platform for the present NONLIN-COUPLE6D simulation are given in Table 4.1. The platform is assumed to behave like a rigid body for the analysis.

Table 4.1: Key Particulars of Spar (Classic JIP Spar)

Parameters	**Rating**	**Unit**
Category	Deep draft spar (DDS)	-
Hull Shape	Cylindrical	-
Hull Length	213.04	m
Radius of cylindrical hull	20.27	m
Hull Draft	198.12	m
Total Mass	2.515E8 kg	Kg
Freeboard	14.92	m
Mooring Point below still sea level	106.62	m
Centre of gravity below still sea level	105.98	m
Distance of Centre of gravity from keel	92.14	m
Distance of Centre of gravity from fairlead	0.64	m
Element type	Rigid beam element	-
Origin orientation (vertical axis)	+z	-
Radius of gyration (Pitch)	62.33	m

Station keeping is maintained by four catenary mooring lines between spar hull and sea bed. The particulars of the catenary mooring lines are explained in Table 4.2. This mooring line system allows the platform to easily move from its position as required under the projected loading. The responses have been studied with the designated configurations in terms of soft (surge, sway, and yaw) and stiff (roll, pitch and heave) degrees of freedom together with mooring line tension. Initially the environmental condition is considered to be a large wave (LW) to incorporate the regular wave loading. The hydrodynamic characteristics considered in the spar-mooring assemblage are as in Table 4.3. The coefficients except in vertical direction are in horizontal direction along wave.

Table 4.2: Mooring line physical properties

Parameters	**Value**	**Unit**
Category	Catenary mooring line (CML)	-
No. of Moorings	4	-
Stiffness (EA)	1.501E9	N
Total line length (upstretched)	2000	m
Line Mass per unit length	1100	Kg/m
Mooring line pre-tension	1.625E+07	N
Material	Steel wire rope	-
Element type	Hybrid beam element	-

The wave forces incorporate the influence of variable submergence. It is noted that the forces experienced at the displaced location of the platform are measured. Morison's equation has been employed maintaining the wave lengths as greater than or equal to five times the diameter of spar cylinder. Dynamic solver in time domain can handle high level of nonlinearities. Response histories are attained for long duration of environmental loading after achieving a steady state.

Table 4.3: Hydrodynamic properties

Element	**Hydrodynamic parameters**	**Value**
Deep draft spar	Drag coefficient	0.6
	Inertia coefficient	2.0
	Added mass coefficient	1.0
	Drag coefficient in vertical direction	3.0
Catenary mooring line	Drag coefficient	1.0
	Inertia coefficient	2.2
	Added mass coefficient	1.2
Sea water depth (m)		1018
Density of Sea water (Kg/m^3)		1000

Along with the regular wave, the effect of current and wind loading have been investigated under numerous sea states. Table 4.4 explains the environmental loading considered in the study. The terminology LW, SG, MG, MW have been quoted as per the guidelines of sea state loading parameter in Chakrabarti (2005). All the nonlinearities associated with the coupled problem are given due consideration. The scheme includes the effect of drag and inertia of mooring lines coupled with Spar hull which can be treated as the effect of integrated coupling. It has been witnessed that the displacement responses in sway together with rotation responses in roll and yaw are indeed trivial because of unidirectional wave loading. Therefore, the present studies focus on surge, heave and pitch responses of spar hull emphasizing the nonlinear coupling effect. Furthermore, the sway, yaw and roll motions are also shown for selected wave loadings.

Table 4.4: Selected environmental conditions of Spar-mooring system

Designation/Case	Parameters	Value	Unit
Large wave (LW)	Wave height	6	m
	Wave period	14	sec
	Wave direction	0	rad
Strong gale (SG)	Wave height	17.15	m
	Wave period	13.26	sec
	Wave direction	0	rad
Moderate gale (MG)	Wave height	11.15	m
	Wave period	10.69	sec
	Wave direction	0	rad
Moderate wave (MW)	Wave height	2.15	m
	Wave period	4.69	sec
	Wave direction	0	rad
Storm Current profile	Depth Sea bed Mean sea level	 0 1.0 (SG), 0.80 (MG), 0.70 (MS),0.40 MW)	 m/s m/s
	Current direction	0	radian
Wind profile	Mean Wind speed (1h@10 m elevation)	26.28 (SG), 20.0 (MG), 10.0 (MW)	m/s
	Fluctuating Wind spectrum	API RP 2A-WSD, Emil Simiu	-
	Wind direction	0	radian
	Wind drag coefficient	2.0	-
Sea bed	Smooth sea bed	Sliding, No friction	-
	Frictional sea bed (Ia, Ib)	Coulomb friction model Friction coefficient 0.4, 0.5	-
Malaysian sea (MS)	Wave height	8.72	m
	Wave period	9.45	sec
	Mean Wind speed (1h@10 m elevation)	17.25	m/s
	Fluctuating Wind spectrum	API RP 2A-WSD	-
	Wind direction	0	radian
	Wind drag coefficient	2.0	-

4.3 Validation of NONLIN-COUPLE6D model with experimental study

Extensive study on the nonlinear coupled Spar/mooring system has been carried out for 1018 m deep water environment. The environmental state comprises large wave (LW) having wave height and wave period as of 6.0m and 14.0 sec respectively. Finite element model done in ABAQUS/AQUA environment incorporates all the structural and hydrodynamic parameters that feature in the OTRC experimental set up. DDS hull and CML components have similar constraints (Table 4.1, Table 4.2 and Table 4.3) as those observed by Chen et al. (2001) in the OTRC wave basin. In their experiment, the surge, pitch and heave motion of a spar and horizontal force at mooring were measured in the three-dimensional wave basin of OTRC at Texas A&M University. The basin is 45.7 m long and 30.5 m wide. It has a uniform water depth of 5.8 m. Scale ratio of the model to prototype is 1:55. Configured JIP Spar of the experiment resembles the present model to a reasonable extent. The mooring lines were attached to the spar at the fairlead which is very close to the centre of gravity of the assembly. The arrangement of the mooring lines is quite identical. Results obtained in the static analysis and free vibration analysis with the present NONLIN-COUPLE6D model are matched with those of the experimental output of Chen et al. (2001). Experimental study at same three-dimensional wave basin of OTRC at Texas A&M University has been adopted by Ran et al. (1996). Dynamic behaviour in terms of Spar responses has been verified with the present study result using similar structural and environmental parameters.

4.3.1. Validation of static characteristics

Top tensions in catenary mooring line at fairlead position have been shown by Chen et al. (2001) against various static off-sets in surge. These values are the net maximum Tension of all the four mooring lines connected with the spar hull and sea bed. A similar configuration is used in the NONLIN-COUPLE6D model. In both researches, the responses are excited by deep water wave loading having wave basin water depth water depth of 318 m and then for 1018 m. Spar configurations are same for both water depths. Keeping similar properties of mooring line the CML length was maintained as 600 m and 2000m for depth of 318 m and 1018 m respectively as presented in Chen et al. (2001) study. Figure 4.1 shows the trends of maximum net tension changes versus the Spar off-set up to the range 0 m to 25 m. Eventually, the top tension in developed model shows the behaviour close to that of Chen et al. (2001) for all the surge off-sets ranging from 10m to 25m. The pattern of the response variation in both studies is reasonably good. The nominal deviation in the numerical values of maximum net tension is mostly caused by the basic variance in the mathematical model. Present model considers slack mooring line where as the experiment chose taut mooting line. The NONLIN-COUPLE6D model contemplates the tangible integrated coupling of the whole system coping with all possible nonlinearities configured in finite element assembly. Besides, Chen et al. (2001) have modelled it in an alternative fashion. The closely matching phenomenon of NONLIN-COUPLE6D model with the study carried out by Chen et al. (2001) shows the validity of the fully coupled mathematical model using the ABAQUS/AQUA finite element module.

It is worth noting that the boundary conditions are appropriately implemented for the required state of equilibrium. Nevertheless, the minute difference in maximum net tension is desirable because of mooring line categories. The OTRC experiment selected the stating keeping system as taut mooring whereas slack (catenary) mooring line is incorporated in the developed model.

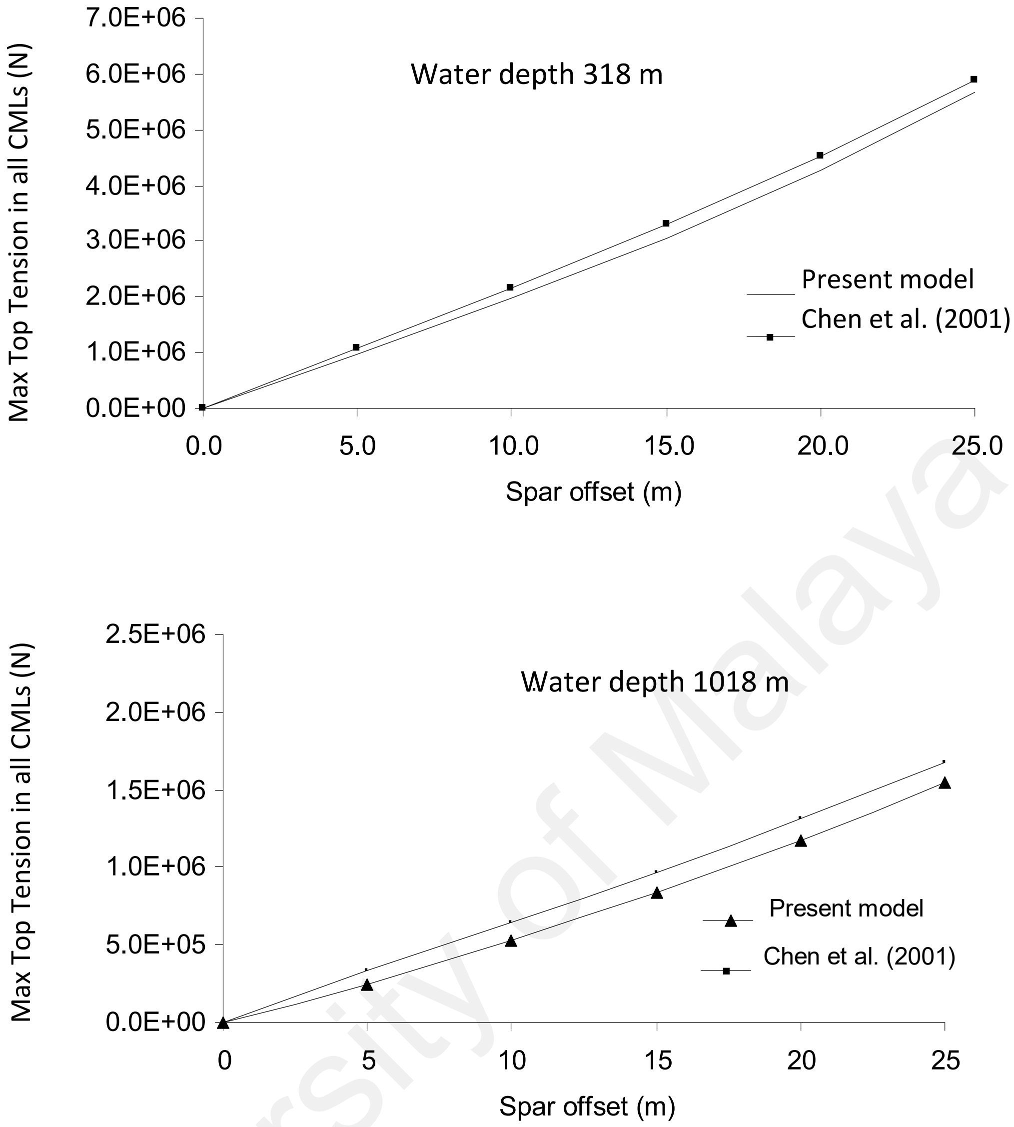

Figure 4.1: Tension comparisons authenticating present model

4.3.2. Validation of free vibration behaviour

In addition to the static analysis, free vibration analysis of Spar platform has been performed to further confirm the validity of the NONLIN-COUPLE6D model. The analysis in frequency domain follows the widely implemented Lanczos algorithm. The progression essentially executes the natural frequencies together with their corresponding mode shapes. Figure 4.2 shows the comparison of natural time periods between Chen et al. (2001) and the present study. The properties of Spar and mooring lines have been mentioned in the preceding section. The natural periods obtained by Chen et al. (2001) are 331.86, 29.03, 66.77 seconds in surge, heave and pitch respectively. Corresponding natural periods 323.97, 25.60 and 59.48 seconds attained by the NONLIN-COUPLE6D model are close to those experimentally measured values as shown in the Figure 4.2. Surge natural periods maintains the marginal alteration in two compared cases. Moreover the natural frequencies experience nominal variance in heave and pitch.

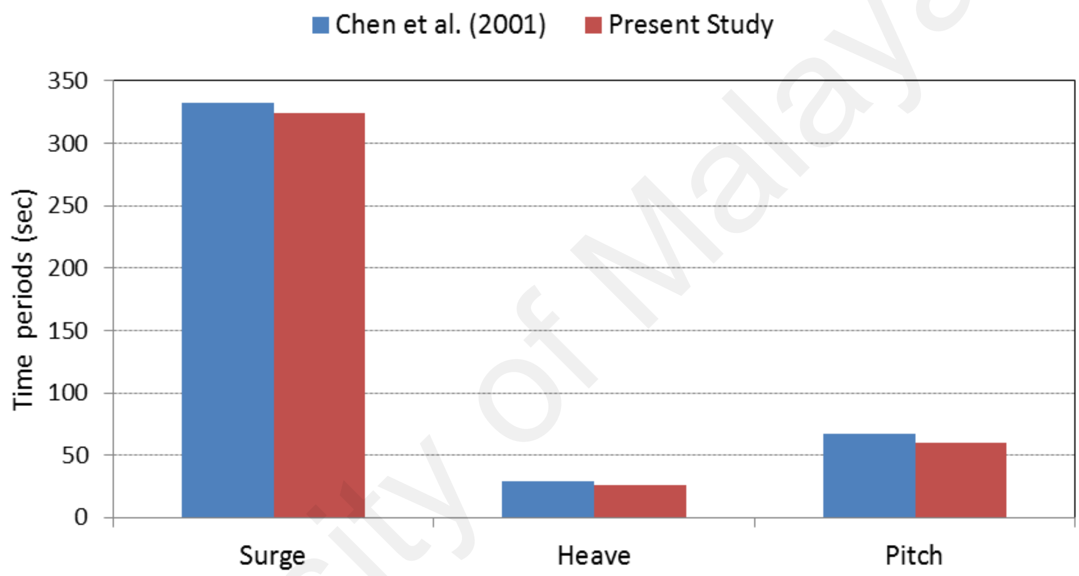

Figure 4.2: Comparison of Natural Time Periods

4.3.3. Validation of dynamic characteristics

The dynamic behaviour of presently modelled moored Spar has been verified with the experimental study of Ran et al. (1996). Their laboratory experiment on Spar platform was carried out at the OTRC wave basin. The Spar hull and mooring line system have similar parameters (Table 4.1, Table 4.2 and Table 4.3) as those of Chen et al. (2001). A water depth of 318 m has been chosen for the experimental study of the floating platform following 1:55 scale (OTRC, 1995) . Large wave (LW) of 6.0m wave height and 14.0 sec wave period has been chosen for the environmental loading. The experimental platform named JIP Spar bears a resemblance to the present model. The finite element model created in ABAQUS/AQUA environment incorporates all the structural and hydrodynamic parameters that feature in the experimental set up. The responses of the nonlinear dynamic Spar- mooring line coupling employed in this study are shown in Figures 4.3~4.7. The structural excursions follow the directions of Ran et al. (1996).

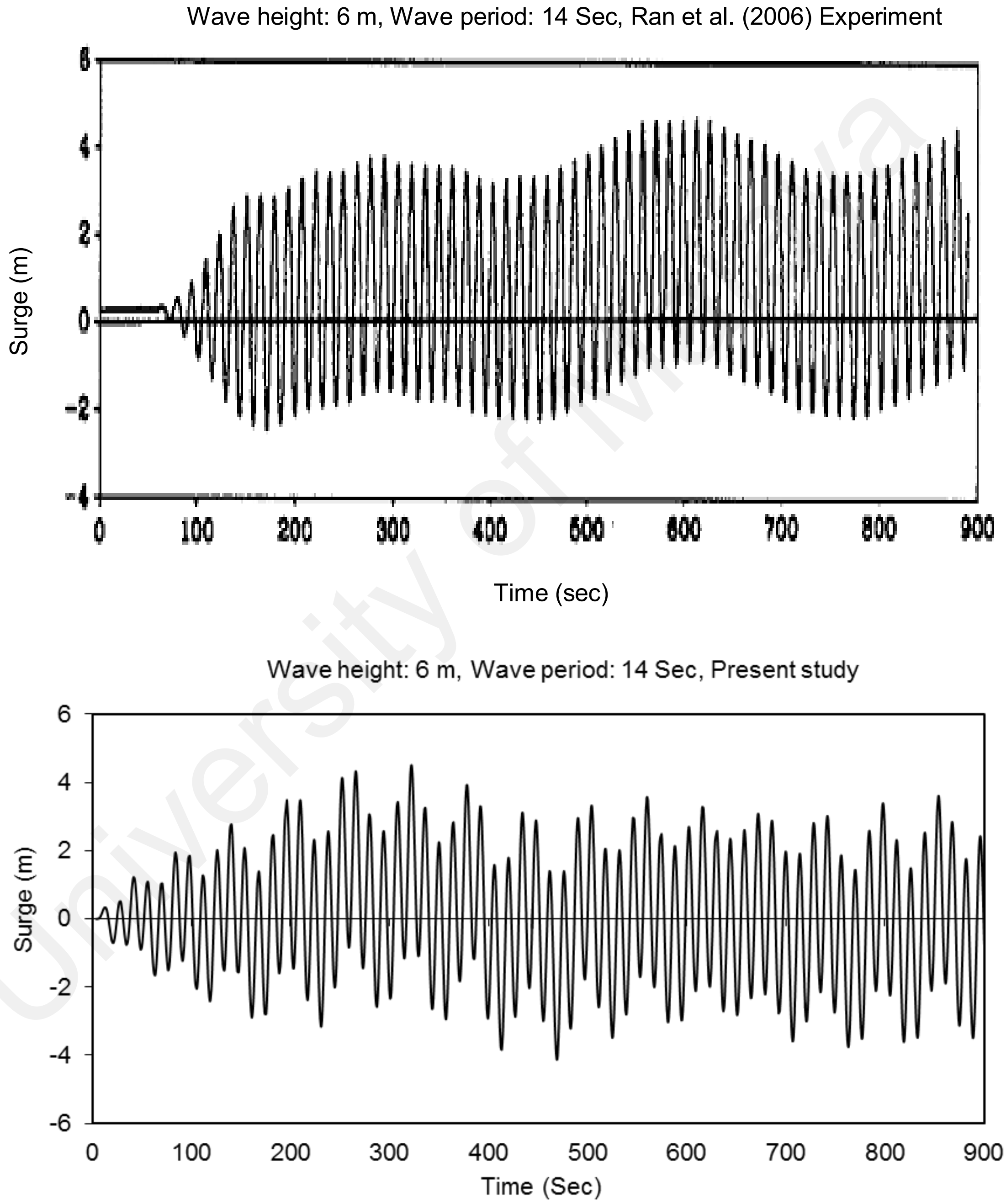

Figure 4.3: Evaluation of Surge time history

The horizontal displacement of Spar in the present study under regular wave environment of the selected wave characteristics has closed trend of fluctuations as that of Ran et al. (1996). It is observed that the maximum and minimum values of surge responses in the published results are 4.2 m and 2.6 m. The present investigation also confirms the value of surge excursions to be close to the experimental results. The statistics of the numerical response exhibit the maximum and minimum values of surge fluctuations to be ±3.8 m.

The system experiences distinct participation of two frequencies. Present FEM modelling produced mean frequency and wave frequency responses in close agreement with the experimental results. The key oscillation is seen to occur at a frequency of 0.14 rad/sec at the experiment along with trivial involvement of surge frequency. Furthermore, a super imposed oscillation exists at a frequency of 0.45 rad/sec. This frequency is actually the wave frequency. Behaviour of the two peaks is clearly understood from the power spectrum in Figure 4.4.

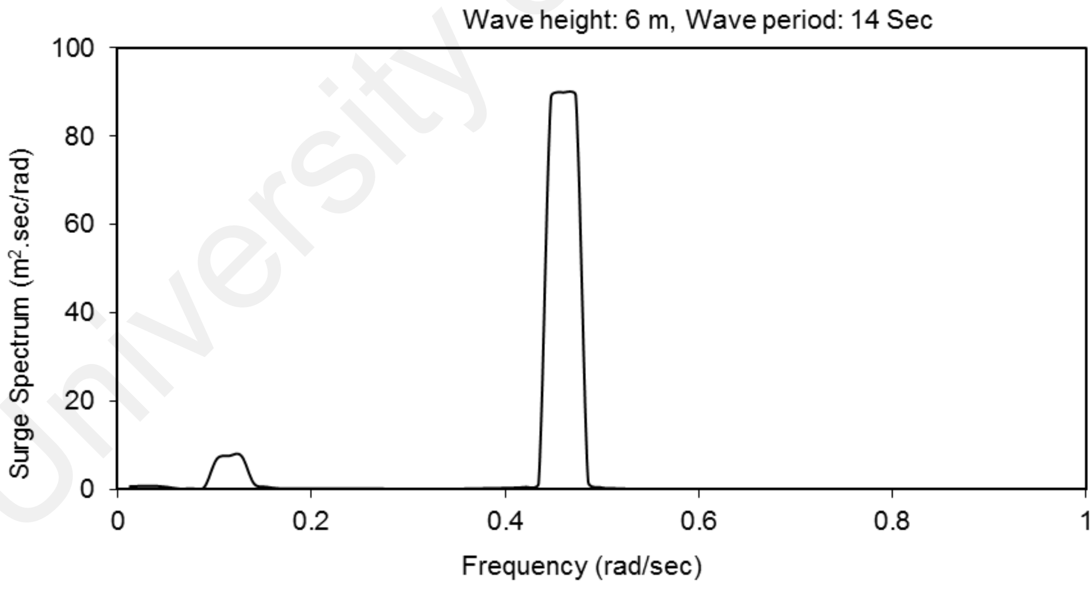

Figure 4.4: Power spectrum of surge motion

In the power spectrum, the lesser peak corresponds to the pitch frequency and the bigger peak indicates the wave frequency of Spar. The concurrent involvement shows the coupling of pitch rotation with surge motion. Present investigations reveal oscillations close to 0.14 rad/sec and 0.45 rad/sec which supports the frequency behaviour of surge response shown in in the work of Ran et al. (1996). Therefore, in the present numerical cases, the Spar translational behaviours along wave direction are reliable. On the other hand, Ran et al. (1996) mentioned that the magnitude of heave response was very small, less than ±1 m, in their experiment. Likewise, the present nonlinear FEM simulation of dynamically coupled Spar-mooring system shows the vertical movement of platform well below the stated magnitude. Figure 4.5 explains the simulated heave response time history. This phenomenon, in actual fact, means that the heave motion response of the floating Spar matches with the experimental excursions. However, the little variation of response behaviour is because the wave basin experiment took the mooring line as taut mooring whereas present model considers catenary mooring line.

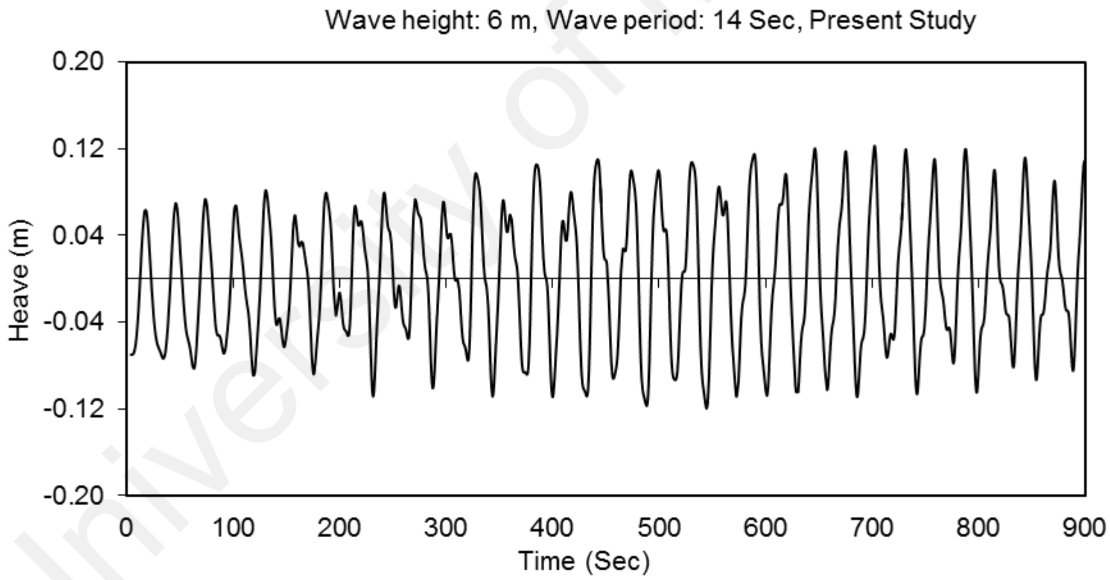

Figure 4.5: Evaluation of Heave time history

The Spar rotation in pitch from the nonlinear coupled dynamic analysis of the currently modelled moored Spar has been presented in Figure 4.6~4.7 for the regular wave environment as chosen in the experiment of Ran et al. (1996). Wave loading is the governing factor on the behaviour of pitch response. This fluctuating frequency matches up to the wave frequency (0.45 rad/sec) of rotation oscillation while pitch frequency of smaller intensity is existent as well. The pitch response in the work of Ran et al. (1996) manifests identical characteristics to those presently obtained. In the experimental investigation also, the main fluctuations resemble the wave frequency. In contrast, the fluctuations at pitch frequency are substantially lessened. The taut mooring lines incorporated in the experimental model induce these constraint characteristics.

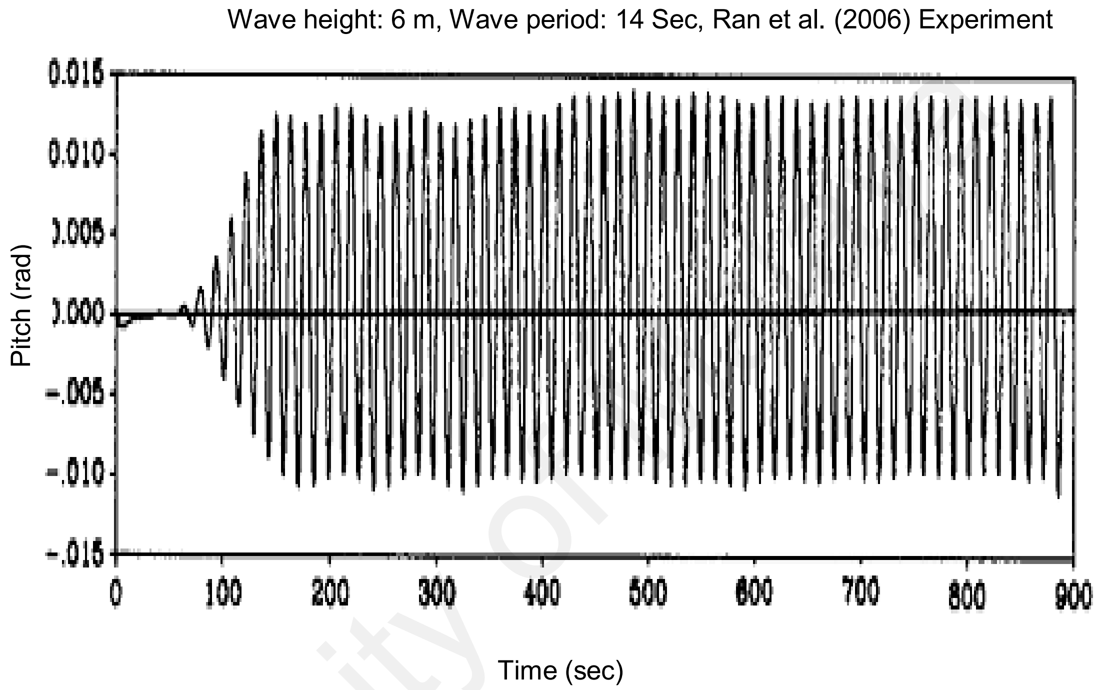

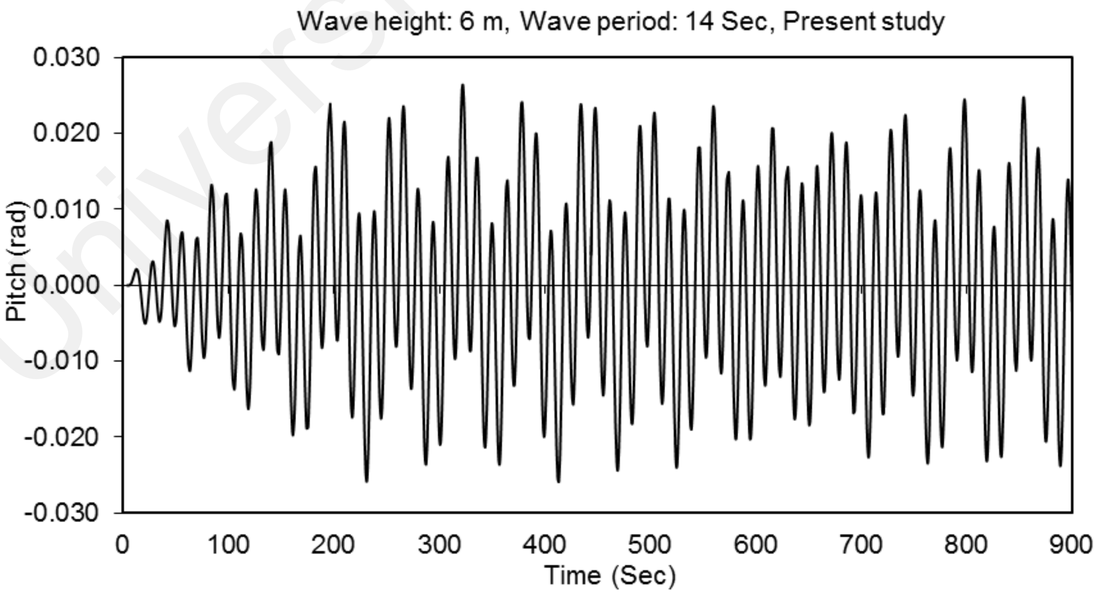

Figure 4.6: Evaluation of Pitch time history

For the present NONLIN-COUPLE6D model, the station keeping system, CML is considered of the actual catenary shape linked to the Spar hull at fair lead position in the vertical direction. Though the peak pitch rotation is higher, ±0.025 rad/sec (Figure 4.6) in the present simulation than the reported pitch value by Ran et al. (1996), mostly occurred regular peaks come out to be close to the value ±0.013 rad/sec obtained in the OTRC wave basin. Slack mooring lines causes the fluctuations of Spar rotation compared to the taut mooring line's involvement. The wide-ranging trend and the response behaviour correspond meticulously.

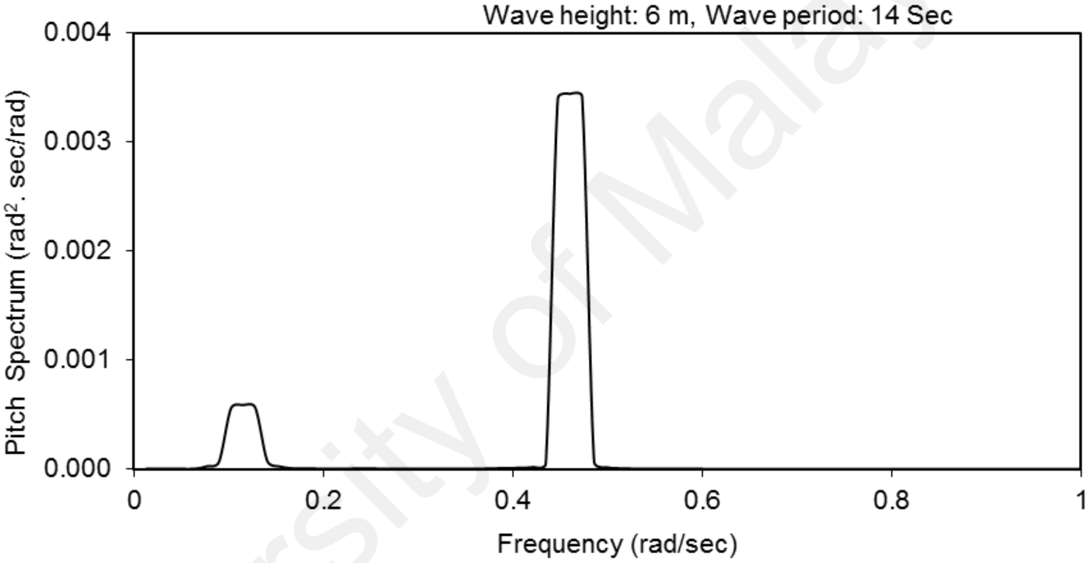

Figure 4.7: Power spectrum of pitch motion

4.4 Numerical Studies of nonlinear coupled Spar

An offshore compliant floating structure like spar platform has been chosen allowing spar-mooring coupling in ocean wave at 1018 m deep water. The system experiences a calm water environment. The sea bed size has been configured as 8000 X 8000 m^2 at ±0 elevation. Hydrodynamic forces are attained from regular wave loading of 6m/ 14 sec (wave height/ wave period) sea state. Top tensions in all the four mooring lines are supposed to be equally distributed. When the wave forces act on the entire structure, participation of mooring lines with rigid hull in the overall response is well depicted.

Variable boundary conditions due to mooring anchor point are appropriately incorporated.

Through the time domain analysis adopts a step-by-step integration technique, the excursion time histories have been obtained for adequate length of time so that the response attains steady state. The analysis of Spar-mooring system for deep water condition has been performed up to a long duration. To understand the mooring damping and coupling effect, two sets of responses are obtained. The responses in terms of surge, heave, pitch and mooring line tension are plotted in subsequent sections as per the sea states under evaluation. As the other responses viz. sway, yaw and roll motion of spar hull are trivial, they are not assessed in this study. Detailed evaluation explicitly explains the Spar-mooring system responses due to coupled analysis, coping with the nonlinearities.

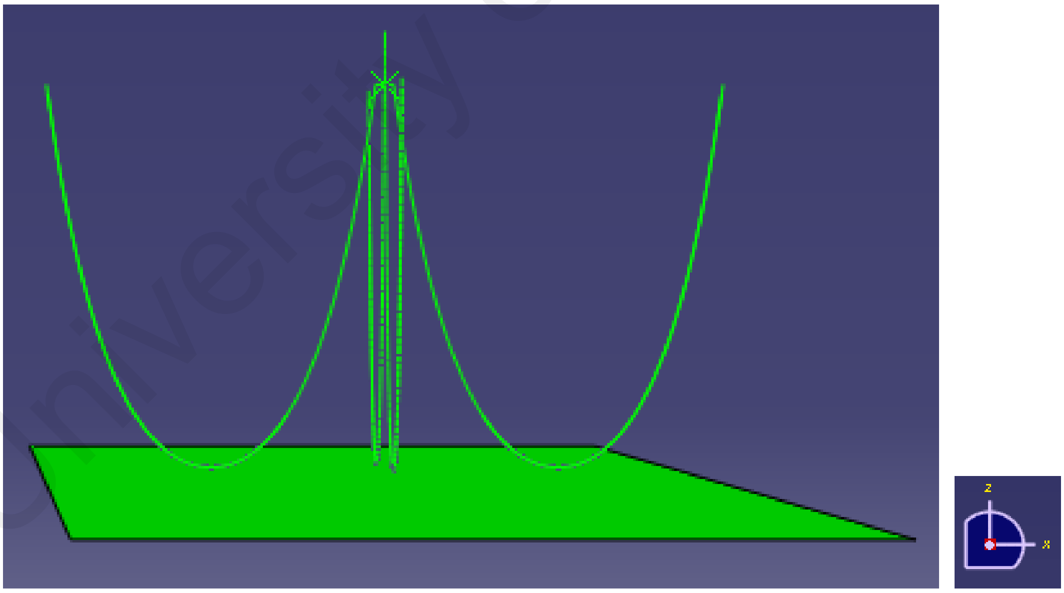

Figure 4.8: Deformed shape of mooring with spar due to its gravity load

4.4.1. Static analysis

Determining the static equilibrium configuration of the floating system is the first challenge in coupled analysis and needs to be accomplished before turning to the dynamic analysis. In this study, the coupled action of deformable mooring to rigid hull has been attained using the FE solver. Due to the ideal modelling, it would not be unusual for the complex solution including nonlinearities to experience difficulty in convergence. However, despite the complexities, forces and moments were seen to converge well. Static analysis was performed from step 1 to until step 4 of the NONLIN-COUPLE6D simulation. The step-wise procedure has been discussed in the previous chapter. Component connector problem is resolved in step 1 through required number of iterations and then convergence is achieved. Only gravity load of mooring line is considered in this stage (Figure 4.8).

In the subsequent stages, the mooring anchors to the sea and achieves the required pretension through step 2 and step 3 respectively. In both the phases, convergence is accomplished in a reliable manner. Once all the structural loadings are applied, the static analysis yields a solution showing the stability of the structure at step 4. Figure 4.9 shows this stable configuration of the moored platform. In all the steps, projected nonlinearities have been duly included.

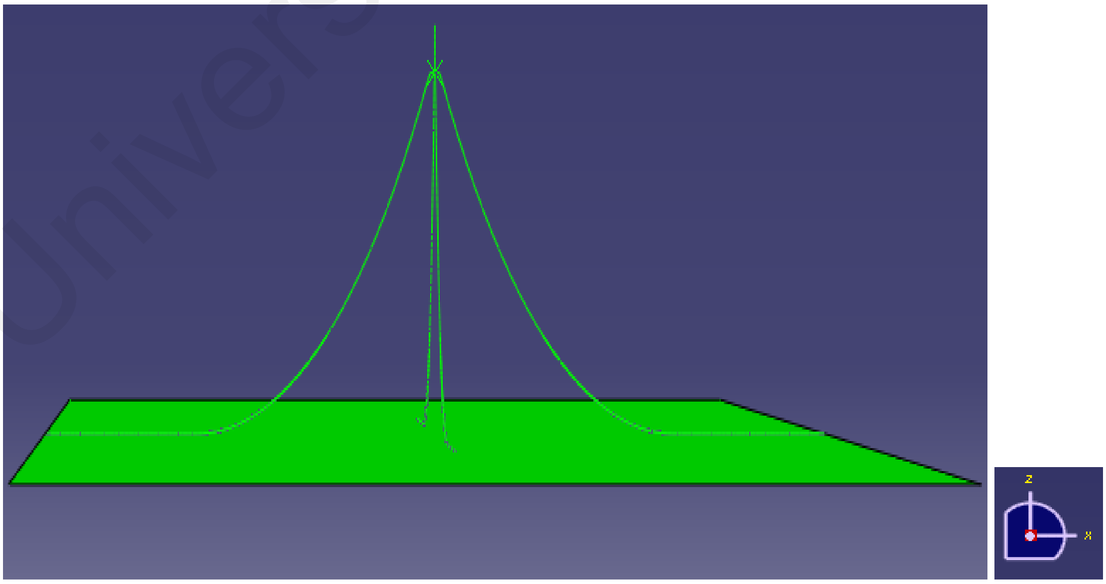

Figure 4.9: Stable Spar-mooring under total structural load through static analysis

4.4.2. Free vibration analysis

In the course of free vibration analysis, Lanczos algorithm has been incorporated to achieve the natural frequencies and respective mode shapes. These frequencies are used to analyse the nonlinear dynamic response of the Spar platform. Mode shapes in the post processing module of finite element code show the trends in the inclusive coupled Spar response. First twenty four mode shapes in ABAQUS/AQUA module have been shown in the subsequent Table 4.5 along with their corresponding frequencies.

Table 4.5: Natural frequencies of present coupled Spar-mooring system

Mode number	Frequency (rad/sec)	Frequency (cycles/sec)
1	1.836E-02	2.92421E-03
2	1.836E-02	2.92421E-03
3	2.078E-02	3.30844E-03
4	2.314E-02	3.68541E-03
5	1.444E-01	2.29954E-02
6	1.445E-01	2.30057E-02
7	1.447E-01	2.30432E-02
8	1.447E-01	2.30432E-02
9	2.778E-01	4.42367E-02
10	2.778E-01	4.42422E-02
11	2.780E-01	4.42625E-02
12	2.780E-01	4.42625E-02
13	3.708E-01	5.90463E-02
14	3.709E-01	5.90635E-02
15	3.709E-01	5.90638E-02
16	3.712E-01	5.91097E-02
17	4.162E-01	6.62753E-02
18	4.162E-01	6.62790E-02
19	4.163E-01	6.62928E-02
20	4.163E-01	6.62930E-02
21	5.544E-01	8.8210E-02
22	5.544E-01	8.8210E-02
23	5.544E-01	8.8210E-02
24	5.544E-01	8.8210E-02

4.4.3. Coupled dynamic analysis in time domain

The solution of the physically coupled dynamic equations in time domain adopting a non-linear integration scheme ensures consistent treatment of spar-mooring system coupling effects. The platform load model accounts for the mass, hydrostatic stiffness, time dependent added mass and damping as well as excitation from environmental forces on the cylindrical hull. Simulations of long duration histories have been employed to acquire extreme response estimates with other statistical values. The perception of FE has been truthfully implemented to establish coupled models of systems with floating Spar connected with mooring lines. Hydrodynamic interaction among the floater-mooring is accounted for subjecting wave forces on the platform. In the automatic time incremental scheme, the time interval (Δt) is selected ensuring stability and accuracy of the solution. This time increment is influenced by Spar platform time periods in different degrees of freedom as well as wave periods. Throughout the studies, stiffness matrices are updated at every time step to incorporate the changes in stiffness due to large deformation, instantaneous mooring tension etc. Subsequent sections describe detailed evaluations of time domain responses of spar and mooring lines.

4.5 Coupled dynamic response for short and long duration of wave loading

The fully coupled responses of Spar platform and mooring lines in deep water conditions have been investigated for 1 and 3 hours of wave excitation. The results are obtained for wide-range of loading time (12000 sec). The responses are plotted for duration of 3000 to 4000 sec. and 11000 to 11800 sec wave loading. To deal the analysis the Spar-mooring system has been subjected to large wave (LW) as chosen by experimental study of Ran et al. (1996). The sea state LW-W comprises regular wave of 6m wave height and 14 second wave period. Comparative evaluation for surge, heave and pitch motion responses has been carried out in terms of time history and power spectrum. The excursions obtained from the coupled analysis have been outlined in terms of surge, heave and pitch motion in Figures 4.10~4.21 [Figures 4.10~4.13 for surge, Figures 4.14~4.17 for heave, Figures 4.18~4.21 for pitch] and Figures 4.22~4.29 for mooring line tension. The other three degrees of freedoms viz. sway, yaw and roll show trivial values and thus the present study does not demonstrate those motions. Both the time histories and motion spectra are presented through corresponding figures. Statistical analysis results in terms of maxima, minima, mean and standard deviation are given in Table 4.6 & Table 4.7 for 1 hour and 3 hour of wave excitation respectively.

4.5.1. Surge response

The time history of surge motion response after 1 hour of wave excitation at the deck level is shown in Figure 4.10. The peak of surge response ranges from +16.194 m to -13.658 m (Table 4.6). The pattern of surge motion at the deck level is largely periodic. For this reason, a solitary governing peak occurs in surge response at pitching frequency (Figure 4.11). The pitch motion (Figure 4.18) occurs concurrently with surge motion and attracts momentous wave energy not far off the pitch frequency.

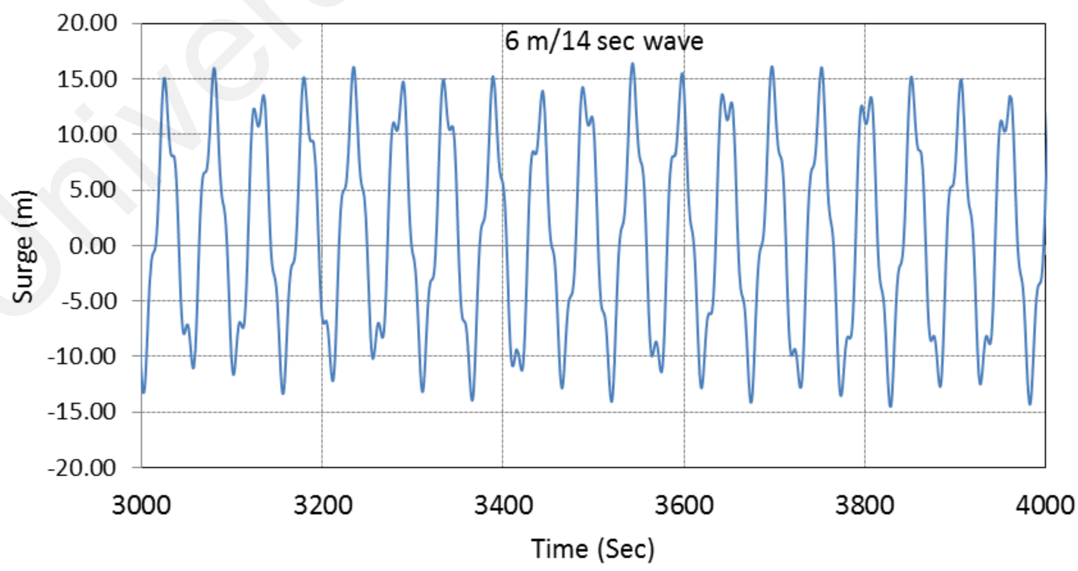

Figure 4.10: Surge time history after 1 hour of wave action

Surge response requires huge energy input because of large inertia and hence does not get excited. However, pitching motion occurring with surge gets excited easily. The surge response at the deck level is mainly dominated by the pitching motion of the hull with insignificant excitation of surge mode. It is mainly due to coupling of surge and pitch. The power spectrum as shown in Figure 4.11 shows the involvement of two frequencies.

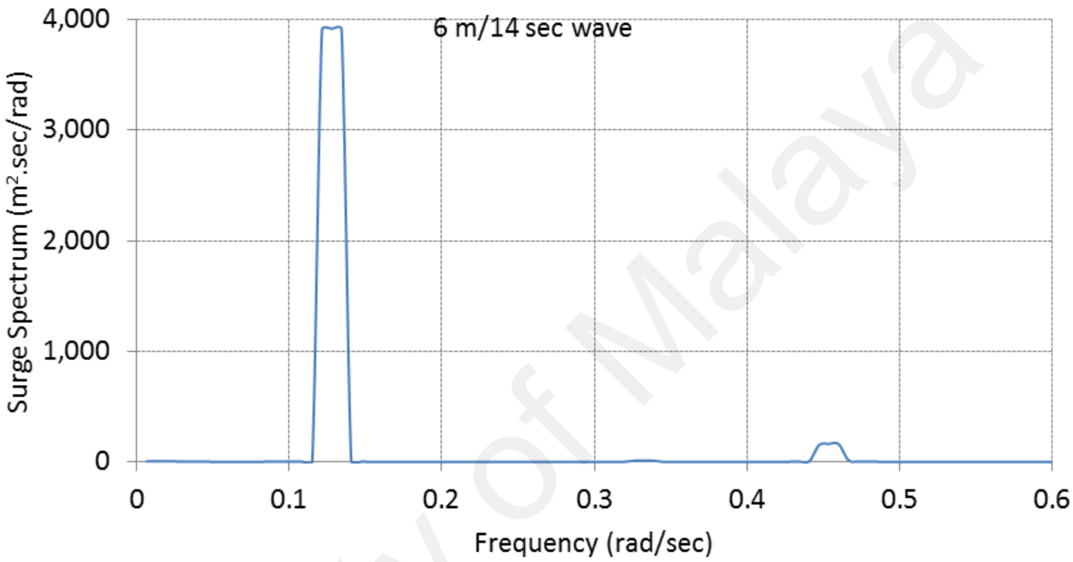

Figure 4.11: Power spectrum of surge after 1 hour of wave action

The small oscillation of harmonic response occurs at a frequency of 0.465 rad/sec, which is frequency of wave loading. Exciting of pitch motion on surge response in short duration causes such little involvement of wave frequency. There is no evidence of any significant involvement of other frequencies. Effect of non-linearity is not very strong on surge motion.

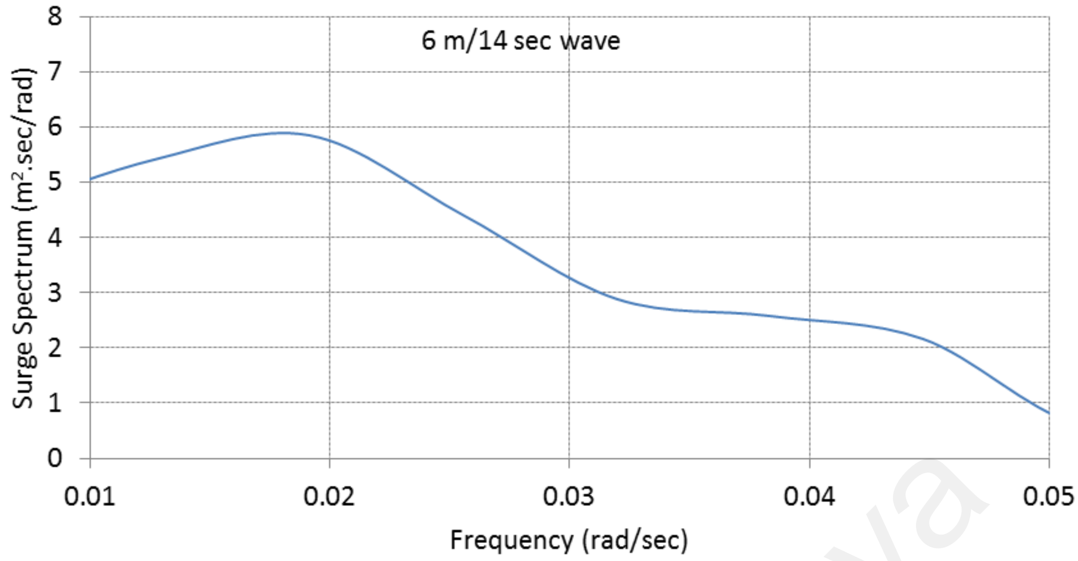

Figure 4.11a: Low frequency (LF) surge behaviour after 1 hour of wave loading

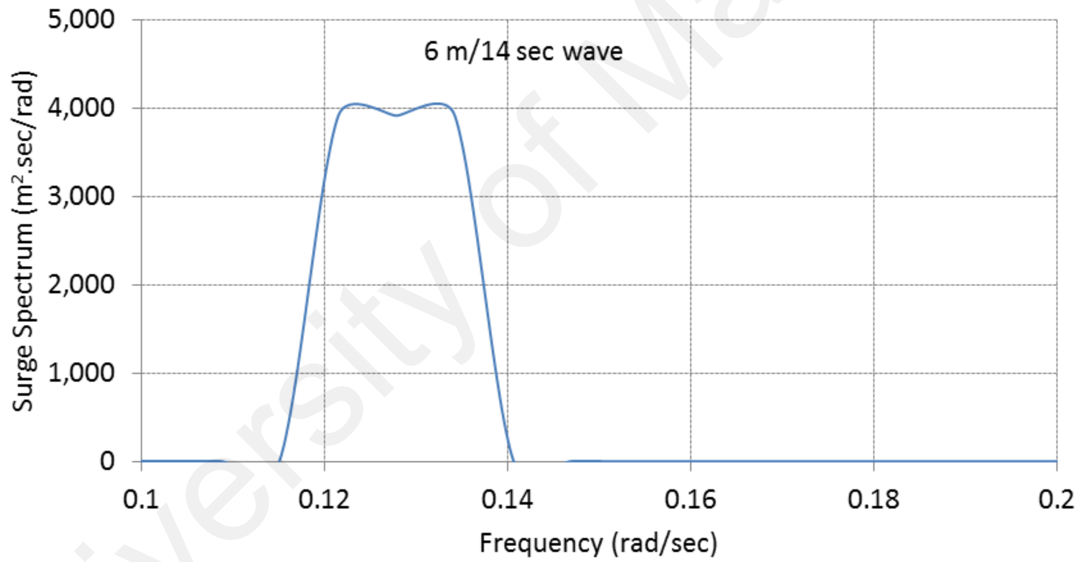

Figure 4.11b: High frequency (HF) surge behaviour after 1 hour of wave loading

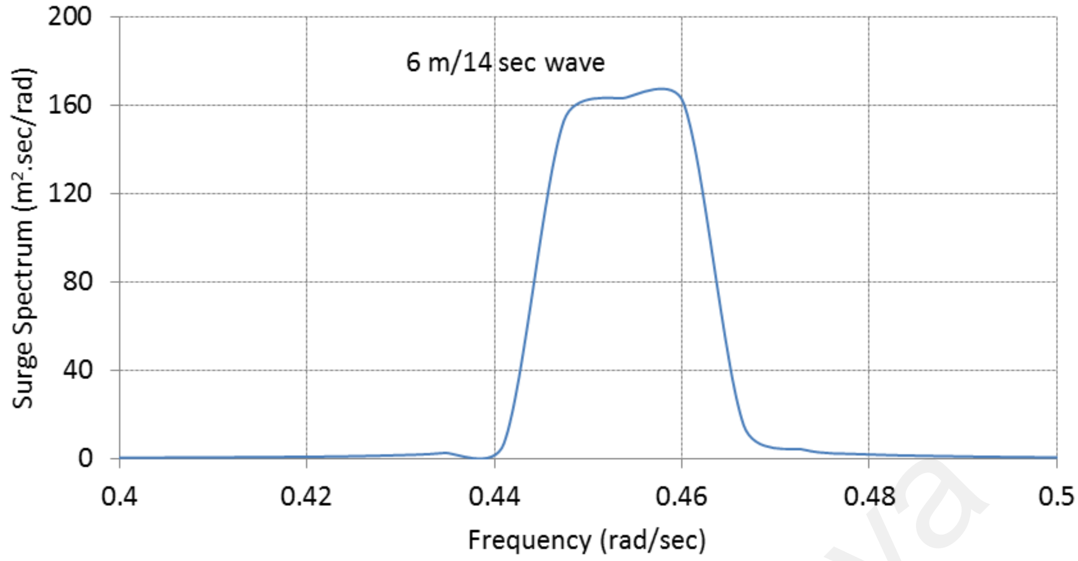

Figure 4.11c: Wave frequency (WF) surge behaviour after 1 hour of wave loading

The power spectra of surge have been shown showing participation of low frequency, high frequency, wave frequency for 1 hour wave loading of large wave at deck level in Figures 4.11a, 4.11b and 4.11c respectively. The involvement of surge frequency and wave frequency is seen in Figures 4.11a and 4.11c. During this time period, surge at platform level is dominated in coupled pitch is also shown in Jameel (2008).

Table 4.6: Statistical analysis results of responses after 1 hour of wave action

Spar motion	Max	Min	Mean	Standard deviation
Surge (m)	16.194	-13.658	1.038	8.663
Heave m)	2.374	-1.981	0.352	1.149
Pitch (rad.)	0.121	-0.122	0.0001	0.074

The time history of surge motion after 3 hours of storm showed a typical regular behaviour as is seen in Figure 4.12. The platform oscillates in regular fashion with maximum and minimum values of +6.431and -6.196 m respectively.

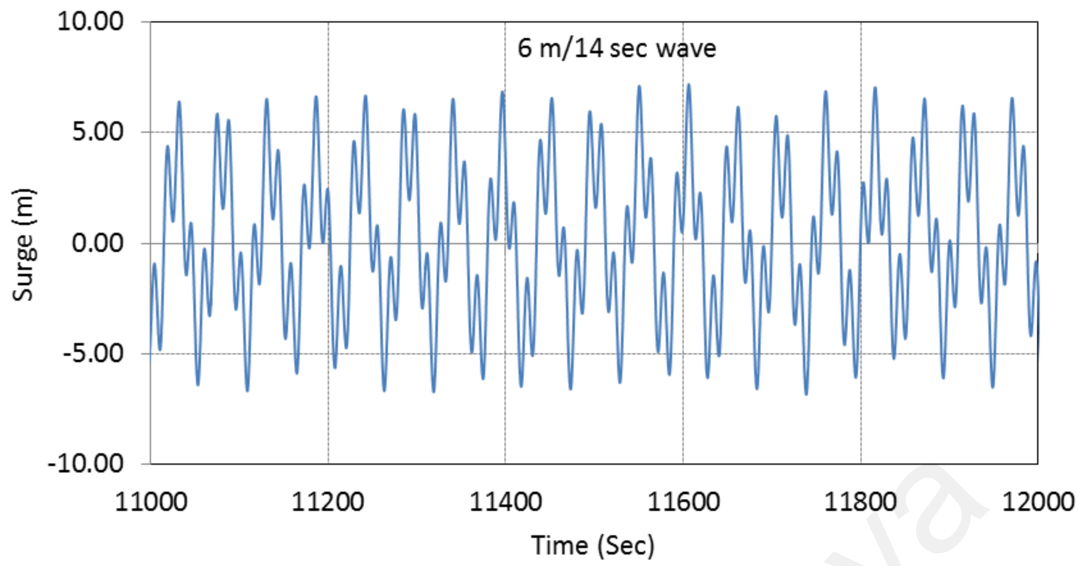

Figure 4.12: Surge time history after 3 hours of wave action

The mean value of surge is given by 0.148 m whereas the standard deviation is found to be 3.568. On comparison of statistics with the surge response in regular wave (Table 4.7), the above trend is established.

Table 4.7: Statistical analysis results of responses after 3 hours of wave action

Spar motion	**Max**	**Min**	**Mean**	**Standard deviation**
Surge (m)	6.431	-6.196	0.148	3.568
Heave m)	1.149	-0.794	0.299	0.423
Pitch (rad.)	0.051	-0.047	0.0000	0.028

The Power spectrum of the surge time history at 3 hours plus time state shows two distinct peaks (Figure 4.13) at 0.121 rad/sec and 0.44 rad/sec. These peaks correspond to frequencies of pitch and wave respectively. It is seen that the magnitude of the spectrum are reduced substantially at 3 hours of wave action at both pitch and wave frequency. This is because of achieving huge energy at 1 hour of runtime, whereas there is a huge reduction of energy for 3 hours' of wave loading caused by damping of mooring line.

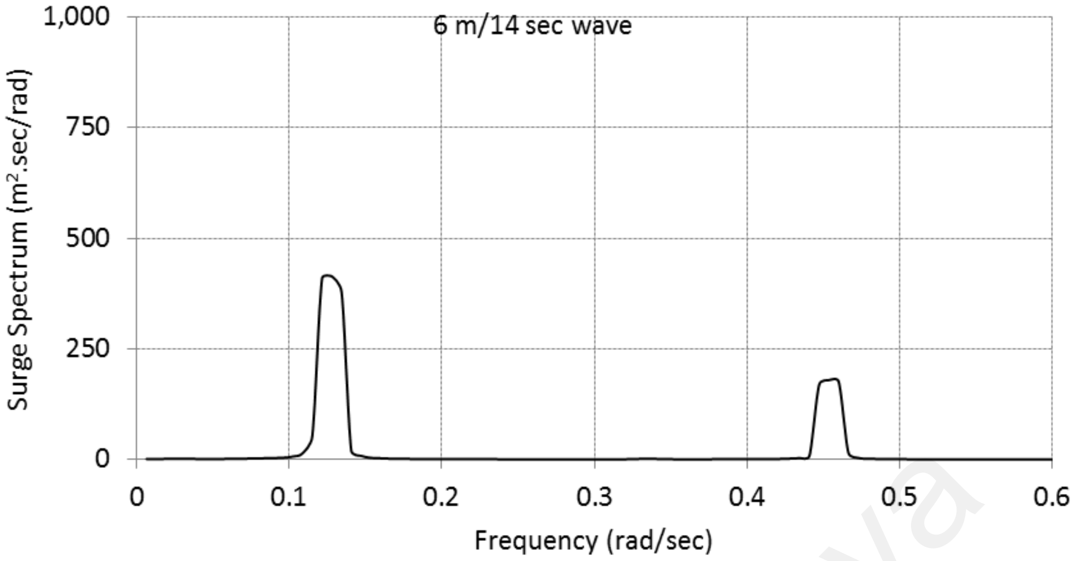

Figure 4.13: Power spectrum of surge after 3 hours of wave action

4.5.2. Heave response

Heave response directly influences the mooring tensions and other operations. The heave responses under regular wave are shown in Figure 4.14. The time history shows the cluster of reversals occurring at varying time intervals. The phenomenon shows regularity in the behaviour. Table 4.6 shows the maximum and minimum responses as 2.374 m and – 1.981 m, while the mean value is 0.352. The heave response fluctuates about the mean position oscillating from smaller to larger heights and repeating the same trend onwards all through the time history as shown in the Figure. The fluctuations gradually increase from narrow to broad by 30 %. Reaching the peak, they gradually reduce by 30 %.

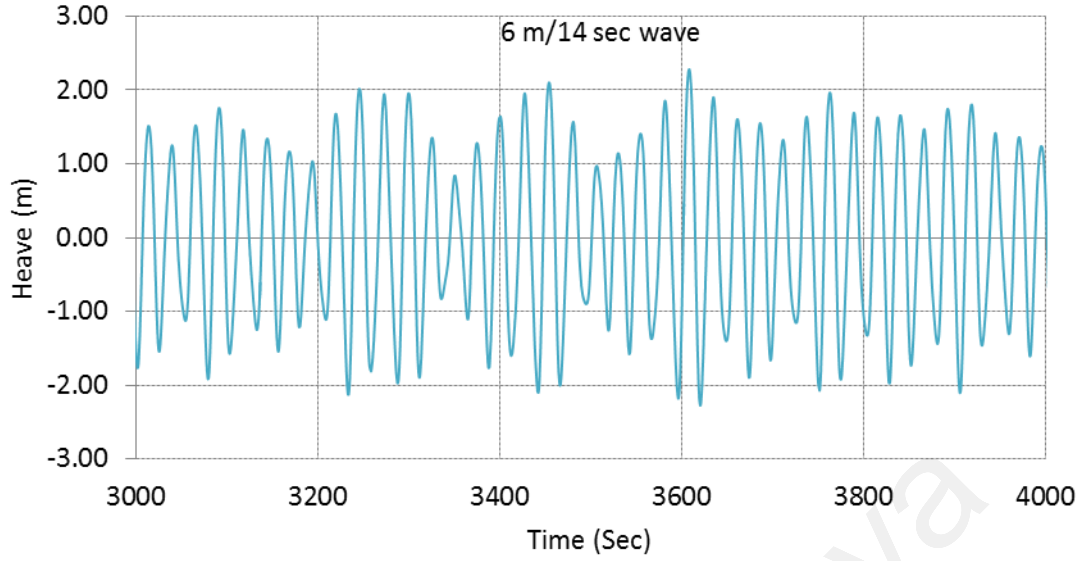

Figure 4.14: Heave time history after 1 hour of wave action

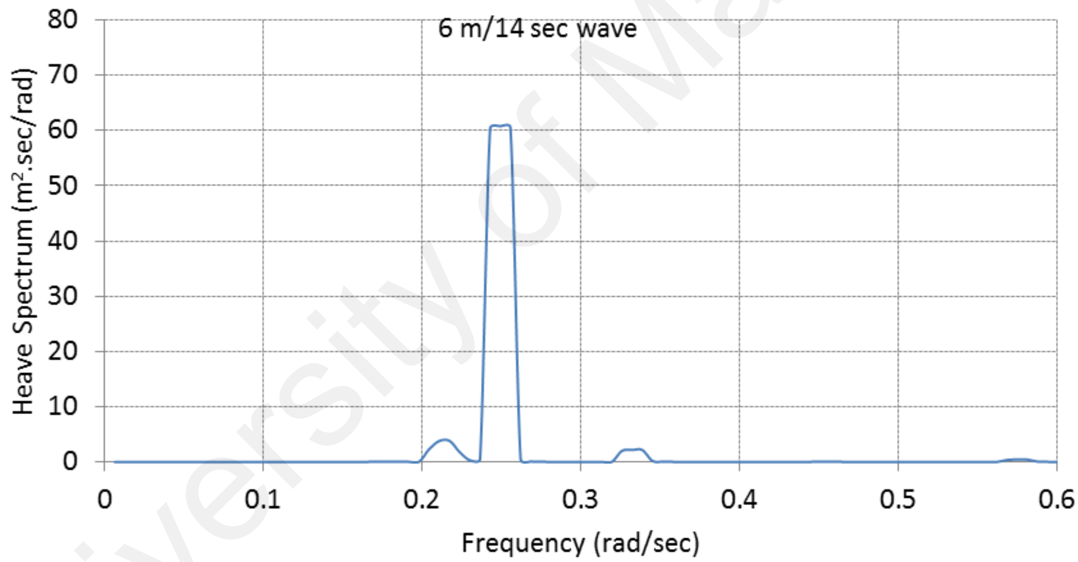

Figure 4.15: Power spectrum of heave after 1 hour of wave action

The response is periodic in nature with superimposed ripples. The local fluctuations near the peaks in the time history are seen to be small in heave motion. The power spectrum of heave response shows a prominent peak at 0.243 rad/sec. The peak is nearby the natural frequency of heave while other peaks (Figure 4.15) have very small energy content. Such peaks may, however, attract more energy at some other sea state occurring in that region.

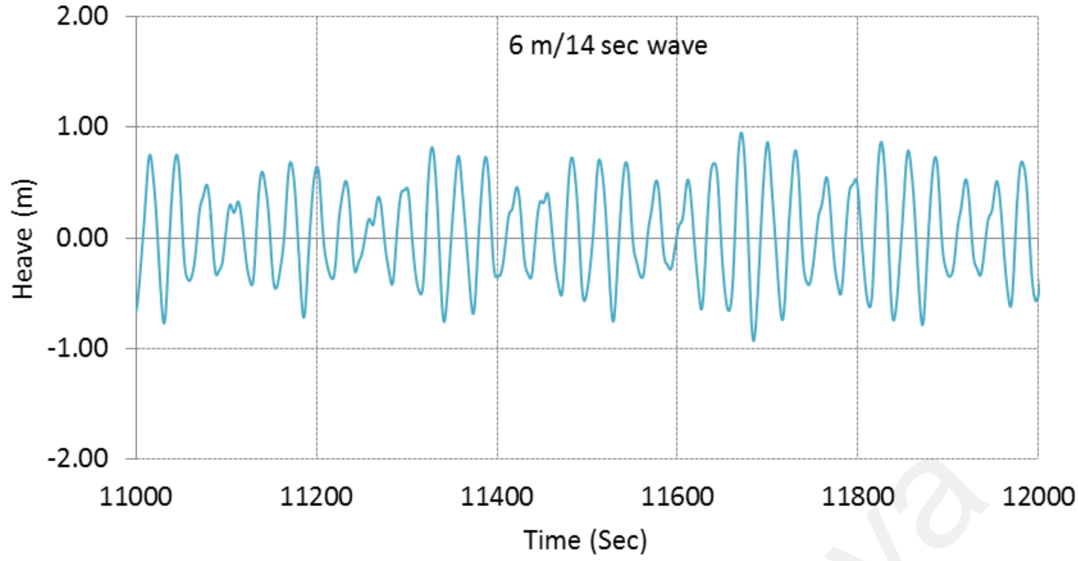

Figure 4.16: Heave time history after 3 hours of wave action

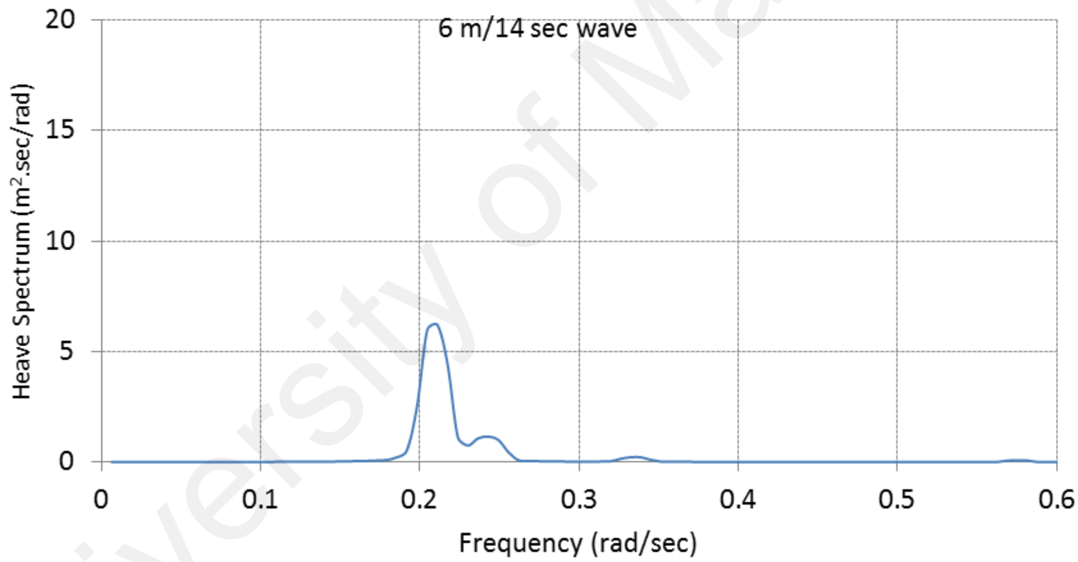

Figure 4.17: Power spectrum of heave after 3 hour of wave action

It is clearly identified that after 3 hours of wave action the maximum heave response in presence of regular wave reduces by approximately 50 %. The heave time history in Figure 4.16 shows the beating phenomenon. The power spectrum in Figure 4.17 shows a solitary peak at natural frequency of heave. But the peak is drastically reduced up to more than 15 times causing a very low magnitude. The damping in mooring lines induces huge reduction of energy progressively which influences such lessening in heave for longer duration of wave loading.

4.5.3. Pitch response

The pitch response after 1 hour time period is shown in Figure 4.18. The time history shows regular fluctuations ranging from ± 0.112 rad. and reducing to small ordinates of ± 0.09 rad. at time station 3130 sec. It takes the energy and further increases to $\pm$ 0.11 rad. Table 4.6 shows maximum positive and negative pitch values of +0.121 and -0.122 rad. The mean value is almost zero and the standard deviation is 0.074 radians. The mean value of zero shows its regular oscillations about the mean position.

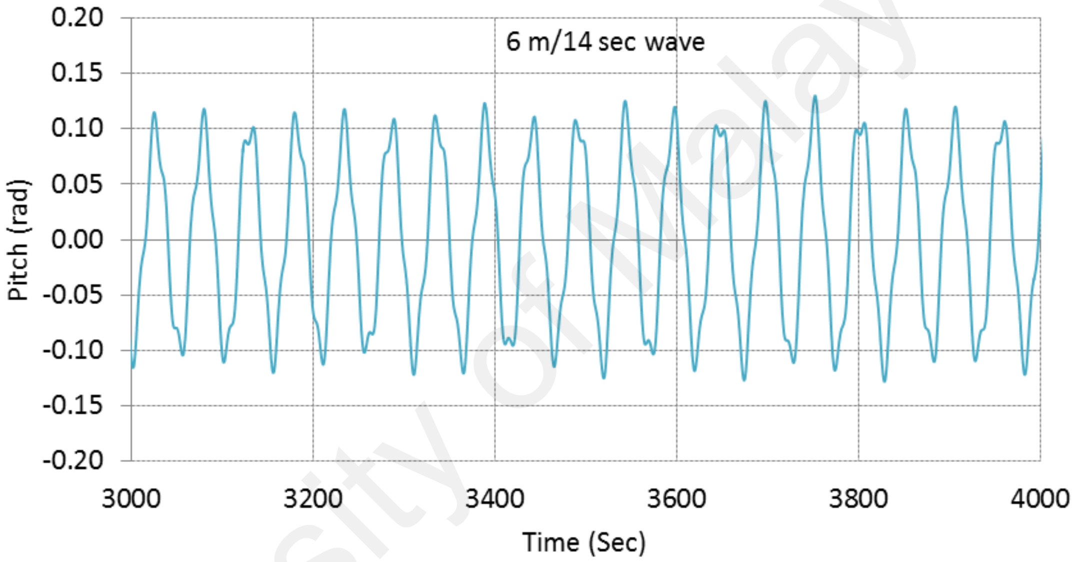

Figure 4.18: Pitch time history after 1 hour of wave action

The significant value of pitch response leads to a substantial surge at deck level. It is coupled with the surge of rigid hull which otherwise is of small magnitude but gets enhanced due to pitch input. This is why the surge time history at deck level shows maximum peak at pitch frequency (Figure 4.11). The pitch time history shows similar behaviour. The periodic response oscillates at frequency of 0.118 rad/sec about the mean position. It is the pitch frequency response. As the pitch drives its force from the wave, participation of another frequency 0.427 rad/sec. is quite close to the wave frequency. However, the energy content at low frequency wave is very trivial.

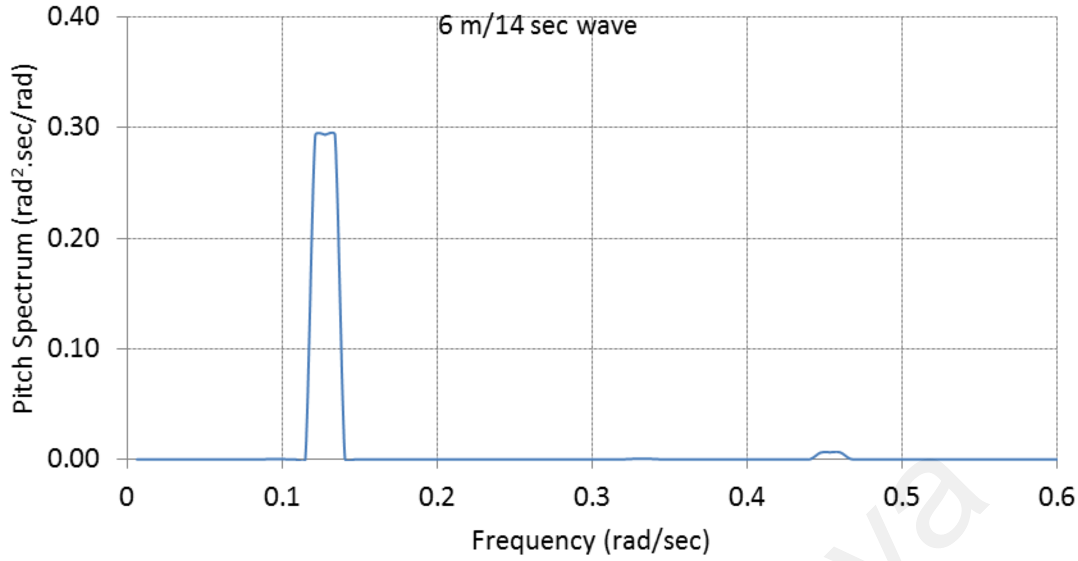

Figure 4.19: Power spectrum of pitch after 1 hour of wave action

Figure 4.20 shows the pitch time history under regular wave after 3 hours of storm. The pitch response after 3 hours gets significantly modified in comparison to the case with 1 hour wave excitation. Pitching motion is regularly distributed about the mean position. Maximum and minimum values of pitch responses are reduced 3 times in comparison to the case with 1 hour time. Damping due to long mooring lines causes a gradual reduction in pitch response.

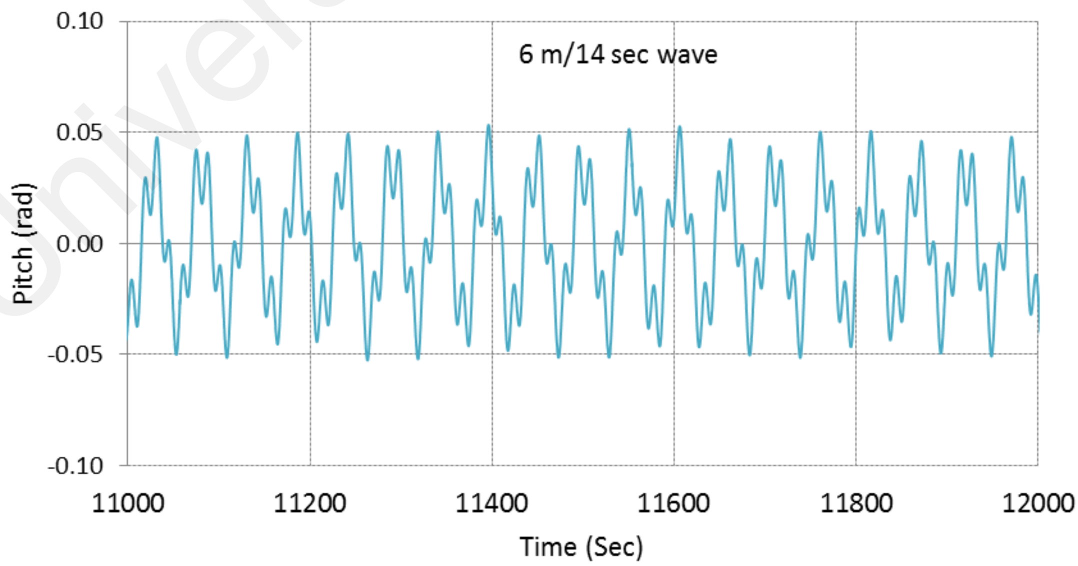

Figure 4.20: Pitch time history after 3 hours of wave action

The Power spectrum of pitch as shown in Figure 4.21 confirms the regular pitch behaviour. The first peak occurs at 0.12 rad/sec close by the pitch natural frequency while the other peak occurs at 0.45 rad/sec which is the dominant wave loading. The energy content of Power spectrum is, however, significantly small in comparison to that with 1 hour (Figure 4.19). The reduction is approximately 10 times.

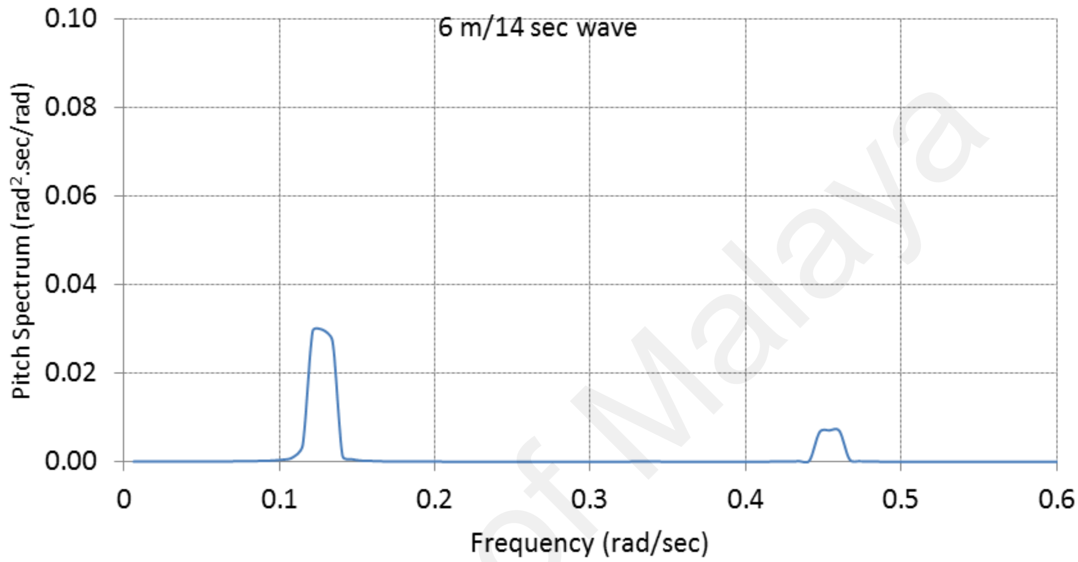

Figure 4.21: Power spectrum of pitch after 3 hours of wave action

4.5.4. Mooring line tension response

The response of mooring lines plays an imperative part in the coupled dynamic analysis of the Spar Platform. Top nodes of catenary mooring lines linked with the Spar hull fairlead experience maximum horizontal forces. In the present finite element model, the wave loading concurrently acts on the rigid hull and deformable mooring lines. The nonlinear analysis of this moored spar yields a consistent coupled response. Mooring line 1 (CML1) and 3 (CML3) are positioned in the direction of wave propagation. As other two mooring lines (CML2 and CML4) are connected in orthogonal direction of wave, these lines get less excited than CML1 and CML3. Therefore, in the sway path, the evaluation of the tension of these two lines is bypassed because of smaller amount of top tension.

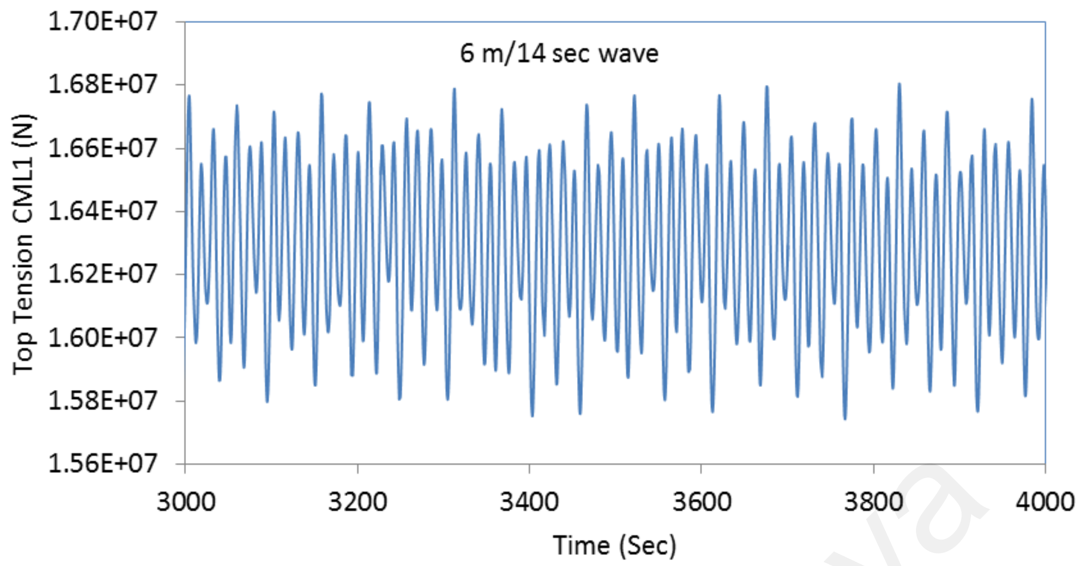

Figure 4.22: Top tension time history of CML1 after 1 hour of wave action

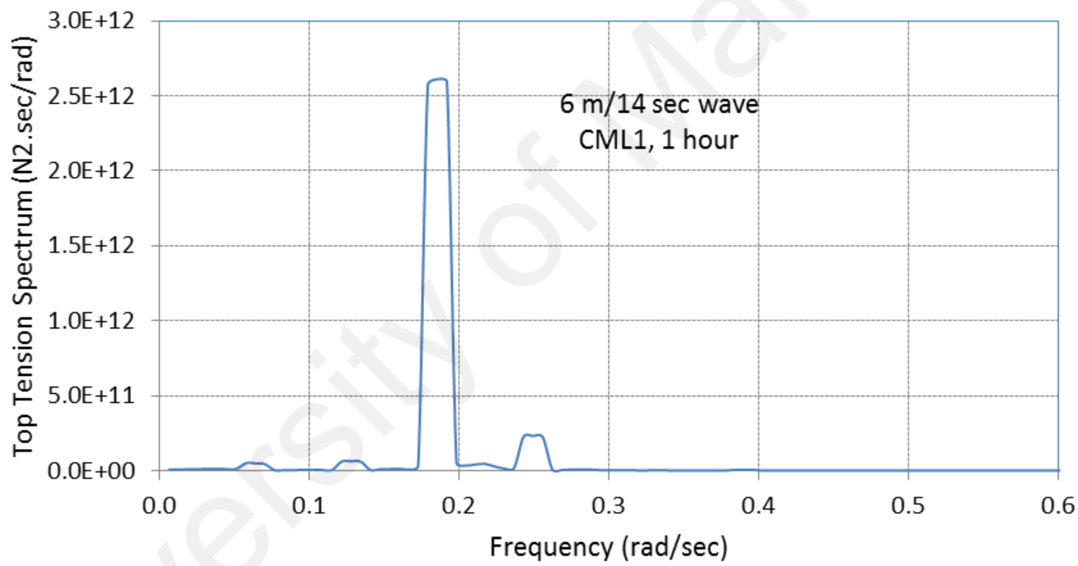

Figure 4.23: Response Spectrum of top tension at CML1 after 1 hour of wave action

The designed pretension in each mooring line of the present problem is 1.625E+07 N (Table 4.2). Mooring line 1 experiences maximum top tension to support surge in the forward direction, while mooring line 3 slackens resulting in the reduction of pretension. Regular behaviour of tension after 1 hour of storm is shown in mooring line 1 (Figure 4.22). The Power spectrum of the line tension is shown in Figure 4.23. At the pitch frequency a small peak of energy gaining is observed. A greater peak is also witnessed at heave frequency. However, among the several peaks, the maximum crest happens approximately at 0.18 rad/sec. which is lower than the heave frequency but larger than the frequency of pitch. This clearly shows the behaviour change in mooring tension due to heave-pitch coupling.

Table 4.8: Statistics of Top Tension in mooring lines after 1 hour of wave action

Parameters (W_H **=6m,** W_P**=14s)**	Rating at 1 hour			
	Max	Min	Mean	Standard deviation
Top Tension in CML1 (N)	1.68E+07	1.58E+07	1.63E+07	2.51E+05
Top Tension in CML3 (N)	1.68E+07	1.57E+07	1.62E+07	2.48E+05

It is expected that heave will significantly influence the mooring tension response. A small peak also occurs, exciting the low frequency surge response. Surge response also causes increase in tension. Other peaks occurring at 0.22 to 0.26 rad/sec are small, but may get excited under other sea states. The statistics show the maximum and minimum values as 1.681E+07 N and 1.583E+07 N respectively in mooring line 1 (Table 4.8).

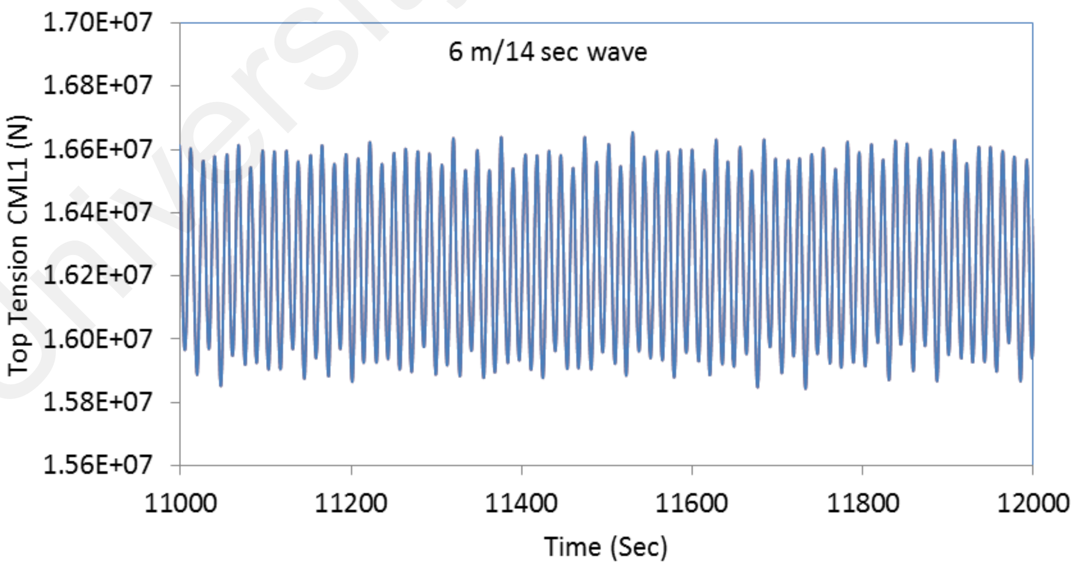

Figure 4.24: Top tension time history of CML1 after 3 hours of wave action

Behaviour of coupled Spar mooring system changes slightly when 3 hours wave loading is considered. It is expected more in case of huge time duration when mooring line is affected with damping. Top tension time history in mooring line 1 is shown in Figure 4.24. Regular oscillations are taking place about the mean value of 1.626E+07 N. The maximum and minimum values of tensions are 1.662E+07 N and 1.581E+07 N, which are less than that at 1 hour time (Table 4.9). Fluctuation of the time history is also less in case of 3 hours of storm. The Power Spectrum (Figure 4.25) shows clearly a prominent single peak at 0.45 rad/sec that is quite different from the 1 hour wave loading condition seen earlier. This frequency is 2.5 times more than that at 1 hour wave excitation and resembles to the wave frequency. For 1 hour the major peak occurs at pitch frequency whereas for 3 hours it occurs at wave frequency (Figure 4.23). It is because the damping effect is active in heave motion for longer time. The surge also contributes to the response but with a small magnitude. Moreover, due to position of mooring line, the peak frequency in spectrum evidently changes to wave frequency.

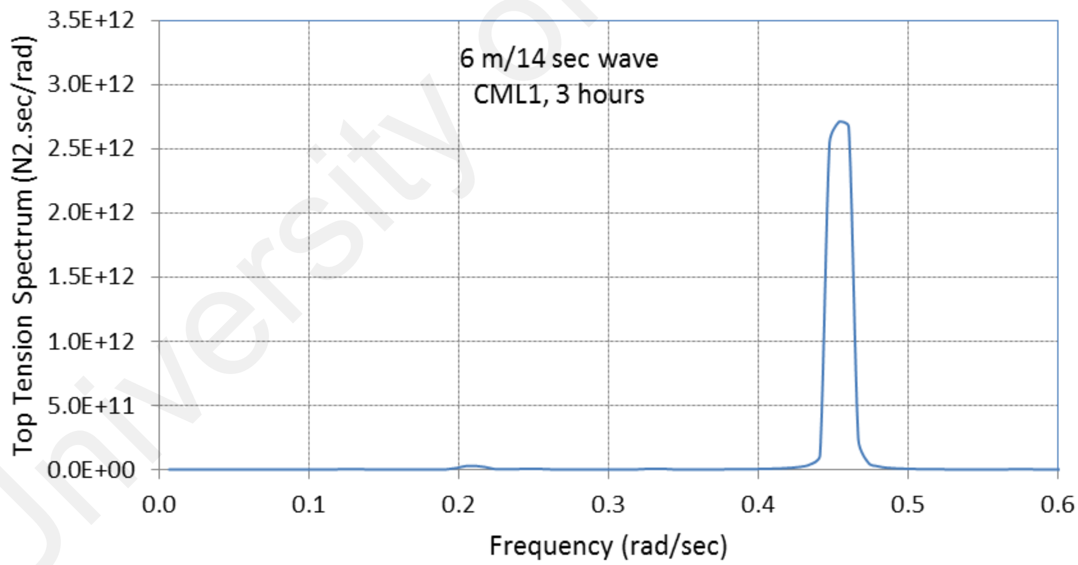

Figure 4.25: Power Spectrum of top tension at CML1 after 3 hours of wave action

Mooring line 3 positioned in the direction of wave propagation slackens resulting in lessening of mooring pretension. Figure 4.22 and Figure 4.26 show the tension fluctuations at 1 hour wave loading when mooring line 1 stretches and mooring line 3 slackens due to surge motion respectively. It is noticed that the tension time history of mooring line 3 is also regular in nature, which is important from fatigue view point. However, there are slight fluctuations in magnitude. Tension fluctuation is of complex periodic nature showing minor ripples near the peaks. For both of these mooring lines at the regular wave, periodic behaviour is observed.

Table 4.9: Statistics of Top Tension in mooring lines after 3 hours of wave action

Parameters (W_H =6m, W_P=14s)	Response at 3 hours			
	Max	Min	Mean	Standard deviation
Top Tension in CML1 (N)	1.66E+07	1.58E+07	1.63E+07	2.34E+05
Top Tension in CML3 (N)	1.67E+07	1.59E+07	1.62E+07	2.34E+05

The major peak frequency as shown in power spectrum matches with the same. The slack mooring line 3 remains in catenary shape with the reduction in tension. Figure 4.26 shows the major peak at the wave frequency. Both the spectrum of CML1 and CML3 show minor peak at pitch frequency. The response also shows a distinct low frequency peak (0.258 rad/sec) close to the natural frequency of heave as shown in Figure 4.27. On this low frequency fluctuation a periodic oscillation at the frequency close to the wave frequency is superimposed. The low frequency response in mooring line 1 and 3 is important as it attracts significant energy. However, the crest in heave frequency of CML3 is slightly greater than that of CML1. This may happen as energy is transferred alternately from pitch to heave motion.

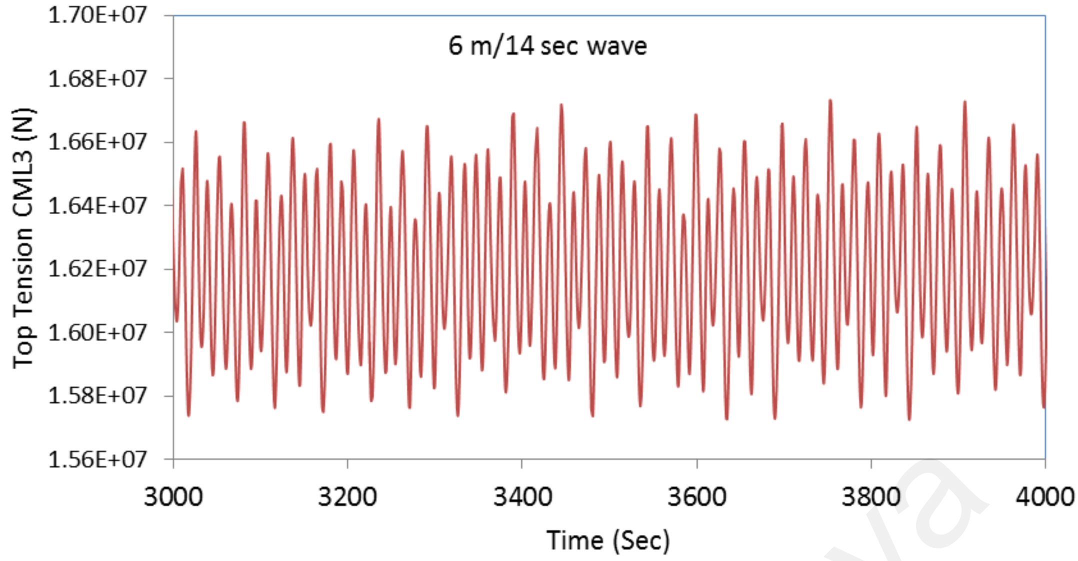

Figure 4.26: Top tension time history of CML3 after 1 hour of wave action

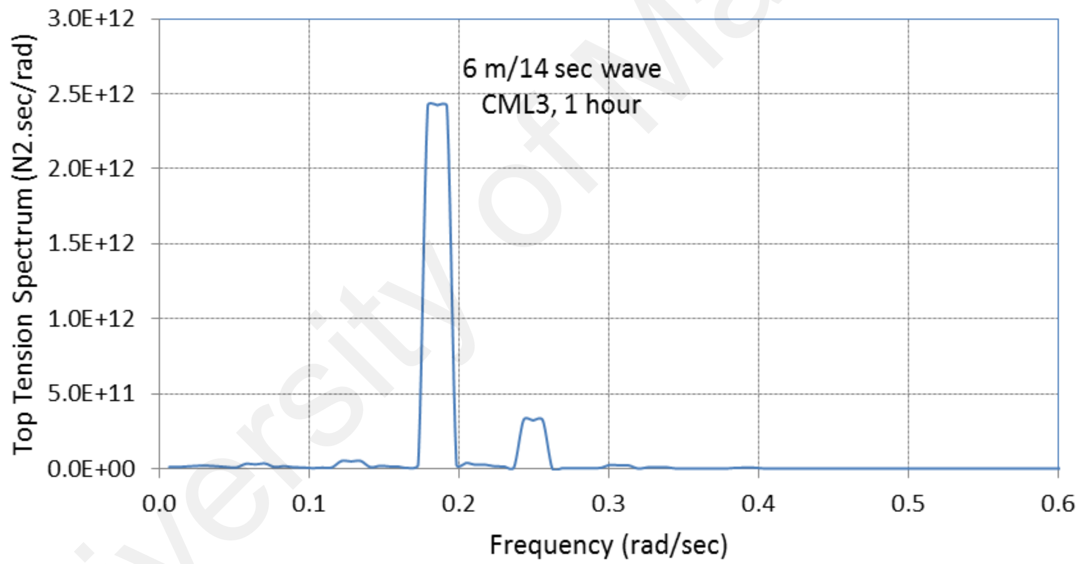

Figure 4.27: Power Spectrum of top tension at CML3 after 1 hour of wave action

Because of heave-pitch coupling the maximum peak occurs at approximately 0.18 rad/sec (Figure 4.27) at the middle of heave and pitch frequency. The peak in case of CML3 is less as the mooring line experiences slightly lesser impact of wave than CML1 owing to its position. Wave frequency response too is quite substantial and should duly be considered. There are very small peaks at several other frequencies whose magnitude is negligible. However, the presence of such peaks shows the tendency of excitation due to changes in mooring line characteristics and forcing behaviour. The non-linear behaviour may also lead to sub and super harmonic resonance. While designing the mooring lines this behaviour should not be ignored.

The time history of mooring line 3 under regular wave shows a damped response of regular nature. The statistics for mooring line 3 show maxima, minima and mean of 1.665E+07 N, 1.585E+07 N, and 1.623E+07 N respectively (Table 4.9). However, for the case of wave at 1 hour plus time the maxima, minima and mean are 1.679E+07 N, 1.574E+07 N and 1.622E+07 N respectively as shown in Table 4.8. The response is damped out with no further increment because of the lateral position of mooring line 3. The tension time history of mooring line 3 under regular wave at 3 hours plus time state shows the mean value smaller than the pretension. Likewise, the maximum value of tension is also smaller in comparison to that in case of response at 1 hour wave excitation. However, the record of minimum magnitude is slightly larger.

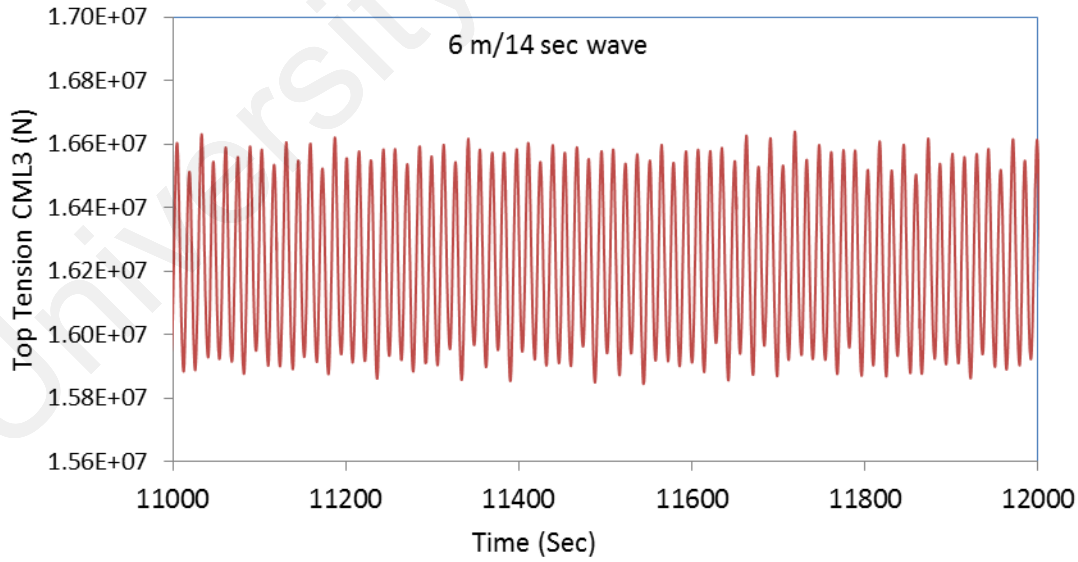

Figure 4.28: Top tension time history of CML3 after 3 hours of wave action

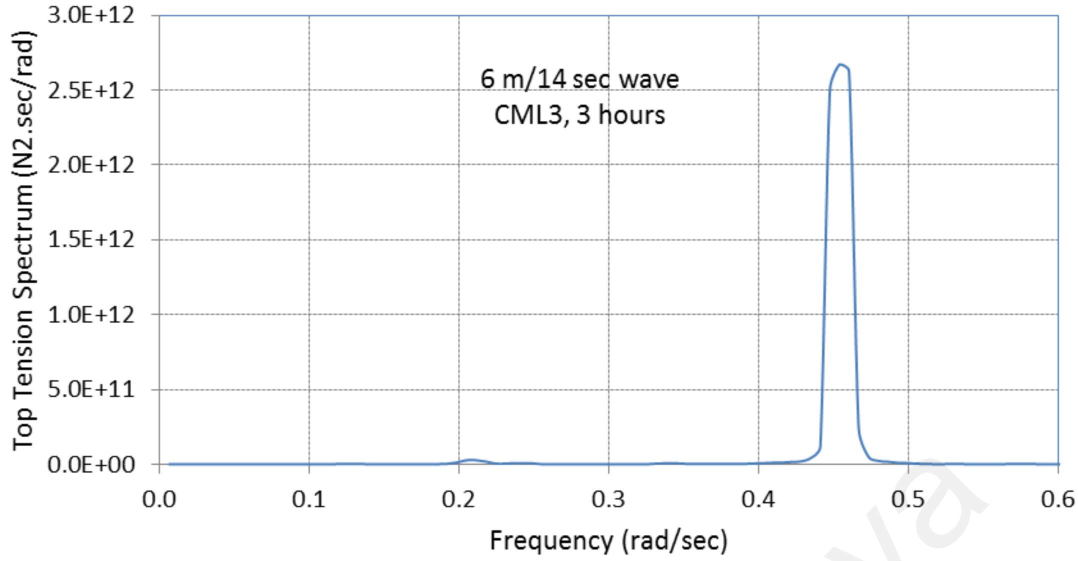

Figure 4.29: Power Spectrum of top tension at CML 3 after 3 hours of wave action

Though the mean tension trend in mooring line 3 increments very slightly, it can be regarded as matching in both cases. Deviation of the tension is still higher in case of 1 hour wave loading. The power spectrum of CML3 tension (Figure 4.29) shows an obvious major single peak at 0.45 rad/sec that is quite different from the 1 hour time condition shown earlier. The value of tension in this frequency is slightly lower than that of the 1 hour wave loading condition. This slight reduction of tension is expected because of the slacking of mooring line 3 at 3 hours wave loading. Response at heave frequency is damped and wave frequency is dominating top tension at longer time.

It is noted that the mooring lines are very long which induces huge damping on the coupled system leading to decrease the platform responses. Numerical damping may arise in interface of one element with another in coupled action but in high frequency. However

1) For Spar platform responses, numerical damping is trivial as its effect on responses is proportional to 1/frequency^2.

2) Present code controls the numerical damping with coefficient -0.05 as maximum 5% numerical damping (ABAQUS, 2009) can arise in coupled action.
3) If numerical damping would vital in the present simulation, the analyses would face convergence problem in solution. In the present case the analysis could be done up to a record length of 18000 seconds with excellent convergence in solution.

The insignificance of numerical damping and the experimental validation also ensures the authenticity of the obtained result.

4.6 Coupled dynamic responses under quartering sea wave loading

It is of great interest to explore the structural coupled responses of the integrated Spar-mooring system whenever the wave forces act at certain angle with the current flow. In this section wave of $\pi/4$ radian angle has been applied to the moored Spar. All the involved complexities as discussed earlier have been considered in the coupled dynamic analysis. Wave height and wave period are chosen as the wave characteristics of sea state LW-W as per Ran et al. (1996). As quartering sea wave is selected the sea state is termed as LW-Wi. A long duration time histories have been obtained to evaluate critical Spar responses in six degrees of freedom motion. Surge, heave and pitch are compared by descriptive statistics for wave at 0 rad and quartering sea wave. Sway. Roll and yaw are evaluated for both the cases through time history and power spectral density function. Following sections discuss the detailed assessments of nonlinear responses of DDS hull and CMLs under the selected wave loadings.

4.6.1. Spar 6 DOF motions

Surge response under quartering sea wave

Wave loading at $\pi/4$ radian gives identical pattern of surge time history with decreased magnitude compared to wave at 0 rad. Similar to the non-quartering sea wave train, the surge response is largely dominated by the pitching motion of the Spar hull. This is induced by the coupling of surge and pitch. Long duration time histories of surge response subjected to wave at π/4 radian angle are compared at 10000-12000 seconds of run time. Table 4.10 shows the descriptive statistics of surge. The table shows the trend for maximum and minimum responses. Standard deviation is not widely varying for inclination of wave. It is seen that steady state surge response has peak value of around 6.52 m whereas the platform displaces around 6.57 m sway. Since the wave is acting at π/4 radian, the load is equally distributed in surge and sway. It also confirms that coupled Spar platform has been appropriately modelled in six degrees of freedom.

Table 4.10: Descriptive statistics of Surge-Sway in wave at 0 rad and quartering sea wave

Parameters	**Wave at 0 rad**		**Quartering sea wave**	
	Surge	**Sway**	**Surge**	**Sway**
Maximum (m)	7.92582	0.00	6.52035	6.57708
Minimum (m)	-7.47578	0.00	-6.42285	-6.57201
Mean (m)	0.113232	0.00	0.109364	-0.01861
Standard Error (m)	0.045426	0.00	0.042604	0.065963
Median (m)	0.06692	0.00	0.102234	-0.05646
Mode (m)	-1.15799	0.00	-1.0135	4.99416
Standard Deviation (m)	3.573668	0.00	3.188183	3.936194
Range (m)	15.4016	0.00	12.9432	13.14909
95.0% Confidence interval	-7.0341~7.2606	0.00	-6.2670~6.4857	-7.891~7.8538

Sway response under quartering sea wave

The maximum and minimum values of sway motion are found as ± 6.57 m (Figure 4.30 and Table 4.10). The roll motion occurring with the sway excites the platform to move orthogonally. Hence, it is noticed that the sway response is largely dominated by the rolling motion of the Spar hull. This is prompted by the coupling of sway and roll.

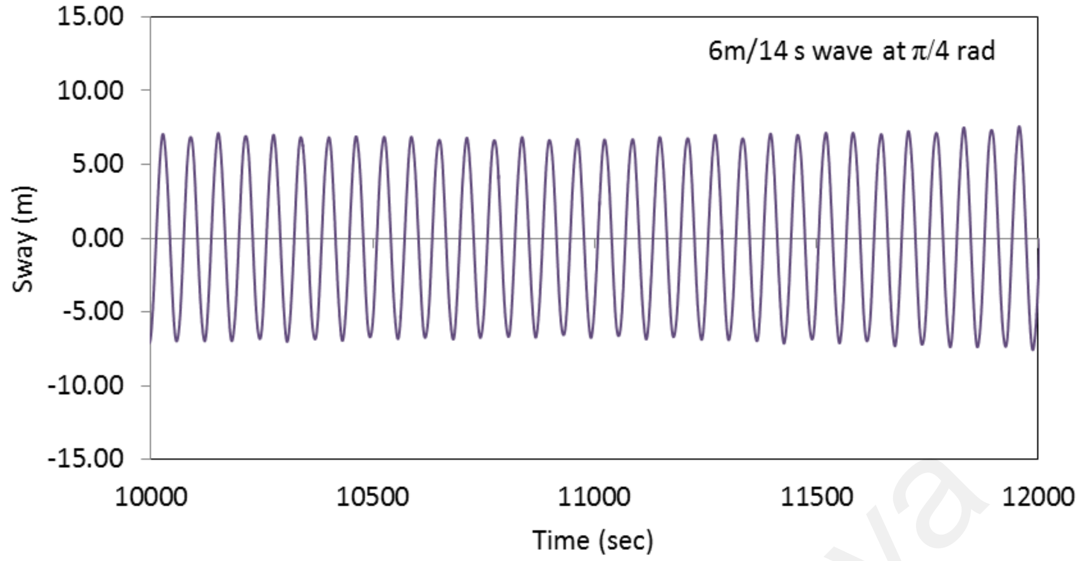

Figure 4.30: Displacement in sway time history under quartering sea wave

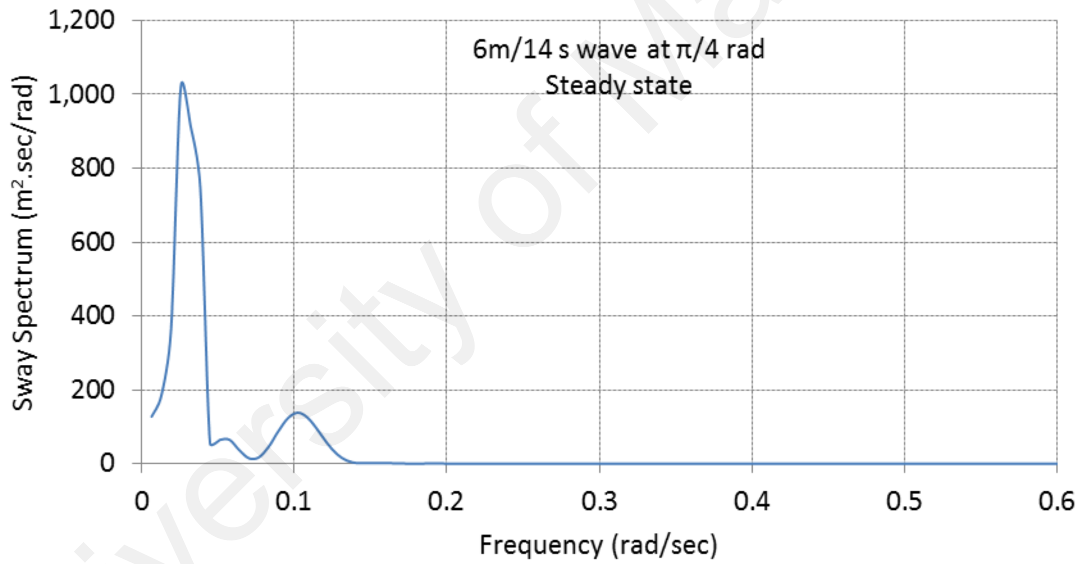

Figure 4.31: Power spectrum of sway under quartering sea wave

The power spectrum for steady state as shown in Figure 4.31 shows the participation of two distinct frequencies. The pattern of sway motion is mostly periodic in nature. Sway frequency gives the governing energy peak at steady state. Moreover the involvement of another frequency close to the roll frequency is observed.

Heave response under quartering sea wave

The statistical comparison of heave responses of the moored spar under quartering sea wave and wave at 0 rad are shown in Table 4.11. Heave response for quartering sea wave ranges between -0.851 m to 0.784 m, while the response due to wave at 0 rad varies between -0.93 m to 0.95 m. However, the pattern of heave time history is identical for both the cases. The slight reduction of heave response is due to inclination of wave train.

Table 4.11: Descriptive statistics of Spar heave in wave at 0 rad and quartering sea wave

Parameters	**Wave at 0 rad**	**Quartering sea wave**
	Heave	**Heave**
Maximum (m)	0.950015	0.783663
Minimum (m)	-0.93105	-0.85074
Mean (m)	0.056765	0.034265
Standard Error (m)	0.005221	0.005197
Median (m)	0.08846	0.04645
Mode (m)	-0.02415	0.39306
Standard Deviation (m)	0.410726	0.388928
Range (m)	1.881065	1.634403
95.0% Confidence interval	-0.7647~0.8782	-0.7436~0.81212

Standard error is the normalized standard deviation with square root of number of heave response data in the individual time history. Standard error shows relative deviation of oscillations for the complete time history under consideration whereas standard deviation is the average deviation of the responses from the mean. The standard error of heave response for wave at 0 rad and $\pi/4$ rad are 0.005221 m and 0.005197 m respectively. This parameter measures the scatter of heave oscillations about its mean with overall time history. For quartering sea wave, the standard error is less than the wave at 0 rad by 1.01% which shows that both responses are of similar pattern. Quartering sea wave induces 6% lower standard deviation than the standard deviation (Stdev) for wave at 0 rad.

The 95% confidence interval means that 95 % of the responses fall between the range mean ± twice standard deviation. For heave response the 95% confidence interval varies between -0.7647 m to 0.8782 m for wave at 0 rad and ranges between -0.7436 m to 0.8121 m for quartering sea wave. Though the maximum heave responses are higher in time history, the estimated confidence level for heave shows the probability of occurrence of these values as 95%.

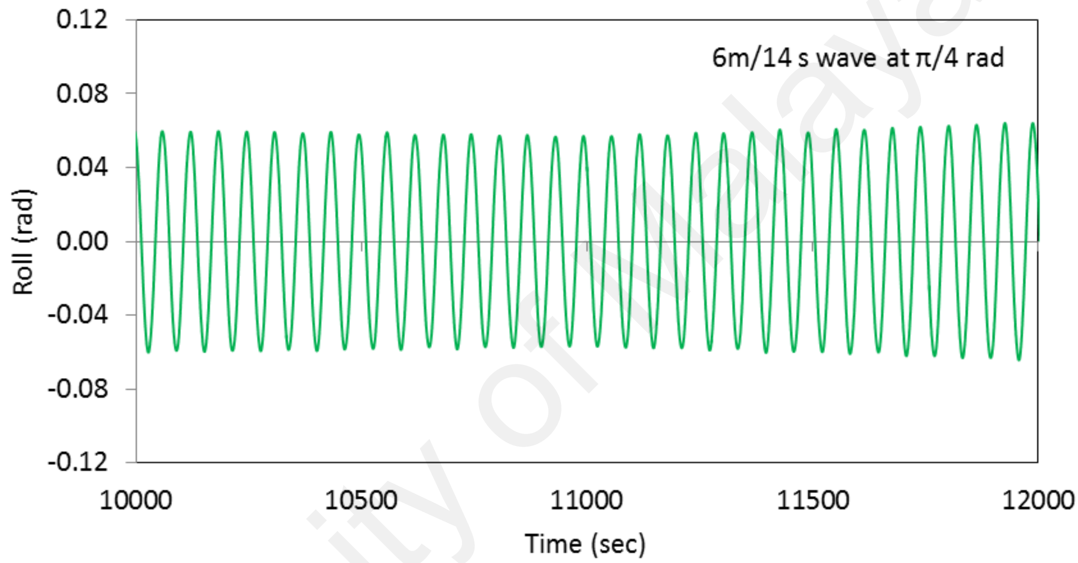

Figure 4.32: Rotation in roll under quartering sea wave

Roll response under quartering sea wave

Similar to the sway time history, the roll motion response is found to be significant after 2000 second of wave loading. The roll response fluctuates about the mean position oscillating from smaller to larger peaks and after around 6000 second steady state is attained. The roll response induces extensive sway at platform. It is coupled with the sway of rigid hull which otherwise is of small magnitude but gets enhanced due to roll input. According to Figure 4.32, the roll time history shows maximum and minimum values as ± 0.06 rad. High energy content is available at sway frequency (Figure 4.33). Furthermore, a distinct peak of energy content has been observed in the periodic response oscillations close to roll frequency. Mooring damping causes gradual reduction in roll response.

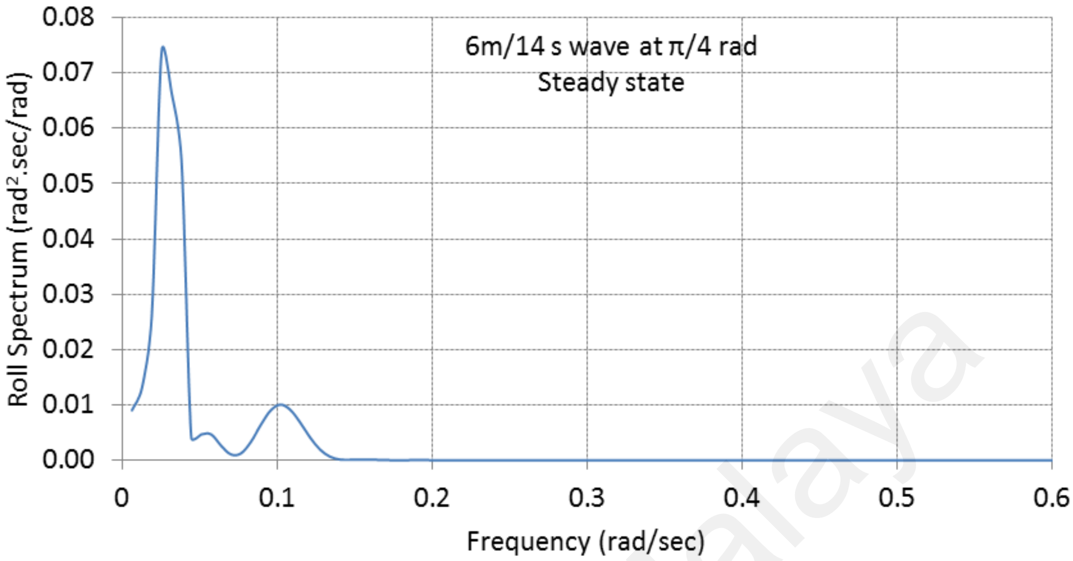

Figure 4.33: Power spectrum of roll under quartering sea wave

The platform experiences significant rotation in both roll and pitch. The steady state rotation in roll shows a peak value of around ±0.06 rad which is very close to the pitch rotation (Table 4.12). This is because the wave at π/4 rad induces substantial platform rotation in roll. For the wave loading at 0 rad, the roll response is nil. The value of mode response of roll also show higher magnitude which indicates most frequent roll response is significant.

Table 4.12: Descriptive statistics of Roll-pitch in wave at 0 rad and quartering sea wave

Parameters	**Wave at 0 rad**	**Quartering sea wave**	
	Pitch	**Roll**	**Pitch**
Maximum (rad)	0.053853	0.064071	0.050006
Minimum (rad)	-0.05384	-0.06434	-0.04998
Mean (rad)	-0.0007	0.000199	-0.00025
Standard Error (rad)	0.000353	0.000564	0.00033
Median (rad)	-0.00128	0.000442	-0.00066
Mode (rad)	-0.01401	-0.0585	-0.01686
Standard Deviation (rad)	0.025804	0.031216	0.024726
Range (rad)	0.107695	0.128408	0.099988
95.0% Confidence interval	-0.0523~0.0509	-0.0622~0.0626	-0.0497~0.0492

Pitch response under quartering sea wave

The statistics of pitch response under quartering sea wave loading and wave at 0 rad is illustrated in Table 4.12. Due to the pitch coupling, the surge time history at platform level experiences maximum peak at pitch frequency which has been shown earlier. The pitch time history is found to be of similar behaviour for both 0 rad wave and quartering sea wave. Pitching motion is regularly distributed about the mean position. Maximum and minimum values of pitch responses are reduced in comparison to the wave at 0 rad case. Damping caused by long mooring lines along with incline-ness of wave leads to reduction in pitch response.

Yaw response under quartering sea wave

Figure 4.34 shows yaw response of platform. For quartering sea wave action the yaw time history shows noteworthy values. The oscillations vary between around ±0.05 rad of maximum yaw. The small mean value of yaw response slightly influences on heave motion and hence the mooring tension. The power spectrum of yaw (Figure 4.35) shows a solitary peak at 0.0196 rad/sec.

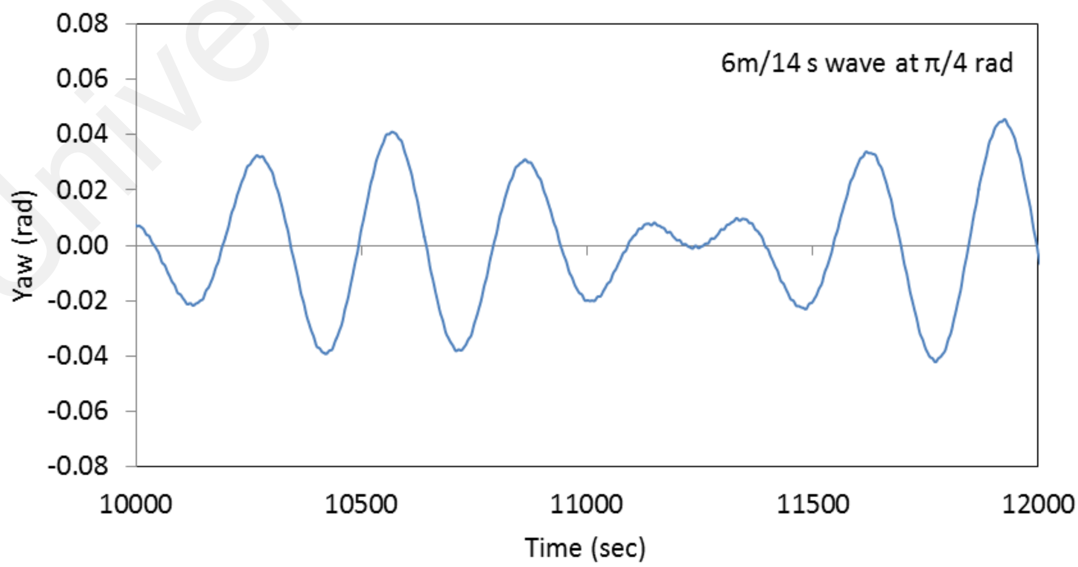

Figure 4.34: Rotation in yaw under quartering sea wave

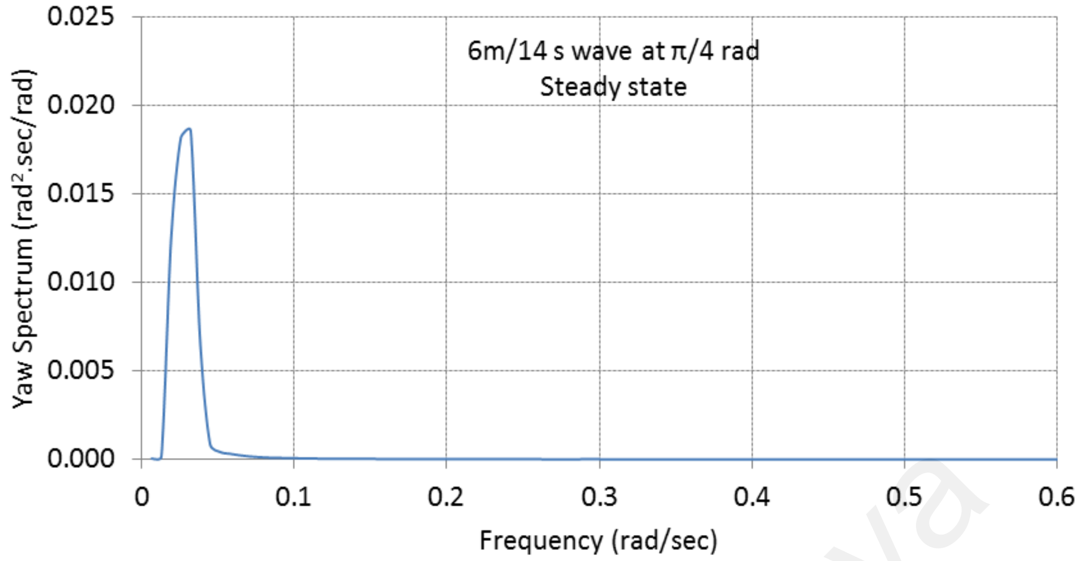

Figure 4.35: Power spectrum of yaw under quartering sea wave

Descriptive statistics of yaw response of the moored Spar are shown in Table 4.13. Because of wave at 0 rad there is no yaw motion of platform, however quartering sea wave poses significant rotation in yaw. The mean and median of yaw response are very small in magnitude showing its firmness in platform rotation.

Table 4.13: Descriptive statistics of Spar yaw in wave at 0 rad and quartering sea wave

Parameters	**Wave at 0 rad**	**Quartering sea wave**
	Yaw	**Yaw**
Maximum (m)	0.00	0.045561
Minimum (m)	0.00	-0.04217
Mean (m)	0.00	0.000881
Standard Error (m)	0.00	0.000296
Median (m)	0.00	0.001039
Mode (m)	0.00	-0.0118
Standard Deviation (m)	0.00	0.021185
Range (m)	0.00	0.087734
95.0% Confidence interval	0.00	-0.04149~0.04325

4.6.2. Mooring line tension in quartering sea wave

The behaviour of top tension in catenary mooring line 1 for quartering sea wave is presented in Figure 4.36 which shows regular oscillations. For the wave at 0 rad the maximum and minimum tension in CML1 ranges between 1.662E+07 N to 1.581E+07

N. But for quartering sea wave the range of maximum tension is 1.656E+07 N to 1.5952E+07 N. The oscillations are reduced by 4% compared to wave at 0 rad. Besides, for 0 rad wave, solitary peak occurs at wave frequency for long duration of wave loading. But for the quartering sea wave the power spectrum is different. The power spectrum of the line tension shows a small peak of energy content close to the heave frequency (Figure 4.37). The governing peak occurs at surge frequency (0.018 rad/sec). This instance clearly shows the behaviour change in mooring tension response.

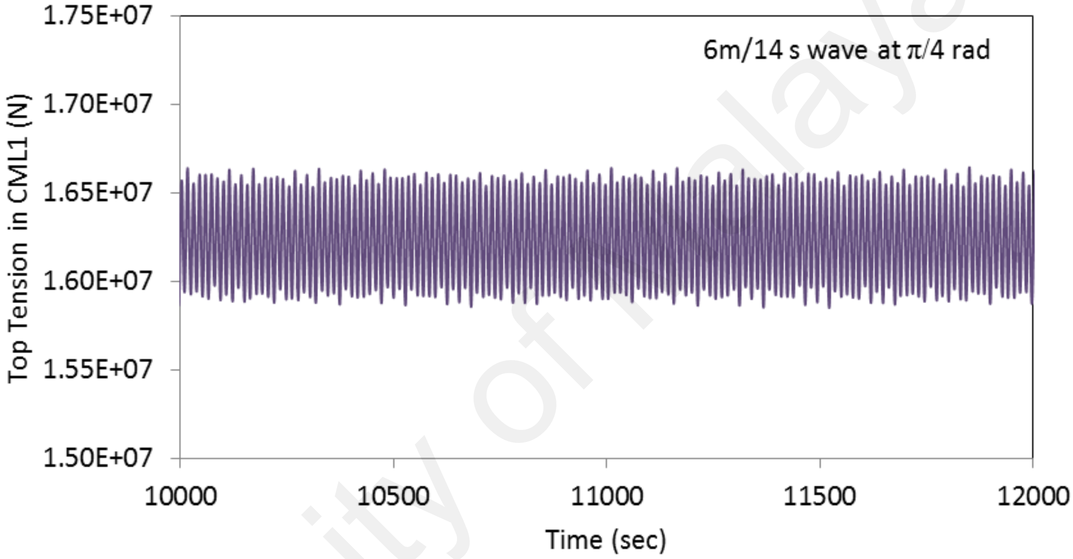

Figure 4.36: Maximum tension in CML1 under quartering sea wave

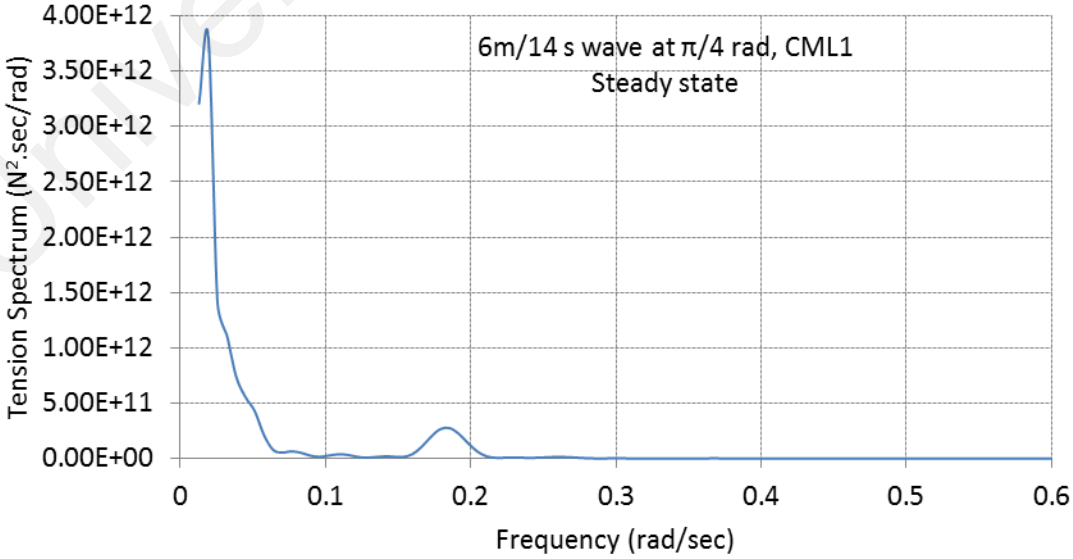

Figure 4.37: Tension spectrum of CML1 under quartering sea wave

For quartering sea wave, the frequency content is seen only at surge/sway frequency for CML2. The tension history of mooring line 2 is also regular in nature with slight variations in magnitude. Figure 4.38 and Figure 4.39 show the tension fluctuations time history and power spectrum of CML2 respectively. Tension fluctuation is of complex periodic nature showing minor ripples near the peaks but the fluctuations are less for this case. For wave at 0 rad, the response is governed by wave frequency whereas for quartering sea wave it is governed by natural frequency of surge/sway.

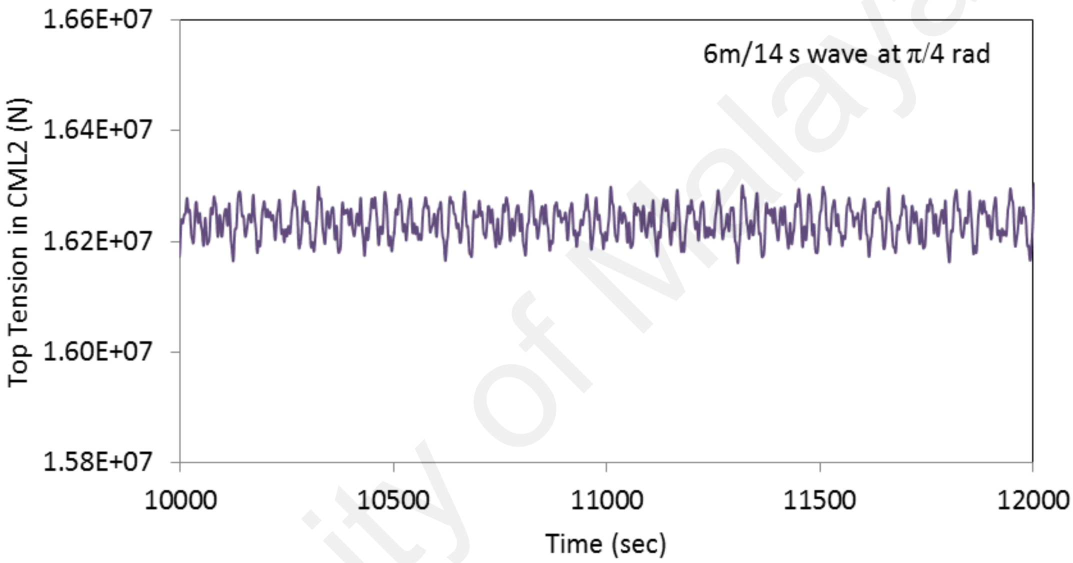

Figure 4.38: Maximum tension in CML2 under quartering sea wave

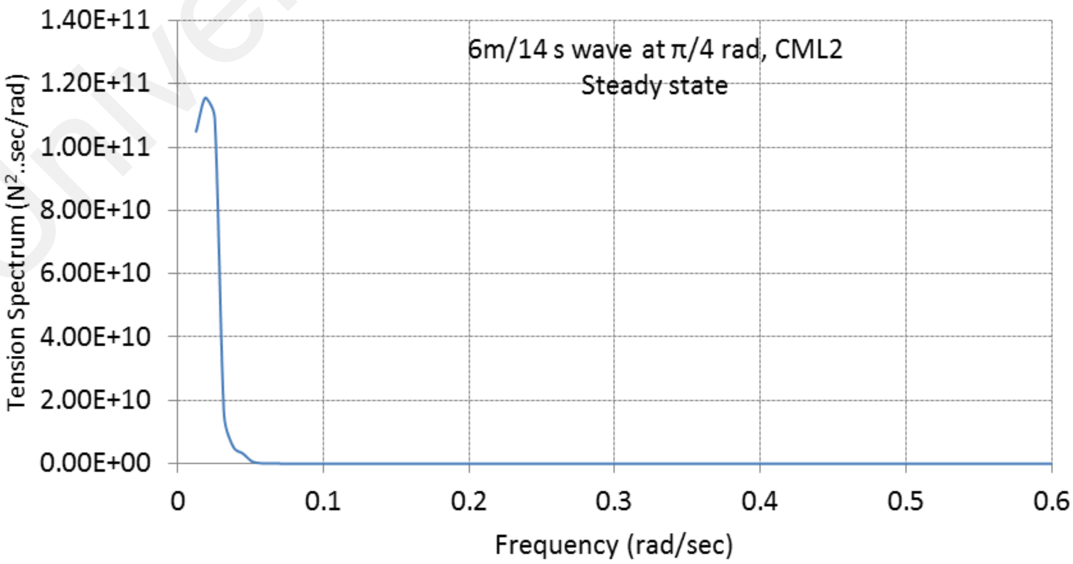

Figure 4.39: Tension spectrum of CML2 under quartering sea wave

4.7 Effect of severe sea states

The nonlinear coupled behaviour of the Spar-mooring system has been evaluated under the anticipated critical sea states to study the behaviour of floating structure. The selected sea states are categorized as severe (Strong gale), mild but critical (Moderate wave) and moderate (Moderate gale). For all the cases only wave condition is chosen for initial evaluation. Moreover, the corresponding current forces of the individual sea states have been included to see the detail behaviour under current plus wave conditions. The excursion time histories are found for sufficient length of time so that the response attains the steady state. The chosen sea states wave data is taken from Jameel and Ahmad (2011). Among all the sea states of their study (Table 3.1), sea state S1 (17.15 m wave height and 13.26 s wave period) is large in loading magnitude but lowest in probability of occurrence. Therefore, this sea state has been selected as extreme case. The wave loading is designated as sea state SG-W. The sea environmental loading S5 from the study of Jameel and Ahmad (2011) has been recognized as moderate gale state. Both the wave period and the wave height are significant in value which can bring about a critical alteration of structural behaviour of moored Spar in the deep ocean. This sea state is labelled as MG-W. Moreover, the sea state S11 in Jameel and Ahmad (2011) is idealized as a moderate wave environment (MW-W). Though the wave period and wave height are lower in magnitude for this case, increased frequency of wave may lead to critical responses of the moored Spar.

4.7.1. Coupled behaviour under severe sea states

For assessing the response characteristics under critical environments, unidirectional regular wave models of the selected sea states are used to compute the incident wave kinematics following the appropriate wave theories. As the ratio of the structure dimension to wave length is small in this deep water, it is assumed that the wave field is virtually undisturbed by the structure and that the Morison's equation is adequate to calculate the wave exciting forces. The wave loads on the moored spar are calculated by assimilating forces along the height of the structure at the instantaneous displaced position. Structural behaviours under the selected sea loadings are discussed subsequently. The response time histories and power spectra of surge, heave, pitch and mooring line tension are plotted for SG-W case. Statistical responses of all three cases of sea states (SG-W, MG-W and MW-W) have been compared.

Spar surge in sea state SG-W

The time history of surge response due to sea state SG-W at the deck level and CG level of the spar platform are illustrated in Figure 4.40 and Figure 4.42 respectively. At these two selected levels, the spar hull movement in horizontal direction is different. The peak of surge response at deck level for sea state SG-W ranges from +25.20 m to -17.50 m at transient stages and reduces from +12.72 m to -6.27 m at steady state. The nature of surge at the deck level is predominantly periodic. Pitch motion occurs simultaneously with surge and attracts significant wave energy at pitch frequency (Figure 4.41). Surge frequency requires huge energy input because of large inertia and hence does not get excited. However, pitching motion occurring with surge gets excited easily. It is understood that the surge response is significantly enhanced and shows a substantial pitch response too. It is mainly due to the surge-pitch coupling. Besides, at longer time of wave action, the energy content in pitching motion is reduced due to the damping and hence the peak is observed in between surge and pitching frequency. After around 9000 sec the surge response attains steady state. Effect of non-linearity is not very strong on surge response. The mean value of surge shows a slight lateral shift of spar at longer time because of high intensity of extreme wave loading. Domination of pitching motion on the hull with insignificant excitation of surge mode in short duration and domination of surge frequency is largely caused by the coupling of surge and pitch.

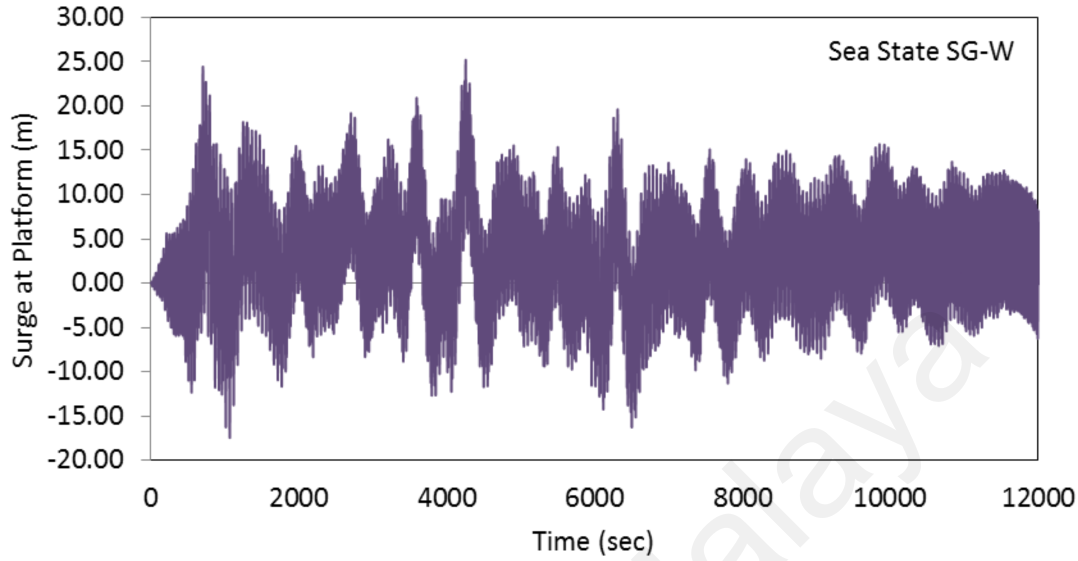

Figure 4.40: Spar response in surge at deck level for Sea state SG-W

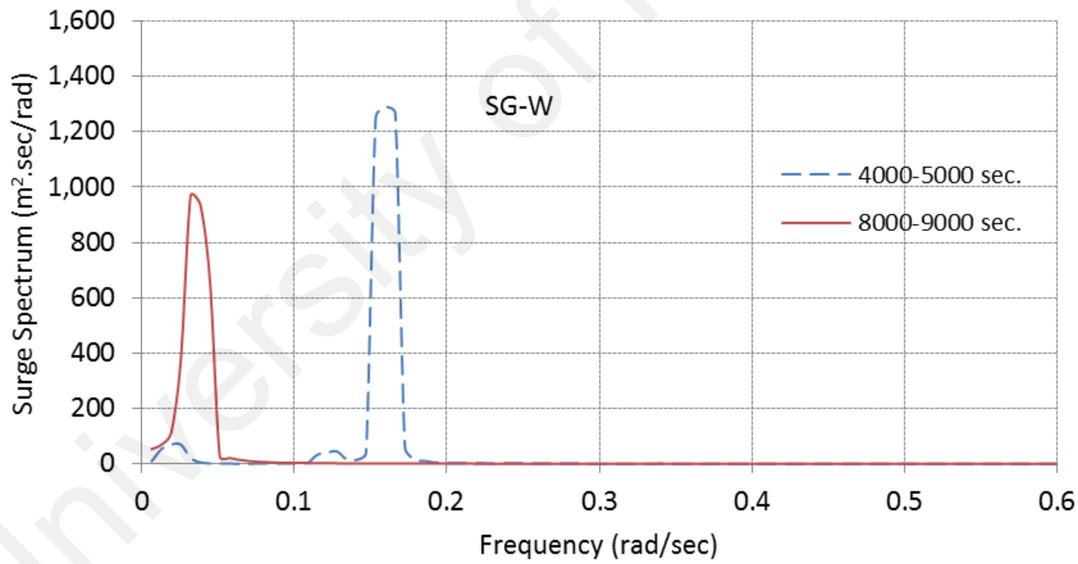

Figure 4.41: Power spectrum of surge at deck level for Sea state SG-W

It is to be noted that the surge is dominating in surge frequency for platform level also at higher duration of wave loading though coupled pitch frequency is dominated at short duration. Surge power spectra at low frequency, high frequency, wave frequency at deck level under strong gale are shown in Figures 4.14a; 4.41b and 4.41c respectively. The involvement of surge frequency and wave frequency has been observed in Figures

4.14a and 4.41c. The wave frequency has less involvement which is reflected in the power spectrum.

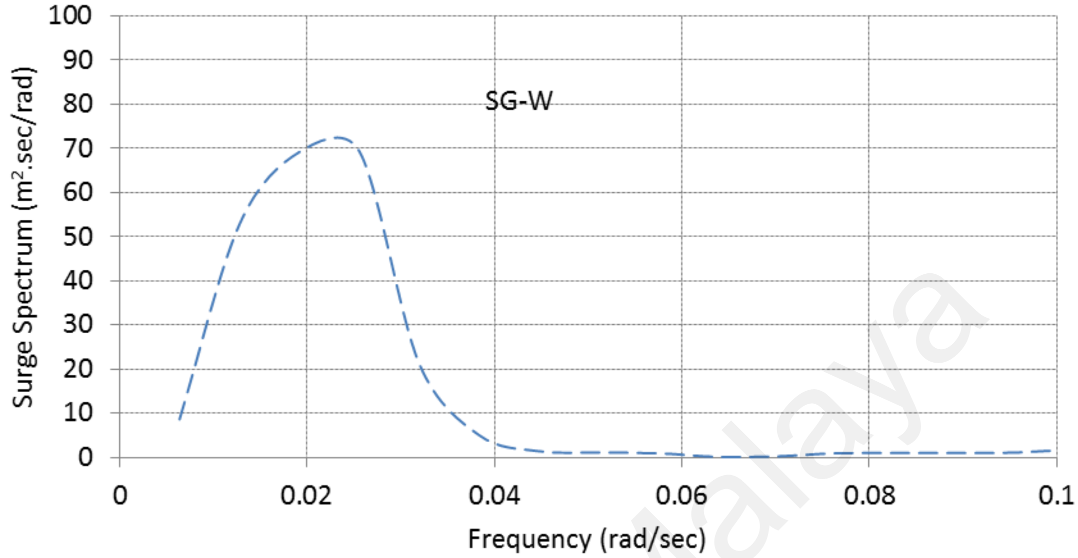

Figure 4.41a: Low frequency (LF) surge behaviour at deck level

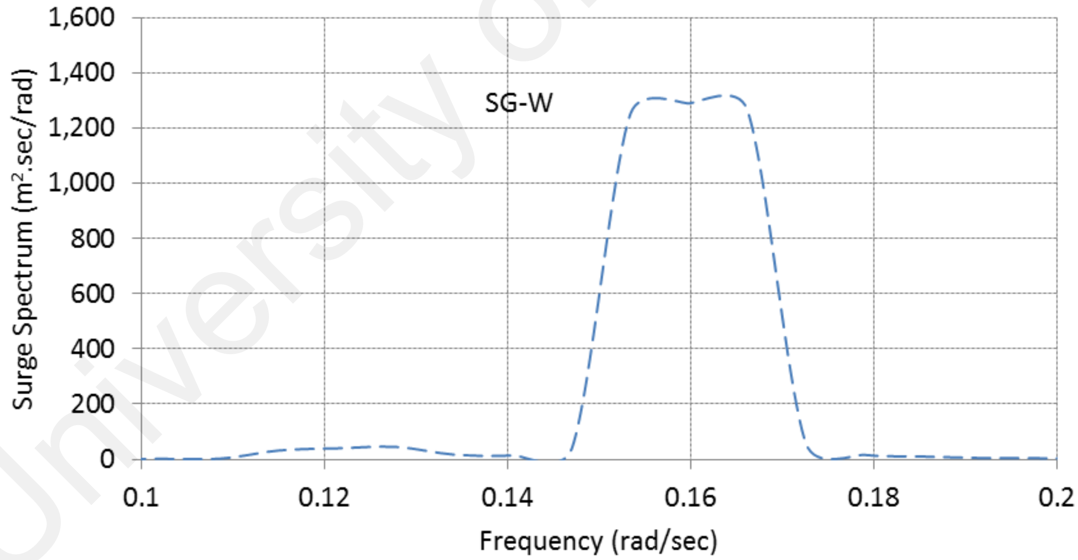

Figure 4.41b: High frequency (HF) surge behaviour at deck level

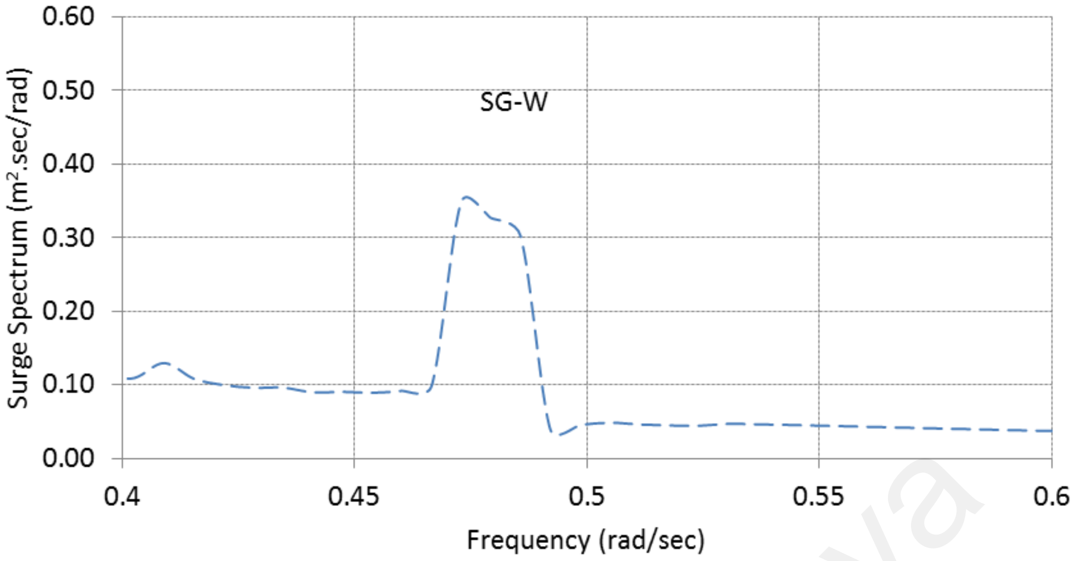

Figure 4.41c: Wave frequency (WF) surge behaviour at deck level

Surge at centre of gravity of spar is shown in Figure 4.42. It shows a marked difference in surge behaviour in comparison to the same at platform level. At CG level it oscillates in a different way as the platform level responses. The response time history shows peak value of surge at 4000 sec to be 16.30m. The fluctuations of surge time history are small in value compared to deck level excursions. There are continuous variations of translational displacement, showing the pronounced non-linear behaviour. The first substantial peak of surge time history occurs at 728 sec. However, there are number of relatively smaller peaks up to 4000 sec, followed by descending peaks later on. It is observed that the surge values gradually lessen due to damping caused by CMLs.

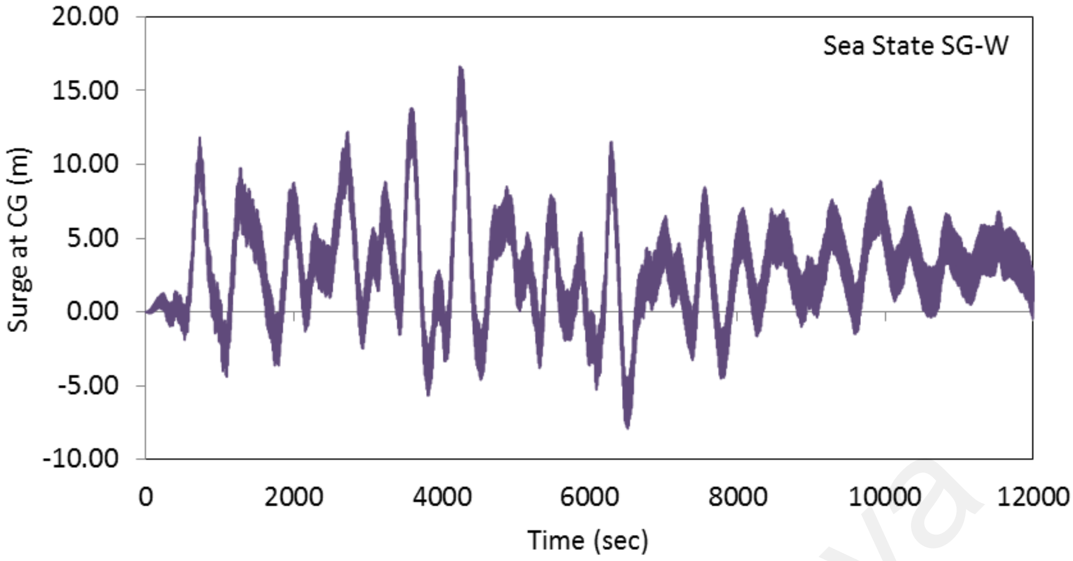

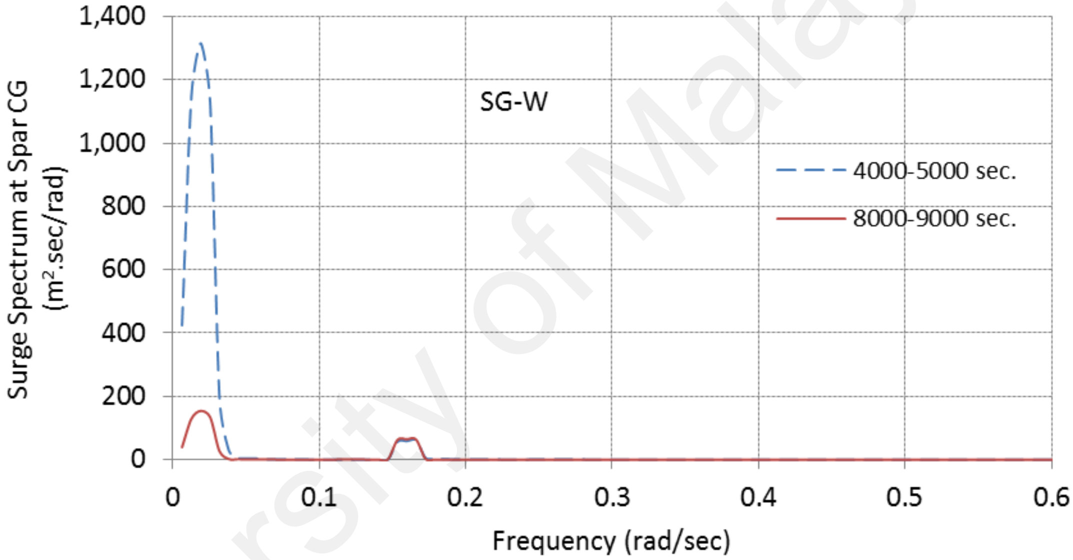

Figure 4.42: Surge response behaviour at Spar CG under Sea state SG-W

The power spectrum of surge response behaviour at centre of gravity shows notable participation of surge motion as shown in Figure 4.42a. The effect of pitch is minimal here (Figure 4.42b) and the participation of wave frequency is very low (Figure 4.42c). The difference in governing frequency at CG level with the platform level reponse is due to difference in position and predicts the actual response behaviour desired at deck level.

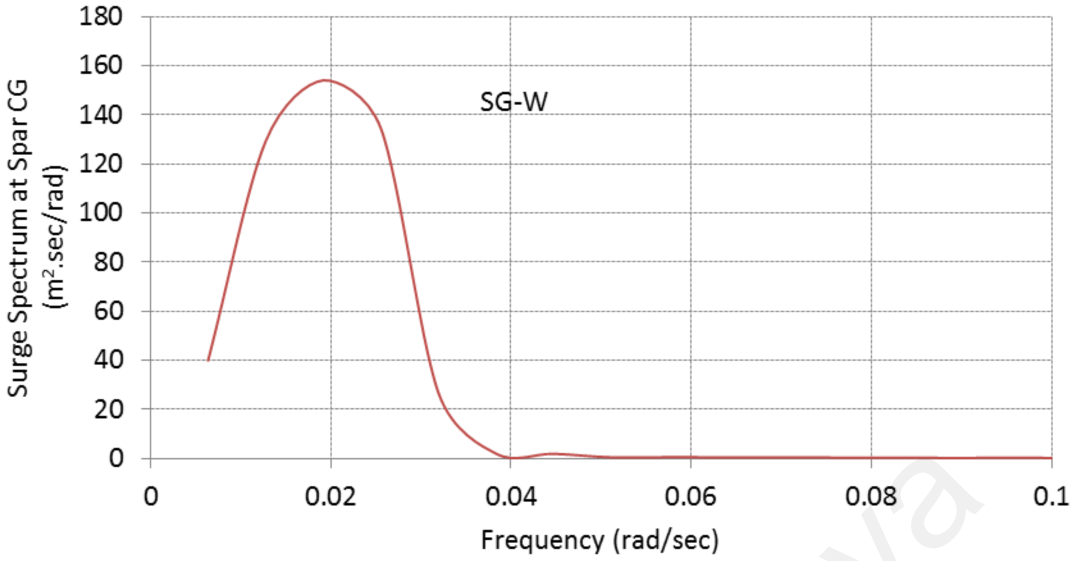

Figure 4.42a: Low frequency (LF) surge behaviour at Spar CG

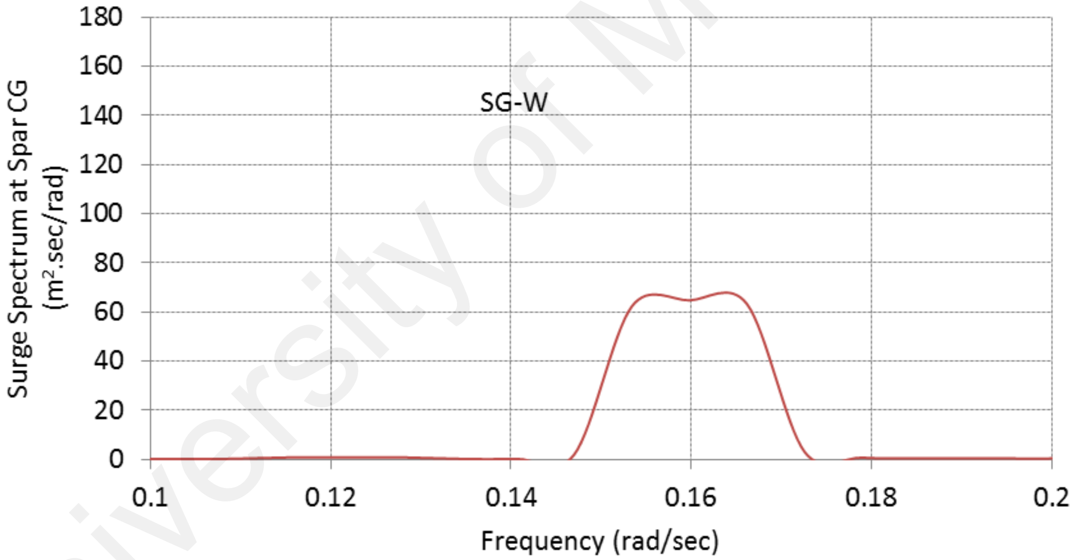

Figure 4.42b: High frequency (HF) surge behaviour at Spar CG

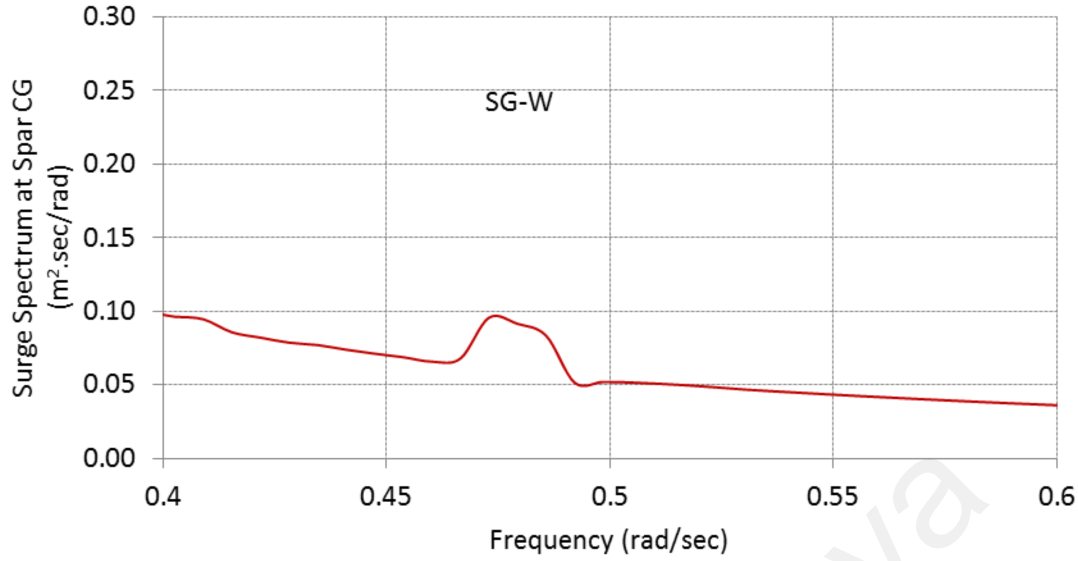

Figure 4.42c: Wave frequency (WF) surge behaviour at Spar CG

Comparison of Spar surge for severe sea states

The surge time history for sea state displays periodic behaviour for all three loading cases. Time history peak of surge response at moderate gale varies from +4.87 m to -2.37 m which are lesser than the strong gale condition. However, the pattern of motion fluctuations is identical (Table 4.14). Nevertheless, under moderate wave, the platform motion oscillates with more fluctuations with a positive peak of 8.93 m and negative crowning as -8.04 m. This is because of higher frequency of wave action caused by lower wave period in moderate wave. The energy attraction and damping characteristics are alike in all the cases. Under moderate gale, the statistical responses are lesser compared to strong gale, which is expected because of low wave intensity. For further lower wave height and wave period (MW-W) higher standard deviation and RMS values shows adverse surge oscillations of platform. The Stdev for strong gale and moderate gale are 5.18 m and 2.16 m which is 5.07 m under moderate wave. This trend is followed by RMS response as well. It should be noted that rather than Morison's equation, for accurate prediction of platform responses under moderate wave MW-W, it is recommended to compute wave forces by wave diffraction theory. Mean and median values of surge response gradually decrease for strong gale to moderate wave case.

Table 4.14: Descriptive statistics of Spar surge under critical wave loadings

Surge	**Strong gale**	**Moderate gale**	**Moderate wave**
Max (m)	12.72	4.87	8.93
Min (m)	-6.27	-2.37	-8.04
Mean (m)	3.36	1.18	0.56
Median (m)	3.07	0.98	0.83
Mode (m)	12.32	3.32	6.97
Standard Deviation (m)	5.18	2.46	5.07
RMS (m)	6.17	2.73	5.09
Skewness	0.05	0.07	-0.08
Kurtosis	-1.32	-1.45	-1.40

Mode value of surge in statistical analysis is the response which has occurred most often in the total time history. Like the statistical mean and median, the mode is a way of expressing, in a single number, important information about random responses. In symmetric unimodal distributions, such as the normal (or Gaussian) distribution, the mean, median and mode all coincide. However, the difference in mode value shows the disturbance of normal distribution to asymmetrical pattern in highly skewed distributions. The mode response of surge under moderate wave (6.97 m) clearly shows that mostly frequent surge response is significant for moderate wave. In probability theory and statistics, kurtosis is a measure of the peaked-ness (width of peak) of the probability distribution of real-valued random responses. The kurtosis is a descriptor of the shape of a probability distribution. Higher kurtosis means that some infrequent extreme deviations from the mean form a high peak. The excess kurtosis is the shape of a given distribution compared to that of the normal distribution (mesokurtic distribution). Distributions with negative or positive excess kurtosis are called platy-kurtic distributions or leptokurtic distributions respectively. The kurtosis coefficient shows platy-kurtic response distribution for strong gale and slightly less peaked-ness of responses around the mean value for moderate gale. For moderate wave, the surge distribution is platy-kurtic with significant flatness in response deviation from the mean.

Coefficient of skewness characterizes the degree of asymmetry of a distribution around its mean. Positive skewness indicates a distribution with an asymmetric tail extending toward more positive values. Negative skewness indicates a distribution with an asymmetric tail extending toward more negative values. For strong gale the positive skewness of surge is 0.05 which is larger for moderate gale (0.07) showing more asymmetric tail in right hand side of distribution curve which means more number of surge response values are greater than its mean. But the surge under moderate wave has negative skewness with asymmetric tail towards left hand side meaning that more numbers of surge response values are slightly less than its mean.

Spar heave in sea state SG-W

The heave response directly influences the mooring tensions and other operations. Responses under regular wave for sea state SG-W are shown in Figure 4.43. Heave time history shows the cluster of reversals occurring at varying time intervals. The response is seen to show regularity. Larger magnitudes of heave responses occur earlier for the SG-W wave loading. Heave response maximum peak touches 1.68 m at transition region and 0.30 m at steady state in case of sea state SG-W. Transition region of heave time history is witnessed up to around 2000 second of wave loading. Within the range, at 1200 s, the maximum peak occurs. And after that, the peaks in the heave response decrease gradually for sea state SG-W case and again increase with a little rise at 6000s wave loading. With a few fluctuating heave peaks, the stable responses appear at around 10000 s of wave loading. Heave response fluctuates about the mean position oscillating from smaller to larger heights and repeating the same trend onwards throughout the time series. The fluctuations gradually increase from narrow to broad by 20 %. Reaching the peak, it gradually reduces by 10 % and again increases ensuring a similar trend. However, after 7200 sec, values of heave are very trivial due to damping of mooring line. Though a few peaks are existent, heave power spectrum shows larger energy peak at heave frequency (Figure 4.44) at 4000-5000 seconds. Later on the energy is transferred towards pitch motion. Therefore, after longer time, energy attraction is seen at pitching motion showing governing peak at pitch frequency zone. These phenomenon shows alternate transactions of energy between heave and pitch response.

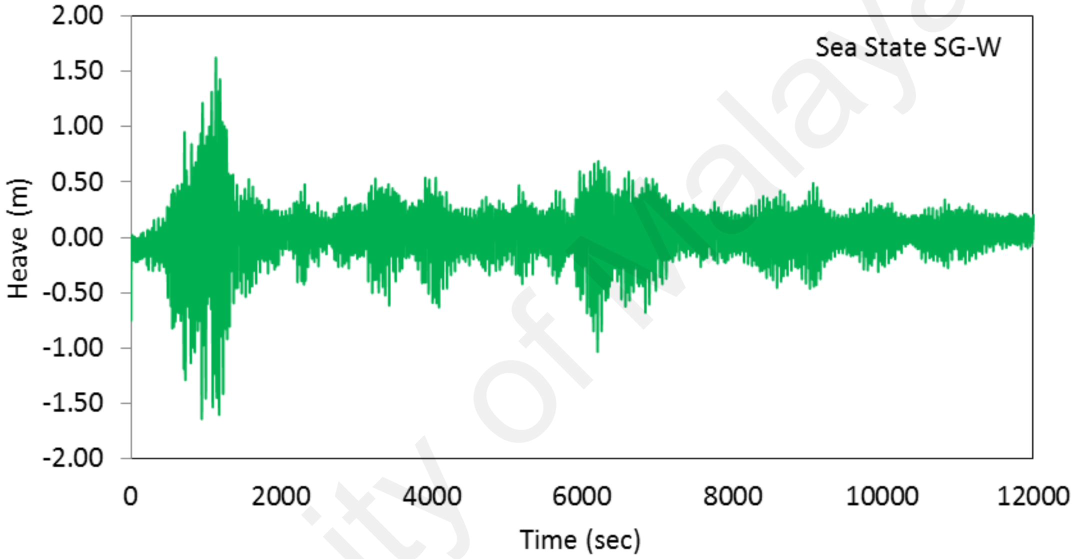

Figure 4.43: Spar response in heave for Sea state SG-W

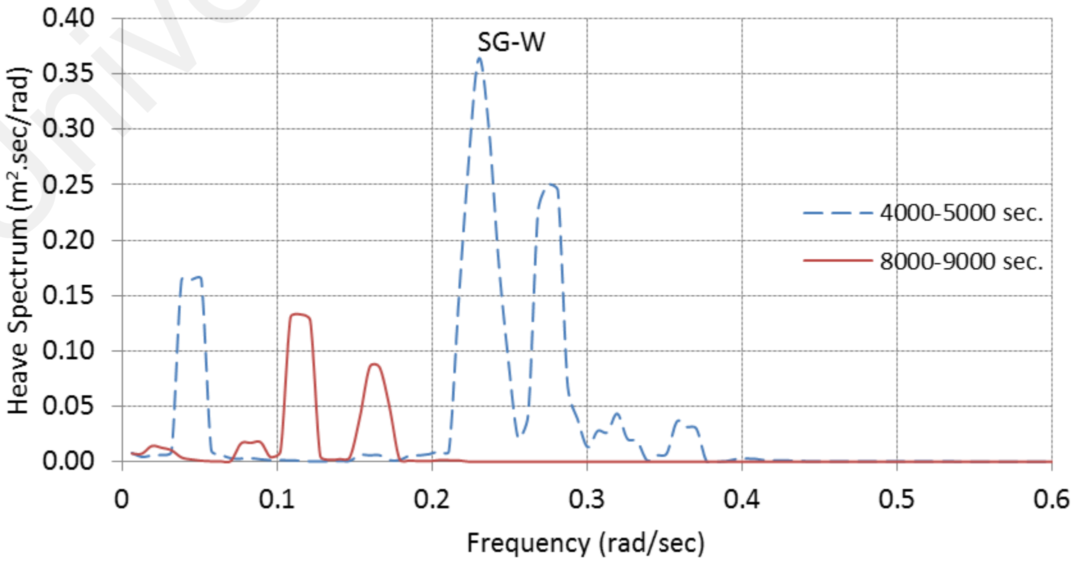

Figure 4.44: Power spectrum of heave for Sea state SG-W

Comparison of Spar heaves for severe sea states

Larger magnitudes of heave responses are seen for sea state MW-W case than those of SG-W and MG-W loading case (Table 4.15). The heave response maximum peak touches ±4.21 m in case of sea state MW-W whereas the magnitude is lower for others. This is because the wave characteristic has a very small wave period. As the wave period is less, the frequency of wave loading becomes significant and the platform experiences additional vertical movement. Numerous clusters of vertical translation fluctuations are witnessed at varying time intervals up to longer time. The heave response fluctuates about the mean position oscillating from smaller to larger amplitudes. For moderate gale, the downward translation of the Spar hull stretches to negative crest of 0.03 m. A long duration of wave loading as 10000 sec. is required to damp out the responses toward smaller value. For moderate wave, the mean, median and mode values are lower than other cases.

Besides, the heave distribution under strong and moderate gale with positive excess kurtosis is seen as leptokurtic. This leptokurtic motion distribution indicates a more acute peak around the mean and fatter tails. But for moderate wave, the negative kurtosis -0.84 is of platy-kurtic nature. Therefore the broad distribution of heave has a lower, wider peak around the mean and thinner tails. This phenomenon indicates the existence of significant amount of heave values around its mean at moderate wave. However, the sea state MW-W induces heave response fluctuations with greater standard deviation and RMS values which show the severity of this sea state.

Table 4.15: Descriptive statistics of Spar heave under critical wave loadings

Heave	**Strong gale**	**Moderate gale**	**Moderate wave**
Max (m)	0.30	0.06	3.09
Min (m)	-0.24	-0.05	-3.13
Mean (m)	0.06	0.01	-0.01
Median (m)	0.07	0.01	-0.02
Mode (m)	0.02	0.02	0.24
Standard Deviation (m)	0.09	0.01	0.51
RMS (m)	0.11	0.02	0.51
Skewness	-0.35	-0.12	-0.01
Kurtosis	0.09	-1.30	-0.84

Spar pitch in sea state SG-W

The pitch response of spar platform for chosen critical cases has been evaluated in this section. The power spectrum shows energy content indicating the governing level of frequency. Pitch motion time history is also studied to assess the characteristics along with the power spectrum. The pitch behaviours of spar hull subjected to sea wave are illustrated in Figure 4.45. The time history output of pitch response shows regular fluctuations initiating from zero up to peak of ± 0.06 rad at steady state which is ± 012 rad at transient zone for sea state SG-W. These peaks of pitch time history occur at transition period of the Spar. The responses reduce periodically and again increase slightly giving a few peaks of lower magnitude. For the sea loading, the stable motion is observed after 9000 seconds. The significant value of pitch response leads to a significant surge at deck level. It is coupled with the surge of rigid hull which otherwise is of small magnitude but gets enhanced due to pitch input. This is why the surge time series shows maximum peak at the frequency of pitch. The pitch time history shows regular behaviour at longer time. Dominant peak in energy content occurs near the pitch frequency itself (Figure 4.46) at 4000-5000 seconds. However, the spectral density shows a solitary peak near surge motion at longer time of wave action. This discrepancy is happened because of reduction of energy in pitching motion due to induced damping.

This incident confirms the fact that pitch motion occurs simultaneously with surge and attracts significant wave energy.

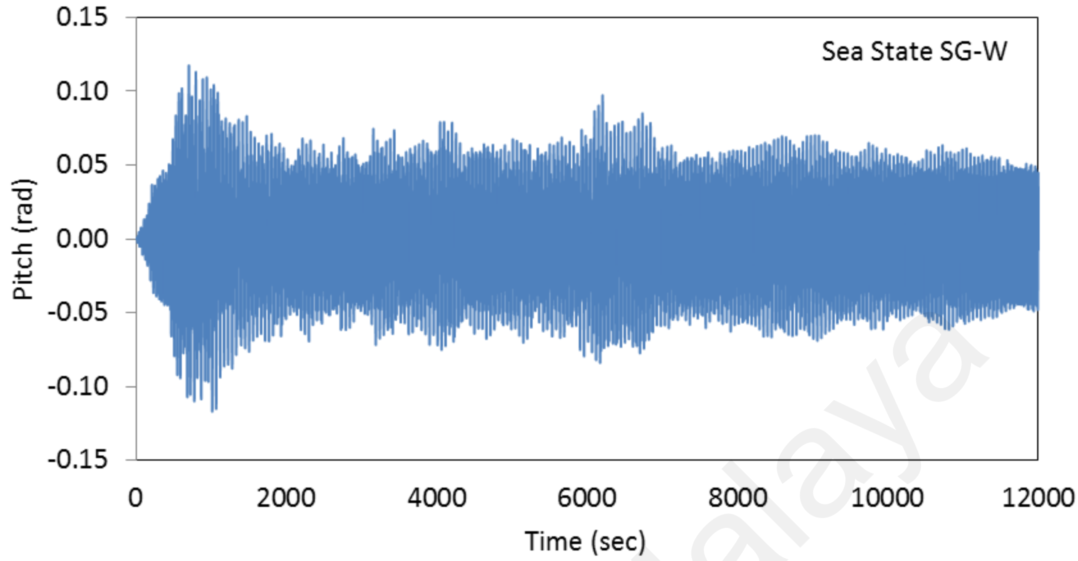

Figure 4.45: Spar response in pitch for Sea state SG-W

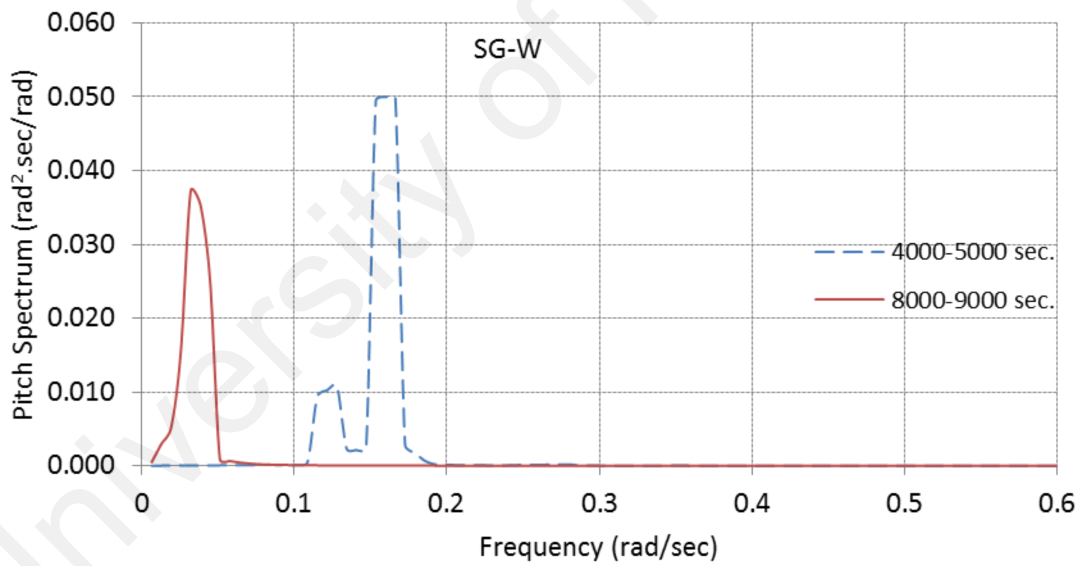

Figure 4.46: Power spectrum of pitch for Sea state SG-W

Comparison of Spar pitch for severe sea states

The platform rotation in pitch shows matching behaviours with the corresponding surge response. The highest peak of pitch response is ±0.02 rad under moderate gale which is less than SG-W case. But pitch of ± 0.07 rad for moderate wave shows the involvement of lower wave period action in deep sea (Table 4.16). Since the surge excursion is directly related to the pitch responses, the responses are regular in fashion for all the cases. This pitching motion occurring with surge gets excited easily. The abrupt lessening and rising of pitch response indicates lock-in phenomenon on the Spar platform system in some time state. It implies that the pitch and surge responses are strongly coupled. The responses are damped out after a long time with decreased steady oscillation. It is seen that though for decreasing wave intensity in moderate gale the pitch response decreases as of usual manner. But for moderate wave the rotation is high due to higher frequency of wave action. The mode response also shows mostly frequent higher value in sea state MW-W. Root mean square is visibly larger for the case along with higher kurtosis. Higher fluctuation of pitch response is seen by the greater standard deviation in this severe sea state.

Table 4.16: Descriptive statistics of Spar pitch under critical wave loadings

Pitch	**Strong gale**	**Moderate gale**	**Moderate wave**
Max (rad)	0.06	0.02	0.07
Min (rad)	-0.06	-0.02	-0.07
Mean (rad)	-0.0003	0.00	0.002
Median (rad)	-0.002	0.00	0.004
Mode (rad)	0.05	0.01	0.05
Standard Deviation (rad)	0.03	0.02	0.04
RMS (rad)	0.03	0.02	0.04
Skewness	0.06	0.07	-0.07
Kurtosis	-1.39	-1.45	-1.40

Top tension in CML at sea state SG-W

The response of mooring lines plays an important role in the coupled dynamic analysis of the Spar Platform. The regular wave loads simultaneously act on the hull and mooring lines. Designed pretension in each mooring line of the present problem is 1.625E+07 N (Table 4.2). Mooring line shows the regular behaviour of tension when subjected to the sea state SG-W (Figure 4.47). Surge response also causes increase in tension. Mooring line 1 is positioned in the direction of wave propagation. It is worth mentioning that the CML1 experiences the top tension to support surge in the forward direction and it experiences maximum value. Tension fluctuation is of complex periodic nature showing minor ripples near the peaks. For the mooring lines at the regular wave, periodic behaviour is seen. The tension responses in mooring line for sea state SG-W reach the larger peak among other crests at 4240 second as 1.78E+07 N and after 6000 s the mooring tension stabilizes with more regular oscillations with 1.73E+07 N tension at 10000 sec of wave loading.

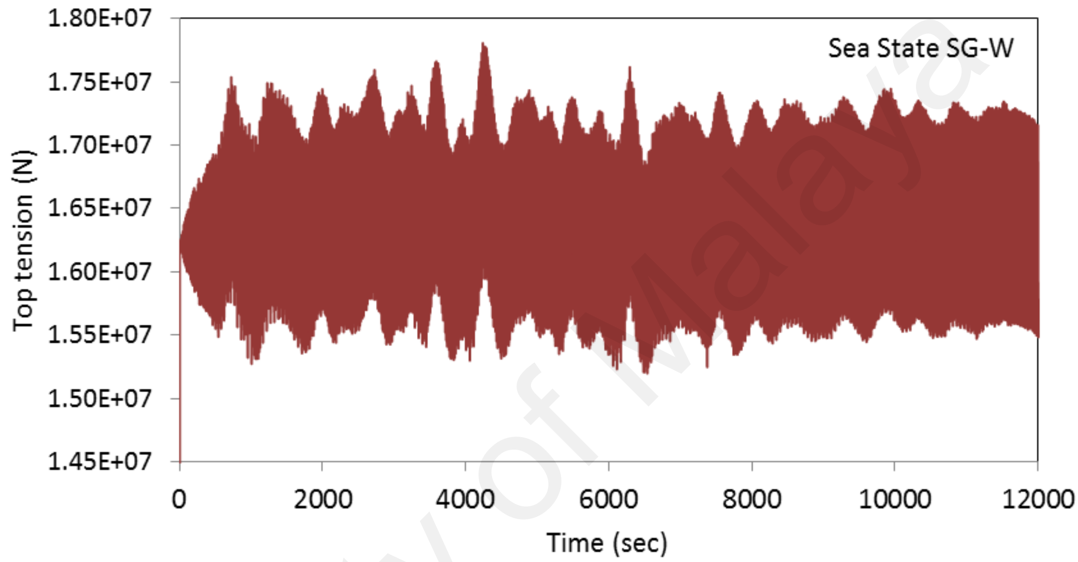

Figure 4.47: Top tension in mooring line for Sea state SG-W

The spectral density of mooring tension at 4000-5000 sec shows governing peak of energy content at frequency 0.181 rad/sec which is in between pitch frequency and heave frequency. Hence, the tension spectrum (Figure 4.48) shows a decent relation of heave-pitch and mooring tension of the moored Spar. Again after long duration distinct peak is observed close to the surge frequency. This indicates that heave and pitching motions has considerable influence on mooring tension together with the participation of surge response.

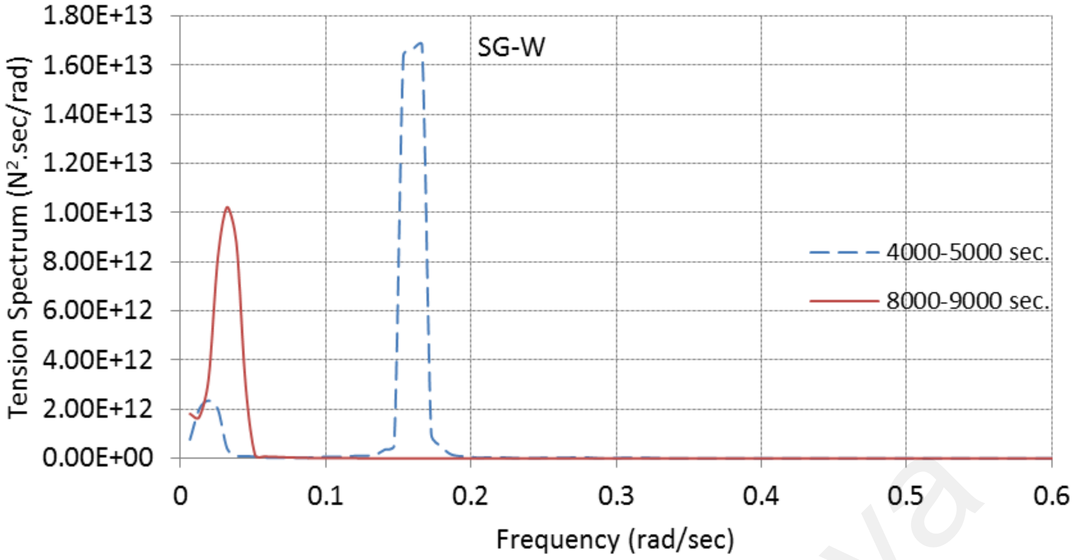

Figure 4.48: Tension spectrum of CML for Sea state SG-W

Comparison of CML Top tension for severe sea states

Complex periodic behaviour is observed in tension fluctuation displaying small amount of undulations near the peaks at sea state MG-W. However, the mooring line in this sea state experience decreased top tension than that of strong gale. The magnitude of tension response peak is 1.68E+07 N which is lower than SG-W case (Table 4.17). The fluctuations of mooring tension follow similar pattern like strong gale environment. The physical difference of values is because of lower hydrodynamic force induced by sea state MG-W. Though the Spar motions are greater in sea state MW-W case than those of other two cases, the mooring tensions decrease under this sea state. Yet, the maximum mooring tension 1.64E+07 N is found to be significant in MW-W case. Furthermore, though the values are less in sea state MW-W, abrupt fluctuations even after longer duration of wave loading indicates the severity of the sea state on the mooring line and hence for the spar-mooring system. But the top tension time series in mooring line for sea state SG-W is quite regular in nature. Larger value in coefficient of skew-ness and kurtosis at moderate wave also show the highly skewed and leptokurtic peaked-ness in tension response distribution. These kinds of adverse variations experienced at lower wave height and lower wave period are substantial and should duly be considered.

Table 4.17: Descriptive statistics of CML tension under critical wave loadings

Mooring top tension	**Strong gale**	**Moderate gale**	**Moderate wave**
Max (N)	1.73E+07	1.68E+07	1.64E+07
Min (N)	1.55E+07	1.57E+07	1.61E+07
Mean (N)	1.64E+07	1.63E+07	1.62E+07
Median (N)	1.63E+07	1.64E+07	1.63E+07
Mode (N)	1.56E+07	1.67E+07	1.63E+07
Standard Deviation (N)	6.10E+05	3.80E+05	4.68E+04
RMS (N)	1.64E+07	1.63E+07	1.62E+07
Skewness	0.15	-0.23	-0.38
Kurtosis	-1.53	-1.43	-0.18

4.8 Effect of current in critical sea states

The time histories of Spar displacements, rotation and top tension in catenary mooring are generated under current and wave action incorporating the time integration technique prescribed earlier. For meaningful statistical analysis, the time histories have been plotted for required length. For all the response estimations, the structure is initially presumed to be at rest. Because of the hydrodynamic and structural damping present in the system, transient responses die out after certain duration. In the present section current force has been incorporated along with wave force in sea environment to study the behaviour of Spar platform under the severe sea state, strong gale condition. This ocean loading is termed as sea state SG-WC. The responses of sea state SG-WC have then been compared with other two cases: moderate gale with current (sea state MG-WC) and moderate wave with current (sea state MW-WC). The current velocity of the selected sea state is considered corresponding to the wave height and wave period. Detailed coupled analysis show the effect of current on the moored Spar in the succeeding section. Time histories of the responses for 0 to 3000 sec & 10000 to 12000 sec have been plotted to evaluate the behaviour at short and long duration of induced loading. Moreover response power spectra for wave and wave + current conditions explain the comparison of energy content.

4.8.1. Spar surge due to current inclusion

For wave plus current, surge response time history and power spectrum in every individual case are evaluated to properly understand the nonlinear coupled physics. As the current force is static, static offset of platform position is expected.

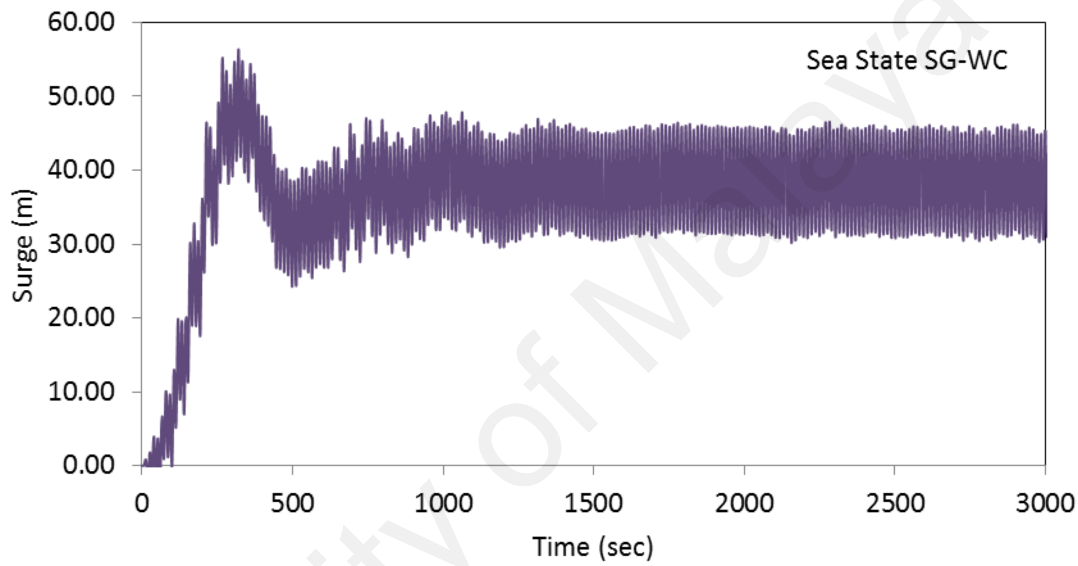

(a) Short duration (0-3000 sec)

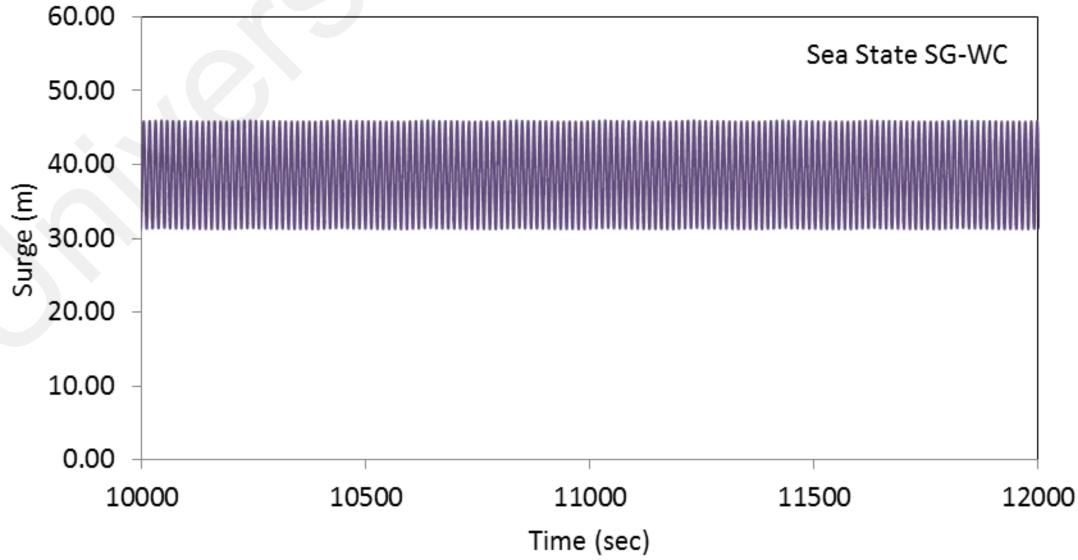

(b) Long duration (10000-12000 sec)

Figure 4.49: Surge time history for Sea state SG-WC (wave + current)

Spar surge in sea state SG-WC

The current force has a static effect on the response. The Spar cylinder is displaced by almost 39 m (Figure 4.49(a)) in the surge due to addition of current. In transient state surge varies between 23.60 m to 56.36 m under sea state SG-WC as shown in Figure 4.49. The static effect of current diminishes the dynamic fluctuations significantly. The regular fluctuation continues throughout the time history with mild alterations in the mean value ranging 31.26 m to 45.97 m (Figure 4.49(b)) at steady state. In case of current, mooring lines get stretched and accordingly stiffness matrix gets modified leading to several stress reversals. Around 1500 seconds the Spar motion stabilizes along wave direction. The current induced force imposes a solitary peak very near to the pitch frequency at 0.156 rad/sec (Figure 4.50). It ensures that the surge response oscillates at frequency equal to that of pitch frequency. The pattern of energy spectrum is not so much different than without current case. The response is seen to be substantially influenced by the high intensity of ocean loading due to addition of current.

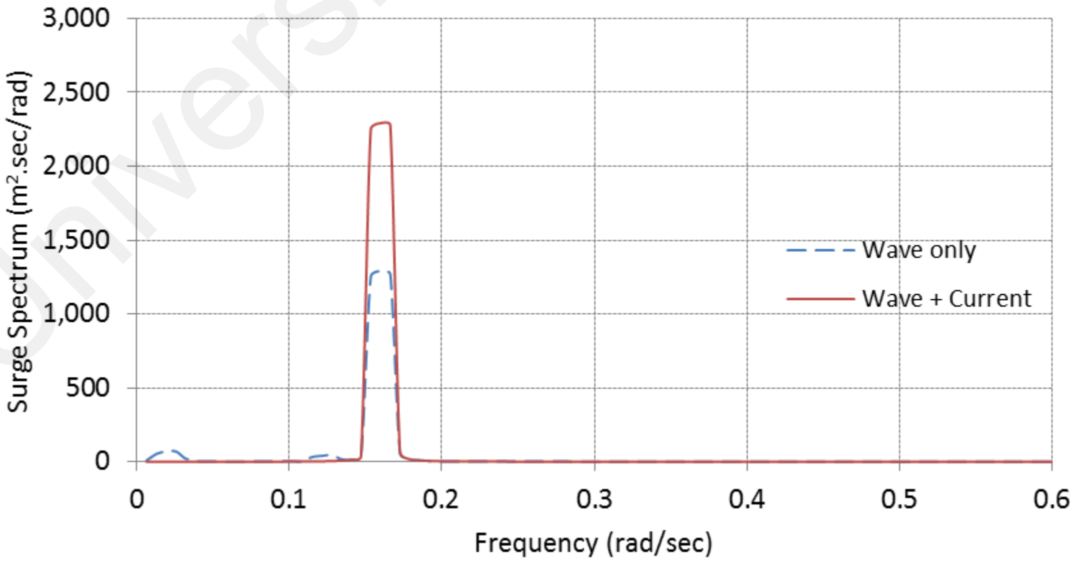

Figure 4.50: Power spectrum of surge for Sea state SG-WC

Variation of Spar surge due to current in severe waves

Static current causes an offset for Spar platform by 22.50 m and 8.06 m under moderate gale and moderate wave respectively whereas under strong gale it is 38.23 m. The oscillating Spar motion in surge ranges from 18.86 m to 26.36 m and -1.82 m to 17.40 m in steady state for MG-WC and MW-WC respectively (Table 4.18). For all the three cases, the spar hull experiences significantly large lateral shifts in wave direction when current is considered. Due to addition of static current force the CMLs experience high pretension and the stiffness matrix is consequently modified. Hence, the increased mooring tension is effect of gradual increment of platform motion for increase in loading intensity. However, highly negative skew-ness in moderate wave displays substantial motion fluctuations.

Table 4.18: Descriptive statistics of Spar surge under critical waves with current

Surge in wave plus current	**Strong gale**	**Moderate gale**	**Moderate wave**
Max (m)	45.97	26.36	17.14
Min (m)	31.26	18.86	-1.82
Mean (m)	38.23	22.50	8.06
Median (m)	37.82	22.58	7.96
Mode (m)	34.72	19.03	13.45
Standard Deviation (m)	5.21	2.51	4.03
RMS (m)	38.58	22.69	9.01
Skewness	0.10	-0.001	-0.02
Kurtosis	-1.54	-1.59	-0.67

4.8.2. Spar motion in heave due to current inclusion

Spar heave in sea state SG-WC

In this case the dynamic fluctuations in heave are milder for sea state SG-WC (Figure 4.51). However, the maximum and minimum responses vary between -0.09 to 0.11 m in SG-WC sea-state less than wave only case. It is observed that static current suppress the heave fluctuations and lessens its magnitude. As shown in Figure, the change in maximum and minimum responses is quite small after 5000 sec for SG-WC case in the presence of current. The mooring line dynamics influence the heave motion under the sea state.

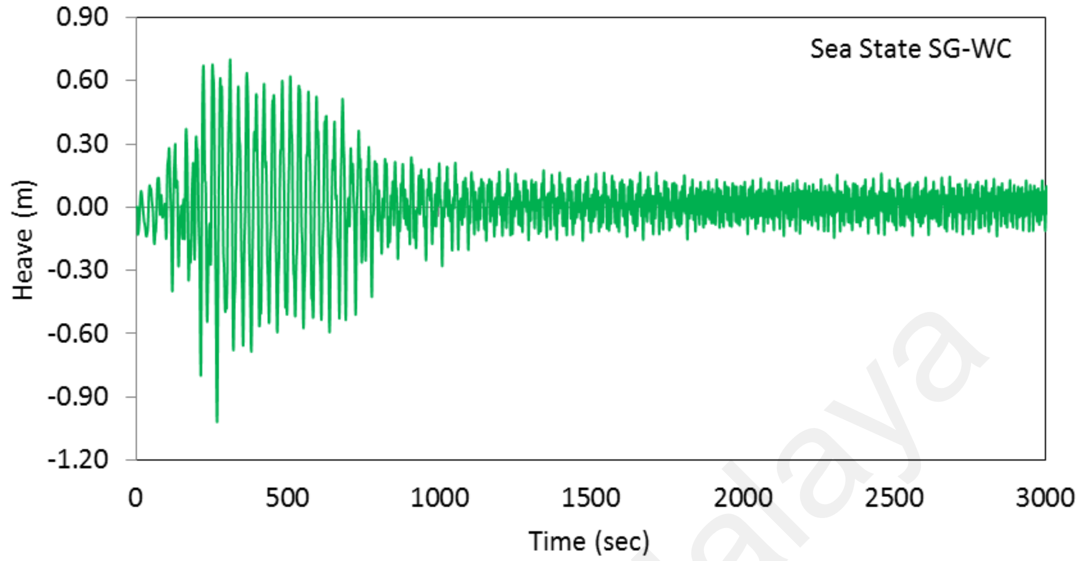

(a) Short duration (0-3000 sec)

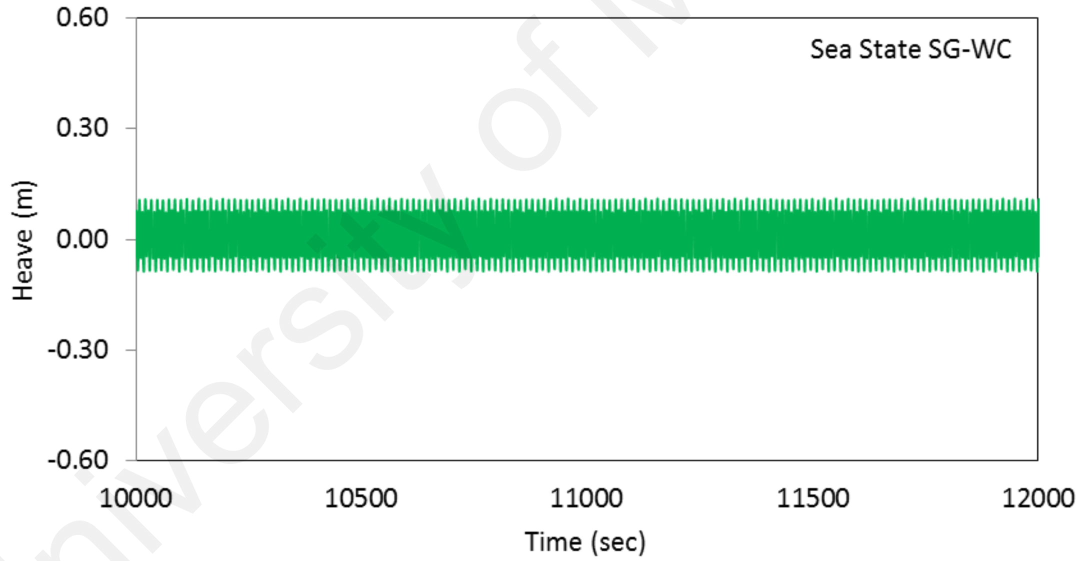

(b) Long duration (10000-12000 sec)

Figure 4.51: Heave time history for Sea state SG-WC (wave + current)

The heave response is predominant showing two sharp peaks at heave frequency zone (Figure 4.52). Another minor peak at pitch frequency shows the upshot of pitching motion on the heave response. Availability of energy content in respective natural frequency is reduced in power spectrum for inclusion of current. At the long duration the heave responses are stabilized with identical peak values in time history. This phenomenon indicates the firmness of the platform with controlled vertical movement when static current is considered.

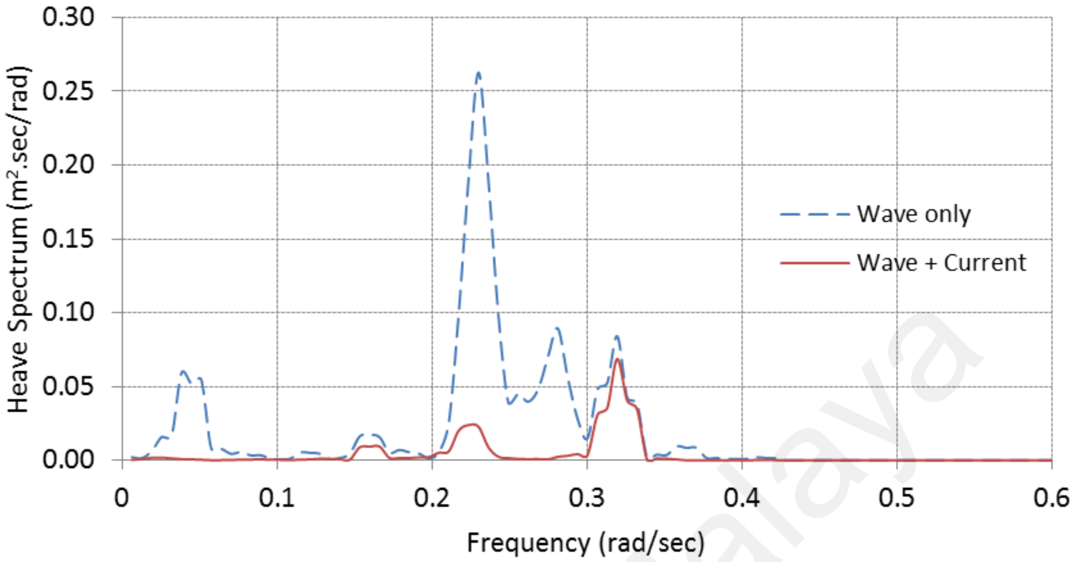

Figure 4.52: Power spectrum of heave for Sea state SG-WC

Table 4.19: Descriptive statistics of Spar heave under critical waves with current

Heave in wave plus current	**Strong gale**	**Moderate gale**	**Moderate wave**
Max (m)	0.11	0.04	2.38
Min (m)	-0.09	-0.02	-2.44
Mean (m)	0.01	0.01	-0.07
Median (m)	0.01	0.01	-0.07
Mode (m)	0.07	0.00	-1.41
Standard Deviation (m)	0.06	0.01	1.23
RMS (m)	0.06	0.02	1.23
Skewness	0.05	-0.08	-0.01
Kurtosis	-1.18	-1.24	-1.25

Variation of Spar heaves due to current in severe waves

The strong gale and moderate gale in presence of current induces similar pattern of platform vertical motion. Maximum heave is approximately 0.04 m for MG-WC which is less than SG-WC case. But for moderate wave, larger heave fluctuations are seen. As shown in Table 4.19, the heave response considering current along with wave are adverse for sea state MW-WC. Though the maximum and minimum responses occur with lower surge motion in SG-WC sea state, the heave oscillation reaches peak of 2.38 m for sea state MW-WC. Less wave period of sea wave makes the wave more frequent.

This additional frequency causes Spar platform to oscillate frequently at CG causing higher heave and pitch response. More accurate response for moderate wave can be computed by diffraction theory rather than Morison’s equation.

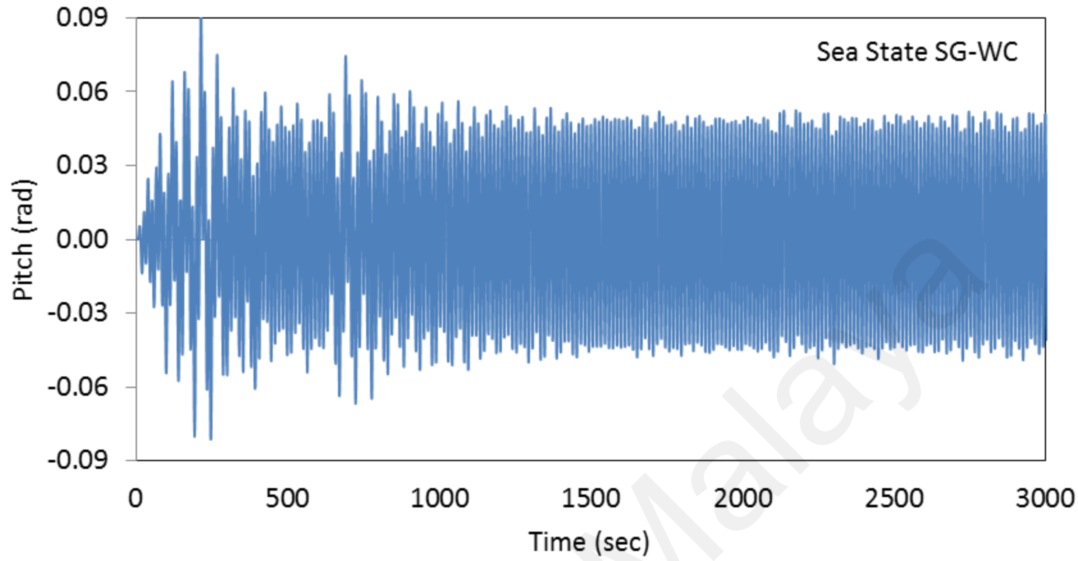

(a) Short duration (0-3000 sec)

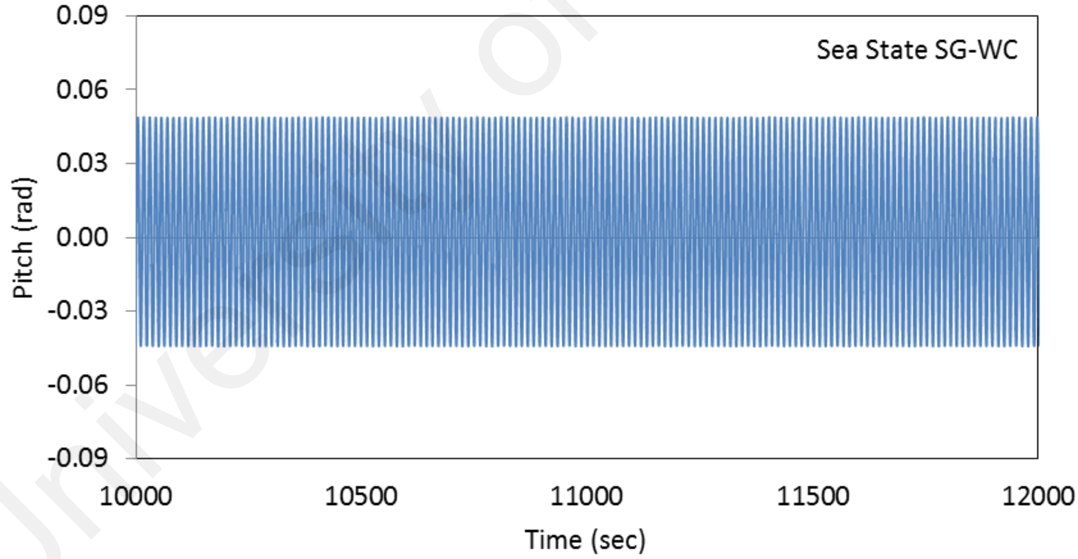

(b) Long duration (10000-12000 sec)

Figure 4.53: Pitch time history for Sea state SG-WC (wave + current)

4.8.3. Spar response in pitch due to current inclusion

Spar pitch in sea state SG-WC

In case of pitch the magnitude of maximum and minimum responses are reduced from ± 0.09 rad to ± 0.05 rad for sea state SG-WC. Figure 4.53 shows the pitch response time history in this sea environment. It is observed that the time history peak values of stress reversals increases when current is considered with wave. This is because of the initial stretching of the moorings which causes high stiffness. The wave loading is then superimposed on already stressed system. At long duration, pitch response reduces for mooring damping and its fluctuation become quite regular with identical peak values. Hence, the platform rotates around its new mean position with controlled manner due to addition of current. The energy spectrum (Figure 4.54) shows a solitary peak at 0.168 rad/sec which is slightly greater than the pitch frequency. The behaviour of pitch response indicates the significance of current involvement. Availability of energy content is slightly increased at the governed pitch frequency for static current force.

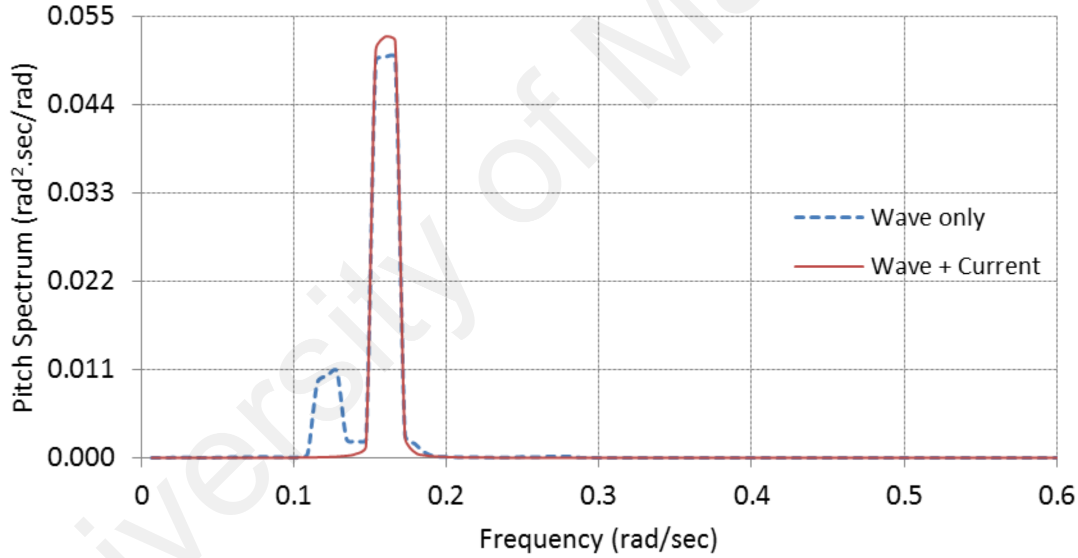

Figure 4.54: Power spectrum of pitch for Sea state SG-WC

Variation of Spar pitch due to current in severe waves

Consideration of current loading in addition to regular wave reasonably changes the Spar rotation in pitch. Similar to the heave response, the pitch is also decreasing when current force is incorporated. Though the rotation change is of small value the alterations are important in coupled response for all the cases. Maximum, mean and RMS values of pitch response shows the behavioural change in Spar rotation (Table

4.20). The peak values of stress reversals are quite low in case of sea state MW-WC compared to sea state SG-WC and MG-WC. Standard deviation, RMS and skew-ness of pitch response gradually decrease for strong gale to moderate gale with current. However, for moderate wave, greater standard deviation in pitch is observed compared to other two cases showing higher fluctuations. Low intensity of wave (moderate wave) causes lower surge and mooring tension but higher heave and pitch. This behaviour may cause discomfort to the crew and affect other operational activities of platform.

Table 4.20: Descriptive statistics of Spar pitch under critical waves with current

Pitch in wave plus current	**Strong gale**	**Moderate gale**	**Moderate wave**
Max (rad)	0.05	0.03	0.05
Min (rad)	-0.04	-0.02	-0.04
Mean (rad)	-0.0002	0.001	0.00
Median (rad)	-0.003	0.001	0.00
Mode (rad)	-0.04	-0.02	0.05
Standard Deviation (rad)	0.03	0.01	0.03
RMS (rad)	0.03	0.02	0.03
Skewness	0.10	-0.0003	0.01
Kurtosis	-1.54	-1.51	-1.39

4.8.4. Mooring line tension due to current inclusion

Top tension in CML at sea state SG-WC

Tension fluctuations in mooring line take place about the mean top tension of 1.80E+07 N (Figure 4.55) at sea state SG-WC. The magnitude of the fluctuations is not so high because of stretched mooring line. The peaks of top tension in mooring line vary from 1.70E+07 to 1.91E+07 N at the steady state. Figure 4.56 shows the tension spectrum of mooring line. The mooring tension for strong gale with current shows one bulky peak at 0.169 rad/sec. This governing frequency is near pitch frequency (Figure 4.56). Because of high pretension in mooring line caused by addition of current force, more energy is available at the same governing pitch frequency.

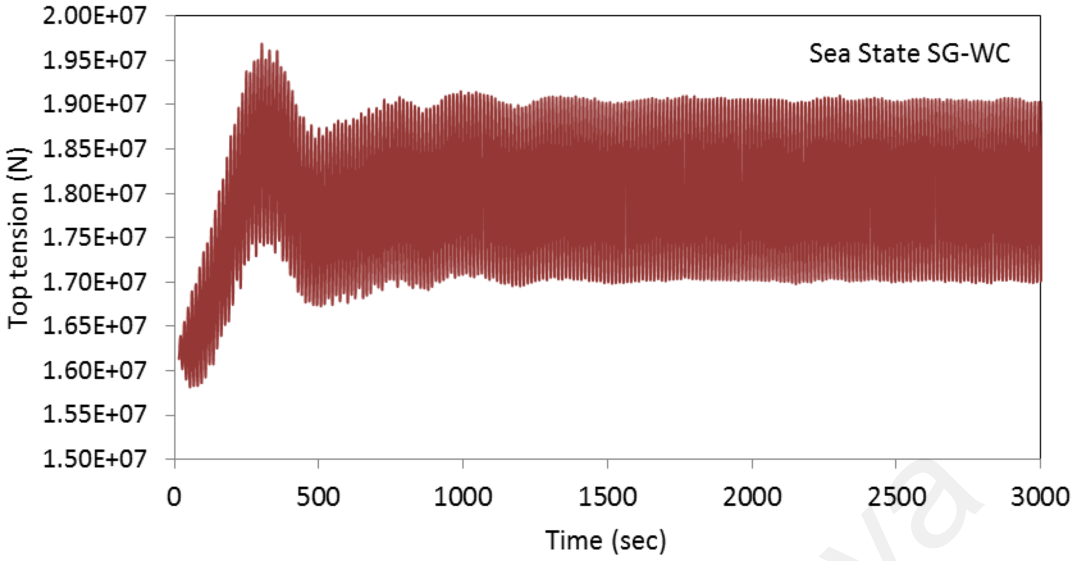

(a) Short duration (0-3000 sec)

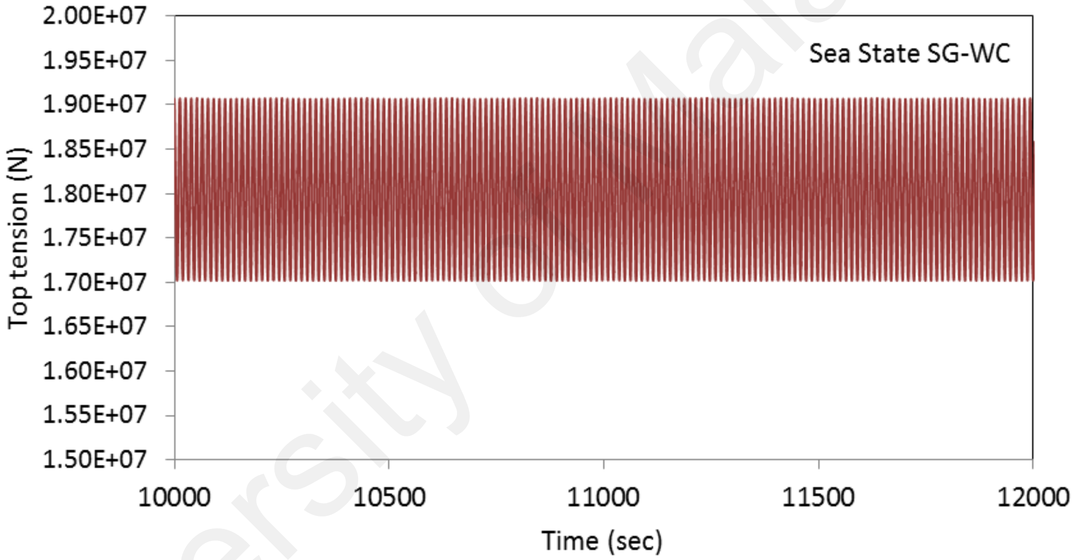

(b) Long duration (10000-12000 sec)

Figure 4.55: Mooring tension time history for Sea state SG-WC (wave + current)

Variation of CML Top tension due to current in severe waves

The current force adds substantial tension in catenary mooring line. The tension response increases by 10.40%, 5.95% and 3.66% due to static current inclusion in strong gale, moderate gale and moderate wave respectively. Maximum, minimum, mean, RMS values of top tension are showing significantly larger value than wave only case. The frequency content of CML tension for longer duration of wave loading shows participation of governing pitch frequency. Earlier it is shown that heave and pitch under moderate wave with current is showing larger value than other sea states. But for mooring tension, the fluctuation is different. Hence, the CML tension increases gradually due to higher pretension in mooring line caused by higher intensity of current loading.

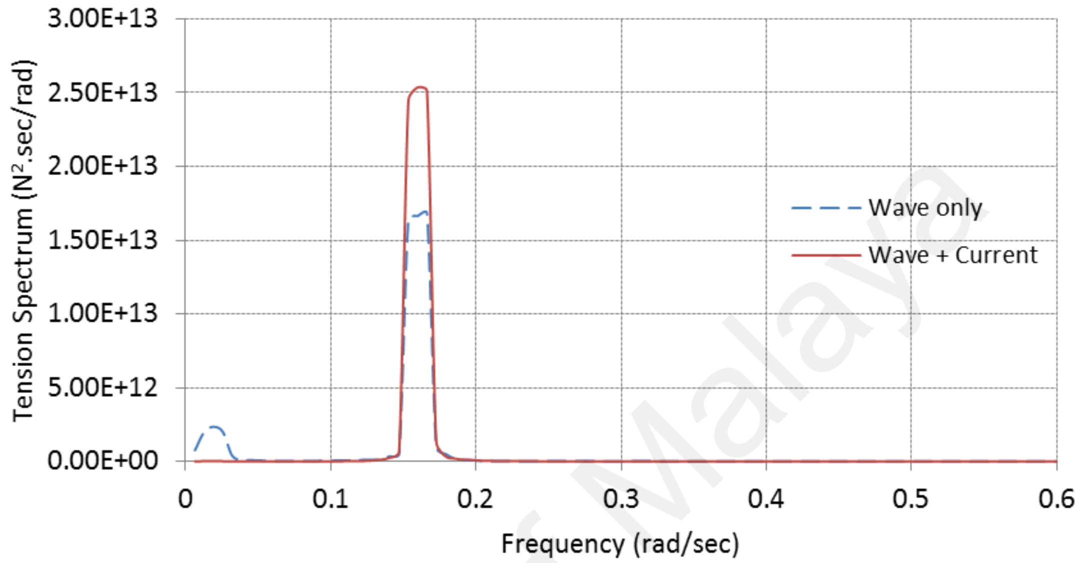

Figure 4.56: Tension spectrum of CML for Sea state SG-WC

Table 4.21: Descriptive statistics of CML tension under critical waves with current

Mooring top tension in wave plus current	**Strong gale**	**Moderate gale**	**Moderate wave**
Max (N)	1.91E+07	1.78E+07	1.70E+07
Min (N)	1.70E+07	1.65E+07	1.62E+07
Mean (N)	1.80E+07	1.72E+07	1.66E+07
Median (N)	1.81E+07	1.73E+07	1.66E+07
Mode (N)	1.91E+07	1.65E+07	1.65E+07
Standard Deviation (N)	7.13E+05	4.58E+05	1.39E+05
RMS (N)	1.81E+07	1.72E+07	1.66E+07
Skewness	-0.02	-0.09	-0.08
Kurtosis	-1.43	-1.50	-0.51

4.9 Effect of wind loading

The solution of equation of motion for coupled Spar platform in deep water experiences more complexities in convergence when aerodynamic loading is incorporated with hydrodynamic forces. The wind force acting on the exposed part of the platform encompasses mean and fluctuating wind components. Accurate prediction of motions of a Spar hull is very important for the integrity and associated costs of the station keeping system. Spar responses in surge, heave and pitch along with top tension in moorings are computed considering aerodynamic loading in addition to wave plus current forces. Aerodynamic loads contribute forces on the wind frontal area. This frontal region includes the topside assembly and the spar hull portion above the sea level. For meaningful statistical analysis, the time histories must be long enough. Therefore, the analyses have been carried out for a long duration of 6000 seconds. For the response analysis, the structure is initially assumed to be at rest. Due to the hydrodynamic and structural damping present in the system, transient response dies out after certain time duration. Hence, time histories recorded for statistical analysis do not contain transient phase of response. Wind velocity follows the density spectrum recommended by API RP 2A-WSD and Emil Simiu as described in the previous chapter.

A severe wind environment may sometimes cause more damage than the normal hydrodynamic loading. Hence, three critical sea states (case SG-WCW, MG-WCW, MW-WCW) have been selected with their individual wind spectrum for comparative evaluation of extreme responses of the moored Spar. The time histories and power spectra give proper assessment of the nonlinear responses. Response behaviours have been evaluated for a number of cases viz. constant + turbulent wind + wave + current, turbulent wind + wave + current, constant + turbulent wind + wave, wave + current and wave only conditions. Influence of different wind spectra has been studied. The variation of response characteristics by varying the wind speed has also been evaluated.

4.9.1. Wind induced surge response

Surge in strong gale

Effect of wind loading on the horizontal movement of platform has been investigated together with wave and current loading. Aerodynamic force added additional lateral shift of DDS hull along wave direction. Hence, the platform is displaced to a high extent in the surge due to sea state SG-WCW. Behaviour of lateral translations at deck level has been presented. It is observed that the platform experiences further lateral shift for constant wind than the current induced static offset. Hence, this constant wind force induced by mean wind speed works as static loading which contributes the additional static offset. Due to the incorporation of constant and turbulent wind force with wave and current environments, platform motion is directly affected and the extreme responses occur under survival conditions. Figure 4.57 illustrates the surge response for inclusion of constant and turbulent wind loading. It is seen that the mean shift of Spar platform is 70.60 m horizontally for total wind. Steady state surge ranges from 61.53 to 79.31 m for total wind whereas for constant wind the values are lower. The surge responses show maximum lateral shift as 65% larger for total hydro-aerodynamic loading than the wave + current induced surge. It is noticed that the static effect of additional loading noticeably diminishes the dynamic fluctuations. Besides, turbulent wind also effects on horizontal displacement contributing considerable amount. Because of hydrodynamic and structural damping in the system, transient responses die out after a certain period. Hence, afterward the Spar motion is seen throughout the time history with mild fluctuations in the mean value.

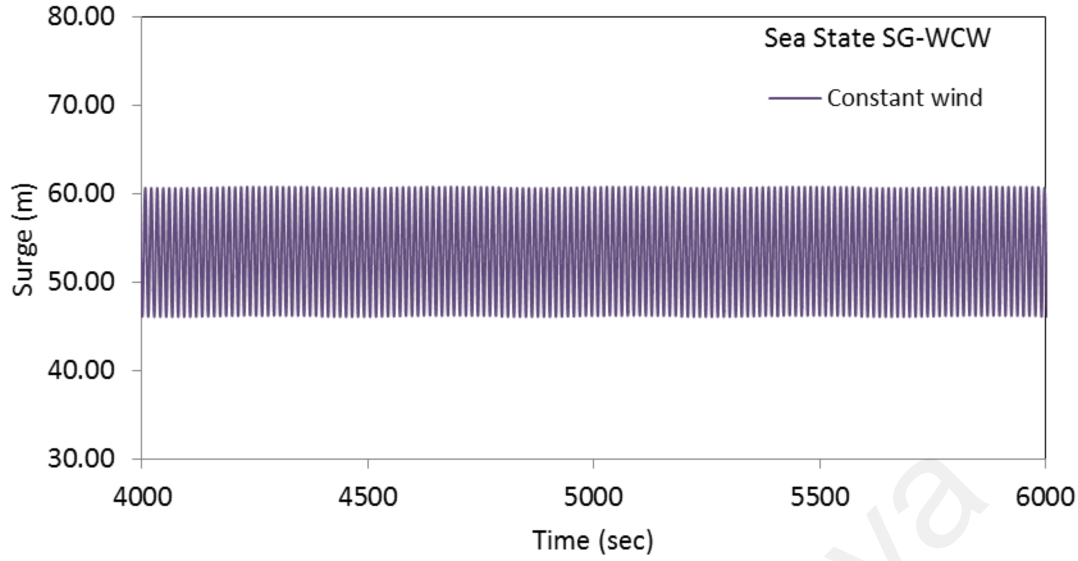

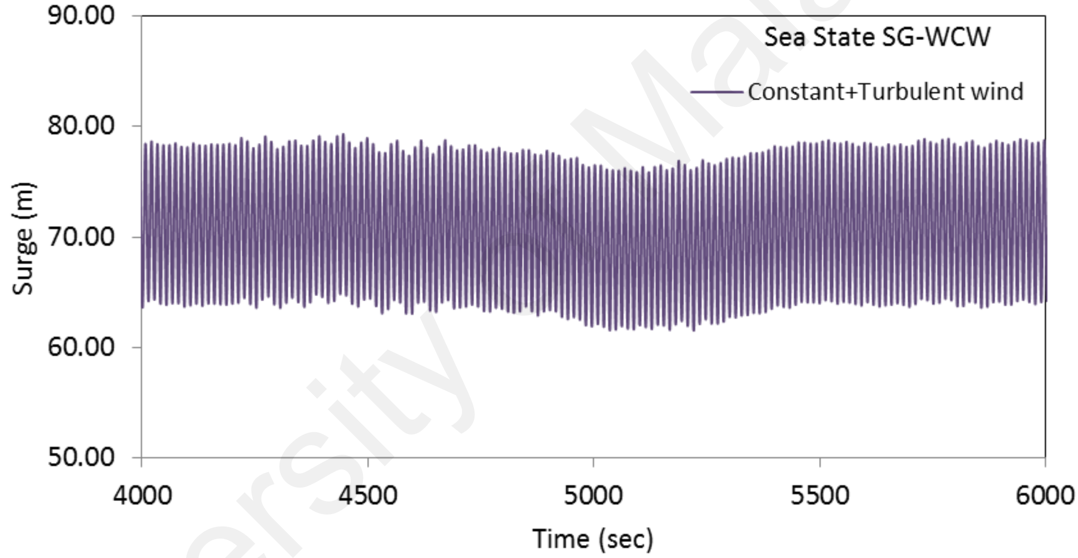

Figure 4.57: Surge at wave + current + wind at deck level for Sea state SG-WCW

Surge response oscillates at frequency 0.167 rad/sec near to the pitch frequency (Figure 4.58). The pattern of energy spectrum is seen to be influenced by the turbulent wind portion of the strong gale. The figure shows the attraction of additional energy content by this fluctuating wind portion.

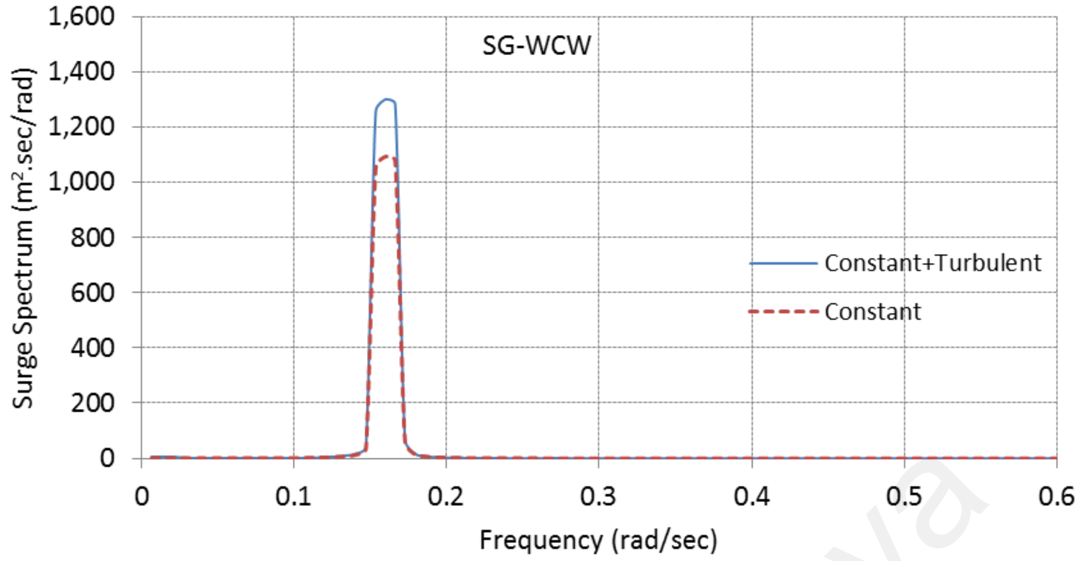

Figure 4.58: Power spectrum of surge for Sea state SG-WCW

Effect of turbulence on surge with wind speed

The effect of turbulent wind on the platform motion in surge of the coupled Spar subjected to the selected waves, currents and winds have been evaluated. The results based on the constant and turbulent wind have been compared to focus the influence of turbulence. In earlier Figures, the surge time history and the surge spectrum for both the constant and the turbulent wind cases are shown under critical environments. In this section the maximum, mean and standard deviation of the responses are obtained through surge time history from individual time domain solutions. The motion characteristics are plotted versus mean wind speed. The mean wind speed refers to the three load cases (strong gale, moderate gale and moderate wave). For increase in wind speed, the maximum value of surge also increases. The maximum surge response for total loading in strong gale decreases by 45% and 55% for moderate gale and moderate wave cases. The variation of Spar surge motion for constant and turbulent wind is shown in Figure 4.59. It is witnessed that the mean value of platform horizontal motion is higher for constant and turbulent wind as expected for surplus translation from turbulence. But the standard deviation for turbulent wind is higher. It shows the contribution of fluctuating behaviour of turbulence.

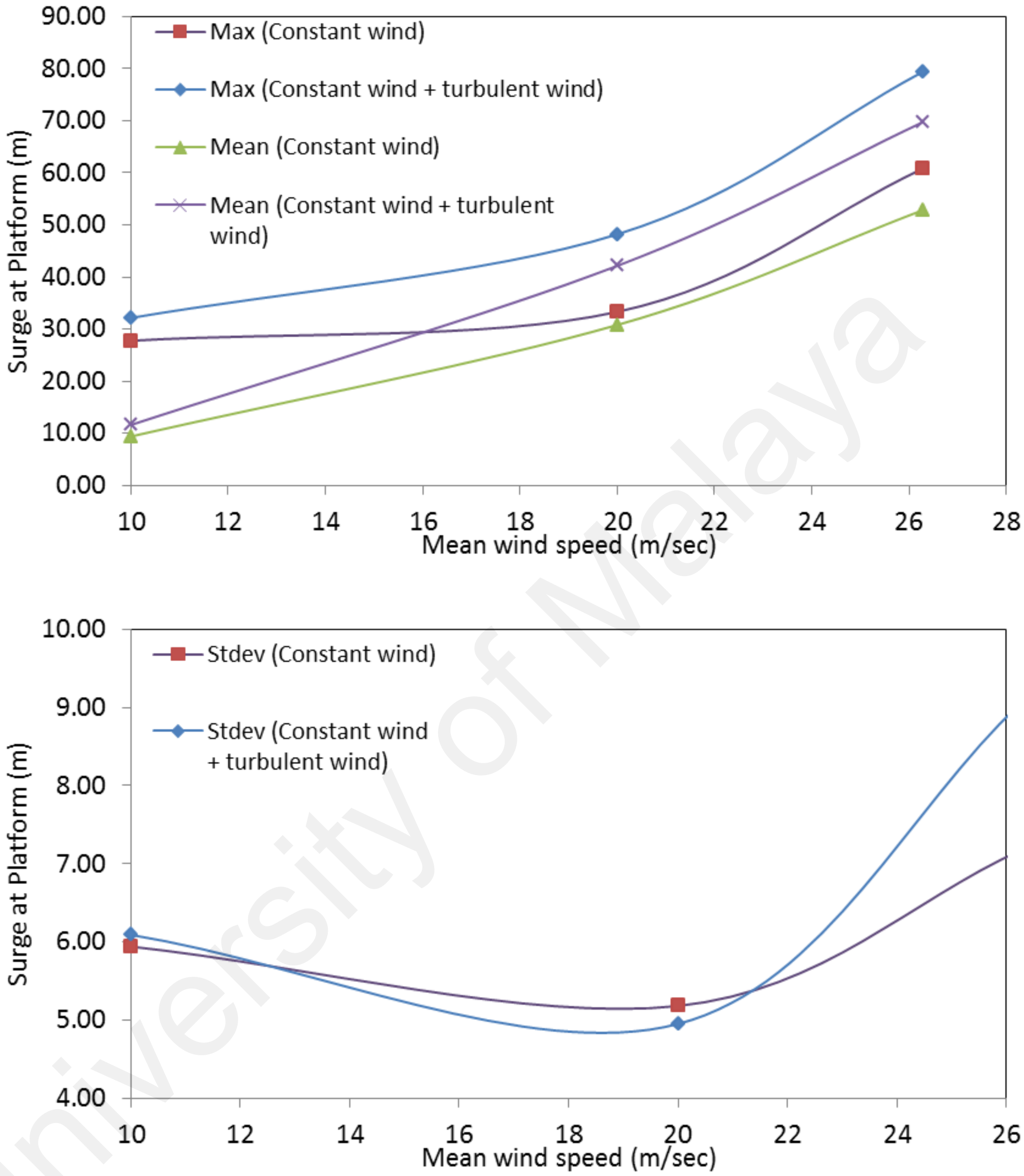

Figure 4.59: Effect of turbulence on Spar surge

Surge variation with wind spectrum

For the comparative study of the spar responses, the fluctuating portion of wind loading on the Spar frontal area has been characterised by Emil Simiu spectrum along with the API RP 2A-WSD spectrum. The wave, current and mean wind speeds are kept similar for both the cases. The varying parameter is only turbulence provided by individual spectrum. Coupled analysis by several cases indicates that the API RP 2A spectra estimates higher deck displacement than the Simiu spectrum in an amount of 11%. Table 4.22 illustrates the characteristics of surge response under the two spectra in different cases.

Table 4.22: Surge response behaviour for different wind spectra

Surge in **Wave + current + total wind**	**Emil Simiu Spectrum**	**API RP 2A-WSD Spectrum**
Strong gale		
Max (m)	71.34	79.31
Min (m)	56.77	61.53
Mean (m)	63.96	70.60
Median (m)	63.65	70.79
Mode (m)	71.32	64.97
Standard Deviation (m)	5.26	6.83
RMS (m)	64.18	70.76
Skewness	0.09	0.02
Kurtosis	-1.36	-1.30
Range	14.57	17.78
Moderate wave		
Max (m)	25.15	37.32
Min (m)	2.93	-5.75
Mean (m)	7.57	11.60
Median (m)	7.30	10.06
Mode (m)	13.93	17.80
Standard Deviation (m)	2.69	6.09
RMS (m)	8.03	13.10
Skewness	0.51	1.20
Kurtosis	0.54	1.73
Range	23.22	43.07

The API RP 2A based responses are highly skewed than the Simiu spectrum induced responses. This means than the deviation of platform surge is more for the API RP 2A spectrum due to more fluctuating behaviour. Higher kurtosis of surge distribution poses the trends in leptokurtic style. These characteristics ensures significant amount of surge values are nearer to the mean showing substantial peaked-ness in Simiu spectrum. However, the magnitudes of highest, lowest average and median show in general lower motion in Simiu spectra. This is due to higher energy available in this spectrum at low frequency. Both the API RP 2A spectrum and Simiu spectrum are advantageous for the low frequency coupled Spar. For moderate wave also, the greater surge is seen for API RP 2A spectrum than Simiu spectrum showing similar pattern like strong gale condition. But the fluctuating tendency of platform motion for API RP 2A spectrum is more in moderate wave case. This can be seen well from the difference of standard deviation for both the cases. The Stdev for API RP 2A spectrum in moderate wave case is considerably higher. Therefore for dense occurrence of wave due to lower wave period, influence of API RP 2A spectrum on platform motion is more significant.

4.9.2. Wind induced heave response

Heave in strong gale

The behaviour of Spar hull in vertical direction subjected to wind also confirms noteworthy differences compared to the case of no current as well as wave + current. In the sea state SG-WCW, the dynamic oscillations are milder than without wind cases (Figure 4.60). The time history peaks of heave oscillations indicate momentous reduction in vertical movement of the platform. The maximum heave motions were 0.69 m for wave only case and 0.16 m for wave plus current case. For addition of constant wind loading with the forces, maximum heave motion lessens to 0.14 m which is 12% less than wave+current case. But again, the turbulence wind increases vertical translation of Spar up to 0.25 m. Influence of turbulence is clearly observed through this characteristics caused by its fluctuating feature. Furthermore, the variation in maximum and minimum excursions is quite trivial after 6000 sec for the aero-hydrodynamic sea loading.

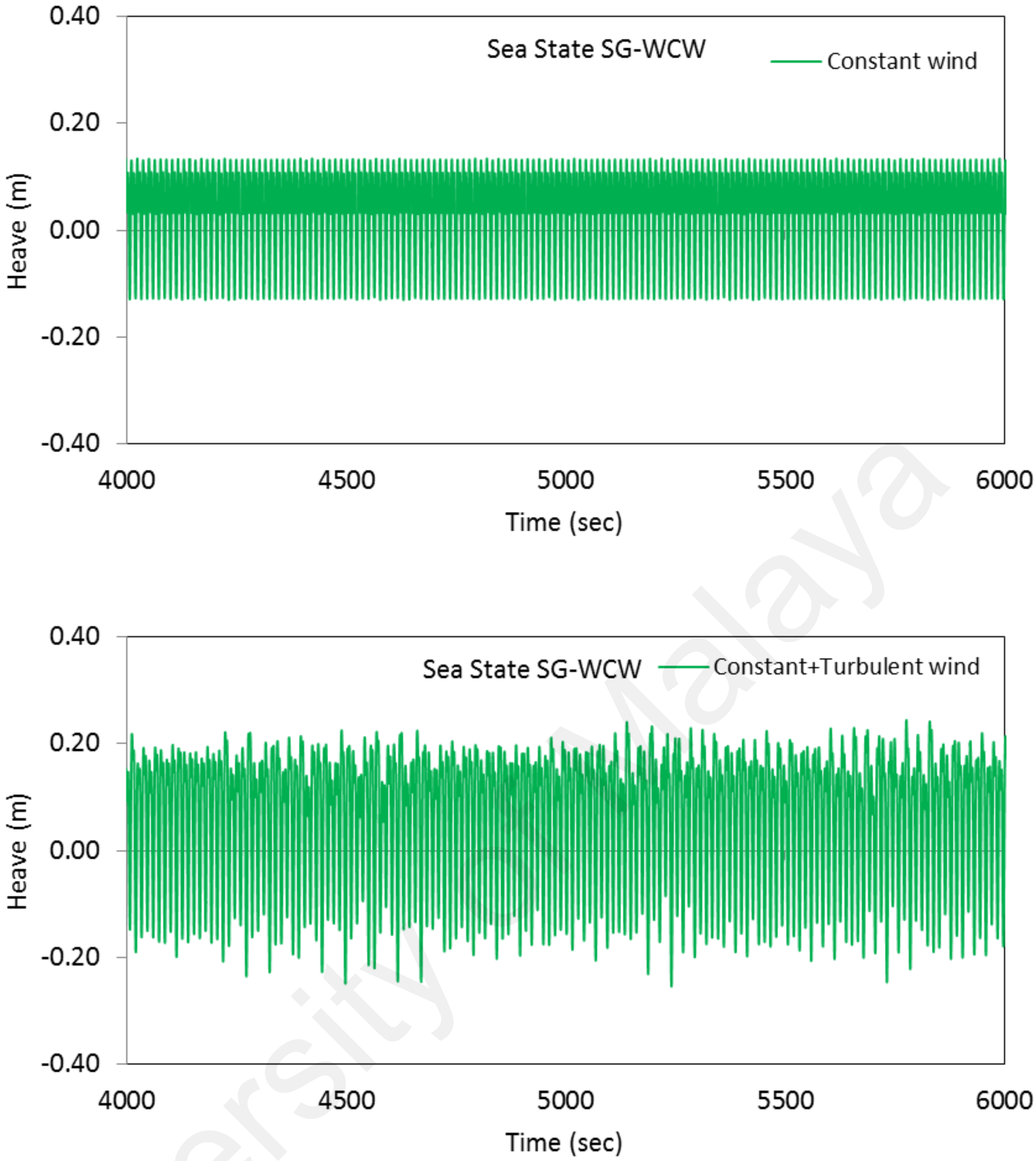

Figure 4.60: Heave under wave + current + wind for Sea state SG-WCW

One large peak in pitch frequency along with two minor peaks in heave frequency region (Figure 4.61) has been seen in heave spectrum. Therefore the energy frequency shows involvement of both heave and pitch on heave response. The constant + turbulent winds attract substantial energy content in pitching motion than the constant wind case. This discrepancy shows the influence of turbulence on Spar vertical motion.

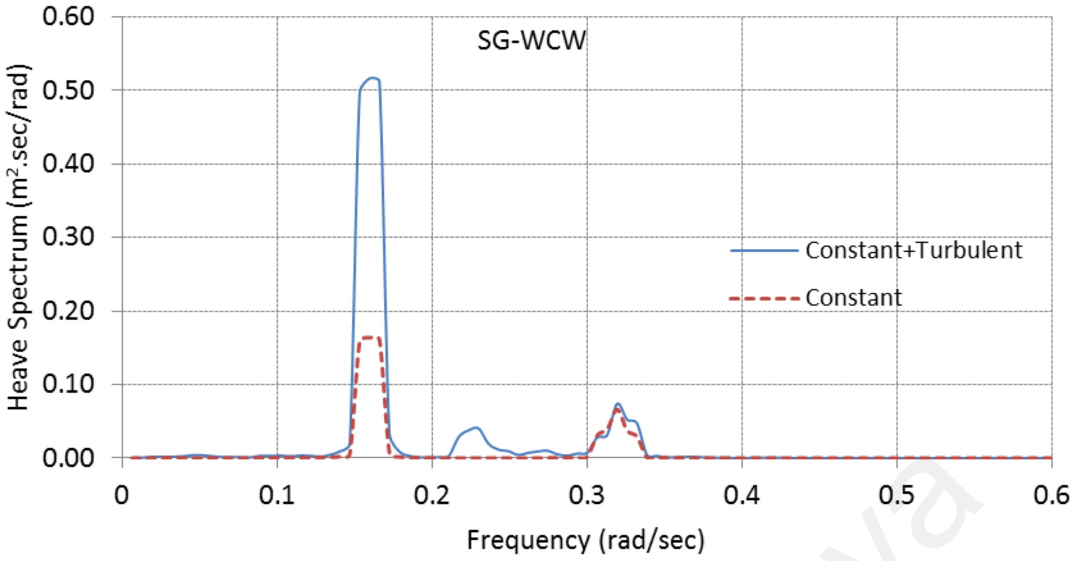

Figure 4.61: Power spectrum of heave for Sea state SG-WCW

Effect of turbulence on heave with wind speed

The maximum, mean and standard deviation of heave responses for constant and turbulent wind are evaluated from time history of heave for every individual load case. The values have plotted against mean wind speed as shown in Figure 4.62. Because of decrement of mean wind speed, the maximum heave is also decreasing for moderate gale by 50% than strong gale. But moderate wave is showing quite larger heave response due to its dense oscillations induced by wave loading. The maximum value of heave response is reduced for the additional influence of constant wind. But turbulent wind increases the heave motion again inducing fluctuation on motion response. Moreover, the standard deviation for turbulent wind is higher which indicates the upshot of fluctuating wind portion.

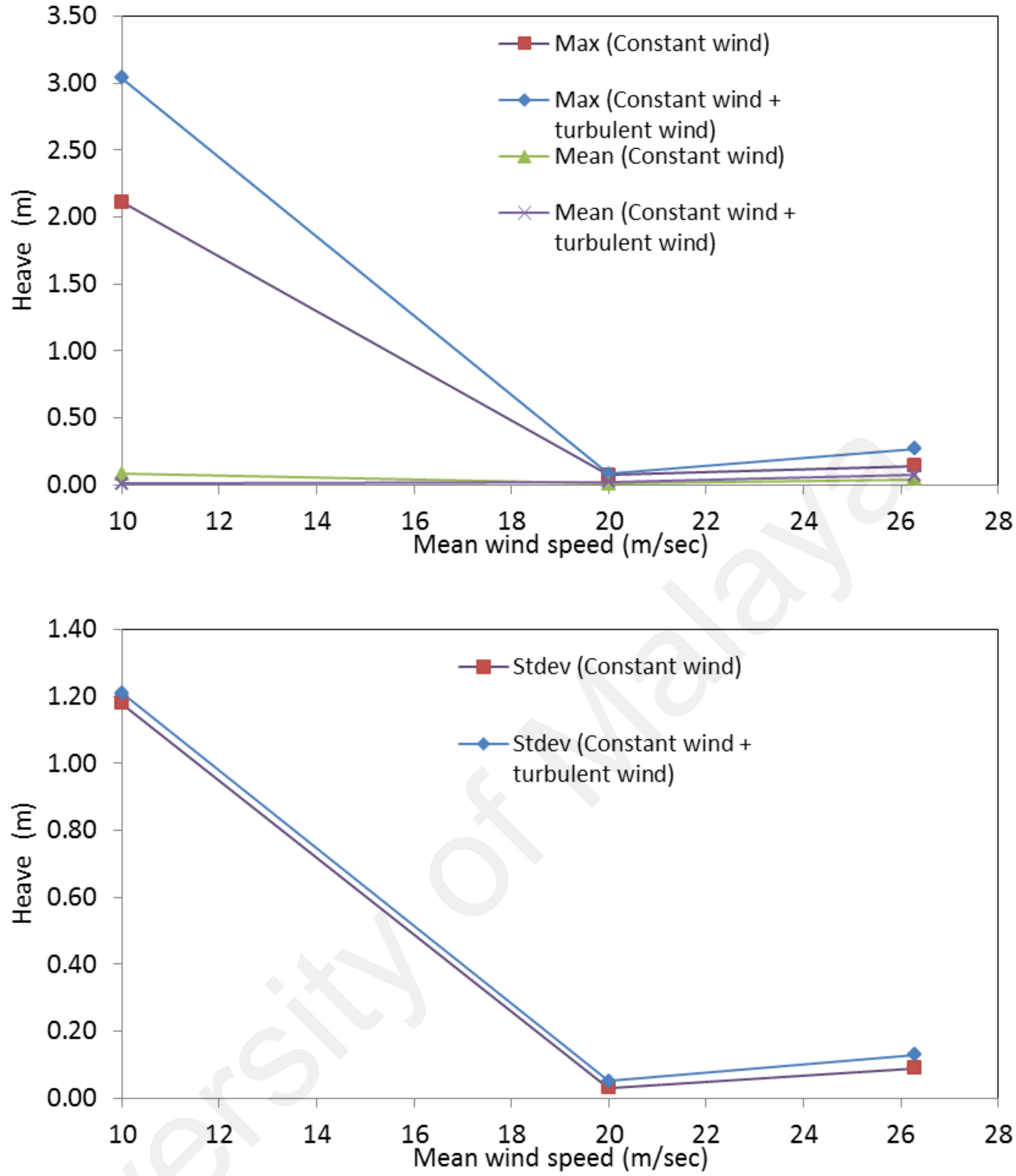

Figure 4.62: Effect of turbulence on Spar heave

Heave variation with wind spectrum

Lower vertical displacement is witnessed under the spectra suggested by Simiu than the API RP 2A spectra. The increase in maximum heave at API RP 2A spectrum is seen by 6% than the Simiu spectrum. Varying behaviours of heave for both spectra are shown in Table 4.23. Slightly more skewed responses are seen in API RP 2A spectra. This discrepancy in negative skew-ness displays a little more fluctuation of vertical motion from the mean value. However, the skew-ness is moderate in nature for both cases.

Similar trend of higher statistical values are seen for API RP 2A spectrum like surge motion. Lower wave period in moderate wave gives higher heave motion for both the spectrum. Nevertheless, the API RP 2A spectrum introduces more fluctuations in greater range than Simiu spectrum case. These can be seen in range of heave time history peak values. For Simiu spectrum, the maximum heave is 0.58 m for moderate wave whereas this is as large as 3.04 m for API RP 2A spectrum case. The root mean square and Stdev of heave motion supports this identical behaviour for the variation of wind spectra.

Table 4.23: Heave response behaviour for different wind spectra

Heave in **Wave + current + total wind**	**Emil Simiu Spectrum**	**API RP 2A-WSD Spectrum**
Strong gale		
Max (m)	0.16	0.24
Min (m)	-0.16	-0.25
Mean (m)	0.04	0.08
Median (m)	0.09	0.12
Mode (m)	0.15	0.15
Standard Deviation (m)	0.11	0.12
RMS (m)	0.12	0.14
Skewness	-0.75	-0.94
Kurtosis	-1.02	-0.38
Range	0.32	0.49
Moderate wave		
Max (m)	0.58	3.04
Min (m)	-0.62	-3.01
Mean (m)	-0.01	0.008
Median (m)	-0.004	0.02
Mode (m)	0.00	0.00
Standard Deviation (m)	0.17	1.21
RMS (m)	0.17	1.00
Skewness	-0.03	-0.12
Kurtosis	0.54	0.59
Range	1.2	6.05

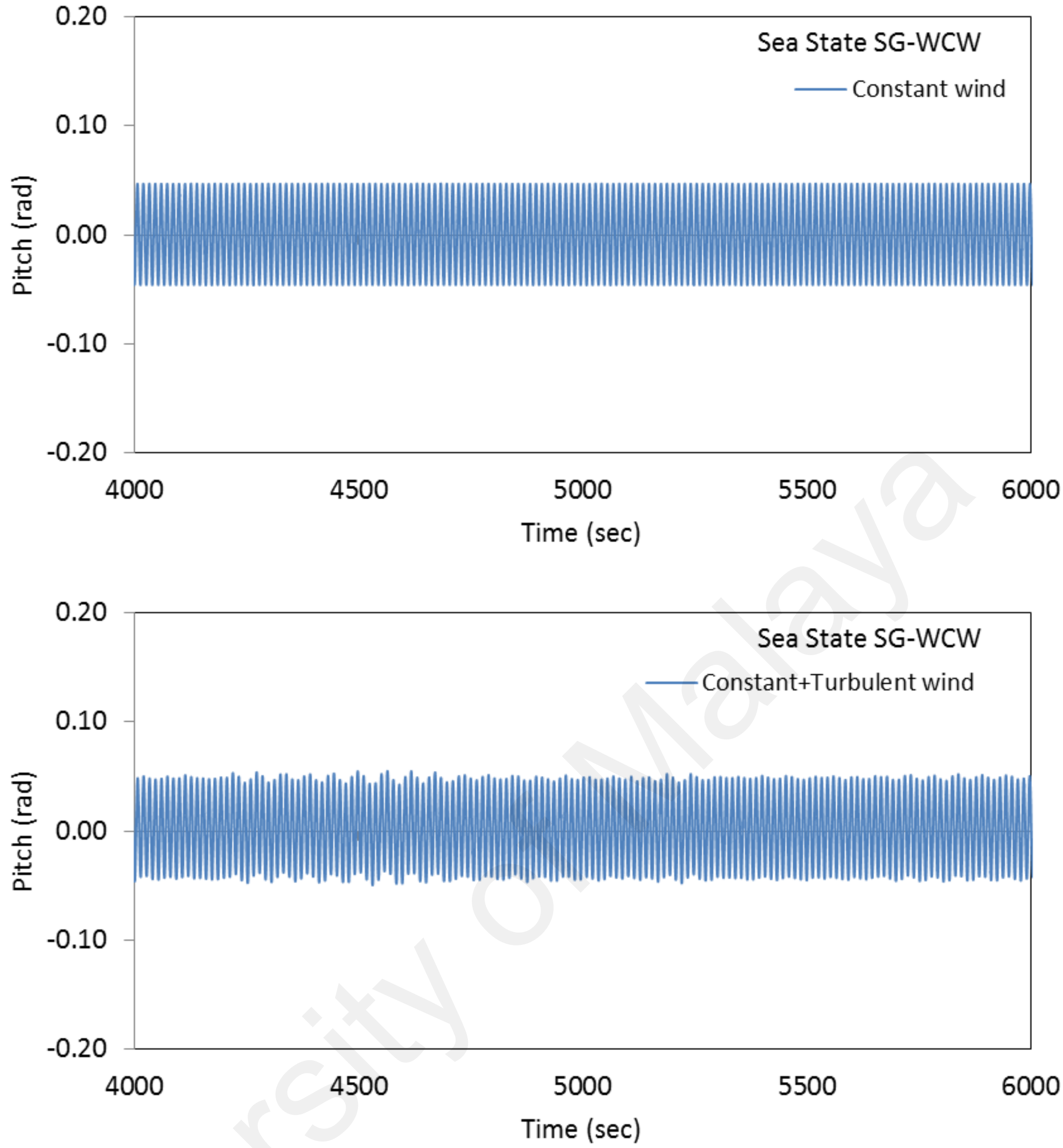

Figure 4.63: Pitch under wave + current + wind for Sea state SG-WCW

4.9.3. Wind induced Pitch response

Pitch in strong gale

Though the inclusion of aerodynamic forces increases Spar surge, the pitch is found to decrease. This is due to additional firmness of platform achieved from constant wind portion of aerodynamic loading. Huge amount of energy content is observed by the pitching motion and hence the Spar experiences reduced rotation. The magnitudes of maximum and minimum pitch responses fall within the range of -0.05 rad to +0.05 rad due to addition of constant wind in strong gale. However, the pitch motion experiences larger value induced by turbulent wind. The amount of increment by turbulent wind is 20% that the wave+current+constant wind loading. Figure 4.63 shows the time series of pitch motion for constant and constant + turbulent wind conditions. Though steady value of pitch is seen for constant wind case, gust wind velocity disturbs the regular shape and reflects fluctuating time history peaks for total wind force.

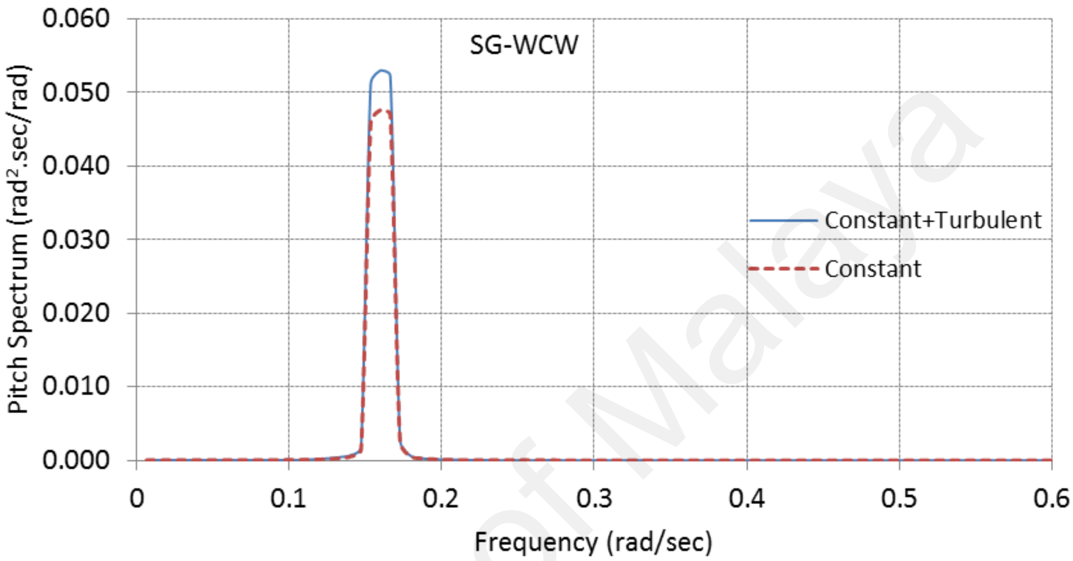

Figure 4.64: Power spectrum of pitch for Sea state SG-WCW

The energy spectrum of pitch shows a governing peak at 0.153 rad/sec which is located at the pitch natural frequency (Figure 4.64). Higher energy is available for constant + turbulent wind at this frequency than the constant wind case. This rise in energy content for total loading indicates the involvement of wind turbulence on pitch response.

Effect of turbulence on pitch with wind speed

Figure 4.65 illustrates the evaluation of hydro-aerodynamic pitch response behaviour of Spar hull. Both the constant wind and total wind includes corresponding wave and current for the selected three sea states; strong gale, moderate gale and moderate wave. Reduced mean wind speed lessens the maximum value of pitch for moderate gale by 42% than strong gale. However, the pitch response increases more than 2 times in case of moderate wave because of its dense fluctuations in lower wave period. For every mean wind speed, effect of turbulence is visible. In case of turbulent wind, the fluctuations causes increase in dynamic responses compared to constant wind. The maximum and mean pitch is dominated by turbulent wind. In addition the fluctuating portion of wind poses higher standard deviation.

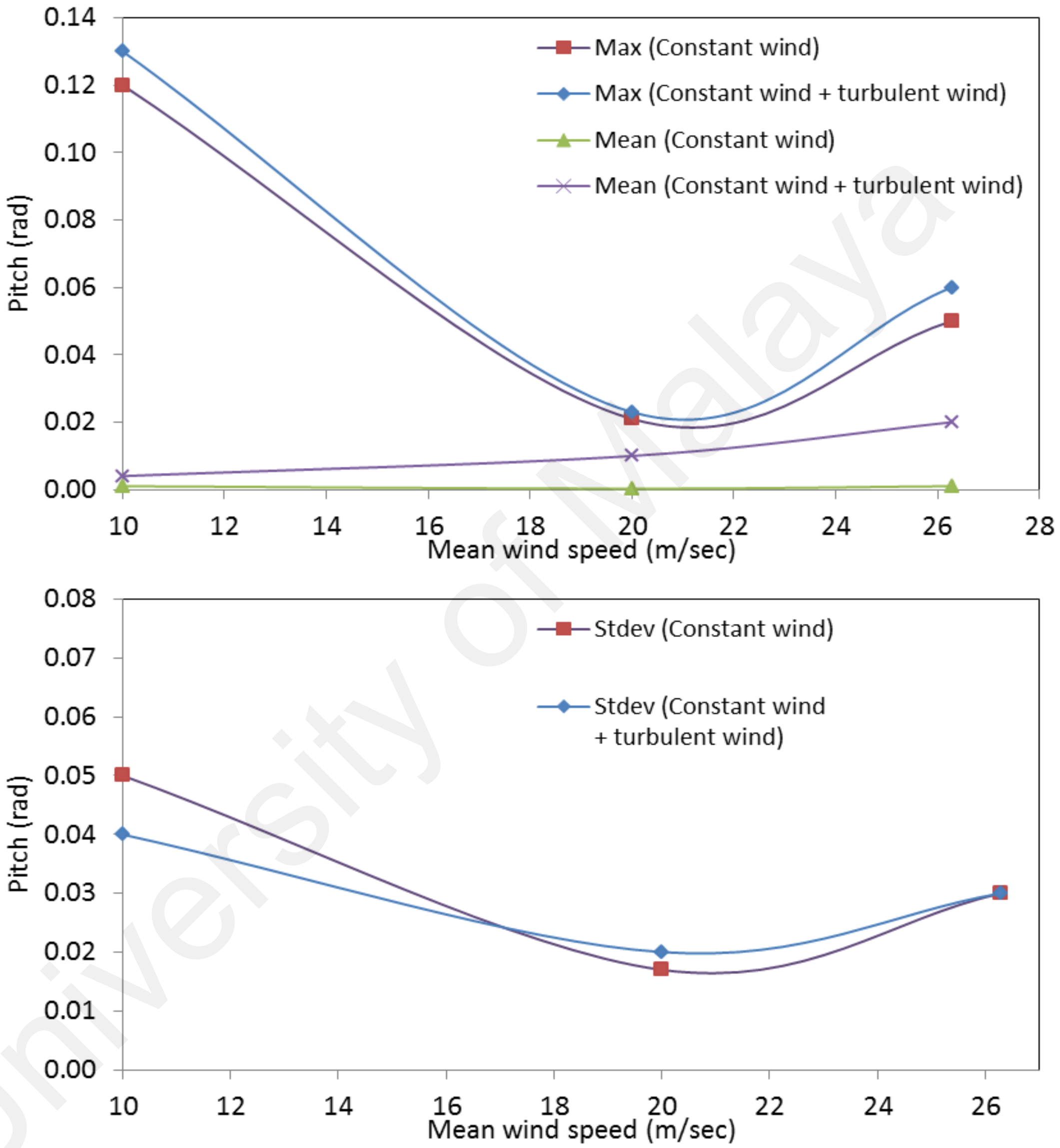

Figure 4.65: Effect of turbulence on Spar pitch

Pitch variation with wind spectrum

Alike the heave response, the spar response in pitch shows similar variation in behaviour for varying wind spectra. Slight reduction in pitch responses is seen in Simiu spectra than the API RP 2A spectra as shown in Table 4.24. For the strong gale condition, influence of spectrum is seen as 20% greater time history peak in API RP 2A spectrum case. But for the moderate wave environment, the API RP 2A adds significant fluctuations on pitch response. The changes of maximum or minimum pitch are more than two times compared to the Simiu spectrum induced platform rotation. Furthermore the pitch distributions are about perfectly skewed showing around 0.0 skew-nesses for both the cases. . This indicates that the pitch responses are quite evenly distributed on both sides of the mean value implying a symmetric distribution. Yet the greater Stdev for API RP 2A spectrum especially in moderate wave shows its more involvement in pitch fluctuation.

Table 4.24: Pitch response behaviour for different wind spectra

Pitch in **Wave + current + total wind**	**Emil Simiu Spectrum**	**API RP 2A-WSD Spectrum**
Strong gale		
Max (rad)	0.05	0.06
Min (rad)	-0.05	-0.05
Mean (rad)	-0.001	0.002
Median (rad)	-0.003	0.002
Mode (rad)	-0.02	-0.04
Standard Deviation (rad)	0.03	0.03
RMS (rad)	0.03	0.04
Skewness	0.04	0.04
Kurtosis	-1.54	-1.35
Range	0.10	0.11
Moderate wave		
Max (rad)	0.06	0.13
Min (rad)	-0.06	-0.12
Mean (rad)	0.0003	0.004
Median (rad)	0.0001	0.003
Mode (rad)	-0.02	0.10
Standard Deviation (rad)	0.02	0.04
RMS (rad)	0.03	0.04
Skewness	0.02	0.00
Kurtosis	-0.002	1.36
Range	0.12	0.25

4.9.4. Wind induced mooring tension

Mooring tension in strong gale

The top tension fluctuations in catenary mooring line takes place around the mean tension of 1.88E+07 N (Figure 4.66) under wave plus current plus constant wind in strong gale. The magnitude of the fluctuations is not high because of high pretension in mooring line but the force magnitude is higher than earlier wave and wave plus current condition. The mooring tension ranges from 1.77E+07 to 1.99E+07 N. In case of turbulent wind significant peaks occur compared to the earlier duration. A dense array of fluctuating peaks is obtained and the higher value peaks occurs showing 2.10E+07 N maximum CML tension for total wind loading with wave+current force. Nonlinear dynamics of the Spar hull reveals that the extreme value of responses can occur when turbulent portion of wind is considered together with other loadings. Therefore, the additional tension response in CML induced by wind turbulence requires is to be considered.

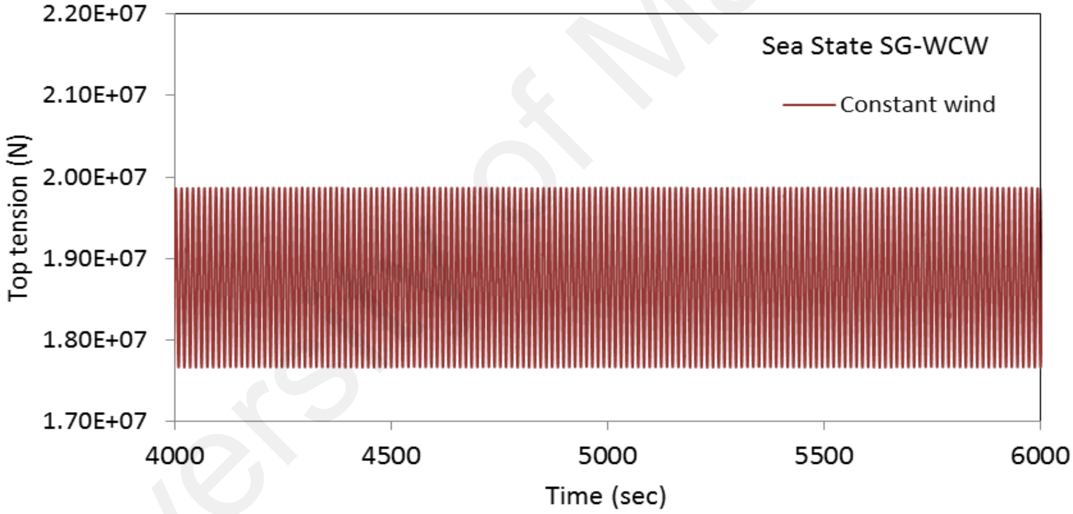

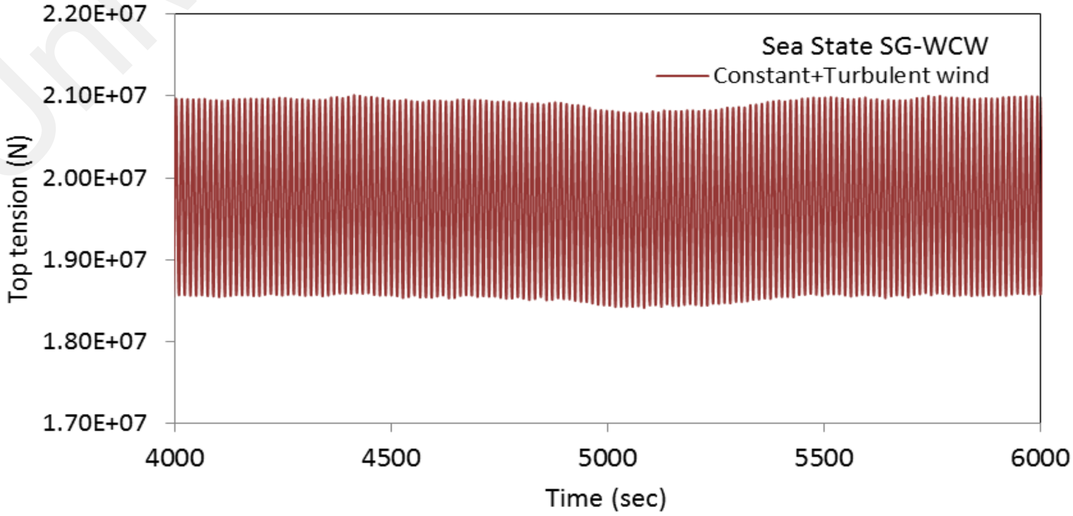

Figure 4.66: Mooring tension under wave + current + wind for Sea state SG-WCW

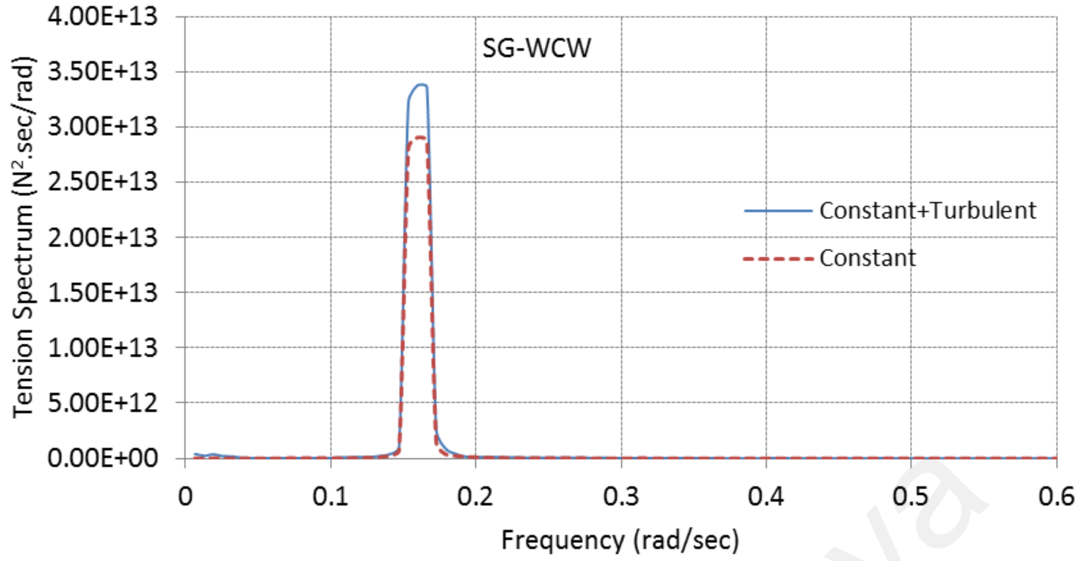

Figure 4.67: Tension spectrum of CML for Sea state SG-WCW

Fluctuating wind together with the constant wind tends to attract more energy than the constant wind case. Frequency content shows solitary peak in pitch frequency region (Figure 4.67). Attraction of huge energy induces such behaviour on mooring tension. Periodic responses are witnessed under aero-hydro dynamic loading with regular value at long duration.

Effect of turbulence on CML tension with wind speed

Turbulent wind force dominates on the mooring tension behaviour of the coupled Spar for all the sea states. The effect of its fluctuating tendency on the CML top is clearly visible as it contributes additional tension. The results based on the constant and turbulent wind have been compared to focus their involvement. It has been noticed that due to decrease in wind speed, the maximum CML tension decreases gradually. Maximum top tension in mooring line for total loading under strong gale in amount of 2.12E+07 N decreases by 10% and 18% for moderate gale and moderate wave cases respectively. For the constant wind portion, mooring tension becomes larger which have been shown earlier. Moreover, the maximum, mean and standard deviation of top tension is governed by wind turbulence. The standard deviation of mooring tension for constant and constant plus turbulent wind is shown in Figure 4.68. Hence, the fluctuating behaviour of turbulence significantly increases the tension in station keeping system.

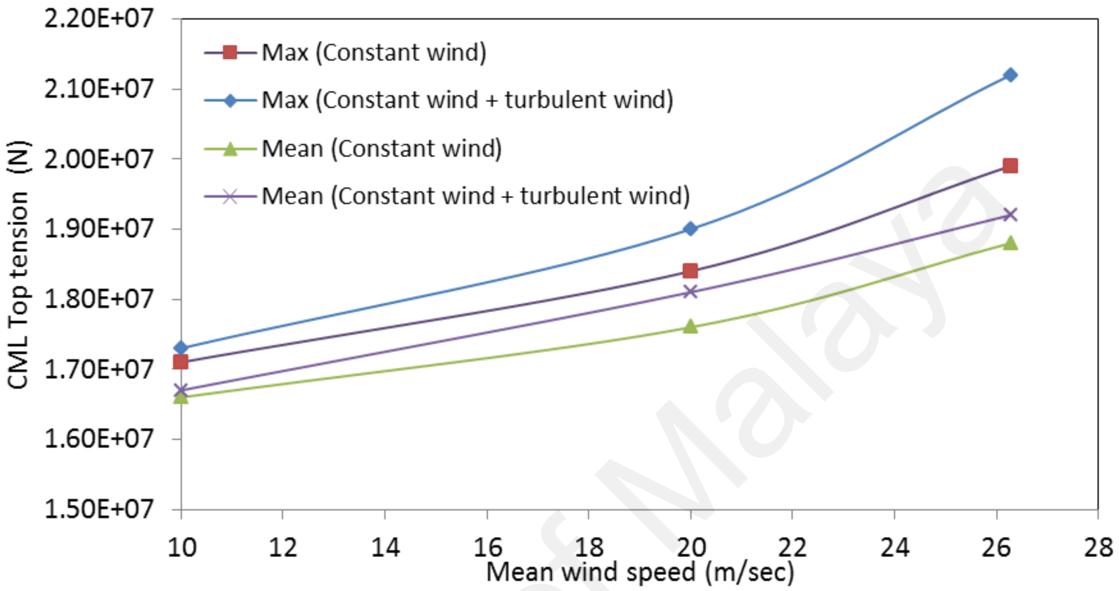

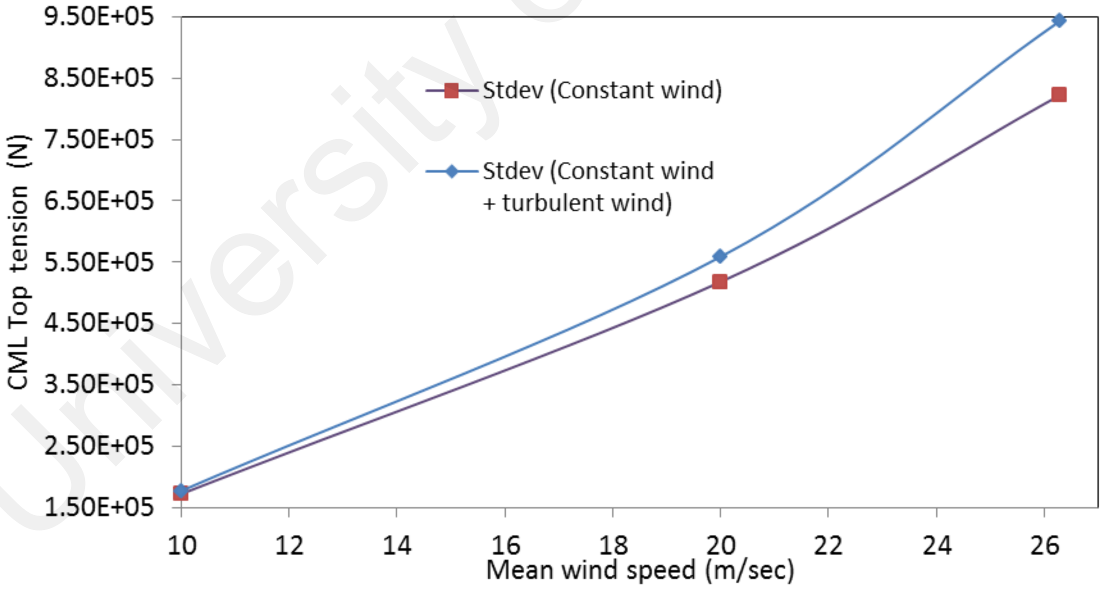

Figure 4.68: Effect of turbulence on CML top tension

Mooring tension variation with wind spectrum

The top tension in mooring line is found to be higher for API RP 2A than Simiu spectra. The increment in mooring tension confirms the participation of fluctuating aerodynamic loading induced by the later spectra. The fluctuations of CML top tension is shown in Table 4.25. It is observed that the lessening of tension in mooring line is of similar pattern like surge response variation with different spectra. Though for heave and pitch response, API RP 2A induces larger fluctuation in maximum response at moderate wave, in case of CML tension the increment of response is around 3 % for both the strong gale and moderate wave cases. However, in case of API RP 2A spectra, the tension behaviour shows significant standard deviation which displays the greater involvement API RP 2A spectrum in fluctuation of mooring tension.

Table 4.25: Mooring tension behaviour for different wind spectra

Mooring top tension in **Wave + current + total wind**	**Emil Simiu Spectrum**	**API RP 2A-WSD Spectrum**
Strong gale		
Max (N)	2.05E+07	2.10E+07
Min (N)	1.82E+07	1.84E+07
Mean (N)	1.93E+07	1.97E+07
Median (N)	1.93E+07	1.97E+07
Mode (N)	2.05E+07	1.86E+07
Standard Deviation (N)	7.81E+05	8.81E+05
RMS (N)	1.93E+07	1.97E+07
Skewness	0.09	0.03
Kurtosis	-1.36	-1.55
Range	2.05E+06	2.60E+06
***Moderate wave*d**		
Max (N)	1.68E+07	1.73E+07
Min (N)	1.65E+07	1.65E+07
Mean (N)	1.65E+07	1.67E+07
Median (N)	1.65E+07	1.67E+07
Mode (N)	1.65E+07	1.66E+07
Standard Deviation (N)	1.06E+05	1.77E+05
RMS (N)	1.65E+07	1.64E+07
Skewness	-29.35	-3.68
Kurtosis	233.48	117.54
Range	3.00E+05	8.00E+05

4.10 Statistical analysis

In order to demonstrate the structural behaviour of platform motions and mooring line tension, statistical analysis has been carried out considering 5 loading combinations. Selected cases are wave only, wave + current, wave + constant wind + turbulent wind, wave + current + constant wind and wave + current + constant wind + turbulent wind subjected to the moored Spar. Every case follows two severe environmental conditions: strong gale and moderate wave. For turbulent wind, API RP 2A spectrum is chosen for the statistical investigation. Ten numbers of statistical parameters are evaluated for surge, heave, pitch and CML top tension.

Statistical analysis of surge response

Effect of current and wind loading on horizontal movement of platform has been investigated with wave force. The maximum value of surge increases gradually for addition of hydrodynamic and aerodynamic forces. Current loading adds around 24% steady drift to the wave induced surge. This offset is also larger than wave plus wind condition. Hence, there is a huge participation of static current on the surge response. Constant wind and turbulent wind add more lateral shift to spar hull compared to wave plus current case. The platform is displaced to higher extent in surge due to total sea loading. Table 4.26 illustrates the statistical analysis of surge response under various cases. Mean, median and mode values support the trend of platform shifting from its original position. RMS responses are increasing significantly for incorporation of current and wind loading. Wave + current force induces more offset of platform than the wave + wind case. Standard deviation is quite high for the wave + current + constant wind + turbulent wind environment than other cases. This is because of the fluctuating wind influence together with other forces.

Table 4.26: Statistics of Surge response for different loading combinations

Surge	**Wave only**	**Wave + current**	**Wave + constant wind + turbulent wind**	**Wave + current + constant wind**	**Wave + current + constant wind + turbulent wind**
Strong gale					
Max (m)	19.63	46.24	44.65	60.81	79.31
Min (m)	-16.28	30.33	30.07	46.11	61.53
Mean (m)	3.00	38.36	37.07	53.13	70.60
Median (m)	3.07	38.18	36.88	52.71	70.79
Mode (m)	10.40	34.72	31.87	47.79	64.97
Standard Deviation (m)	6.19	5.20	5.06	5.07	6.83
RMS (m)	6.97	38.71	37.41	53.37	70.76
Skewness	0.05	0.05	0.09	0.10	0.02
Kurtosis	-0.47	-1.54	-1.46	-1.47	-1.30
Range	35.91	15.91	14.58	14.70	17.78
Moderate wave					
Max (m)	10.31	20.03	18.15	27.75	32.15
Min (m)	-10.01	-10.34	-16.01	-4.85	2.11
Mean (m)	-0.02	8.25	4.33	9.38	11.60
Median (m)	0.12	7.66	4.11	8.46	10.06
Mode (m)	12.97	13.45	19.49	11.58	17.80
Standard Deviation (m)	8.90	6.69	8.97	5.94	6.09
RMS (m)	8.90	10.62	9.96	11.10	13.10
Skewness	-0.10	-2.48	0.04	0.95	1.20
Kurtosis	-0.52	0.50	-0.98	2.14	1.73
Range	20.32	30.37	34.06	32.60	30.04

For both strong gale and moderate wave, the static effect of additional loading noticeably diminishes the dynamic fluctuation which is seen from the range of surge fluctuations. The increment in maximum surge response than wave+ current loading is seen as 28% and 38% for wave+current+constant wind as well as 65% and 60% for total loading in strong gale and moderate wave environment respectively. On the other hand for wave + total wind case maximum surge response shows lower value by 4% for strong gale and 9% for than the wave+ current case. But this offset induced by wind is significant to be considered properly. Turbulence of aerodynamic load induces this larger variation. However, platy kurtic manner of the surge probability distribution is caused by current and constant wind force. This steady effect of loading on the platform allows the spar to oscillate in a controlled manner with reduced oscillations.

Statistical analysis of heave response

Table 4.27 shows that the maximum heave response gradually decreases for wave + current and wave + current + constant wind respectively than the wave only. This is because static forces of current and constant wind suppress the dynamic fluctuations of the platform vertical movement. This phenomenon shows firmness of the moored Spar under these loadings. However, the turbulence wind induces little fluctuation in heave motion adding some platform translation vertically. Besides, the standard deviation is dominated by wave only case. The mean heave magnitude is changing compared to the no wind case. Therefore, the aerodynamic load visibly distinguishes the motion behaviour. But for both strong gale and moderate wave environments, in place of current and wind loading combination, heave motion diminishes to a reasonable amount showing lower ranges of time history peak values. RMS responses increases reasonably for turbulent wind which supports the pattern of standard deviation. It is seen that for addition of current the maximum heave response reduces by 75%. This vertical movement again decreases by 12% for addition of constant wind to wave+current loading. Therefore, it is clear that static force suppress the vertical movement of Spar. Moreover, it is turbulence wind force which increases the heave fluctuations. Though for wave+total wind surge response was less than wave +current case, maximum heave increases by 17~19% for wave+wind. And for wave+current+total wind it raises to 38~68%. However, it is interesting that even all the loadings are incorporated the heave value shows quite less vertical movement of spar than wave only case.

Table 4.27: Statistics of heave for different loading combinations

Heave	**Wave only**	**Wave + current**	**Wave + constant wind + turbulent wind**	**Wave + current + constant wind**	**Wave + current + constant wind + turbulent wind**
Strong gale					
Max (m)	0.69	0.16	0.17	0.14	0.24
Min (m)	-1.03	-0.17	-0.18	-0.15	-0.25
Mean (m)	0.05	0.01	0.05	0.04	0.08
Median (m)	0.07	0.01	0.11	0.05	0.12
Mode (m)	0.18	-0.05	0.14	0.07	0.15
Standard Deviation (m)	0.223	0.06	0.15	0.08	0.12
RMS (m)	0.23	0.06	0.13	0.08	0.14
Skewness	-0.57	0.02	-0.91	-0.85	-0.94
Kurtosis	9.25	-1.16	-0.70	-0.46	-0.38
Range	1.72	0.33	0.35	0.28	0.49
Moderate wave					
Max (m)	3.02	2.19	2.56	2.11	3.01
Min (m)	-3.07	-2.12	-2.55	-2.10	-3.01
Mean (m)	0.004	0.02	0.047	0.08	0.008
Median (m)	0.00	0.01	0.02	0.12	0.02
Mode (m)	0.00	0.00	0.00	0.00	0.00
Standard Deviation (m)	1.41	1.27	1.38	1.18	1.21
RMS (m)	1.41	1.27	1.38	1.18	1.00
Skewness	-0.10	-0.07	0.01	-0.10	-0.12
Kurtosis	-0.52	0.50	-0.20	2.14	0.59
Range	6.09	4.31	5.11	4.21	6.02

Statistical analysis of pitch response

The pitch response statistics generated from different loading combinations are described in Table 4.28. The maximum, minimum and mean values of pitch show that the responses reduces gradually due to inclusion of static force like current and constant wind loading. Therefore, the range of pitch fluctuations diminishes. The mean, median and mode response indicate uni-modal distribution of pitch as these values are nearly similar in magnitude. Very low magnitudes of standard deviation and RMS show the reduction in rotation fluctuations by the environmental loading. It is seen that for wave+current, the pitch reduces by 60% than the wave only case. Inclusion of constant wind again lessens the rotation by 12~16% than wave+current case. But turbulent wind improves the pitch motion for both strong gale and moderate wave environment because of its fluctuating tendency. It is observed that for total loading, the maximum pitch increases by 11~60% than wave +current force. The firmness of platform is disturbed by fluctuating wind loading.

Table 4.28: Statistics of pitch for different loading combinations

Pitch	**Wave only**	**Wave + current**	**Wave + constant wind + turbulent wind**	**Wave + current + constant wind**	**Wave + current + constant wind + turbulent wind**
Strong gale					
Max (rad)	0.10	0.053	0.048	0.045	0.059
Min (rad)	-0.10	-0.047	-0.045	-0.046	-0.053
Mean (rad)	0.004	0.003	0.001	0.001	0.002
Median (rad)	0.0002	-0.003	0.002	-0.004	0.002
Mode (rad)	-0.02	-0.04	0.04	0.04	-0.04
Standard Deviation (rad)	0.04	0.03	0.033	0.03	0.03
RMS (rad)	0.04	0.03	0.033	0.03	0.04
Skewness	0.02	0.05	0.09	0.10	0.04
Kurtosis	-0.86	-1.54	-1.46	-1.47	-1.35
Range	0.20	0.10	0.12	0.10	0.11
Moderate wave					
Max (rad)	0.13	0.08	0.08	0.07	0.13
Min (rad)	-0.13	-0.08	-0.09	-0.07	-0.12
Mean (rad)	0.005	0.0001	0.007	0.001	0.004
Median (rad)	0.0003	0.0002	0.0003	0.001	0.003
Mode (rad)	0.03	-0.05	0.13	-0.01	0.10
Standard Deviation (rad)	0.07	0.05	0.07	0.05	0.04
RMS (rad)	0.07	0.05	0.033	0.05	0.04
Skewness	-0.02	0.002	0.03	0.005	-0.003
Kurtosis	-0.88	0.28	-1.14	1.84	1.36
Range	0.26	0.16	0.17	0.14	0.25

Statistical analysis of CML tension

Table 4.29 describes the statistical analysis of top tension in mooring line. It is observed that the maximum and mean top tension in mooring line for both strong gale and moderate wave are gradually increasing for wave only, wave plus current, wave plus current plus constant wind and wave plus current plus constant wind plus turbulent wind.

Table 4.29: CML tension statistics for different loading combinations

Mooring top tension	**Wave only**	**Wave + current**	**Wave + constant wind + turbulent wind**	**Wave + current + constant wind**	**Wave + current + constant wind + turbulent wind**
Strong gale					
Max (N)	1.76E+07	1.91E+07	1.89E+07	1.99E+07	2.10E+07
Min (N)	1.52E+07	1.70E+07	1.69E+07	1.77E+07	1.84E+07
Mean (N)	1.64E+07	1.80E+07	1.78E+07	1.88E+07	1.97E+07
Median (N)	1.63E+07	1.81E+07	1.78E+07	1.89E+07	1.97E+07
Mode (N)	1.55E+07	1.70E+07	1.69E+07	1.99E+07	1.86E+07
Standard Deviation (N)	6.19E+05	7.09E+05	7.02E+05	7.87E+05	8.81E+05
RMS (N)	1.64E+07	1.80E+07	1.78E+07	1.88E+07	1.97E+07
Skewness	0.11	0.01	0.08	-0.10	0.03
Kurtosis	-1.41	-1.42	-1.50	-1.49	-1.55
Range	2.40E+06	2.10E+06	2.00E+06	2.20E+06	2.60E+06
Moderate wave					
Max (N)	1.66E+07	1.70E+07	1.67E+07	1.71E+07	1.73E+07
Min (N)	1.58E+07	1.58E+07	1.59E+07	1.63E+07	1.65E+07
Mean (N)	1.62E+07	1.69E+07	1.64E+07	1.66E+07	1.67E+07
Median (N)	1.63E+07	1.66E+07	1.64E+07	1.66E+07	1.67E+07
Mode (N)	1.62E+07	1.66E+07	1.63E+07	1.66E+07	1.66E+07
Standard Deviation (N)	2.03E+05	1.69E+05	1.98E+05	1.72E+05	1.77E+05
RMS (N)	1.62E+07	1.66E+07	1.78E+07	1.66E+07	1.64E+07
Skewness	-2.40	-2.48	-6.01	-3.99	-3.68
Kurtosis	49.81	64.58	133.05	126.42	117.54
Range	8.00E+05	1.20E+06	8.00E+05	8.00E+05	8.00E+05

The increment in mooring tension confirms the participation of steady current and the aerodynamic loading. The maximum mooring tension increases from 1.76E+07 to 2.10E+07 N for only wave to total loading for strong gale and 1.66E+07 N to 1.73E+07 for moderate wave. Therefore, CML is seen to be influenced by the hydrodynamic and aerodynamic forces. Standard deviation and RMS shows the increment of tension indicating influence of current and wind forces. Similar to surge response the mooring tension increases for each additional force acting in the Spar-mooring system. It is seen that current loading adds 9% tension in catenary mooring line for strong gale. Moderate wave also follows similar behaviour of tension variation. Furthermore, wave+current+constant wind and wave +current+constant wind+turbulent show rise in tension by 1~4% and 2~10% than wave+current case. However, wave+total wind shows lower tension response than wave+current loading by around 2%. But this tension for wave plus wind is significantly larger than wave only case. Therefore both the current and wind loading plays important role on mooring tension.

4.11 Suitability of Spar platform in Malaysian deep water regions

Malaysian energy sector is dependent mostly on primary energy sources such as oil and gas. Rapidly growing demand of these hydrocarbons is experienced in this region. Therefore, finding new sources and techniques for oil and gas exploration is important to meet the intensely increasing fuel demand. Emphasis has to be made for deep water exploration to achieve the projected demand. The oil and gas scenario in Malaysia and feasibility to install Spar platform in its deep water regions have been described in Chapter 2. Thorough study of nonlinear coupled Spar platform subjected to Malaysian deep water environment is conducted in this section. Based on the known oil and gas reserves as well as possible future deep water exploration and production activities, the location for the satellite wave data is chosen for offshore Sarawak, longitude 111°E, latitude 6°N in Malaysia. The raw wave data has been collected and analysed to obtain competent sea environment. Frequency analysis and probability analysis have been carried out. The wave data is then used for coupled analysis of Spar platform in deep waters of Sarawak. The structural behaviour of Spar-mooring system under wave, current and total wind loading under Malaysian deep water conditions has been evaluated. Sea bed friction effect and stability analysis of coupled Spar platform have been performed. These studies appraise the suitability of coupled Spar platform in Malaysian deep water regions.

4.11.1. Processing of collected wave data

The wave data collected from WorldWaves (2010) is raw in nature spanning a recording duration of 1-year. This data period is considerably short for estimating the possible wave heights for a 100-year return period as required in offshore engineering design. Suitable wave height distribution model is constructed based on the available data in order to properly estimate the probability of higher wave heights occurring in 100 years (How, 2011). The "frequency" mentioned in this section refers to the frequency of occurrence for a particular wave height. Offshore Sarawak sedimentary basin has water depth around 1000 m. Other deep water sedimentary basins also exist around 1000 m water depth with similar environmental characteristics. Therefore, this region is selected as representative of Malaysian deep water sedimentary basins. Moreover, the procedure adopted for wave data analysis and coupled dynamics of Spar platform is applicable to any region in the world.

4.11.2. Wave data analysis

The collected wave data as shown in Table 3.3 of Chapter 3 is analysed using CumFreq program. It is capable of calculating the best-fitting cumulative frequency distribution of input data. The program tests various linear, logarithmic, exponential and double exponential cumulative frequency functions and selects the best fitting function automatically. The results obtained from frequency analysis are summarized in Table 4.30. In the table, wave period and wind velocity for corresponding mid-point of wave height has been estimated using the equations (3.120) and (3.121) respectively.

Table 4.30: Processed satellite wave data

Wave height, H (m)	Midpoint (m)	Wave Period, T (sec)	Wind Velocity u, (m/s)	Frequency of Occurrence
5-6	5.5	7.5075	13.8077	2
4-5	4.5	6.7908	12.4896	12
3-4	3.5	5.9889	11.0148	53
2-3	2.5	5.0616	9.3092	138
1-2	1.5	3.9207	7.2109	593
0-1	0.5	2.2636	4.1632	662

When the CumFreq program detects a discontinuity in the function, it gives choice to permit a break point. The function fitting procedure starts with ranking the data (X) in ascending order and assigning rank frequencies F_r = R/ (N+1), where R is the rank number and N the total number of data. Linear regressions are then made of F_r on the transformed data. The transformations are of a different kind corresponding to the type of function tried. The program also divides the range of X-data into a number (A) of equal intervals and calculates an interval frequency distribution.

Table 4.31: Statistical summary of wave data

<table>
<tr><td colspan="3">Summary: Sarawak wave data (6°N, 111°E)</td></tr>
<tr><td colspan="3">Number of wave data: 1460</td></tr>
<tr><td>Average: 1.29</td><td>Median: 1.04</td><td>Standard Dev.: 0.753</td></tr>
<tr><td>Cumulative frequency function:
Twice Gumbel</td><td colspan="2">Breakpoint :
P = 1.06</td></tr>
</table>

To find the best cumulative distribution function for representing the wave height occurrence data, the program is set so that a break-point is allowed and may be taken account for, if it is detected. The break-point is found from the best-fit method. The wave data is analysed by comparing how well it fits into the resulting frequency. The statistical summary of the 1-year wave data offshore Sarawak is shown in Table 4.31. The wave data is found to be best fitted to Gumbel frequency distribution.

Table 4.32: Sarawak sea states and their 100-year probability of occurrences

Sea State	Wave height, H (m)	Occurrence Probability
S_a	0.5	6.5273E-02
S_b	2.0	7.8414E-01
S_c	3.5	1.3353E-01
S_d	5.0	1.5244E-02
S_e	6.5	1.6204E-03
S_f	8.0	1.7094E-04
S_g	9.5	1.8019E-05
S_h	11.0	1.8992E-06
S_i	12.5	2.0017E-07

The 100 year probability occurrence of various sea states are shown in Tables 4.32. Nine sea states (S_a~S_i) have been considered to evaluate the probability of occurrences. The statistics show that among the nine selected sea states, the probability of occurrence of S_b is higher. For other sea states the probability of occurrence is significantly less.

4.11.3. Prediction of wave periods and wind velocities

The wave periods and wind velocities corresponding to wave heights for 100 year return period in Sarawak basin is shown in Figure 4.69. A graphical relationship is useful to obtain wind velocities corresponding to wave height and wave period. For this purpose, wave periods and wind velocities are computed using equations (3.120) and (3.121) and then plotted against wave height. This figure shall be useful in computing wave and wind characteristics in Sarawak basin.

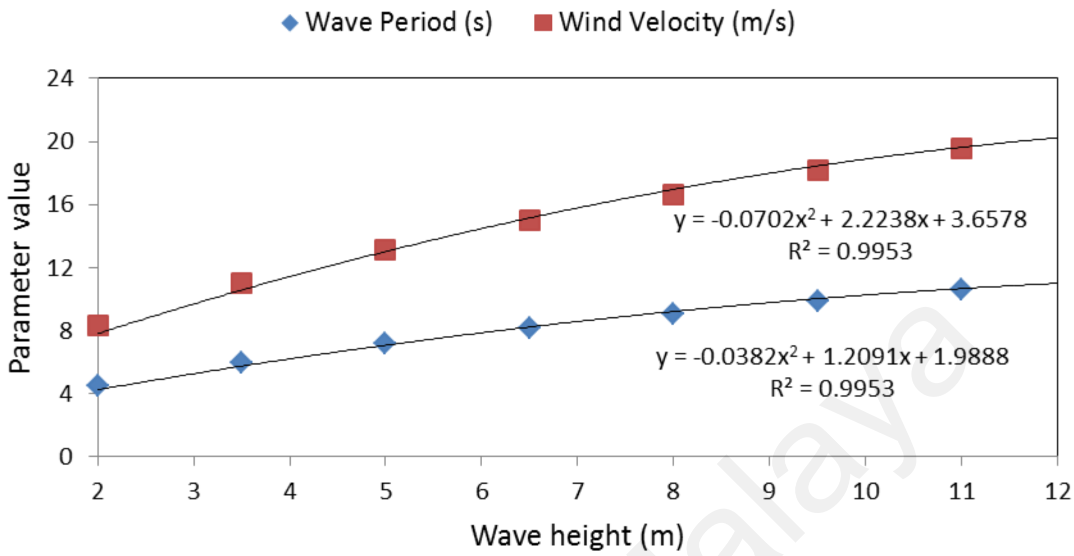

Figure 4.69: Wave period and wind velocity against wave height

The wind velocity is seen to be gradually increasing with the increment of wave period and wave height. The raising pattern of wind speed against wave height is steep. However, the increasing nature of wave period with respect to wave height is moderate. Both the lines show the regression as $R^2 = 0.9953$.

4.11.4. Sea states and their return periods

The wave data describing wave heights, wave periods and probability of occurrences is shown in Table 4.33. Wave height distribution is studied in detail to predict probability of occurrences of different sea states for 1000-year return periods. Wave and wind data for 100 years return period has been selected for response evaluation of coupled spar platform in Malaysian deep water. According to Table 4.33, wave height and wave period are 8.72 m and 9.45 sec respectively for 100 year return period. The mean wind speed is obtained as 17.25 m/s from Figure 4.69. The sea state falls in the category of moderate gale (Chakrabarti, 2005).

Table 4.33: Wave occurrence with return period

Return Period	Wave height	Mean Wave Period	Probability of Occurrence
1	5.649222722	7.608687904	0.000342
2	6.111434968	7.913835511	0.000205
5	6.722363916	8.299968258	6.84E-05
10	7.184484854	8.580512703	3.42E-05
20	7.646594382	8.852163943	2.05E-05
50	8.257461715	9.198959488	6.84E-06
100	8.719562117	9.452849854	3.42E-06
200	9.181661378	9.700096566	2.05E-06
500	9.79252255	10.01757752	6.84E-07
1000	10.2546209	10.25121227	6.84E-07

4.11.5. Coupled analysis of Spar platform in Malaysian deep water region

The Spar platform is a deep water structure with favourable sea keeping characteristics to explore oil and gas in Malaysian deep water region. Hence, assessing detail behaviour of Spar is of great interest. The structural system consists of essential features of Spar platform subjected to combination of all major types of environmental loading. The sea state is named as MS-WCW which includes the wave 8.72 m/ 9.45 sec, mean wind speed 17.25 m/s and wind induced current velocity 0.7 m/s. Turbulent wind speed has been considered as per the API RP 2A spectrum. Two types of sea beds have been considered namely frictionless and frictional sea bed. Subsequent sections discuss the structural responses for both cases.

Responses in frictionless sea bed

The environmental condition surrounding the Spar-mooring system is considered as sea loading of Malaysian deep water, MS-WCW. Sea bed in this study has been treated as a flat bed with no friction. The responses of platform along with top tension in catenary mooring lines are evaluated. Surge and mooring tension have been presented with time histories and probability histograms. The platform responses in surge, heave, pitch and CML tension are also evaluated by statistical analysis.

Spar surge in frictionless sea bed

Figure 4.70 shows that the platform is shifted to an offset of almost 22.95 m in surge. Platform reaches maximum surge of 45.40 m in transient state. In steady state the minimum and maximum responses are observed to be oscillating in the range of 17.28 to 27.38 m. The offset of platform from origin shows the influence of aerodynamic stress and steady current loading. Transient response shows adverse fluctuations of surge. After 2500 seconds the oscillation of surge motion diminishes and milder fluctuations occur. At 9300 sec slight rise in fluctuation is seen. However, after this time again the surge stabilizes to regular responses because of damping characteristics. Gradual lessening of surge shows the coupled behaviour of the responses.

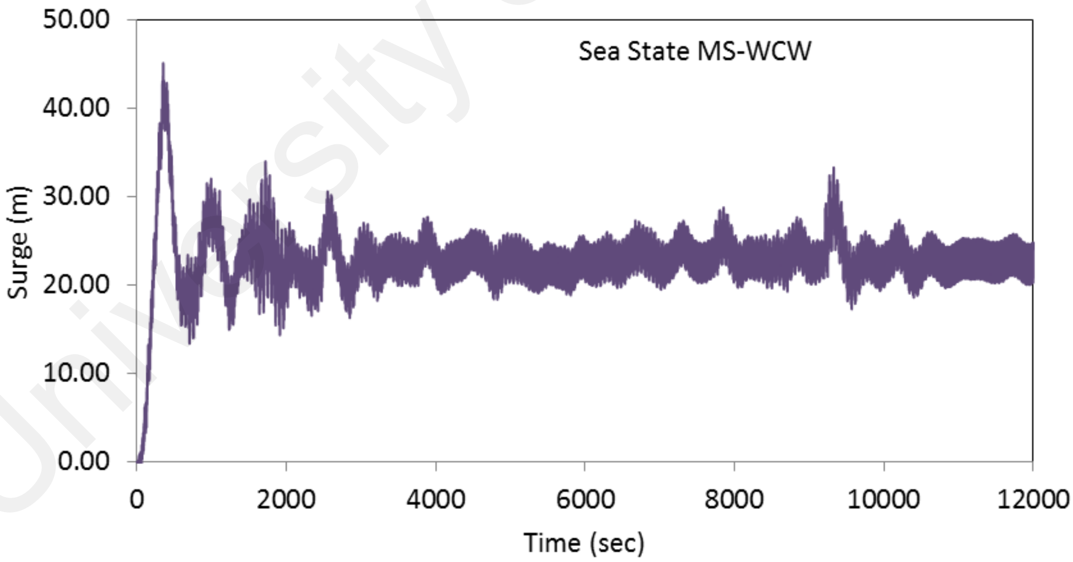

Figure 4.70: Surge time history under sea state MS-WCW

Statistical analyses of surge in frictionless sea bed

The surge histogram for total loading in Malaysian sea is shown in Figure 4.71. The histogram shows normal distribution of platform motion around mean. The distribution shows a few time history peaks of less than 15 m and higher than 35 m. Large number of responses occur within 20~30 m and very few are in 40~50 range as shown in the probability histogram. Therefore, the responses within the range 20~30 m can be treated as the maximum probable surge. Mode and median value of surge are close to the mean position as shown in the statistical analysis. Hence, the surge distribution is uni-modal showing symmetric nature of response fluctuation around the mean.

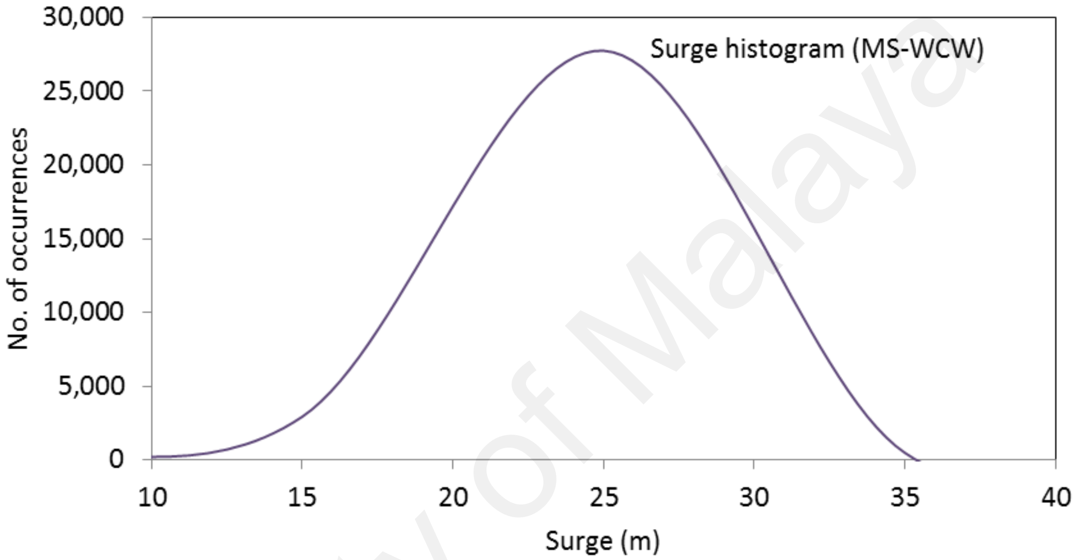

Figure 4.71: Probability histogram of surge in Malaysian sea (MS-WCW)

The descriptive statistics of surge response is shown in Table 4.34. From the table it is witnessed that maximum and minimum peak of surge are 27.38 m and 17.28 m respectively. In steady state, the mean, median and RMS values of surge are around 23 m. Most frequent occurrence of surge peak is seen by mode value as 25.24 m. The probability histogram also confirms that most of the surge values fall in the range 20~30 m. The coefficient of surge skew-ness show moderately skewed nature with slightly negative skew-ness in left hand side of distribution. Low value of standard deviation is induced from the turbulent wind loading.

Table 4.34: Statistics of Spar motions and mooring tension

Wave + current + wind in Malaysian sea	Surge (m)	Heave (m)	Pitch (rad)	Mooring top tension (N)
Max	27.38	0.128	0.027	1.80E+07
Min	17.28	-0.129	-0.028	1.64E+07
Mean	22.95	0.001	0.002	1.72E+07
Median	23.22	0.001	0.004	1.71E+07
Mode	23.23	0.004	0.014	1.66E+07
Standard Deviation	1.80	0.033	0.011	4.46E+05
RMS	23.02	0.033	0.011	1.72E+07
Skewness	-0.29	-0.06	-0.28	0.16
Kurtosis	-0.90	1.58	-1.27	-1.42
Range	10.10	0.257	0.055	1.60E+05

Spar heave in frictionless sea bed

The time history of platform motion in heave under Malaysian sea condition MS-WCW is shown in Figure 4.72. Because of involvement of aerodynamic and hydrodynamic loads, heave motion shows adverse fluctuations at transition zone. However, the fluctuations of heave time history diminish after transition region. The time history shows small rise in time history peak at 9800 sec with ±0.20 m. Again the heave motion stabilizes to ±0.13 m at long duration and regular value is evolved. Damping characteristics causes the response die out. Moreover, the steady behaviour is accomplished for the suppression of heave response by current stress and constant wind loading.

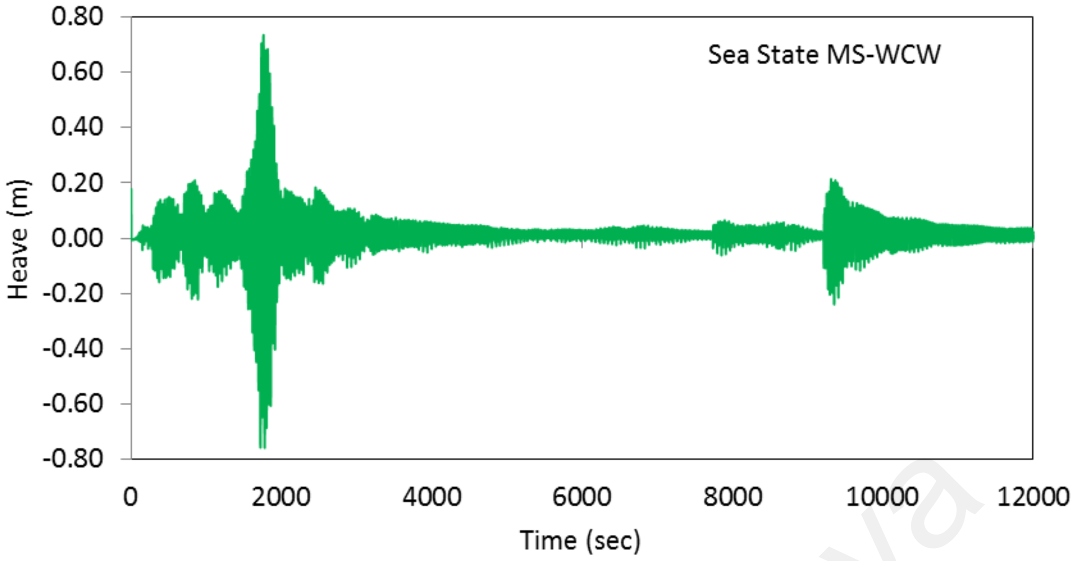

Figure 4.72: Heave time history under sea state MS-WCW

Statistical analyses of heave in frictionless sea bed

In case of heave response, the probability histogram shows normal distribution of platform motion with slight skew-ness of responses in left hand side. Around the mean value of heave 0.001 m, huge numbers of responses occur. Though the heave motion is fluctuates much showing significant peak in transition zone, most of the response peaks in time history oscillates within the range -0.2 m to 0.2 m. Among them most frequent occurrence near the mean heave indicates vertical firmness of the platform. Mode and median value are also close the mean position as shown in statistical analysis at Table 4.34. Hence, the heave distribution is uni-modal. Figure 4.73 illustrates the heave probability histogram. The kurtosis coefficient for heave is of leptokurtic nature showing higher peaked-ness of vertical motion. Yet low value of standard deviation indicates huge numbers of occurrences are around the mean with very less variation in magnitude. Such response behaviours show suitability of coupled Spar platform in Malaysian deep water.

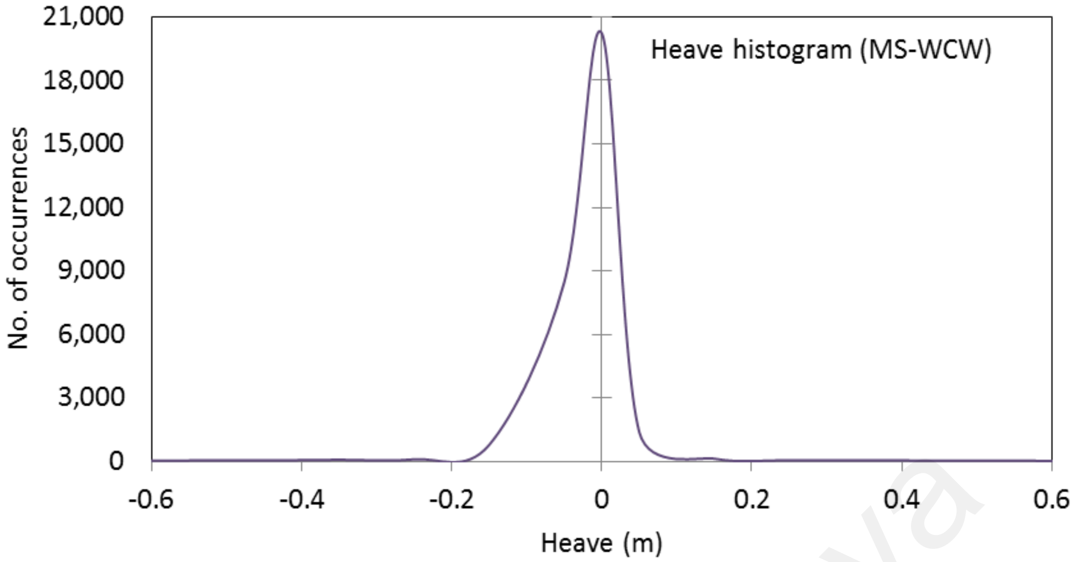

Figure 4.73: Probability histogram of heave for Malaysian sea (MS-WCW)

Spar pitch in frictionless sea bed

The pitch response ranges from -0.028 rad to 0.027 rad in steady state. This time history peaks are considerably less than the values at transition region. This decreased magnitude of Spar rotation in pitch is due to damping. Figure 4.74 shows the time histories of pitch response in sea state MS-WCW. The fluctuation of the responses causing a number of reversals is occurred by fluctuating tendency of turbulence wind on Spar rotation. A sudden increase in pitch response is seen at 9200 sec for a while and immediately after this occurrence regular values of pitch stabilizes to ± 0.027 rad at long duration of ocean loading.

Statistical analyses of pitch in frictionless sea bed

The distribution of pitch response follows identical pattern as the heave probability distribution. As an alternate transfer of energy is existent in between heave and pitch response, this similarity is desirable. The pitch probability histogram is illustrated in Figure 4.75. It is seen that a large numbers of responses are existent near the mean value 0.005 rad. Median and RMS value of heave are both 0.001 rad shown in Table 4.34.

Very close value of mean, median and RMS responses show the controlled rotation of the platform around its mean position. Static loading of current and constant wind supress the platform from greater rotation and hence massive statistics of occurrences are observed showing the Spar rotation in the range -0.028 to 0.027 rad. The occurrences of pitch response shows moderately skewed distribution and also flatness of pitch distribution.

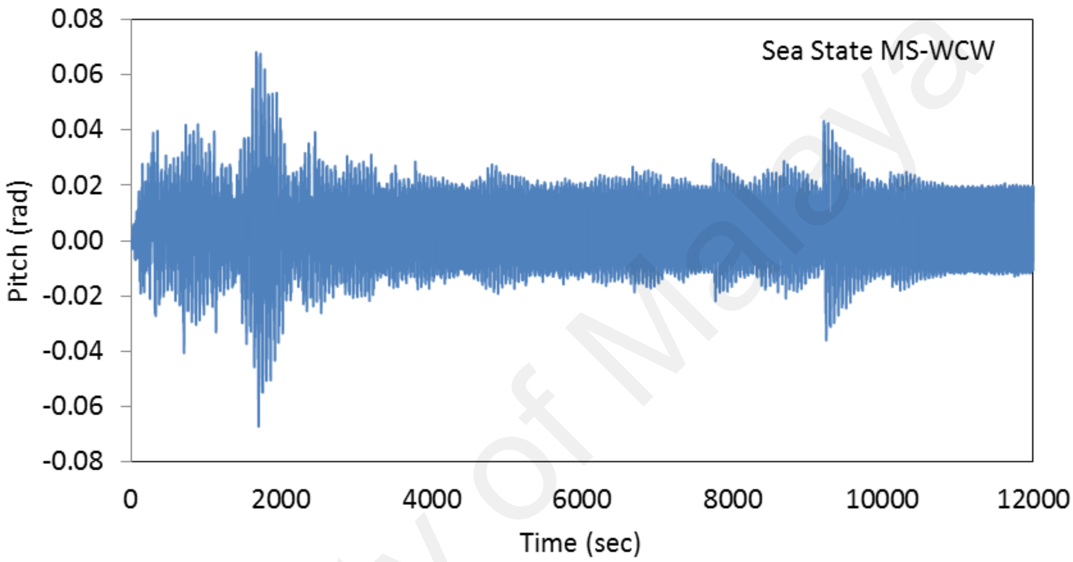

Figure 4.74: Pitch time history under MS-WCW sea state

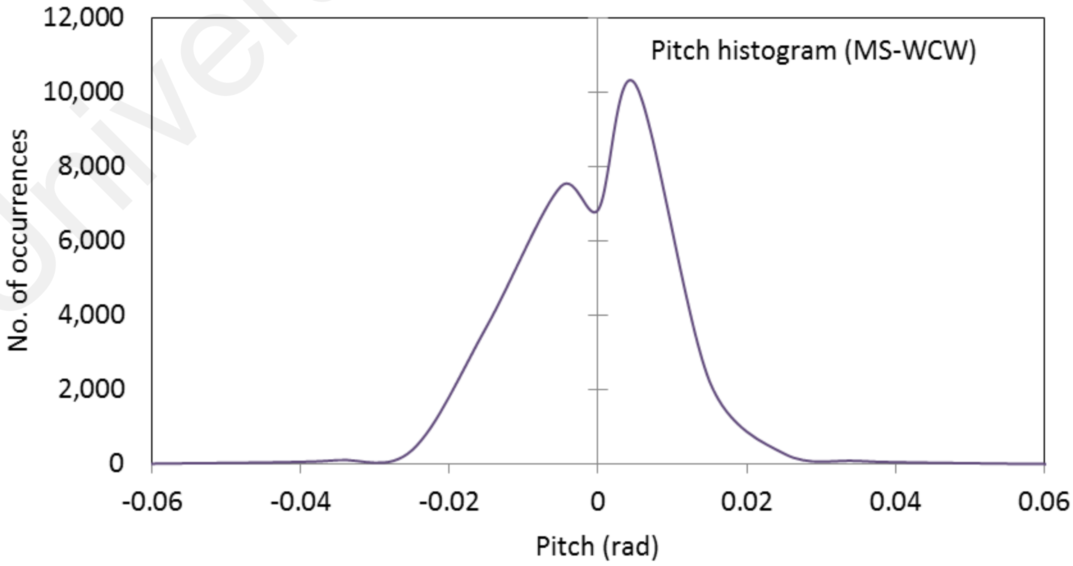

Figure 4.75: Probability histogram of pitch for Malaysian sea (MS-WCW)

Mooring line tension in frictionless sea bed

The mean value of top tension response in catenary mooring line is 1.72E+07 N under the sea state MS-WCW (Figure 4.76). Adverse fluctuations of top tension occur in transient period. Just after this tension variation, the dense fluctuating peaks change to more scattered responses. However, slight shoot out of tension response is seen at around 9300 sec. After this long period of loading the tension response stabilizes to regular value due to the mooring line damping. The tension response has maximum value of 1.80E+07 N. In this region, the station keeping system, CML experiences steady tension around the mean value.

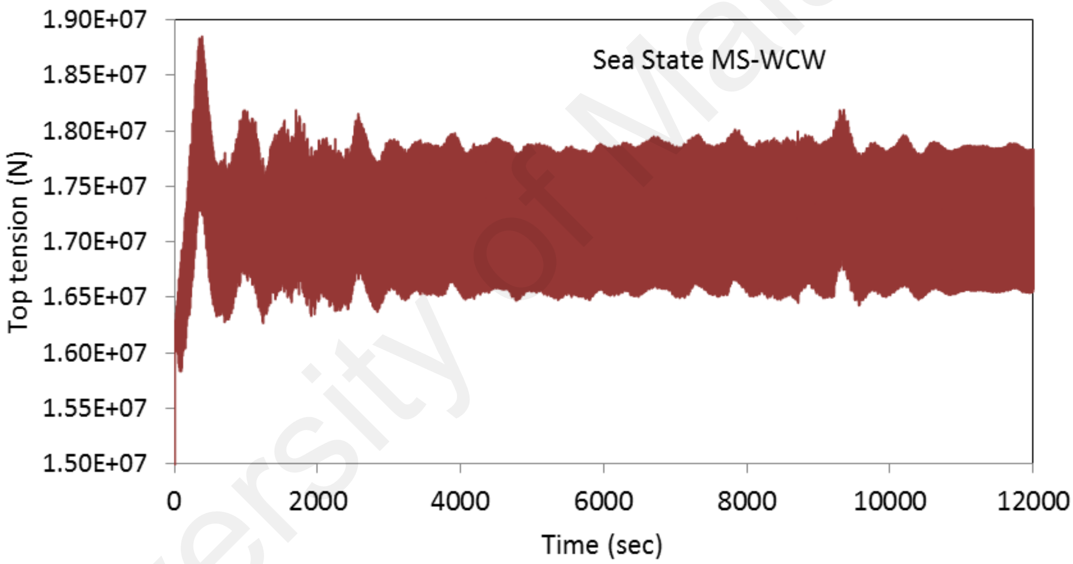

Figure 4.76: Mooring tension time history under sea state MS-WCW

Statistical analyses of CML tension in frictionless sea bed

The catenary mooring line experiences tension response ranging from 1.64E+07 N to 1.80 E+07 N (Table 4.34). The median and mean values of top tensions are 1.71E+07 N and 1.72E+07 N respectively, the mode value is 1.66E+07 N. The histogram shows maximum numbers of occurrences around the range of 1.60E+07 N to 1.80E+07 N making almost normal distribution of tension responses. The probability histogram of mooring tension shows the nature of distribution in Figure 4.77. The distribution of tension responses is moderately skewed. Platy-kurtic nature in flatness of tension responses agrees with the regular distribution of CML tension under Malaysian sea environment. Such behaviour of CML tension indicates the firmness of mooring lines in long duration of loading.

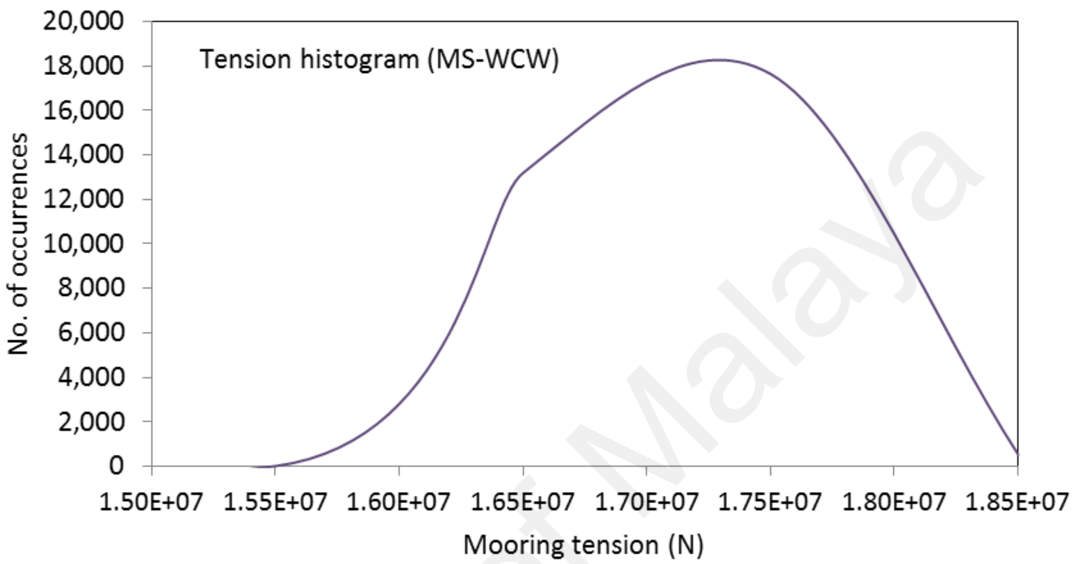

Figure 4.77: Probability histogram of CML tension for Malaysian sea (MS-WCW)

4.12 Effect of Sea bed friction

This section focuses on the effect of sea bed friction on mooring line and hence on the coupled Spar platform system. The mooring lines experiences frictional resistance at seabed. Proper investigation is required to address the friction effect. In the present study, sea bed friction is considered as basic Coulomb friction model. Two friction coefficients FC1 and FC2 are incorporated with values 0.4 (Yu and Tan, 2006) and 0.5 respectively. Corresponding sea states are named as MS-WCWIa, and MS-WCWIb. Frictional seabed provides vertical/normal support to mooring line and lateral/tangential resistance to CML through the frictional mechanism. Platform motions and mooring tension are compared to assess the behaviour in frictional and frictionless sea bed case under total loading in Malaysian condition. Moreover, the contact shear stresses experienced by mooring lines at different positions have been evaluated.

4.12.1. Surge behaviour in frictional seabed

The analysis shows that inclusion of sea bed friction changes the pattern of response along with slight reduction in magnitude. The mooring touch down point and sea bed friction contributes additional nonlinearity to the system. Difficulty in convergence of solution arises because of these nonlinearities. A large number of iterations are required at different time stations. Maximum surge in transient state for MS-WCWIa is around 38.62 m which is 14.41% less than the frictionless sea bed case (Figure 4.78). At steady state the maximum and minimum surge ranges for 24.55 m to 19.71 m which are less compared to 27.38 m to 17.28 m in frictionless sea bed. Lateral shift of platform decreases by 10.34% for addition of friction. As the friction coefficient increases, the platform motion in surge decreases. This is because of additional interruption caused in mooring line due to frictional resistance.

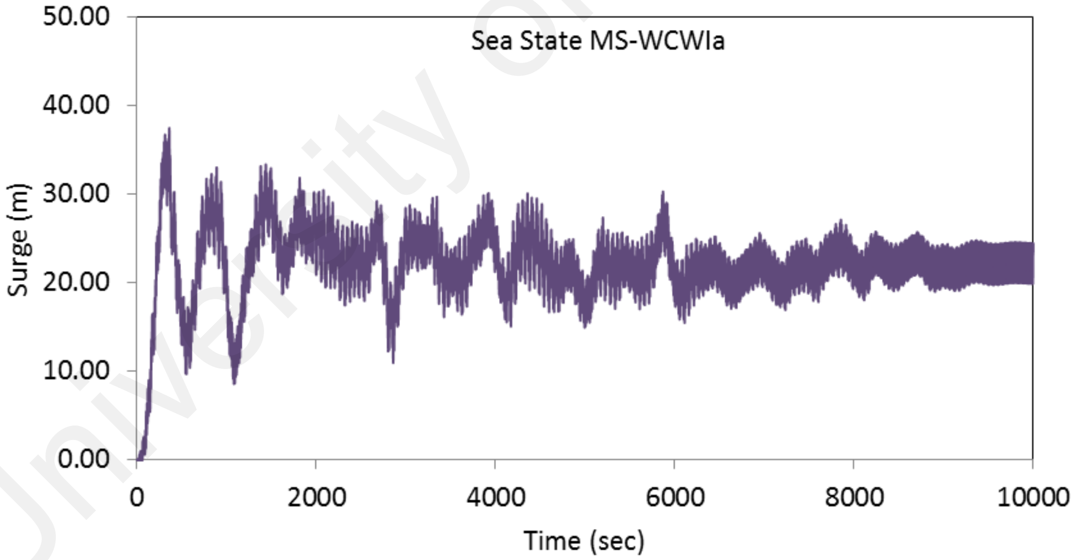

Figure 4.78: Spar surge for frictional sea bed

A solitary peak at low frequency in surge is observed with lower energy content for frictional sea bed. Comparative power spectra of surge response are shown in Figure 4.79. For frictionless sea bed case little involvement of 0.065 rad/sec frequency is seen. However, in both cases governing peak is at surge frequency. The decrease in energy content in the governing frequency is because of high pretension in CMLs.

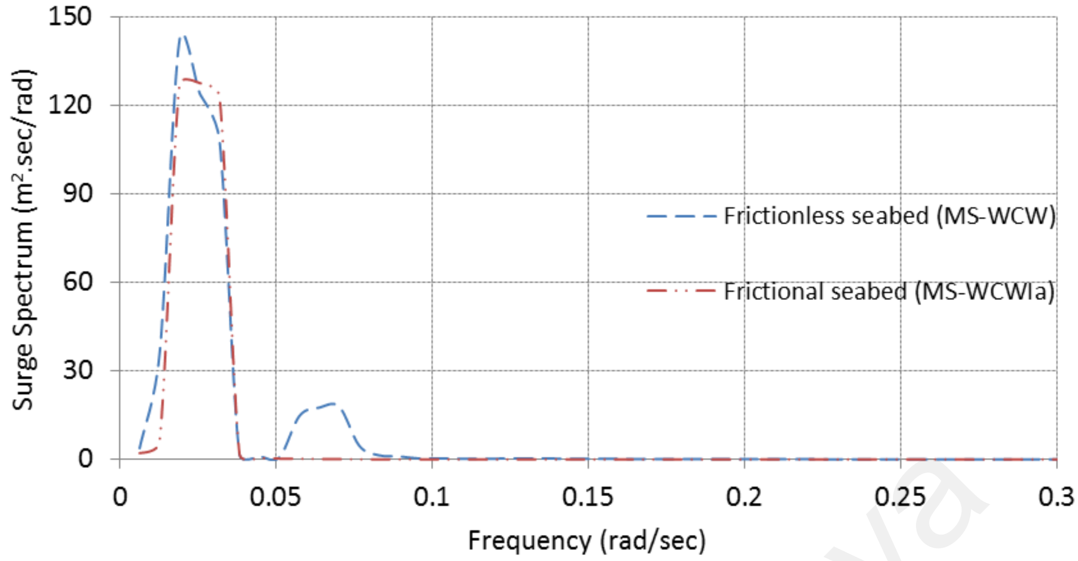

Figure 4.79: Comparative power spectrum of surge for sea bed friction

Statistical analysis of surge response has been shown in Table 4.35. Gradual decrement of surge response from FC1 to FC2 is observed. The mean, median, mode and RMS values of surge responses decrease for increase in friction coefficient. Standard deviation of surge is gradually decreasing for increasing friction. Higher friction restricts the movement of mooring line more and hence it lessens the platform surge. Though the effect of friction on surge response is not so much, it should not be ignored.

Table 4.35: Descriptive statistics of surge response due to sea bed friction

Surge	**Frictionless sea bed**	**Frictional sea bed (FC1)**	**Frictional sea bed (FC2)**
Max (m)	27.38	24.55	24.38
Min (m)	17.28	19.71	19.90
Mean (m)	22.95	22.01	21.38
Median (m)	23.22	21.86	21.26
Mode (m)	23.23	20.04	19.92
Stdev (m)	1.80	1.64	1.58
RMS (m)	23.02	22.07	21.41
Skewness	-0.29	0.13	0.16
Kurtosis	-0.90	-1.52	-1.42

4.12.2. Heave response in frictional sea bed

Significant reduction in heave response is observed when friction is considered. The descriptive statistics of heave and pitch for frictionless and frictional sea bed case is given in Table 4.36. Detail evaluation of heave and pitch are discussed in the section of Mathieu instability with respective time histories in Figure 4.91 and Figure 4.92. The heave response in steady state decreases by 84% for frictional resistance in sea bed. Power spectrum of heave in frictionless sea bed shows governing peak at heave frequency with two minor peaks at surge frequency (Figure 4.80). However, frictional resistance alters the behaviour of power spectrum. The energy content in heave frequency is substantially reduced and surge frequency is governed with lower energy. This is because of higher resistance and additional damping induced in mooring line due to addition of friction.

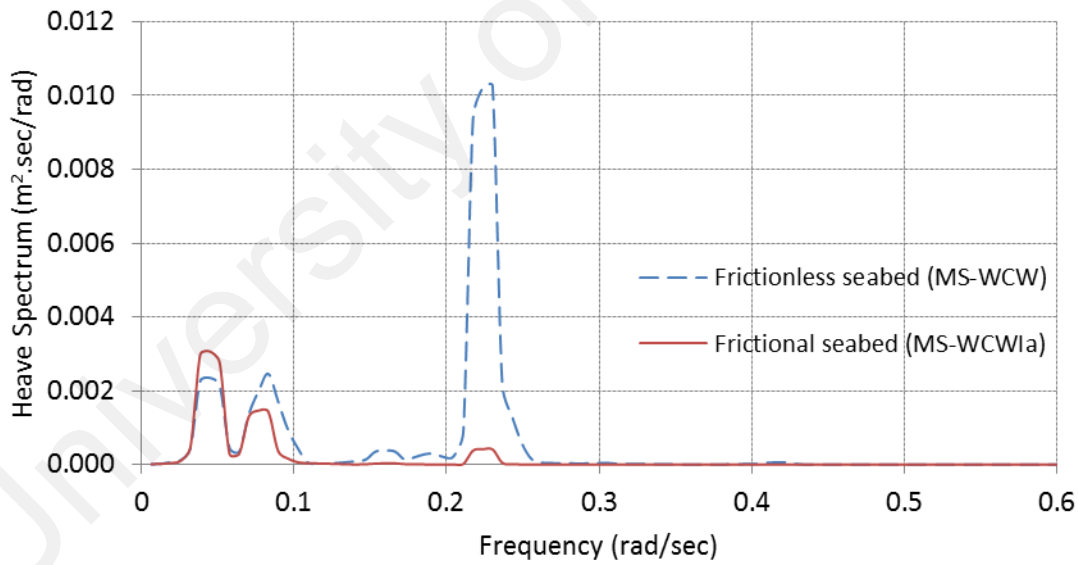

Figure 4.80: Comparative power spectrum of heave for sea bed friction

Mean and RMS values of heave responses reduces because of friction. Gradual decreasing in heave response is observed for increase in friction coefficient. The kurtosis coefficient for heave shows more leptokurtic distribution of response.

Moreover, lower value of standard deviation indicates dense occurrence of heave response around mean with less variation in magnitude.

Table 4.36: Descriptive statistics of heave response for friction

Heave	**Frictionless sea bed**	**Frictional sea bed (FC1)**	**Frictional sea bed (FC2)**
Max (N)	0.128	0.020	0.019
Min (N)	-0.129	-0.019	-0.019
Mean (N)	0.001	0.005	0.006
Median (N)	0.001	0.008	0.009
Mode (N)	0.004	0.010	0.010
Stdev (N)	0.033	0.010	0.009
RMS (N)	0.033	0.011	0.011
Skewness	-0.06	-0.80	-0.95
Kurtosis	1.58	-0.53	-0.26

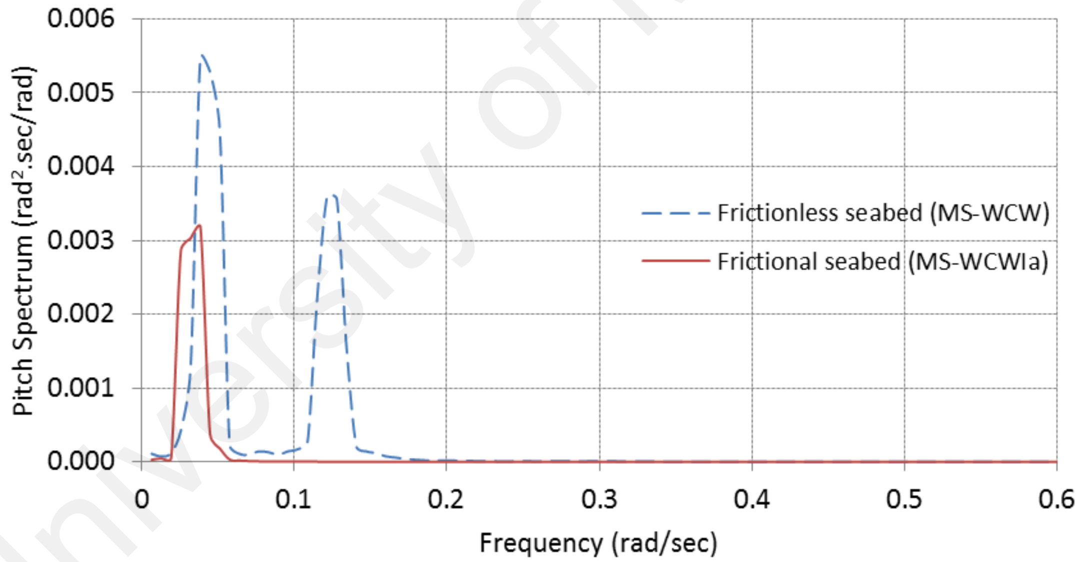

Figure 4.81: Comparative power spectrum of pitch for sea bed friction

4.12.3. Pitch response in frictional sea bed

Maximum pitch response in steady state reduces by 40% for addition of frictional resistance. Statistics of pitch shows maximum value of 0.027 rad and 0.016 rad for frictionless and frictional sea bed case respectively (Table 4.36). Comparative power spectrum of pitch response in frictionless and frictional sea bed case is shown in Figure

4.81. Pitch power spectrum in frictionless sea bed shows governing peak at surge frequency with significant involvement of pitch frequency. Due to inclusion of friction in sea bed, the participation of pitch frequency disappears and only solitary peak is available in surge frequency with lower energy content.

Table 4.37: Descriptive statistics of pitch responses for friction

Pitch	**Frictionless sea bed**	**Frictional sea bed (FC1)**	**Frictional sea bed (FC2)**
Max (N)	0.027	0.016	0.015
Min (N)	-0.028	-0.016	-0.016
Mean (N)	0.002	-0.001	-0.001
Median (N)	0.004	-0.002	-0.003
Mode (N)	0.014	-0.014	0.008
Stdev (N)	0.011	0.011	0.011
RMS (N)	0.011	0.011	0.011
Skewness	-0.28	0.13	0.16
Kurtosis	-1.27	-1.52	-1.42

Lower values of mean, median and RMS responses in frictional sea bed case indicate controlled rotation of the platform around its mean position. This is because of friction induced damping in the system. The pitch response is gradually decreasing in little amount for increase in frictional resistance. Steady and stabilized response behaviours show the firmness of platform and hence suitability of moored Spar under Malaysian deep water in frictional sea bed.

4.12.4. Mooring tension behaviour in frictional seabed

Inclusion of sea bed friction causes change in pattern of mooring tension fluctuations. In case of sea state MS-WCWIa, slight reduction in top tension is seen due to friction coefficient FC1. The maximum time history peak in steady state reduces to 1.787E+07 N (Figure 4.82) which is 1.796E+07 N in frictionless sea bed case MS-WCW. This minor change in mooring tension is due to the friction induced damping of mooring line. As the pretension in mooring line is very high, the change in tension value is insignificant. This trend is in line with the behaviour of mooring tension for various loading cases.

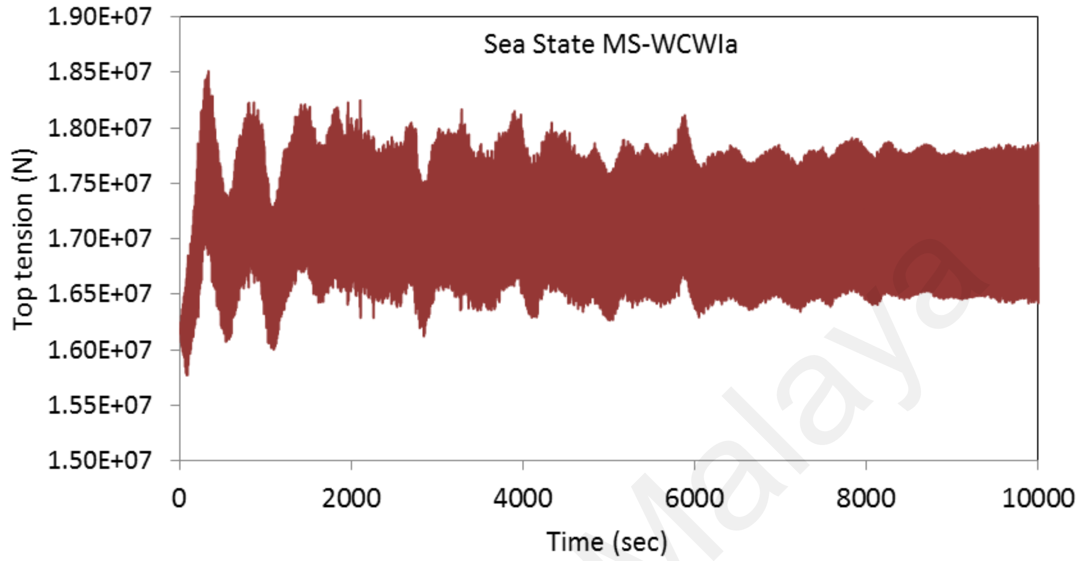

Figure 4.82: CML Top tension for frictional sea bed

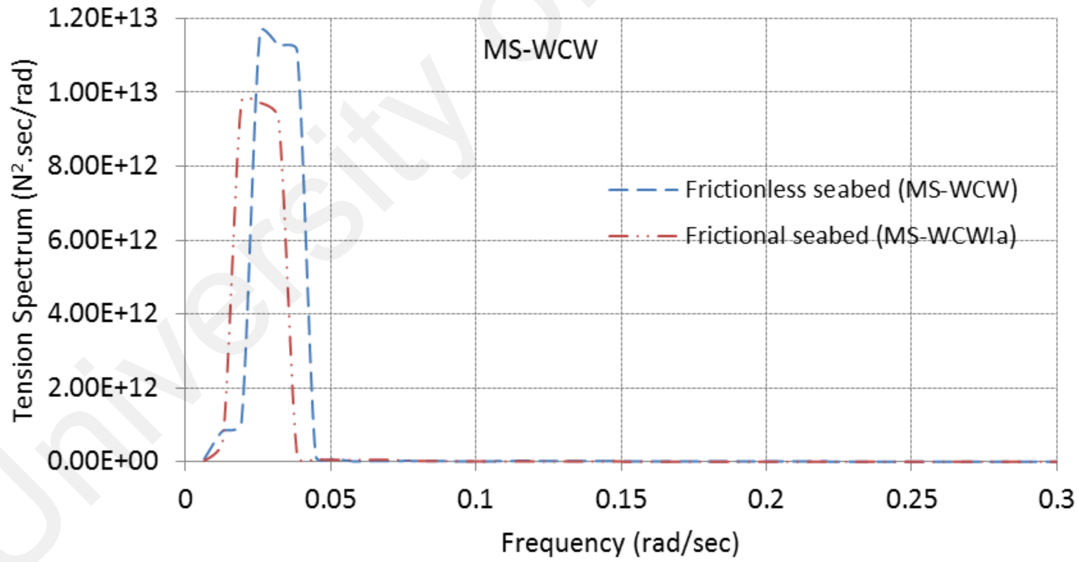

Figure 4.83: Comparative power spectrum of CML Top tension for sea bed friction

Figure 4.83 shows the power spectrum of mooring tension for frictionless and frictional sea bed. In both cases, the power spectrum shows a single peak at low frequency which is near to surge natural frequency. Inclusion of friction causes slight shift in governing frequency with minor reduction in magnitude. Because of friction induced damping, there is little change in behaviour of tension response which is reflected in power spectrum.

The statististical analysis of mooring tension is shown in Table 4.38. Further addition of frictional resistance FC2, causes gradual reduction in tension magnitude of mooring line compared to the frictionless and frictional sea bed (FC1) case. Mean, median, mode and RMS values of mooring tension also show the decreasing nature of tension response. This evaluation indicates that sea bed friction induces supplementary damping. Due to increase in friction, the tension response distribution becomes more moderately skewed. More flat reponses of tension response is shown by the platykurtic distribution of responses.

Table 4.38: Descriptive statistics of CML tension variation due to sea bed friction

Mooring tension	**Frictionless sea bed**	**Frictional sea bed (FC1)**	**Frictional sea bed (FC2)**
Max (N)	1.796E+07	1.787E+07	1.778E+07
Min (N)	1.643E+07	1.642E+07	1.649E+07
Mean (N)	1.715E+07	1.717E+07	1.711E+07
Median (N)	1.711E+07	1.722E+07	1.727E+07
Mode (N)	1.660E+07	1.655E+07	1.667E+07
Stdev (N)	4.460E+05	4.459E+05	3.116E+05
RMS (N)	1.716E+07	1.717E+07	1.711E+07
Skewness	0.16	-0.13	-0.26
Kurtosis	-1.42	-1.43	-1.44

When the mooring line comes in contact with sea bed, the friction causes resistance of mooring movement as well. Sea bed friction induces addition damping to the heave motion which is mentioned by Koo et al. (2004). This eventually effects on the platform vertical motion causing its reduction and hence on the pitch response as there is coupled action in between Spar hull and mooring lines. In the coupling effects on the floater mean position and dynamic response, the restoring force comes from 1) Static restoring force from the mooring and riser system as a function of floater offset, 2) Current loading and its effects on the restoring force of the mooring and riser system, 3) Seafloor friction (if mooring lines and/or risers have bottom contact). In addition the damping forces are induced by 1) Damping from mooring and riser system due to dynamics, current, etc. and 2) Friction forces due to hull/riser contact. The frictional effect is interrelated with the displacement history (DNV, 2010).

Damping of slow-drift motions comprise i) wave drift damping, ii) drag forces on hull and mooring lines/risers, iii) variation of wind loads with the velocity of the structure as well as iv) friction of the mooring lines on the sea-floor. With increasing the wave intensity, the slow-drift damping component for viscous damping by sea-floor friction also increases (Molin, 1994). Sea floor soil friction leads to reduced tension fluctuations for the portion of the mooring table in contact with sea floor, causing an increase of the line stiffness. It has some effect on wave frequency tensions (Triantafyllou et al., 1994). Hence the alterations of spar hull motions in coupled system due to the effect of sea bed friction on mooring lines are reasonable.

4.12.5. Contact shear

Frictional sea bed causes lateral/tangential resistance to mooring line. Small change in magnitude and pattern of platform responses as well as mooring tension is noticed. For frictionless sea bed no contact shear is induced on mooring line. The frictionless sea bed allows the catenary mooring line to slide without any resistance. Thus the contact shears in the part of mooring line lying on sea bed is zero. However, the frictional sea bed provides contact shear because of frictional resistance. The mooring line interacts with sea bed continuously because of platform movements. Hence, the tangential shear induced to the CML is essential to be considered in design of catenary mooring line.

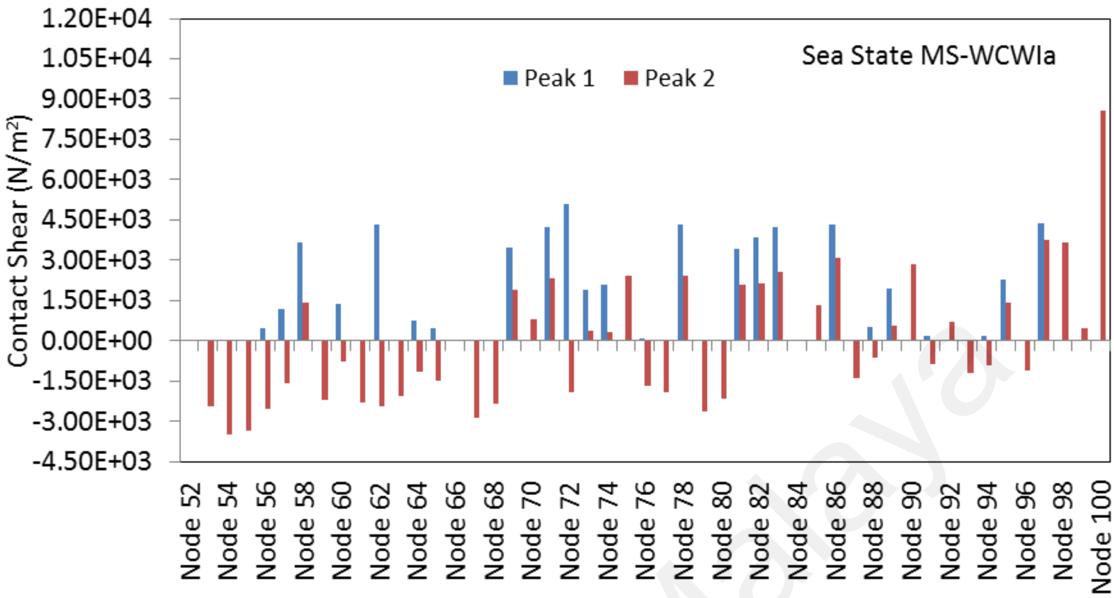

Figure 4.84: Maximum Contact shear on mooring line for frictional sea bed

Figure 4.84 shows the behaviour of contact shear in frictional sea bed. In the Spar platform model, catenary mooring line is linked at node 1 with Spar fairlead position. Another end of CML having node no 101 is anchored at sea bed. For the sea state MS-WCWIa, CML experiences maximum contact shear 8.560E+03 N/m^2 at node no 100. Node numbers 1 to 52 are hanging above the sea bed and never come in contact. Therefore, this part of mooring line doesn't have any amount of contact shear. As the element 52 of CML partly hangs and partly comes in contact with sea bed, node 53 experiences first contact shear stress due to CML-sea bed contact. Contact shear of this region of mooring line can be noticed as -2.446E+03 N/m^2. Lying portion of CML shows varying shear stresses at different locations. Maximum positive and negative contact shears are 4.333E+03 N/m^2 and -3.459E+03 N/m^2 respectively in the laid portion. The contact shear in lying portion and transition zone is 50% and 30% of the mooring end contact shear.

Table 4.39: Statistics of contact shear for frictionless and frictional sea beds

Maximum Contact Shear (N/m ^{2})		**Frictionless sea bed**	**Frictional sea bed (FC1)**	**Frictional sea bed (FC2)**
Mooring end		Null	8.560E+03	10.701E+03
Laying portion	Positive	Null	4.333E+03	5.455E+03
	Negative	Null	-3.459E+03	-4.058E+03
Transition region		Null	-2.446E+03	-2.984E+03

Table 4.39 shows the statistical analysis of contact shear for frictionless and frictional sea beds. In case of sea state MS-WCWIb, the contact shear value is -2.980E+03 N/m^2 at node 53. Increment in frictional resistance from sea bed increases mooring contact shear by approximately 22%. Due to increase in frictional resistance (FC2), maximum contact shear at mooring end increases by 10.701E+03 N/m^2. More frictional resistance in sea bed induces more contact shear on mooring line. Hence the sea bed frictional resistance should be considered for the design of mooring line. Contact shear is rapidly increasing in the lying node than the transition node. The transition zone and adjacent lying elements are of important concern. Together with the potentially high mooring tensions, frictional resistance give rise to locally very high contact shear stress between mooring and sea bed. The shear may amplify at the turn crossovers where the mooring line runs over high frictional soil.

Small amplitude sliding of the mooring line relative to the supporting soil causes local wear, especially at the crossovers. Such wear can become severe and lead to significant number of localised mooring strands breaks. It can be seen that there is a rapid increase in contact shear in the lying element of CML than its adjacent transition element. These high contact shears, under the action of high loading can also lead to plastic deformation of mooring surface, displacing them from their position. This can have an extreme effect on fatigue performance.

4.13 Stable response analysis

The fully coupled Spar platform exhibits nonlinear behaviour because of inherent nonlinearities in the system. These nonlinearities are produced by damping nonlinearity, nonlinearity in the restoring force and nonlinear excitation force which may lead to complex response behaviour of the moored structure. Nonlinear restoring force is from the geometric nonlinearity or the catenary effect of the mooring lines where the CMLs are allowed to adjust the structural balance. Nonlinear coupled responses of the system are analysed to investigate different kinds of dynamic instability phenomena. Malaysian sea state comprising all the hydrodynamic and aerodynamic forces has been chosen as environmental loading. Frictional sea bed incorporates the Coulomb friction model with FC1 (Sea state MS-WCWIa) to consider the effect of sea bed friction. Following sections discuss the results from the two selected stability techniques.

4.13.1. Stable response analysis by bifurcation technique

Responses of the nonlinear coupled Spar-mooring system have been obtained in terms of platform motion and respective velocity time histories of DDS hull. Afterward, the velocity responses are plotted in abscissa with displacement/rotation responses in horizontal axis. Through these phase portraits of surge, heave and pitch, stability and instability of Spar responses are assessed. The plots display different kinds of instability phenomena in patterns of symmetry breaking bifurcations caused by mT sub harmonic/super harmonic oscillations and aperiodic responses of the moored Spar along with the pattern of limit cycle. It is to mention that, when a system approaches periodic behaviour and a closed curve in phase plane is appeared, the closed path is called a limit cycle. Two-dimensional manifolds as closed trajectories reported by phase plots are evaluated in stability recognition of Spar-mooring system.

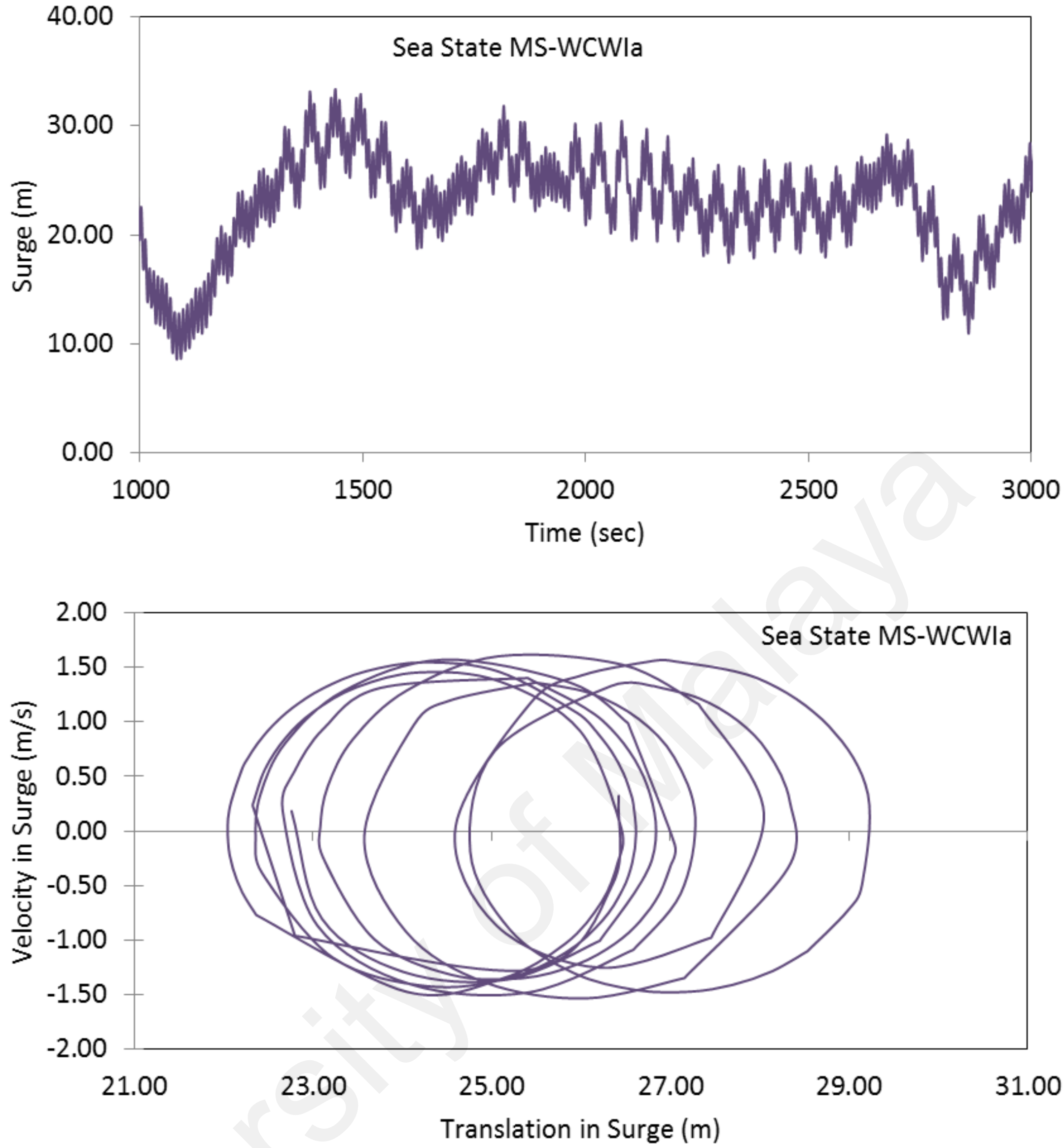

Figure 4.85: Short duration surge history and phase plot for sea state MS-WCWIa

Surge response

To clarify the stability and instability phenomena, the surge response behaviour of fully coupled Spar platform under sea state MS-WCWIa has been investigated in shorter and longer duration of loading. The horizontal motion in surge shows abrupt fluctuation in Spar motion at short duration of environmental condition. Repeated reversals in oscillations exist with a large range of platform movement (Figure 4.85) inducing lateral shift of platform. The variation of surge response in shorter duration is found to be aperiodic in nature at the start and then periodic later on. The phase plot of the surge responses at deck level shown in Figure 4.85 displays the behaviour of horizontal motion against its exciting velocity. In the time history, sub-harmonic or super-harmonic characteristics are existent. Furthermore, the phase plot is not symmetric. The limit cycle in two-dimensional manifold is a bit unstable. Hence, the possibility of dynamic instability of the response is exhibited.

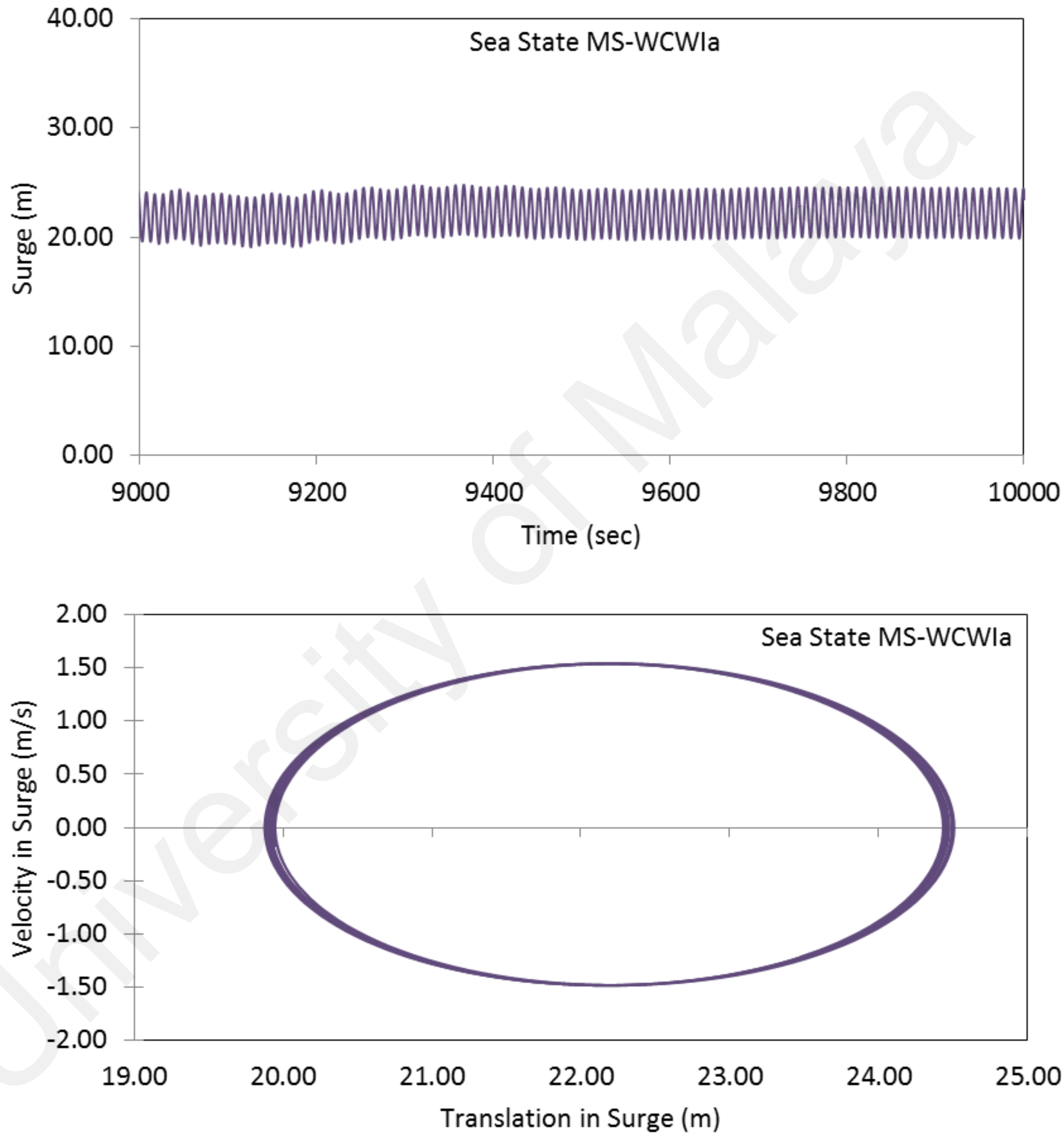

Figure 4.86: Long duration surge history and phase plot for sea state MS-WCWIa

On the other hand, for long duration of sea state MS-WCWIa, the platform motion shows excellently periodic surge with oscillating envelope. The lessened values of surge motion indicate identical peaks of maximum response around 25 m. The phase plot (Figure 4.86) shows the stable behaviour. The limit cycle in the two-dimensional manifold is found as stable. Reduced surge fluctuations and its steady phase plot confirm the behaviour of system stability. Though in short duration of loading, unstable platform motions are seen with symmetry breaking bifurcation, at long duration responses are stable with excellent stable close trajectory.

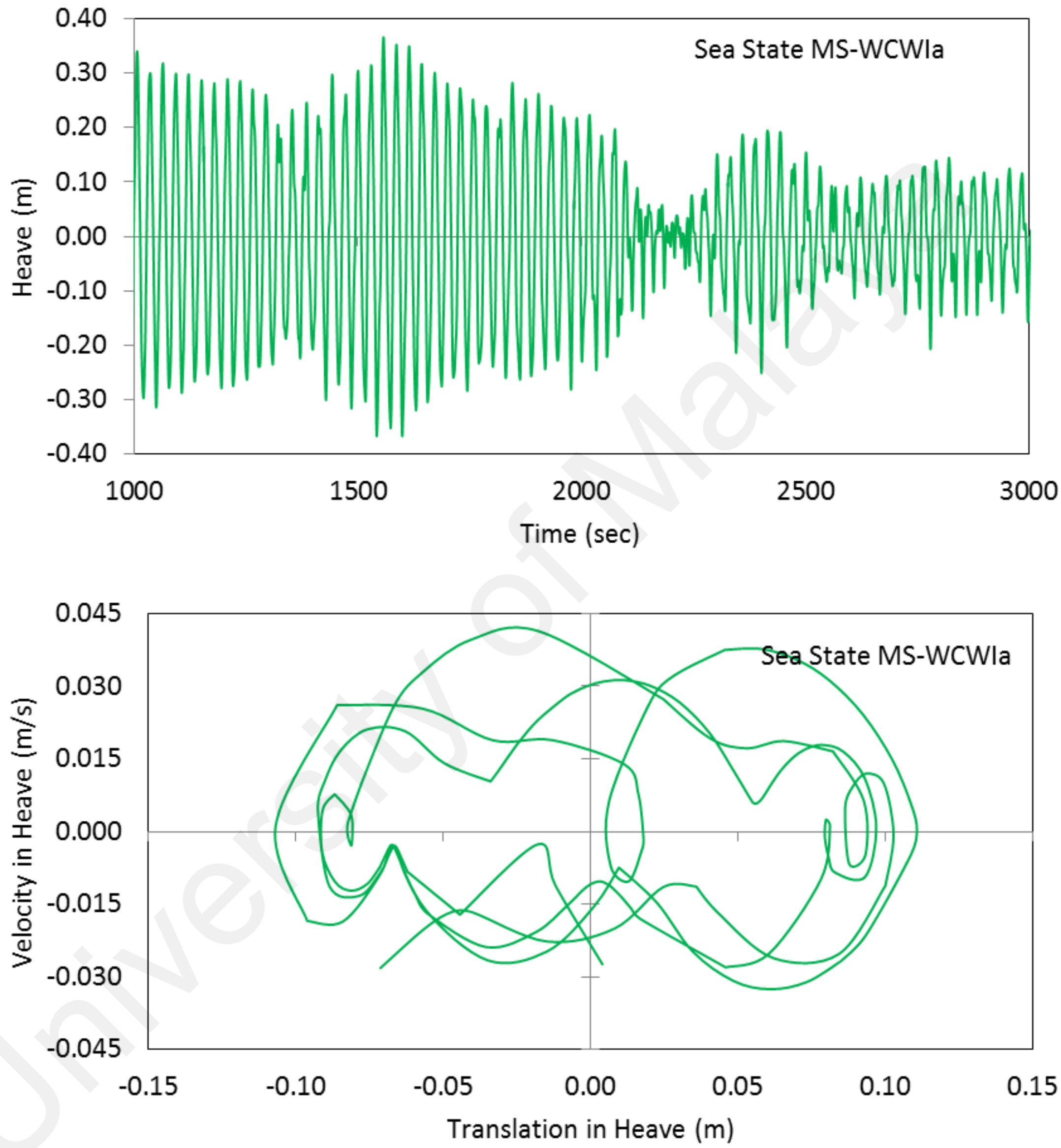

Figure 4.87: Short duration heave history and phase plot for sea state MS-WCWIa

Heave response

The time histories of heave motion and corresponding phase plots are plotted at Figure 4.87 for shorter duration and Figure 4.88 for longer duration of sea state MS-WCWIa. In heave response oscillations at shorter duration, significant range of fluxes indicates the possibility of instability. The responses are not harmonic but periodic in nature and sub harmonics/super-harmonic characteristics of heave motion occur. The sub harmonics in the surge response history are induced by the nonlinearities in the system. The phase plot of the heave responses in Figure 4.87 articulates the motion as asymmetric in nature with supercritical Hopf bifurcations. The Spar platform experiences tendency of instability in this neighbourhood. It is also seen that no limit cycle is existent or the limit cycle is unstable in the two-dimensional manifold. Therefore, possibility of dynamic instability in terms of bifurcation of response as well as nT solution exists.

Conversely, at long duration of MS-WCWIa sea state, the nature of heave fluctuation and its corresponding phase plot dismisses the existence of instability (Figure 4.88). The platform motion in heave behaves periodically offering an oscillating envelope. Added damping reduces the long duration response to some extent. However significantly lower values of heave motion show identical peaks of maximum response (around 24 m) at this stage. T-periodic behaviour along with closed path in phase portrait exists in the heave motion. From the phase plot it is seen than the platform moves downward and then come upward vertically. After the maximum upward movement, the platform moves slightly downward and then slightly upward creating a loop in velocity-displacement relation. Again the platform moves downward showing an overall symmetric closed path and hence stable behaviour of response. Stabilized heave fluctuations in periodic manner confirm the system more stable at long duration, though in short duration the heave response is unstable because of sub harmonic/super harmonic nature with supercritical Hopf bifurcations.

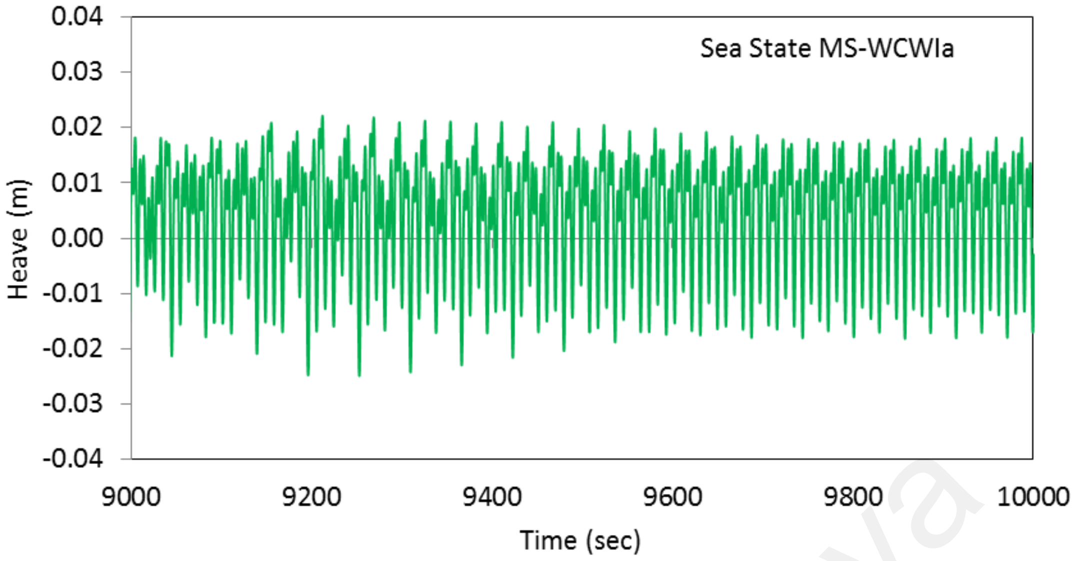

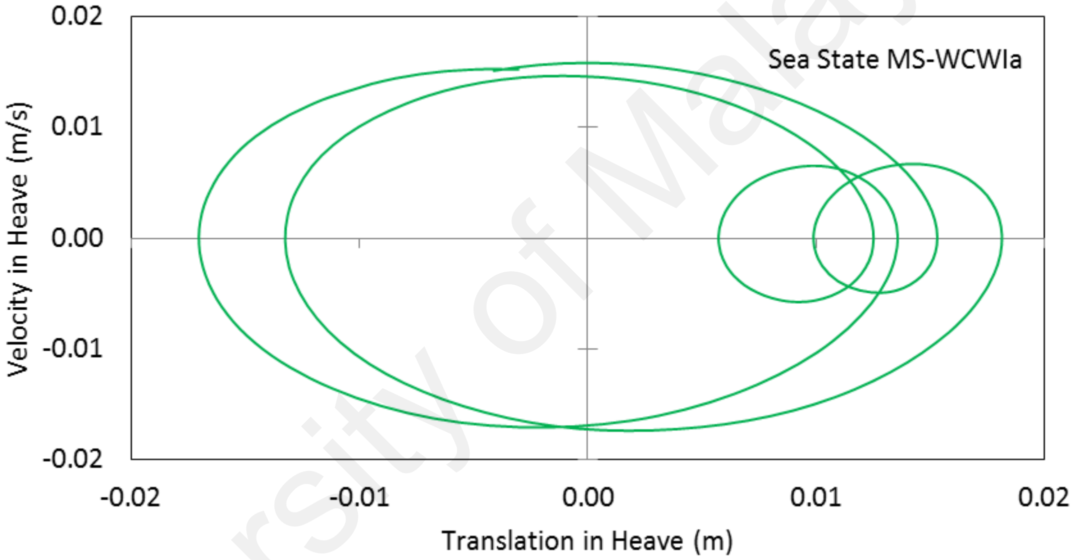

Figure 4.88: Long duration heave history and phase plot for sea state MS-WCWIa

Pitch response

Short duration of loading at sea state MS-WCWIa shows the possibility of instability in platform rotation as shown in Figure 4.89. The pitch phase portrait doesn't show the symmetric close path which indicates unstable bifurcation. Increase of pitch changes the oscillations of Spar rotation to sub harmonic and super harmonic nature. Abrupt movement of platform pitch is visualized. In the system nT solution subsists even though the pitch response may endure within finite bounds. The limit cycle in two dimensional phase plane is unstable. The phase plot breaks its symmetry at short duration and the Spar platform experiences instability in this time zone.

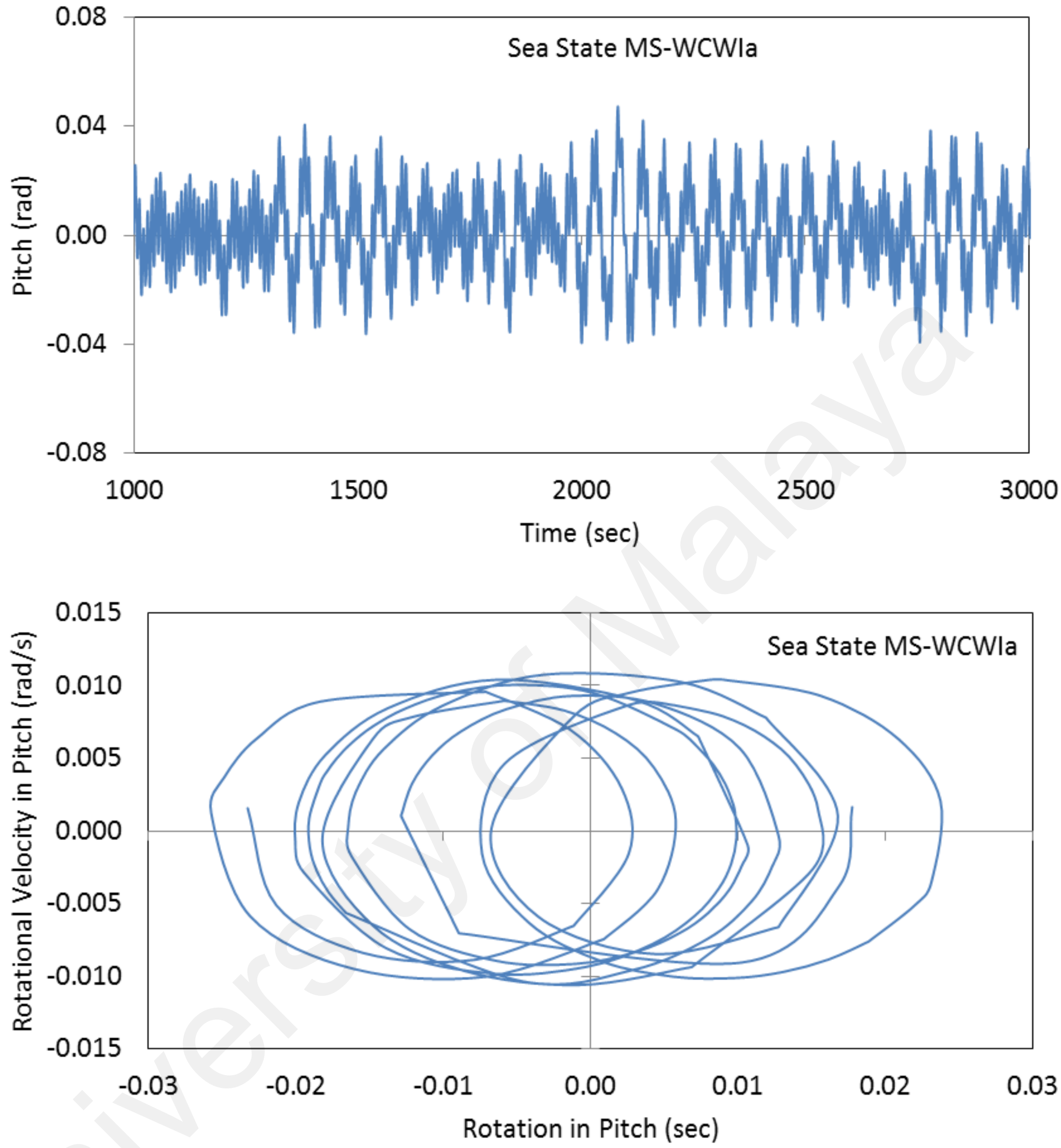

Figure 4.89: Short duration surge history and phase plot for sea state MS-WCWIb

Though at shorter duration, the platform experiences unstable behaviour, at longer duration, the pitch response is periodic and the two dimensional manifold of velocity-rotation shows symmetric path. The platform shows a stable configuration at this duration of ocean loading. The pitch time history and its phase plot are shown in Figure 4.90. The phase plot shows stable limit cycle with nice close trajectory. No sub harmonic and super harmonic bifurcations are existent. Hence, the platform is stable on pitch rotation for long durational ocean environment.

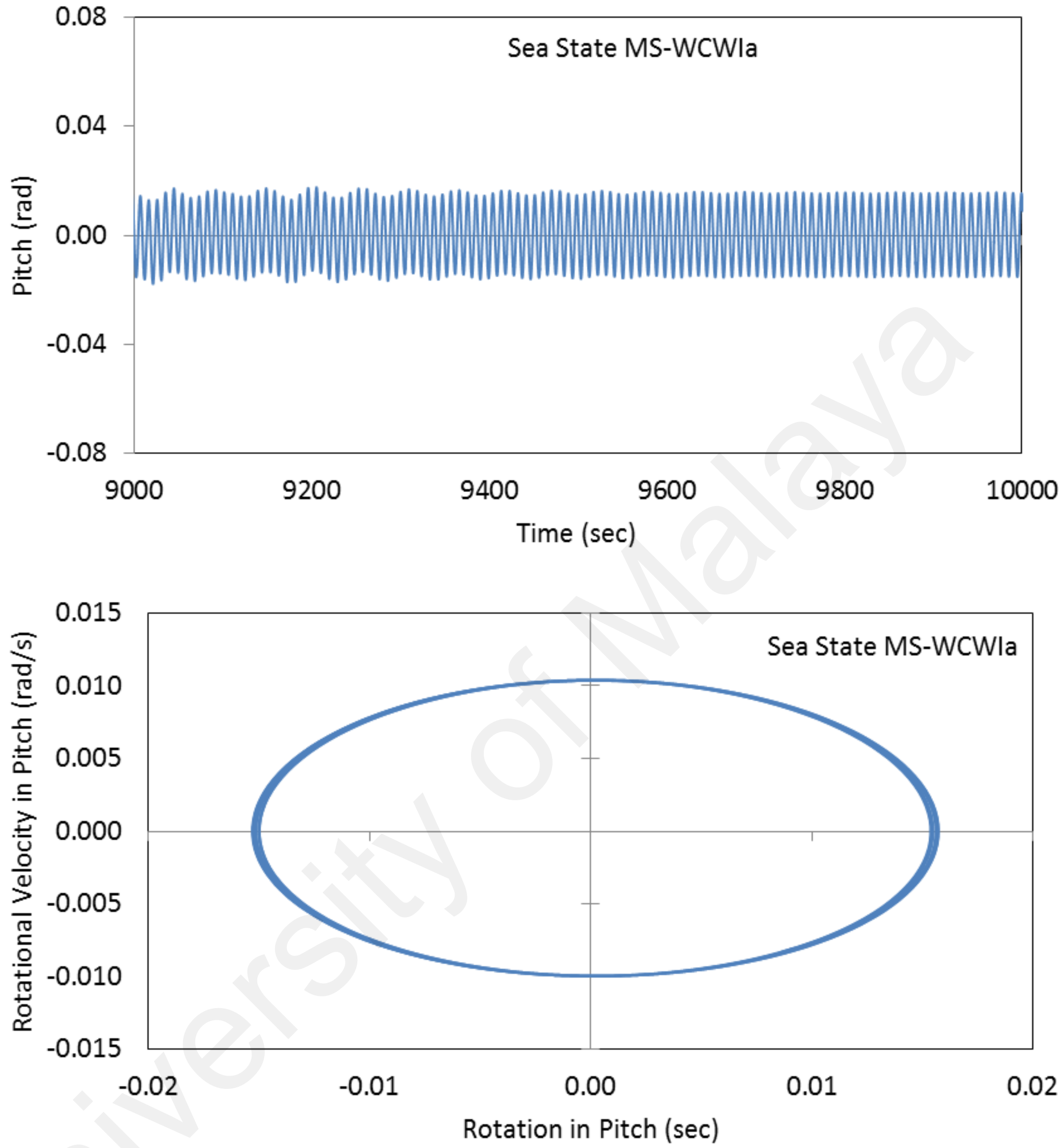

Figure 4.90: Long duration surge history and phase plot for sea state MS-WCWIb

4.13.2. Mathieu's Instability

Mathieu's instability may occur when the pitch natural period is double than that of heave motion and the harmonic variation of pitch exist due to large heave motion. Due to existence of Mathieu instability, heave and pitch coupling creates a lock-in phenomenon. In this section, the heave and pitch responses are evaluated to see the existence/non-existence of Mathieu instability in short and long duration of Malaysian environmental loading. The sea state is MS-WCWIa which considers frictional coefficient FC1. More sea states with wave periods near to heave natural period along with various damping coefficients should be considered for detail evaluation of Mathieu instability phenomenon in Spar platform.

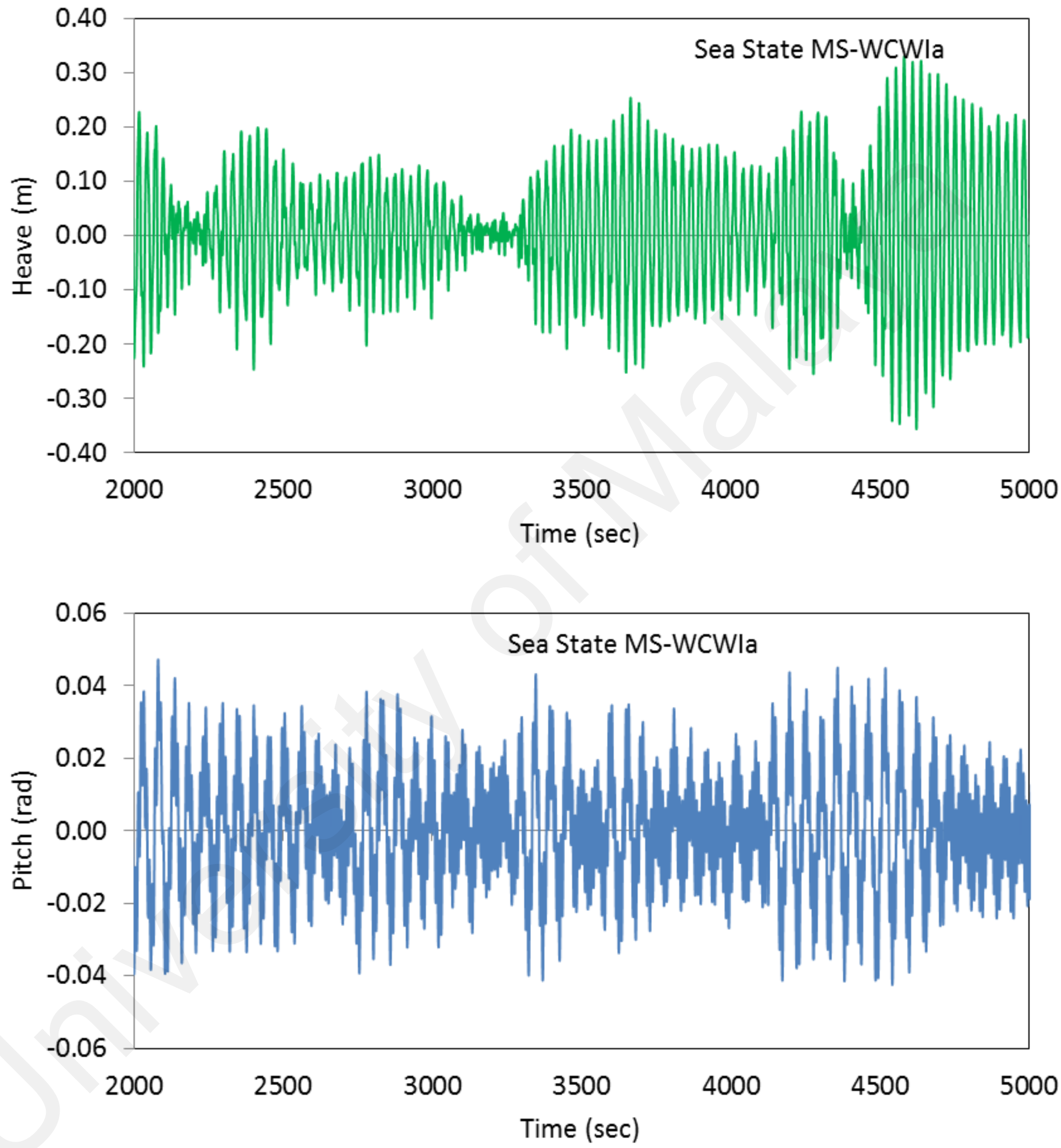

Figure 4.91: Short duration heave-pitch time history under sea state MS-WCWIa

Mathieu's instability in Malaysian condition

The free decay simulation of fully coupled Spar platform show the natural periods as 25.60 second and 53.48 seconds for heave and pitch motion respectively. Drag coefficients are chosen as 0.6 and 1.0 for Spar hull and catenary mooring line respectively. Additional damping is induced from Coulomb friction model of sea bed friction. It is observed that most of the heave damping on the moored Spar comes from CML. As the heave natural period is around half of pitch natural period, the Spar platform may have Mathieu instability. Long range time history of heave and pitch up to 10000 sec has been evaluated to check Mathieu instability of the moored Spar.

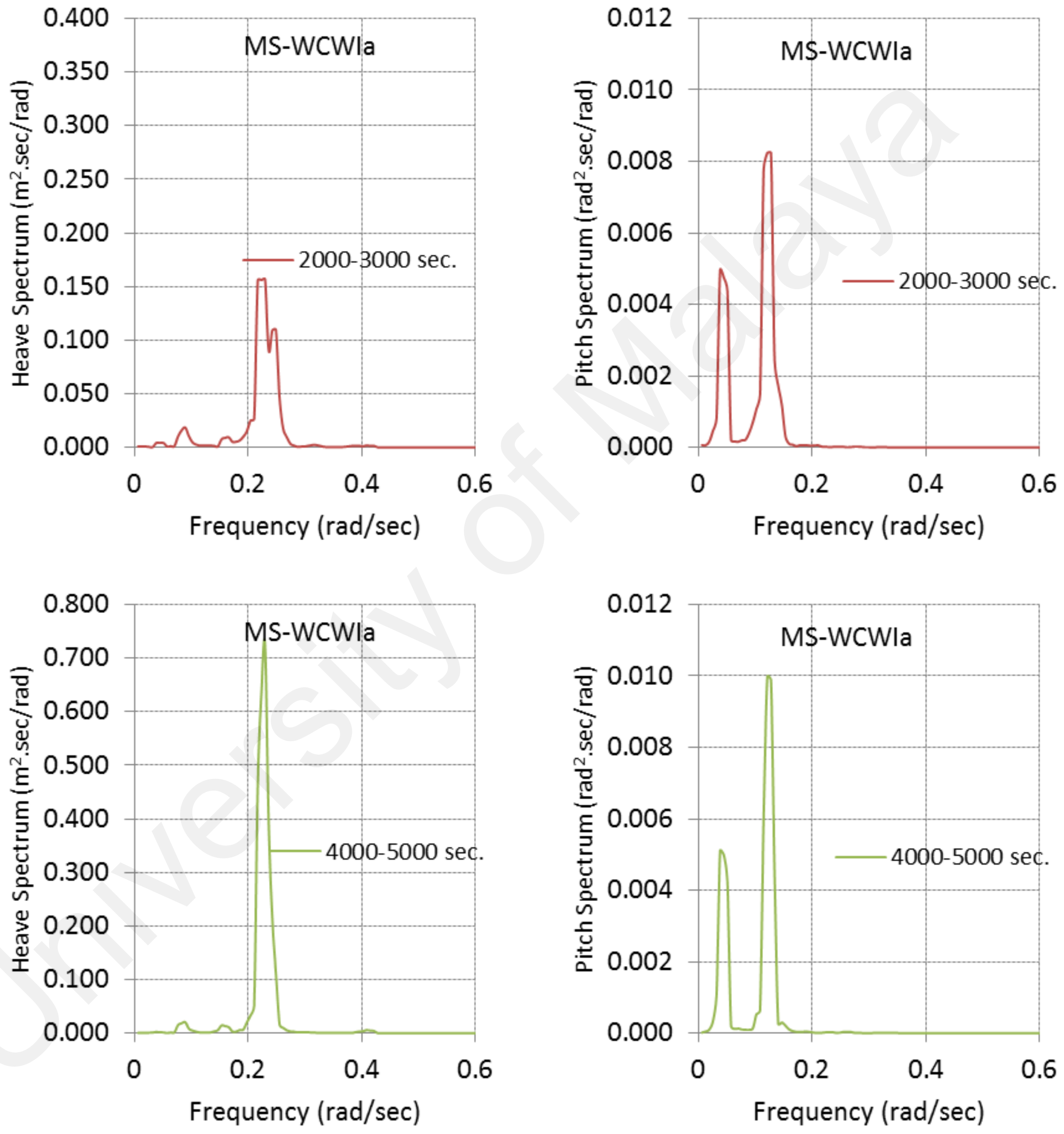

Figure 4.92: Short duration heave-pitch spectra under sea state MS-WCWIa

It is seen that at several time station in short duration, there are sudden radical rise and fall of heave responses (Figure 4.91). At these stages, the pitch motions are also disturbed. It can be noticed that heave and pitch are slightly dependent on each other.

The heave-pitch coupling exists around 2400 sec, 3500 sec and 4400 sec of ocean loading. The pitch response spectrum (Figure 4.92) shows largest peak in pitch natural period. Heave response is governed by heave natural frequency. Heave and pitch coupling creates a lock-in phenomenon at this stage showing slight Mathieu instability. Alternation of energy transfer is observed between heave and pitch motion. Such behaviour of responses falls around the damped tongue of instability in nonlinear damped Mathieu instability diagram (Figure 3.18). However, the magnitudes of heave and pitch are not very high for the Spar to show significant Mathieu instability.

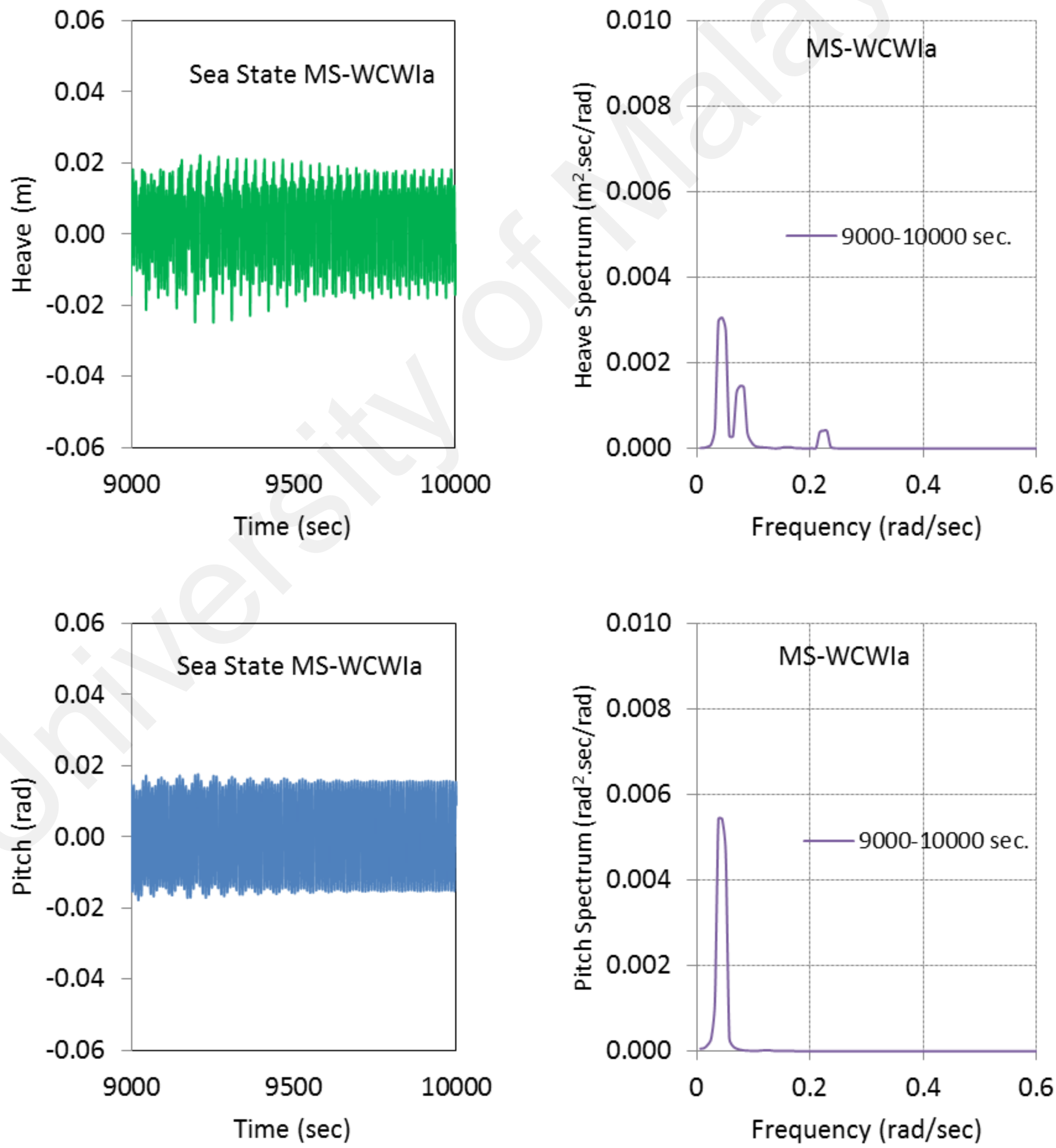

Figure 4.93: Long duration heave-pitch stable behaviour for sea state MS-WCWIa

After around 9000 seconds of loading, the heave and pitch motion stabilizes and appears to be steady. There is no existence of heave-pitch coupling in this zone and pitch is not dependent on heave motion. Both heave and pitch spectra show governing peak at surge frequency (Figure 4.93). The heave motions are not adequately large to trigger the Mathieu instability and the heave-pitch motion becomes stable. Periodic motion of heave and pitch indicates the stability of platform. The behaviour of Spar motion shows that the structural damping is adequate to conquer the Mathieu instability. Therefore, for the chosen damping parameters and structural configuration Mathieu instability is not existent for selected Malaysian condition. The Spar platforms show excellent motion behaviour in this sea state. However, when the swell condition is considered with wave period close to heave natural period, the heave motion of spars can be largely amplified and Mathieu instability may occur.

4.14 Effect of riser

A key aspect in the design of a Spar platform is the coupling of the associated risers and the impact they have on the platform. The risers provide means for drill strings and production tubings to reach the oil well deep down at the ocean floor. Increase in water depth has a direct impact on the design of the riser, primarily due to the increase in riser weight as well as larger hydrodynamic drag. As risers are integral parts of drilling and production activities in offshore environments, proper investigation for the effect of risers on coupled dynamics of Spar is of great importance. Hence, the response of coupled Spar in surge, heave and pitch along with top tension in mooring lines are evaluated in the present study.

4.14.1. Integrated Spar-mooring-riser simulation

Adopted methodology for nonlinear coupled dynamic analysis of floating Spar-mooring system in deep water has been discussed earlier. The riser component has been modelled which allows coupled analysis of the whole integrated Spar-mooring-riser system. The properties of rigid riser (Khan and Ahmad, 2010) for the present simulation are given in Table 4.40. The riser is modelled as hybrid beam element with six degrees of freedom in ABAQUS finite element program. Single equivalent rigid riser comprising of four individual risers has been considered in the Spar-mooring-riser system. The bottom end of rigid riser is hinged. It allows rotation but restrained in horizontal and vertical directions. The top end of riser is linked with the Spar keel. Rotation in roll, pitch and yaw has been permitted. Furthermore, horizontal and vertical movement of riser top is allowed with Spar keel. This assemblage provides coupled action of Spar hull with riser at the Spar keel. Required pretension is maintained at riser top end. The analysis comprises nonlinearities caused by large deformation, time-varying variation of submergence, added mass, buoyancy and drag force.

Table 4.40: Properties of equivalent riser

Parameters	**Value**	**Unit**
Category	Rigid riser (RR)	-
Total line length	819.88	m
Stiffness (EA)	1.0706E11	N
Wall thickness	0.01588	m
Elastic modulus	2.068E11	N/mm^2
Torsional shear modulus	1.034E11	N/mm^2
Riser pre-tension	1.20E+07	N
Element type	Hybrid beam element	-
Drag co-efficient	1.1	-
Inertia co-efficient	2.5	-

4.14.2. Numerical study for riser effect

Nonlinear analysis of integrated platform, mooring lines and riser is carried out under hydro-aerodynamic loading. The hydrodynamic characteristics considered in the spar-mooring-riser assemblage are given in Table 4.3 and Table 4.41. A severe sea environment may sometimes cause more damage than the normal hydrodynamic loading. Hence, critical sea state, strong gale for wave only (case SG-W) has been selected for comparative evaluation of extreme responses of the coupled Spar. The time histories recorded for statistical analysis is 9200 to 9700 sec for with riser case and 11500 to 12000 sec of wave loading for without riser case. Because, in these stages, stabilized responses are seen. Response behaviours in steady state have been evaluated for Spar-mooring system and Spar-mooring-riser assemblage though time histories, power spectra and statistical analysis.

Table 4.41: Hydrodynamic properties for riser

Element	**Hydrodynamic parameters**	**Value**
Rigid riser	Drag coefficient	1.1
	Inertia coefficient	2.5
	Added mass coefficient	1.2
Sea water depth (m)		1018
Density of Sea water (Kg/m^3)		1000

4.14.2.1. Surge behaviour for inclusion of riser

Platform surge

The effect of riser coupling on platform surge in the moored Spar has been studied under wave only case in strong gale. The riser adds additional restrain against environmental forces. Behaviour of surge responses at deck level is shown in Figure 4.93 for w/o (without) riser and with riser case. Maximum values of surge are 12.72 m and 10.20 m in case of without riser and with riser. It is seen that the surge response reduces by 20%. The surge response oscillates from -6.27 m to 12.72 m (Figure 4.93a) and -4.69 m to 10.20 m (Figure 4.93b) in w/o riser and with riser case respectively. Therefore, the fluctuation of surge is significantly decreased due to inclusion of riser in the coupled system.

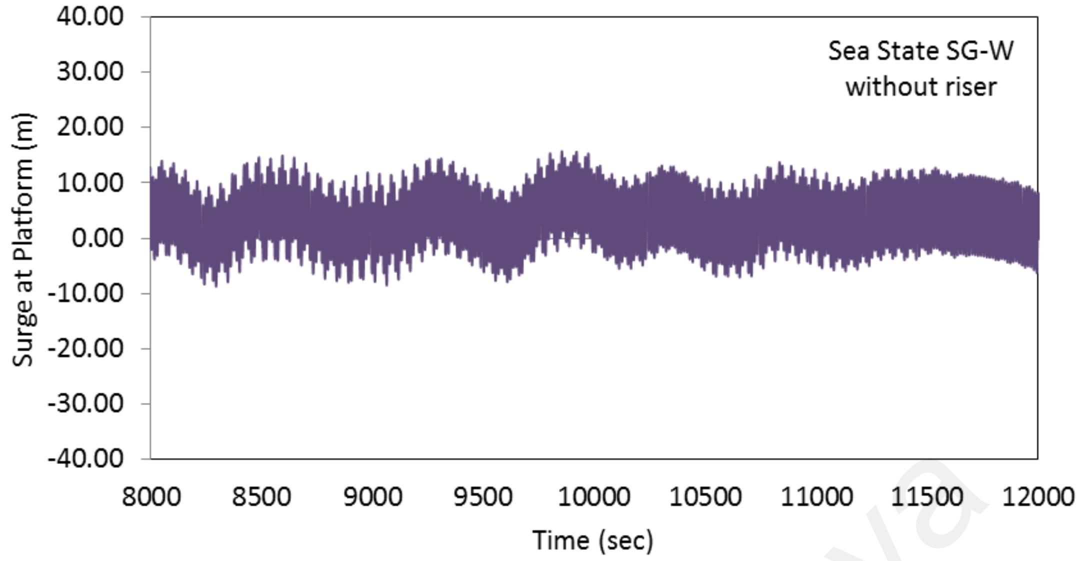

a) Without riser

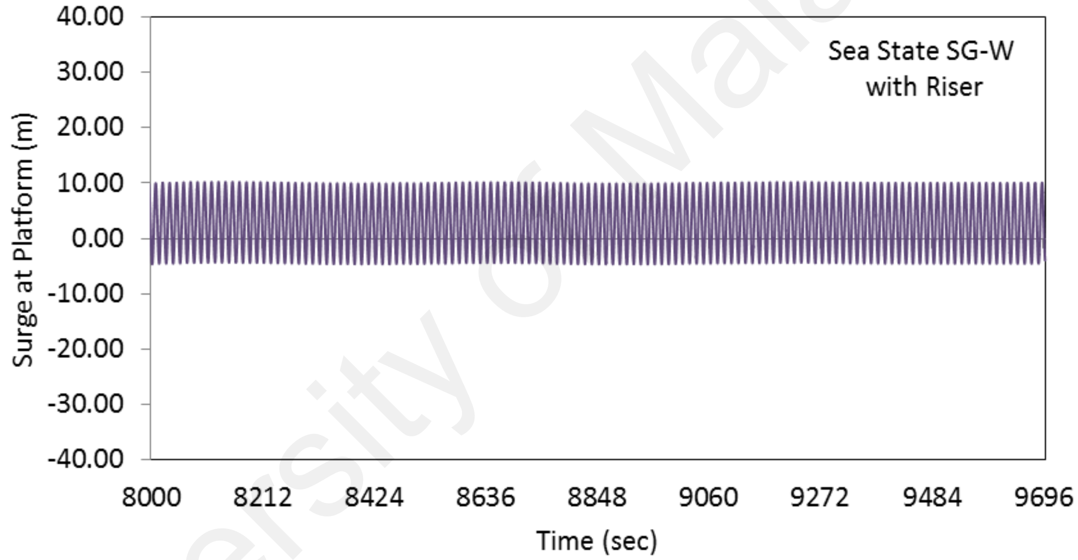

b) With riser

Figure 4.93: Surge time history with and w/o riser

A governing peak near pitch frequency is observed for inclusion of riser. However, the energy content in this frequency is less than without riser condition. Comparative power spectra of surge response for with riser and without riser cases have been shown in Figure 4.95. In without riser case participation of surge frequency is also seen along with the governing peak at pitching motion. The change in surge behaviour of platform is due to additional damping induced by the rigid riser in Spar-mooring-riser system.

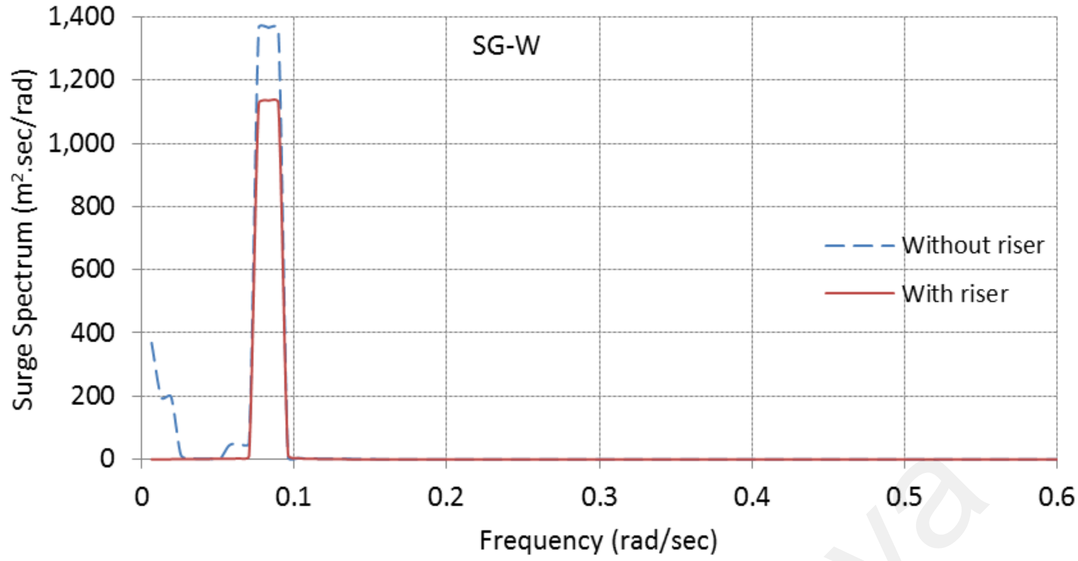

Figure 4.95: Power spectrum of surge with riser and without riser

Statistical analysis of surge response

Table 4.42 illustrates the statistical analysis of surge response under various cases. When riser is not considered, the surge RMS values are seen as 6.20 m under strong gale. But inclusion of riser decreases these corresponding statistical values to 5.91 m in surge response. Reduced standard deviation with riser confirms the suppression of platform response. Hence, overestimation of platform motion in surge can be eliminated by proper incorporation of riser in the coupled Spar platform assemblage.

Table 4.42: Effect of riser on surge response behaviour

Surge	**Wave w/o riser**	**Wave with riser**
Max (m)	12.72	10.20
Min (m)	-6.27	-4.69
Mean (m)	3.51	2.88
Median(m)	3.32	3.07
Mode (m)	12.32	10.04
Stdev (m)	5.11	5.17
RMS (m)	6.20	5.91
Skewness	0.02	-0.05
Kurtosis	-1.33	-1.50
Range	18.98	14.89

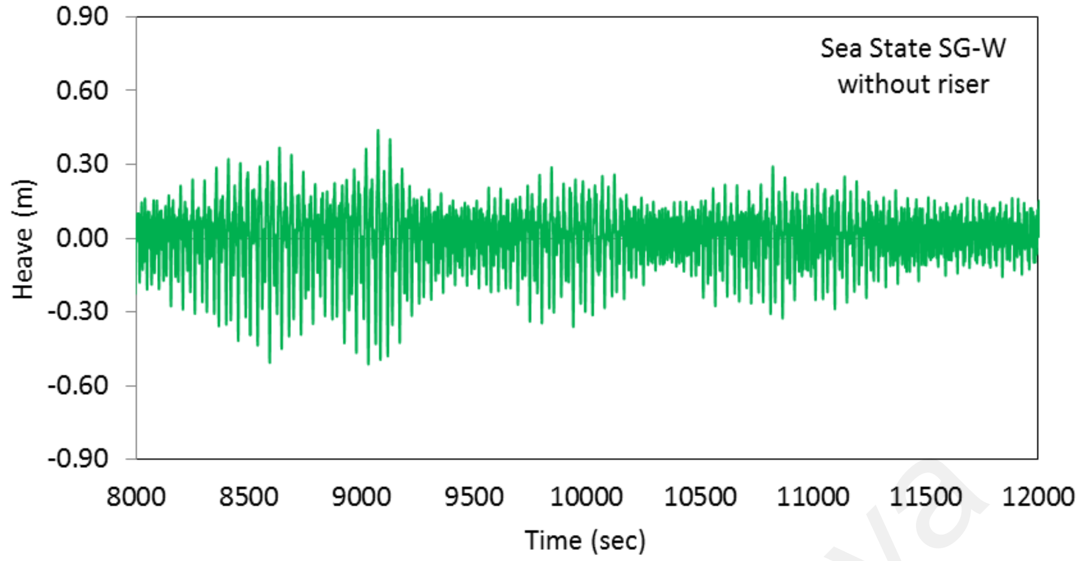

a) Without riser

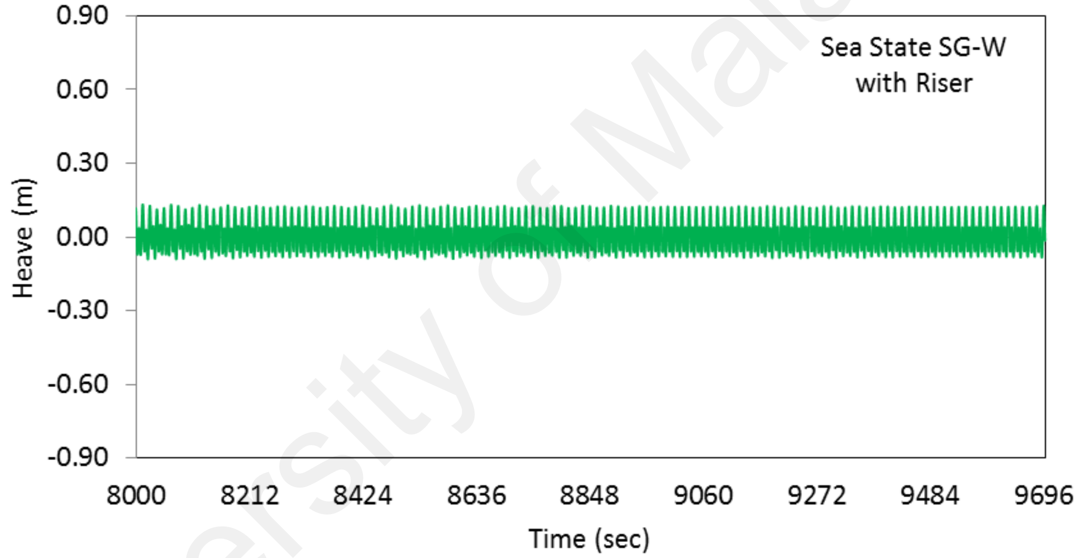

b) With riser

Figure 4.96: Heave time history with and w/o riser

4.14.2.2. Heave behaviour for inclusion of riser

Platform heave

Inclusion of riser in coupled Spar-mooring system changes the behaviour of platform vertical motion. The heave responses for without and with riser case, are shown in Figure 4.96a and Figure 4.96b respectively. Maximum heave response for without riser case is 0.17 m whereas it decreases to 0.13 m for with riser case. It is seen that the heave motion reduces by 23% when riser is incorporated. Therefore, more steadiness in platform vertical movement is achieved due to riser. It is possible that for Spar-mooring system, more time is needed to stabilize, whereas Spar-mooring-riser responses stabilize early.

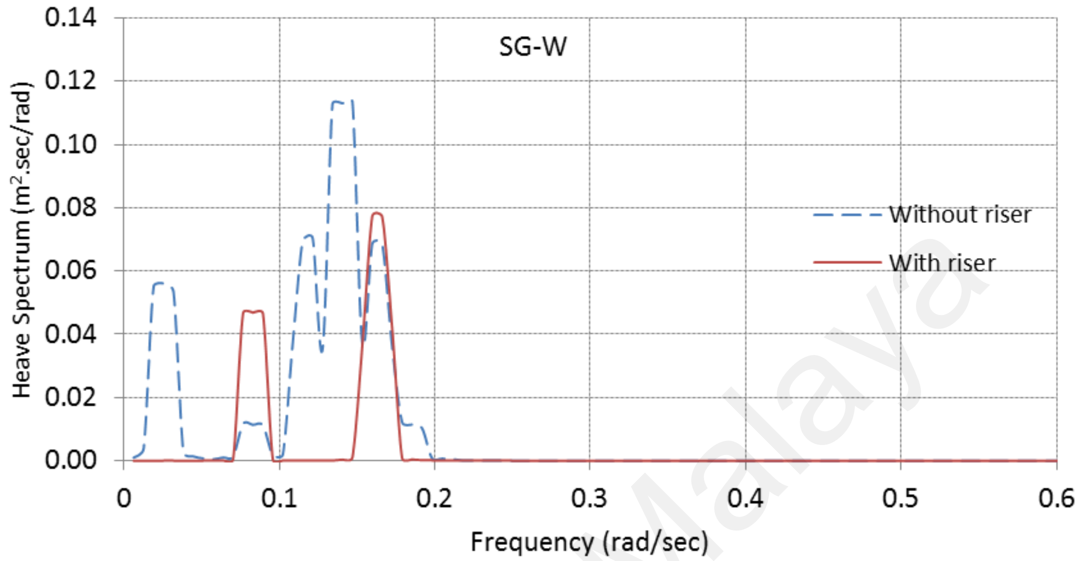

Figure 4.98: Power spectrum of heave with riser and without riser

In case of without riser, one large peak and two minor peaks in pitch frequency region (Figure 4.98) has been seen in heave spectrum along with little involvement of surge frequency. However, pitch frequency is significant for with riser case. The power spectra show that the energy contents at governing frequency are diminishing when riser is considered.

Table 4.43: Effect of riser on heave response behaviour

Heave	**Wave w/o riser**	**Wave with riser**
Max (m)	0.17	0.13
Min (m)	-0.16	-0.09
Mean (m)	0.02	0.01
Median(m)	0.02	0.00
Mode (m)	-0.03	0.04
Stdev (m)	0.07	0.06
RMS (m)	0.07	0.06
Skewness	-0.12	0.43
Kurtosis	-0.74	-0.93
Range	0.32	0.22

Statistical analysis of heave response

Statistical illustration of the heave responses are given in Table 4.43. RMS responses are seen as 0.07 m and 0.06 m for w/o riser and with riser respectively. Mean and median value of heave responses decreases due to riser inclusion. The standard deviation of heave response with riser coupling also decreases. More platy-kurtic distribution of heave responses is seen for with riser case indicating less fluctuation around the mean position than without riser condition.

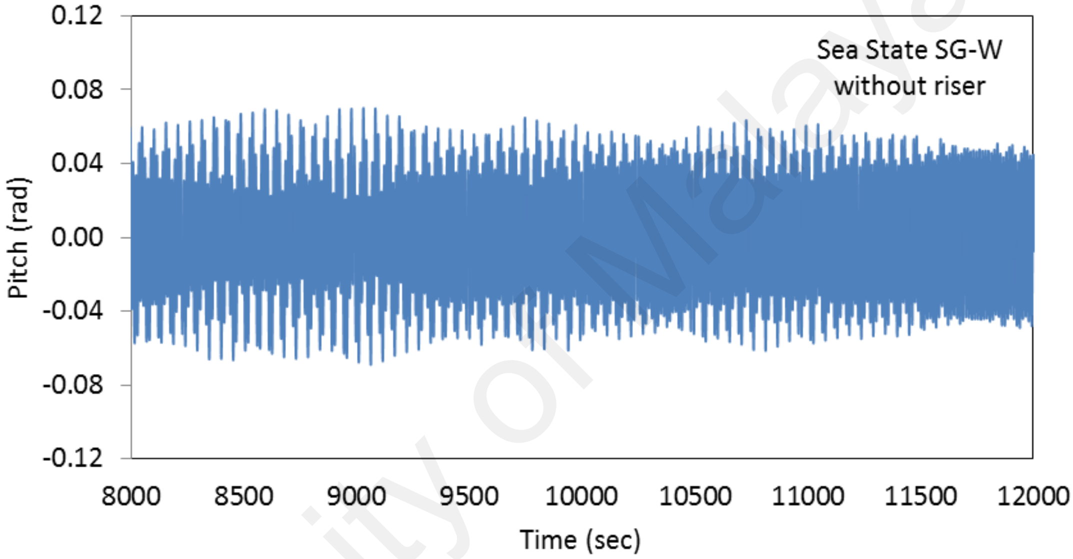

a) Without riser

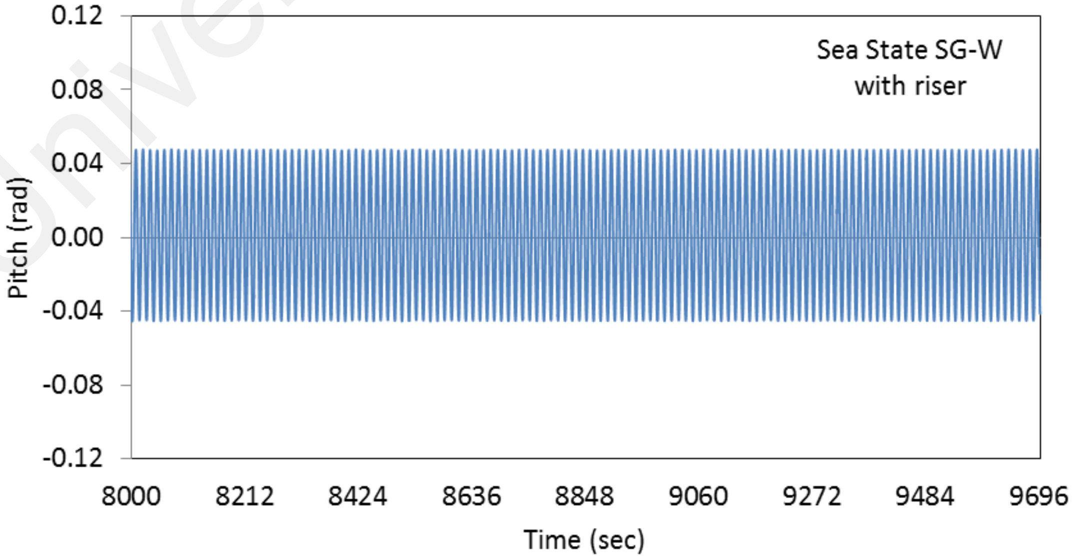

b) With riser

Figure 4.99: Pitch time history with and w/o riser

4.14.2.3. Pitch behaviour for inclusion of riser

Platform pitch

The pitch response decreases due to coupled action of riser with platform and mooring line. Maximum value of pitch reduces by 10% when riser is considered. It shows that the platform rotation is overestimated by 1.10 times if riser is ignored. Figure 4.99 displays the time series of pitch motion for w/o riser and with riser case. The maximum and minimum response in pitch are +0.053 rad, -0.050 rad for w/o riser and +0.048 rad, -0.045 rad with riser. However, the RMS values are not showing significant difference in pitch for riser inclusion.

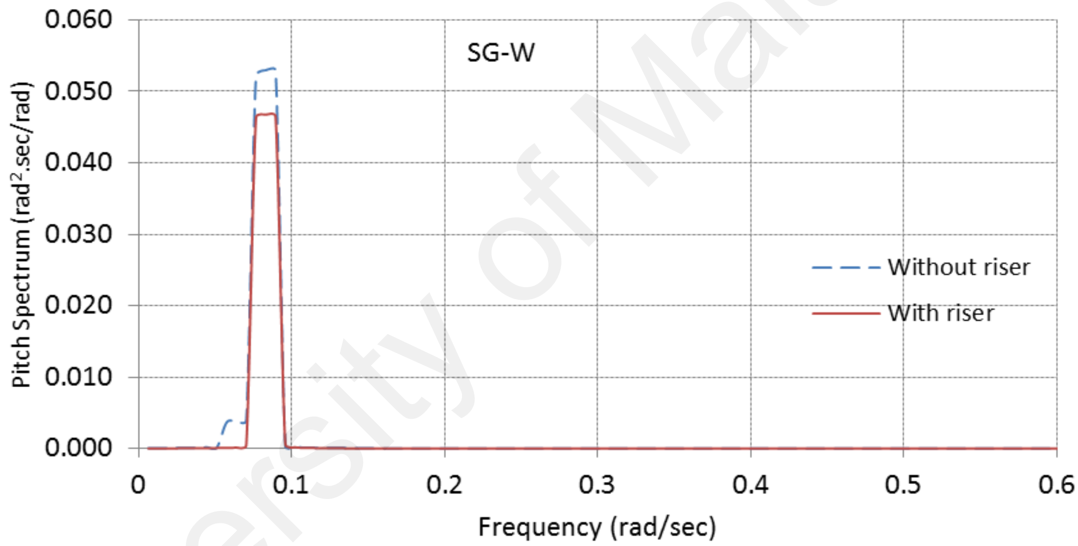

Figure 4.101: Power spectrum of pitch with riser and without riser

The energy spectrum of pitch shows a governing peak at 0.093 rad/sec which is located near the pitch natural frequency (Figure 4.101). Slightly higher energy is available for without riser case, but this amount reduces when riser is considered. Coupled action in Spar-mooring-riser system enhances to decrease the energy content which is reflected in power spectra.

Statistical analysis of pitch response

The mean and mode values of pitch response show reduction of platform rotation due to inclusion of riser. Maximum pitch response decreases for riser case. The statistics of pitch time history for without riser and with riser are discussed in Table 4.44. Very low value of mean and median (around zero) shows the firmness in rotation of platform. Uni-modal distribution of pitch response is seen for both the cases. Moreover, reduction of standard deviation with riser case shows reduced fluctuations of pitch.

Table 4.44: Effect of riser on pitch response behaviour

Pitch	**Wave w/o riser**	**Wave with riser**
Max (rad)	0.053	0.048
Min (rad)	-0.050	-0.045
Mean (rad)	0.001	0.002
Median(rad)	-0.0004	0.003
Mode (rad)	0.05	-0.04
Stdev (rad)	0.03	0.03
RMS (rad)	0.03	0.03
Skewness	0.04	-0.05
Kurtosis	-1.45	-1.50
Range	0.10	0.09

4.14.2.4. Mooring tension behaviour for inclusion of riser

Top tension in mooring line

The effect of riser on CML tension has been shown in Figure 4.102 under strong gale environment. Damping of riser decreases the maximum CML tension by 2%. The fluctuation of wave induced tension without riser ranges from 1.73E+07 N to 1.54E+07 N which reduces by 1.70E+07 N to 1.55E+07 N due to addition of riser. This lower fluctuation in tension response is because of additional damping caused by riser.

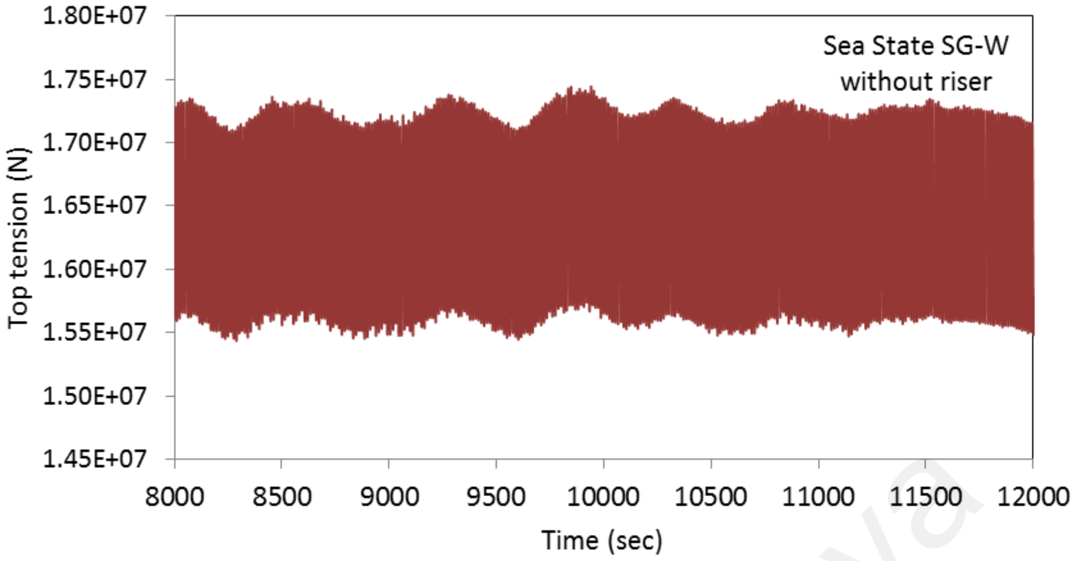

a) Without riser

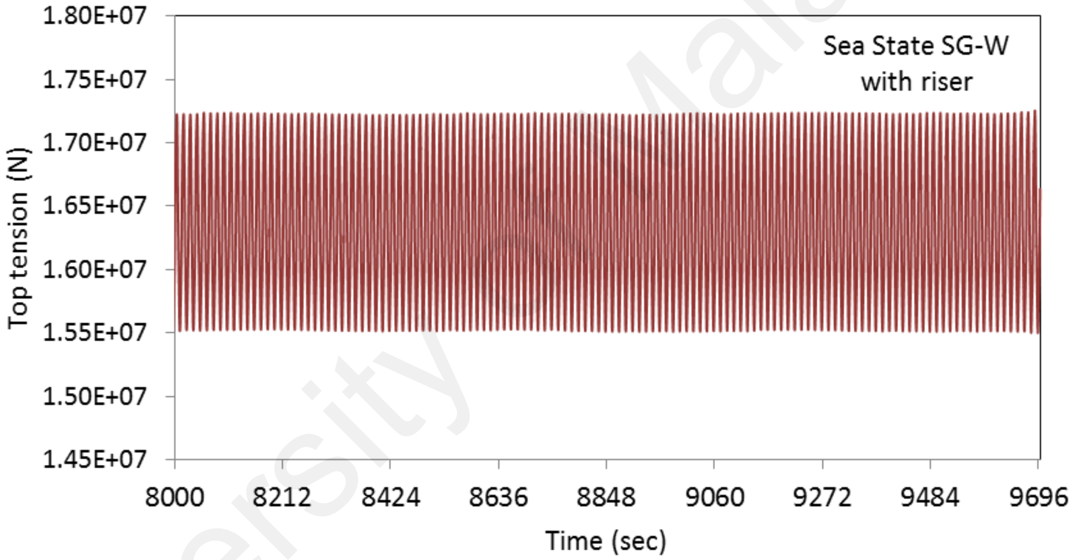

b) With riser

Figure 4.102: Mooring tension time history with and w/o riser

Power spectrum of mooring top tension (Figure 4.104) shows governing peak in pitch frequency and very little involvement of surge motion for without riser case. Due to inclusion of riser, solitary peak of energy content is seen at pitch frequency. However, the energy content at the governing frequency decreases in very little amount. The behaviour of tension response does not change significantly which is reflected in power spectrum.

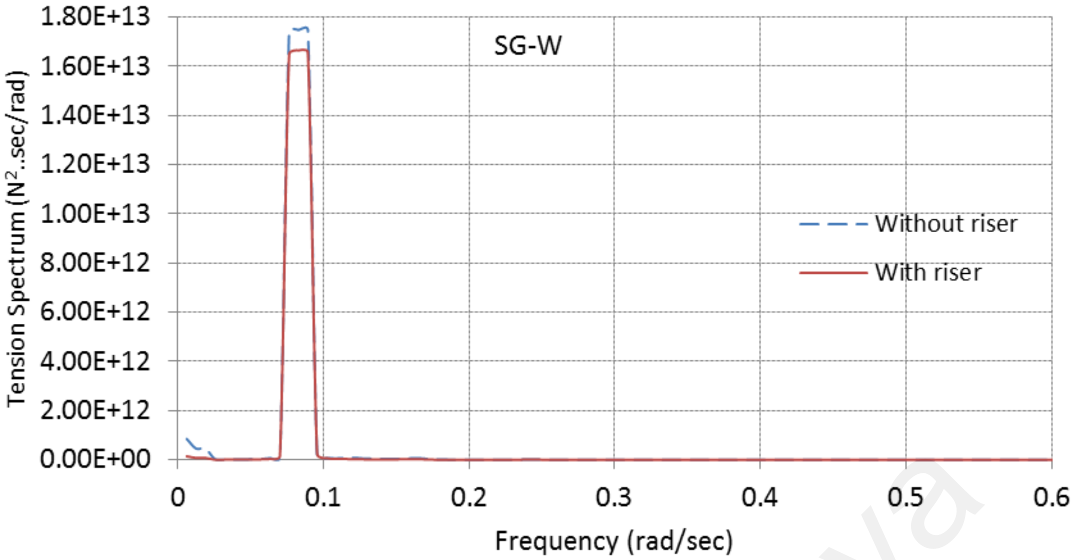

Figure 4.104: Power spectrum of mooring tension with riser and without riser

Statistical analysis of mooring tension

Table 4.17 shows the statistical analysis of tension responses for without riser and with riser cases. The mean, median, mode values of CML tension are seen to be slightly changed for inclusion of riser. Reduction of standard deviation in tension for inclusion of riser is observed by 5% than without riser case. The stdev decrement in mooring tension shows the participation of riser component in coupled analysis contributing milder oscillations.

Table 4.45: Effect of riser on mooring tension behaviour

Mooring top tension	**Wave w/o riser**	**Wave with riser**
Max (N)	1.73E+07	1.70E+07
Min (N)	1.54E+07	1.55E+07
Mean (N)	1.63E+07	1.62E+07
Median (N)	1.62E+07	1.63E+07
Mode (N)	1.56E+07	1.55E+07
Stdev (N)	6.12E+05	5.85E+05
RMS (N)	1.64E+07	1.64E+07
Skewness	0.21	0.11
Kurtosis	-1.51	-1.46
Range	1.86E+06	1.73E+06

CHAPTER 5: CONCLUSIONS

5.1 General

A fully coupled integrated NONLIN-COUPLE6D model of Spar mooring system has been developed and validated with published experimental results. Nonlinear coupled analysis of Spar platform has been carried out under various sea waves, current forces and wind loading. Nonlinearities arising due to long flexible mooring geometry, variable submergence, added mass, damping and mooring line interaction with sea bed are duly considered. Oil and gas energy status in Malaysian scenario has been assessed. Wave data of Malaysian sedimentary basins have been simulated. Suitability of coupled spar-mooring system in Malaysian deep water is evaluated. It includes evaluation of sea bed friction effect and stable response analysis of the moored Spar. Moreover, Spar-mooring-riser system has been modelled as integrated system and the effect of riser in fully coupled analysis is assessed.

5.2 Conclusions

Based on the present study, following important conclusions are drawn.

5.2.1. Developing fully coupled integrated model (NONLIN-COUPLE6D) of Spar platform

a) The fully coupled Spar platform model employed in the present study is realistic because it maintains the continuity of the structure, incorporates the instantaneous stiffness due to time-wise response, curvature of catenary, tension fluctuations, geometric and other essential nonlinearities.

b) Nonlinear coupled dynamic response behaviours obtained from the developed model have been validated and the results are found to be in reasonable agreement with the published experimental results.

c) In finite element model, the entire structure acts as a continuum. This model can handle all nonlinearities, loading and boundary conditions. The commercial finite element code ABAQUS/ AQUA is found to be suitable for the simulation.

d) The physical coupling of mooring lines at Spar fair lead and the variable contact condition at the touch down point near sea bed model the mooring line dynamics in a realistic fashion. However, the solutions are convergence sensitive and require large number of iterations, at each time station.

5.2.2. Nonlinear coupled dynamic analysis for long duration wave loading

a) Nonlinear dynamic analysis of fully coupled Spar platform has been performed in time domain up to 12000 seconds of wave loading. High degree of non-linearity involved causes irregular response characteristics of mooring lines at low frequency and wave frequency levels. Power spectra are more informative to highlight the important features.

b) Platform responses are influenced by natural frequencies for both short (4000 sec.) and long (12000 sec.) duration of wave. At longer duration, wave frequency becomes relatively significant for surge, heave and pitch. Mooring tension is governed only by wave frequency for longer duration of wave loading.

c) Surge response at platform level is deeply influenced by the coupled pitch. It significantly appears at pitch frequency in power spectrum.

d) The responses in surge, heave and pitch considerably decrease for long duration of wave loading. However, because of high pretension, CML tension does not show any appreciable change even after long duration of wave loading.

e) The energy contents of power spectra of surge, heave and pitch responses at 3 hours significantly reduce compared to 1 hour of wave loading. It is mainly due to the damping of CMLs in the integrated coupled Spar- mooring system.

f) The CML tension at short duration of wave loading show the participation of higher modes in pitch frequency apart from exciting an appreciable low frequency response. In case of longer duration, the response is observed to be predominant only at wave frequency.

g) Touch down point of the mooring line is a time dependent phenomenon that directly influences the boundary condition. This parameter substantially influences the convergence of solution of governing equations.

5.2.3. Nonlinear coupled dynamic analysis for quartering sea wave loading

a) The responses of platform under wave at $\pi/4$ radian are equally divided for surge & sway, roll & pitch and top tension in mooring line 1 & 2. The yaw response of platform is also activated. It confirms that coupled Spar platform has been appropriately modelled in six degrees of freedom.

b) For heave response, the 95% confidence interval varies between -0.7647 m to 0.8782 m under wave at 0 rad and ranges between -0.7436 m to 0.8121 m for quartering sea wave. Though the maximum heave responses are higher in the time history, the estimated confidence level for heave shows the probability of occurrence of these values as 95%.

c) The roll response occurring with the sway excites the platform to move and rotate around its position. Hence, it is noticed that the sway response is influenced by rolling motion of the Spar hull which is similar to surge response coupled with pitch in case of wave at 0 rad.

d) There is no yaw motion for wave at 0 rad which is an expected phenomenon. In case of quartering sea wave the yaw response varies between -0.042 rad to 0.046 rad.

e) For the wave at 0 rad the maximum and minimum CML tension ranges between 1.662E+07 N to 1.581E+07 N. But for quartering sea wave the range of maximum tension is from 1.656E+07 N to 1.5952E+07 N. The oscillations of time history shows reduction of maximum tension by 4% compared to the wave at 0 rad.

f) The maximum CML tension is governed by wave frequency under longer duration wave at 0 rad whereas for quartering sea wave it is governed by natural frequency of surge/sway.

5.2.4. Effect of severe waves

a) For surge response at long duration of wave loading, energy content reduces due to hydrodynamic damping showing solitary peak in surge frequency. Governing peak in pitch power spectrum occurs near pitch frequency at short duration. A solitary peak in surge at long duration is existent. Hence, the pitch motion occurs simultaneously with surge and attracts significant wave energy.

b) Response at hull centre of gravity is significantly different than that of platform level. Fluctuations of surge time history in CG are milder compared to deck level responses. The frequency content is dominated by natural frequency of surge. Both the responses at deck level and CG level are important for various functions of Spar platform.

c) Surge time histories display periodic behaviour for all the severe sea states. With decreasing wave intensity, surge response gradually decreases. However, moderate wave causes higher RMS, mode and stdev showing more surge oscillations due to higher frequency of wave/low wave period.

d) Power spectrum in heave shows larger energy content in heave frequency at lower time of wave loading. Afterward the energy is transferred towards pitching motion. Therefore, at long duration, governing peak of energy attraction occurs at pitch frequency. This phenomenon shows alternate transactions of energy between heave and pitch response.

e) The mean, median and mode values of heave and pitch decrease due to lower intensity of wave. Distribution of heave under strong and moderate gale is leptokurtic with more acute peak and platy-kurtic for moderate wave with wider peak around the mean. Greater stdev and RMS values show higher heave-pitch fluctuations which indicate severity of moderate wave.

f) Complex periodic behaviour is observed in tension fluctuation for the severe sea states. Though the Spar motions are higher in moderate wave than those of other two cases, mooring lines experience lesser top tension for lower wave height and wave period. Larger coefficients of skew-ness at moderate wave show higher skewed nature in tension distribution.

g) Tension spectrum at short duration of wave loading shows governing peak of energy content at frequency 0.18 rad/sec. However, at long duration, it is governed by natural frequency of surge.

h) For accurate prediction of platform responses under moderate wave, it is recommended to compute wave forces by wave diffraction theory rather than Morison's equation.

5.2.5. Effect of current in severe waves

a) The current force causes major static offset of Spar platform leading to appreciable changes in the dynamic characteristics of mooring system and hence the platform & CML responses.

b) The platform experiences increase of maximum surge for current inclusion by 2.25 times of wave induced surge. Top tension in CML increases by 10.40% for wave + current loading.

c) Heave and pitch response reduces by 54.17% and 16.67% respectively for addition of current. Moreover, current loading diminishes the dynamic fluctuations. This phenomenon shows firmness of the moored Spar with controlled oscillations around its new mean position.

d) The governing frequency of energy content in power spectrum of surge, pitch and CML tension do not change for inclusion of current. However, heave oscillates at different frequency for inclusion of current. Availability of energy content in power spectra is reduced due to current.

e) For moderate wave, surge and mooring tension are relatively less compared to higher sea states of strong gale and moderate gale. However, heave and pitch values are higher for moderate wave. Due to more frequent wave action, the Spar oscillates at CG causing higher pitch and heave. This behaviour may cause discomfort to the crew and affect other operational activities of platform.

f) The Stdev, RMS and skew-ness show gradual reductions of oscillations in heave and pitch around mean for strong gale to moderate gale with current. However greater Stdev indicates higher fluctuations for current in moderate wave.

g) For longer duration of wave + current loading, platform responses and CML tension stabilize with identical peak values in time history. This phenomenon indicates platform firmness and suitability for deep water exploration.

5.2.6. Incorporating aerodynamic wind loading on coupled spar

a) Wind induced forces significantly affect Spar responses as well as mooring line tension. The platform experiences 65% larger lateral shift under total hydro-aerodynamic loading than the wave + current induced surge. The mooring tension increases by 10%.

b) Heave and pitch response reduces by 12% and 16% respectively due to current and constant wind. However, turbulent wind increases heave and pitch by 60% and 28% causing corresponding increase of 48% and 12% for total loading. Yet under all loadings, these are significantly less than wave only case.

c) Inclusion of constant wind causes static offset and turbulent wind induces more magnitudes of oscillations. Moreover, the wind force diminishes the dynamic fluctuations. The steady offset from constant wind allows the spar to oscillate in a controlled manner about the new mean position.

d) The offset of platform is dominated by constant wind and the standard deviation is turbulent wind induced. Extreme value of responses can occur under the aerodynamic forces.

e) The extent of tension fluctuations under wind loading is not high because of high pretension in mooring line but the force magnitude is higher than wave and wave plus current condition.

f) As wind speed decreases, the maximum values of surge and mooring tension reduces nonlinearly. However, heave and pitch responses increases significantly due to dense oscillations induced by lower wave period.

g) The API RP 2A spectrum estimates higher surge and mooring tension than Simiu spectrum by 11% and 3% respectively. Heave and pitch responses are higher by 50% and 20% compared to Simiu spectrum. Both spectra can be advantageously used for the coupled Spar platform.
h) Influence of API RP 2A spectrum on platform motion is more significant in dense occurrence in moderate wave due to higher Stdev for its significant fluctuating behavior.

5.2.7. Suitability of Spar platform in Malaysian deep water regions

5.2.7.1. Malaysian sedimentary basins and wave data

a) Malaysian deep water fields can play a vital role to meet the nation's energy demand. Except Kebabangan field, all the offshore hydrocarbon reserves are located at deeper water around 1000 m. Present Spar concept indicates suitability of Spar platform in Malaysian deep sedimentary basins for efficient oil and gas exploration.
b) Procedure for wave data simulation in deep water Malay basin is presented. The record contributes wind and wave characteristics for 1000 years return period indicating the physical properties of the Malaysian deep sea. The 100 year return period wave and wind characteristics are 8.72 m/ 9.45 sec and 17.25 m/s respectively.

5.2.7.2. Coupled behaviour and influence of sea bed friction

a) Sea bed friction induces additional damping to the mooring line and hence on the floating system. There is minute change in pattern and magnitude of surge and mooring tension.
b) The mooring touch down point and sea bed friction contributes additional nonlinearity to the system. Difficulty in convergence of solution arises because of these nonlinearities. A large number of iterations are required at different time intervals.
c) Heave and pitch responses decreases by 84% and 40% respectively for addition of frictional resistance. Friction causes little increase in mooring pre tension leading to reduced responses in heave and pitch. Moreover, the addition of

friction induced damping also effect these responses. As the friction coefficient increases heave and pitch responses reduces gradually.

d) Power spectrum of heave in frictionless sea bed shows governing peak at heave frequency. Due to frictional resistance, the energy content in heave is substantially reduced and surge frequency is governed with lower energy.

e) For inclusion of friction in sea bed, participation of pitch frequency disappears in pitch power spectrum and only solitary peak is available in surge frequency with lower energy content.

f) Inclusion of friction causes slight shift in governing frequency of tension power spectrum with minor reduction in magnitude. Because of friction induced damping, there is little change in behaviour of tension response which is reflected in power spectrum

g) Small amplitude sliding of mooring line relative to the supporting soil causes local wear, especially at the crossovers. Such wear can be severe and lead to significant localised breaks of mooring strands. High contact shears, under extreme loading can also lead to plastic deformation of mooring surface, displacing them from their position. This may affect the fatigue performance.

h) Though inclusion of friction causes severe convergence issues, it has significant effect on platform heave and pitch. Increase in frictional resistance give rise to locally high contact shear in mooring line. Therefore the friction effect should be considered for final design of mooring line.

5.2.7.3. Stable response analysis

a) For short duration of loading, unstable platform motions in surge and pitch are seen with symmetry breaking bifurcation. However, at long duration responses are stable with excellent stable close trajectory in phase plot.

b) Stabilized heave fluctuations in T-periodic manner confirm the system more stable at long duration, though in short duration the heave response is unstable because of sub harmonic/super harmonic nature with supercritical Hopf bifurcations.

c) The Spar platforms show excellent motion behaviour in Malaysian sea state. The selected damping parameters are adequate to conquer the Mathieu instability. More sea states with wave periods near to heave natural period along with various damping coefficients should be considered for detail evaluation of Mathieu instability.

5.2.8. Effect of riser in coupled spar

a) Inclusion of riser reduces dynamic fluctuations of platform motions and mooring line tension. For Spar-mooring system, more time is needed to stabilize, whereas Spar-mooring-riser responses stabilize early.

b) Incorporation of rigid riser causes reduction in maximum and minimum responses of platform. Maximum surge, heave, pitch and mooring tension decreases by 20%, 23%, 10% and 2% respectively. More steadiness in platform movement and rotation is achieved due to riser.

c) The mean, median and mode values of responses decrease for inclusion of rigid riser showing suppression of motions. Reduction of standard deviation shows the participation of riser component leading to milder oscillations.

d) More platy-kurtic distribution of platform motions is seen for with riser case indicating less fluctuation around the mean position than without riser condition.

e) The governing frequency of energy content in power spectrum of surge, pitch and mooring tension do not change significantly for inclusion of riser. However, heave oscillates at different frequency for riser. The availability of energy content in respective natural frequencies is reduced in power spectrum for riser incorporation.

5.3 Recommendations

Present study illustrates that the spar platform is suitable for deep water oil and gas exploration. Spar platform has huge potential in the future. It is expected to greatly promote operations in deep sea exploration. Following are the important recommendations required to be addressed for future work in this area.

i. Synthetic mooring lines and composite risers can be incorporated to make the structure more economical and efficient.

ii. Inclusion of wave directionality effect, wave diffraction and higher order wave forces will make the analysis more realistic.

iii. Vortex induced vibration of catenary mooring lines, risers and Spar should be properly investigated.

iv. There is an ample scope to improve the solution technique of nonlinear system of dynamic equations. Accuracy and faster convergence may be achieved if an improved algorithm is adopted.

v. Comprehensive reliability analysis of spar platform and mooring lines is essential. Stability and serviceability limit state are required to be incorporated. For the entire structure reliability, fault tree approach may be adopted.

vi. Undulations in sea bed at mooring touch down point may cause sudden increase and decrease in tension which will further affect the responses of Spar platform. Hence, the sea bed irregularity needs to be considered properly.

vii. To understand the wearing/abrasion of mooring line, proper simulation of soil and mooring line interaction is essential.

References

ABAQUS. (2006). ABAQUS documentation version 6.9.

Agarwal, A. K., and Jain, A. K. (2003). Nonlinear coupled dynamic response of offshore Spar platforms under regular sea waves. *Ocean Engineering, 30*(4), 517-551.

Ahmad, S. (1996). Stochastic TLP response under long crested random sea. *Computers & Structures, 61*(6), 975-993.

Ahmad, S., Islam, N., and Ali, A. (1997). Wind-induced response of a tension leg platform. *Journal of Wind Engineering and Industrial Aerodynamics, 72*(1-3), 225-240.

Ahmad, S. K., and Ahmad, S. (1999). Active control of non-linearly coupled TLP response under wind and wave environments. *Computers & Structures, 72*(6), 735-747.

Anam, I. (2000). *Non-linear dynamic analysis and reliability assessment of deepwater floating structure.* PhD Thesis, Texas A & M University, Texas, USA.

Anam, I., Roesset, J. M., and Niedzwecki, J. M. (2003). *Time domain and frequency domain analysis of Spar platforms.* Paper presented at the Proceedings of the Thirteenth International Offshore and Polar Engineering Conference, 25-30 May Honolulu, Hawaii, USA.

API-RP2A. (1993). *Recommended Practice for Planning, Designing and Constructing Fixed Offshore Platforms–Working Stress Design*. Washington, DC: American Petroleum Institute (API).

API-RP2A. (2000). *Recommended practice for planning, designing and constructing fixed offshore platforms*. Washington, DC: American Petroleum Institute (API).

Arcandra. (2001). *Hull/mooring/riser coupled dynamic analysis of a deep water floating platform with polyester lines.* PhD Thesis, Texas A & M University, Texas, USA.

Argyris, J., and Mlejnek, H. P. (1991). *Dynamics of Structures* (Vol. 5). North Holland: Elsevier Science Publication Co.

Arnoult, É., Lardeur, P., and Martini, L. (2011). The modal stability procedure for dynamic and linear finite element analysis with variability. *Finite Elements in Analysis and Design*, *47*(1), 30-45.

Astrup, O. C., Nestegård, A., Ronæs, s. M., and Sødahl, N. (2001). *Coupled Analysis Strategies for Deepwater Spar Platforms.* Paper presented at the The Eleventh International Offshore and Polar Engineering Conference, 17-22 June Stavanger, Norway.

Biswas, A., and Kara, A. H. (2011). Conservation Laws for Regularized Long Wave Equation and R(m, n) Equation. *Advanced Science Letters, 4*(1), 168-170.

Brennodden, H., Lieng, J. T., Sotberg, T., and Verley, R. L. P. (1989). An energy-based pipe-soil interaction method. *PROC. 21ST ANNUAL OFFSHORE TECHNOLOGY CONF., HOUSTON, U.S.A., MAY 1-4, 1989, 3 , Richardson, U.S.A., Offshore Technology Conference, 1989,* 147-158.

Bruce, T. (1984). *"Energy Methods". Advanced Dynamics for Engineers*. United States of America: CBS College Publishing.

Caires, S., and Sterl, A. (2005). 100-Year Return Value Estimates for Ocean Wind Speed and Significant Wave Height from the ERA-40 Data. *Journal of Climate, 18*(7), 1032-1048.

Chakrabarti, S. K. (1987). *Hydrodynamics of Offshore structures*. Plainfield, Illinois, USA: CBI Industries, Inc.

Chakrabarti, S. K. (2005). *Handbook of Offshore engineering*. Plainfield, Illinois, USA: Elsevier Science Publishers, Amsterdam, Netherlands.

Chandrasekaran, S., Chandak, N. R., and Anupam, G. (2006). Stability analysis of TLP tethers. *Ocean Engineering, 33*(3–4), 471-482.

Chaudhary, G. (2001). *A new method for coupled dynamic analysis of platforms.* Paper presented at the Eleventh international offshore and polar engineering conference June 17-22, Stavanger, Norway.

Chaudhury, G., and Ho, C.-Y. (2000). *Coupled Dynamic Analysis of Platforms, Risers, and Moorings*. Paper presented at the Offshore Technology Conference.

Chen, X. (2002). *Studies on dynamic interaction between deep-water floating structures and their mooring/tendon systems.* PhD Thesis, Texas A & M University, Texas, USA.

Chen, X., Zhang, J., and Ma, W. (2001). On dynamic coupling effects between a spar and its mooring lines. *Ocean Engineering, 28*(7), 863-887.

Chen, X., Zhang J., and Ma W. (1999). *Coupled time-domain analysis of the response of a spar and its mooring system.* Paper presented at the International Offshore Polar Engineering Conference (ISOPE).

Chen, X. H., Zhang, J., Johnson, P., and Irani, M. (2000). *Studies on the dynamics of truncated mooring line*. Paper presented at the Proceedings of the Tenth International Offshore and Polar Engineering Conference, Seattle, USA.

Chernetsov, V. A., and Karlinsky, S. L. (2006). *Ice-Resistant Spar-Type Platform for Middle Sea Depth.* Paper presented at the The 16th International Offshore and Polar Engineering Conference, May 28-June 2 San Francisco, California, USA.

Chillamcharla, G. K., Thiagarajan, K. P., and Winsor, F. (2009). *Mooring Analysis of a Weathervaning FPSO in Bi-Directional Sea-States*. Paper presented at the Omae 2009, Vol 6, 585-590. Retrieved from <Go to ISI>://WOS:000283008400064

Colby, C., Sodahl, N., Katla, E., and Okkenhaug, S. (2000). *Coupling Effects for a Deepwater Spar.* Paper presented at the Offshore Technology Conference, 1-4 May Houston, Texas, USA.

Culla, A., and Carcaterra, A. (2007). Statistical moments predictions for a moored floating body oscillating in random waves. *Journal of Sound and Vibration, 308*(1-2), 44-66.

Davison, I., and Miles, I. (2013). A SPAR Modelling Platform Case Study: Skynet 5. *Procedia CIRP, 11*(0), 431-434.

Dean, R. G., and Dalrymple, R. A. (1991). *Water Wave Mechanics For Engineers And Scientists, Vol. 2*: World Scientific.

Deo, M. C. (2012). Waves and Structures, Free Courseware, http://www.civil.iitb.ac.in/~mcdeo/waves.html retrived at 06th August,2012. Indian Institute of Technology Bombay Powai, Mumbai, India.

Ding, Y., Kim, M., Chen, X., and Zhang, J. (2003). *A Numerical Code (COUPLE6D) for Coupled Dynamic Analysis of Moored Offshore Structures* Houston, Texas, USA.

DNV. (2010). *Recommended Practice DNV-RP-F205, Global performance analysis of deep water floating structures*: DET NORSKE VERITAS (DNV).

Esmailzadeh, E., and Goodarzi, A. (2001). Stability analysis of a CALM floating offshore structure. *International Journal of Non-Linear Mechanics, 36*(6), 917-926.

Fenton, J. (1985). A Fifth-Order Stokes Theory for Steady Waves. *Journal of Waterway, Port, Coastal, and Ocean Engineering, 111*(2), 216-234.

Garrett, D. L. (1982). Dynamic analysis of slender rods. *Journal of Energy Resources Technology, Transactions of ASME, 104*, 302-307.

Garrett, D. L. (2005). Coupled analysis of floating production systems. *Ocean Engineering, 32*(7), 802-816.

Gupta, H., Finn, L., and Weaver, T. (2000a). *Effects of Spar Coupled Analysis.* Paper presented at the Offshore Technology Conference 1-4 May Houstan, Texas, USA.

Gupta, H., Finn, L., and Weaver, T. (2000b). *Effects of Spar Coupled Analysis.* Paper presented at the Offshore Technology Conference, 1-4 May, Houstan, Texas, USA.

Hasan, S. D., Islam, N., and Moin, K. (2011). Multihinged Articulated Offshore Tower under Vertical Ground Excitation. *Journal of Structural Engineering-Asce, 137*(4), 469-480.

Haslum, H. A., and Faltinsen, O. M. (1999). Alternative shape of spar platforms for use in hostile areas. *Proceedings of the 31st Offshore Technology Conference (OTC 10953), 3-6 May, Houston, Texas, 2*, 217-228.

How, T. L. T. (2011). *Nonlinear finite element analysis of riser.* BSc. Thesis, University of Malaya, Kuala Lumpur, Malaysia.

Huang, S. (1999). Stability analysis of the heave motion of marine cable-body systems. *Ocean Engineering, 26*(6), 531-546.

Huang, T. S., and Leonard, J. W. (1990). Lateral stability of a submarine flexible hoseline. *Ocean Engineering, 17*(1–2), 35-52.

Irani, M. B., Rouckout, T., and Johnson, R. P. (2000). *Dynamics of a Spar Platform.* Paper presented at the The 10th International Offshore and Polar Engineering Conference, May 27-June 2 Seattle, USA.

Islam, N., and Ahmad, S. (2007). Reliability of articulated tower joint against random base shear. *Structural Engineering and Mechanics, 27*(1), 33-48.

Islam, N., Zaheer, M. M., and Ahmed, S. (2009a). Double hinged articulated tower interaction with wind and waves. *Journal of Wind Engineering and Industrial Aerodynamics, 97*(5-6), 287-297.

Islam, N., Zaheer, M. M., and Ahmed, S. (2009b). Response of double hinged articulated tower platforms to wind forces. *Wind and Structures, 12*(2), 103-120.

Jameel, M. (2008). *Non-linear dynamic analysis and reliability assessment of deepwater floating structure.* PhD Thesis, Indian institute of technology, Delhi, india.

Jameel, M., and Ahmad, S. (2011). *Fatigue Reliability Assessment of Coupled Spar-Mooring System* Paper presented at the ASME 30th International Conference on Ocean, Offshore and Arctic Engineering, (OMAE 2011-49687), 19-24 June Rotterdam, The Netherlands.

Jha, A. K., de Jong, P. R., and Winterstein, S. R. (1997). *Motion of spar buoy in random seas: comparing predictions and model test results.* Paper presented at the Behaviour of Offshore Structures-97, Vol. 2 (Hydodynamics), 333-347, Delft, Netherlands.

Kamarudin, M. H., Thiagarajan, K. P., and Czajko, A. (2007). *Combined effects of waves and currents on offshore pipeline bundles.* Paper presented at the Proceedings of the 26th International Conference on Offshore Mechanics and Arctic Engineering, Vol 3, 337-345.

Kareem, A. (1985). Wind-Induced Response Analysis of Tension Leg Platforms. *Journal of Structural Engineering-Asce, 111*(1), 37-55.

Khan, R. A., and Ahmad, S. (2010). Probabilistic Fatigue Safety Analysis of Oil and Gas Risers Under Random Loads. *ASME Conference Proceedings, 2010*(49101), 345-352.

Kim, B. W., Sung, H. G., Kim, J. H., and Hong, S. Y. (2013). Comparison of linear spring and nonlinear FEM methods in dynamic coupled analysis of floating structure and mooring system. *Journal of Fluids and Structures, 42*(0), 205-227.

Kim, M. H., Koo, B. J., Mercier, R. M., and Ward, E. G. (2005). Vessel/mooring/riser coupled dynamic analysis of a turret-moored FPSO compared with OTRC experiment. *Ocean Engineering, 32*(14-15), 1780-1802.

Kim, M. H., Ran, Z., and Zheng, W. (2001). Hull/Mooring Coupled Dynamic Analysis of A Truss Spar in Time Domain. *International Journal of Offshore and Polar Engineering, 11*(1), 42-54.

Kim., M. H., Ward, E. G., and Harnig, R. (2001). *Comparison of Numerical Models for the Capability of Hull/Mooring/ Riser Coupled Dynamic Analysis for Spars and TLPs in Deep and Ultra Deep Water.* Paper presented at the Proceedings of the Eleventh International Offshore and Polar Engineering Conference.

Kiu, K. Y., Stappenbelt, B., and Thiagarajan, K. P. (2011). Effects of uniform surface roughness on vortex-induced vibration of towed vertical cylinders. *Journal of Sound and Vibration, 330*(20), 4753-4763.

Koo, B. J., Kim, M. H., and Randall, R. E. (2004a). The effect of nonlinear multi-contact coupling with gap between risers and guide frames on global spar motion analysis. *Ocean Engineering, 31*(11-12), 1469-1502.

Koo, B. J., Kim, M. H., and Randall, R. E. (2004b). Mathieu instability of a spar platform with mooring and risers. *Ocean Engineering, 31*(17-18), 2175-2208.

Lee, C.-H. (1995). *WAMIT Theory Manual. Report 95-2* Massachusetts Institute of Technology Cambridge,MA, USA.

Li, Y., and Kareem, A. (1990). Stochastic response of tension leg platforms to wind and wave fields. *Journal of Wind Engineering and Industrial Aerodynamics, 36, Part 2*(0), 915-926.

Lim, S. J., Rho, J. B., and Choi, H. S. (2005). *An experimental study on motion characteristics of cell spar platform.* Paper presented at the Fifteenth International Offshore and Polar Engineering Conference-2005.

Liqin Liu, B. Z., and Zhang, Y. (2013). *The Coupled Motion of Hull Heave and Moonpool Water of Spar Platform* Paper presented at the ASME 2013 32nd International Conference on Ocean, Offshore and Arctic Engineering, 9-14 June Nantes, France.

Liu, J.-Y., Huang, C.-F., and Shyue, S.-W. (2001). Effects of seabed properties on acoustic wave fields in a seismo-acoustic ocean waveguide. *Ocean Engineering, 28*(11), 1437-1459.

Low, Y. M., and Langley, R. S. (2007). *A Comparison of Methods for the Couple Analysis of Floating Structures.* Paper presented at the Proceedings of the 26th International Conference on Offshore Mechanics and Arctic Engineering (OMAE), San Diego, USA.

Low, Y. M., and Langley, R. S. (2008). A hybrid time/frequency domain approach for efficient coupled analysis of vessel/mooring/riser dynamics. *Ocean Engineering, 35*(5-6), 433-446.

Ma, Q. W., and Patel, M. H. (2001). On the non-linear forces acting on a floating spar platform in ocean waves. *Applied Ocean Research, 23*(1), 29-40.

Ma, W., and Webster, W. C. (1994). *An Analytical approach to cable dynamics: Theory and user manual* (No. PB--95-173456/XAB; TRN: TRN: 50761821 United States, TRN: 50761821 Mon Dec 01 07:25:44 EST 2008NTISGRA; SCA: 022000; 020900; PA: GRA-95:61821; EDB-95:055403; SN: 95001358118; TVI: 9509 English).

Marghany, M., and Hashim, M. (2010). Simulation of sea surface current velocity from synthetic aperture radar (SAR) data. *International Journal of the Physical Sciences, 5*(12), 1915-1925.

Mazaheri, S., and Downie, M. J. (2005). Response-based method for determining the extreme behaviour of floating offshore platforms. *Ocean Engineering, 32*(3-4), 363-393.

MMS. (2010). Malaysian Meteorological Service, Monthly Summary of Marine Meteorological Observations. Kuala Lumpur.

Molin, B. (1994). Second-order hydrodynamics applied to moored structures-a state-of-the-art survey.

Montasir, O. A., and Kurian, V. J. (2011). Effect of slowly varying drift forces on the motion characteristics of truss spar platforms. *Ocean Engineering, 38*(13), 1417-1429.

Montasir, O. A. A., Kurian, V. J., Narayanan, S. P., and Mubarak, M. A. W. (2008). *Dynamic response of Spar platforms subjected to waves and current.* Paper presented at the The international conference on construction and building technology (ICCBT 2008) 16 - 20 June Kualal Lumpur, Malaysia.

Munipalli, J., Pistani, F., Thiagarajan, K. P., Winsor, F., and Colbourne, B. (2007). *Weathervaning instabilities of a FPSO in regular waves and consequence on Response Amplitude Operators*. Paper presented at the Proceedings of the 26th International Conference on Offshore Mechanics and Arctic Engineering, Vol 1, 405-412. Retrieved from <Go to ISI>://WOS:000249556900045

Muzathik, A. M., Nik, W. B. W., Samo, K. B., and Ibrahim, M. Z. (2011). Ocean Wave Measurement and Wave Climate Prediction of

Peninsular Malaysia. *Journal of Physical Science, 22*(1), 77-92.

NDCo. (2012). North Drilling Company, Types of Spar. Retrieved 29th August, 2012, from http://www.ndco.ir/fa/goonagoon/display.aspx?id=273

Nishimura, H., Isobe, M., and Horikawa, K. (1977). Higher Order Solutions of Stokes and Cnoidal Waves. *Journal of Faculty Engineering, University of Tokyo (B), 34*(2), 267-293.

Nordgren, R. P. (1974). On Computation of the Motion of Elastic Rods. *Journal of Applied Mechanics, 41*(3), 777-780.

Ochi, M. K., and Shin, Y. S. (1988). Wind turbulent spectra for design consideration of offshore structures. *Twentieth Annual Offshore Technology Conference, Houston, U.S.A., , 2 ,OTC 5736*, 461-467.

Offshore technology. (2012a). Kikeh Floating Production, Storage and Offloading Development, Malaysia Retrieved 29th August, 2012, from http://www.offshore-technology.com/projects/kikeh/kikeh3.html

Offshore technology. (2012b). Tahiti, United States of America. Retrieved 29th August, 2012, from http://www.offshore-technology.com/projects/tahiti-field/

Onni Suhaiza, S., Salim, S., and Frederik, J. P. (2007). Flood frequency analysis for Sarawak using Weibull, Gringorten and L-Moments formula. *The Journal of the Institution of Engineers, Malaysia, 6*(1), 2671-2680-.

Ormberg, H., and Larsen, K. (1998). Coupled analysis of floater motion and mooring dynamics for a turret-moored ship. [doi: DOI: 10.1016/S0141-1187(98)00012-1]. *Applied Ocean Research, 20*(1-2), 55-67.

Ormberg, H., Stansberg, C. T., and R., Y. (1999). *Integrated vessel motion and mooring analysis applied in hybrid model testing.* Paper presented at the Proceedings of the Nineth International Offshore and Polar Engineering Conference, Brest, France.

OTRC. (1995). *Spar Model Test: Joint Industry Project-216*. Texas, USA: Offshore Technology Research Center.

Palmer, A. C., Steenfelt, J. S., Steensen-Bach, J. O., and Jacobson, V. (1988). Lateral resistance of marine pipelines on sand. *IN: OTC '88 PROC. TWENTIETH ANNUAL OFFSHORE TECHNOL. CONF., (HOUSTON, U.S.A.: MAY 2-5, 1988), 4 , Richardson, U.S.A., Offshore Technol. Conf., 1988, Paper OTC 5853*, 399-408.

Patel, M. H. (1989). *Dynamics of offshore structures*. London: Butterworth & Co.

Paulling, J. R., and Webster, W. C. (1986). *A consistent, large-amplitude analysis of the coupled response of a TLP and tendon system.* Paper presented at the Proceedings of the 5th International Conference on Offshore Mechanics and Arctic Engineering (OMAE 86).

Petronas. (2010). *PETRONAS Oil & Gas Company, Petroliam Nasional Berhad*

QLEE. (2011). SPAR Platform - UT, *Turbosquid [Cited 11 May, 2012] Available at <http://www.turbosquid.com/3d-models/3d-max-spar-platform--/589373>*.

Ran, Z., and Kim, M. H. (1997). Nonlinear Coupled Responses of a Tethered Spar Platform in Waves. *International Journal of Offshore and Polar Engineering, 7*(2), 111-118.

Ran, Z., Kim, M. H., Niedzwecki, J. M., and Johnson, R. P. (1996). Response of a Spar platform in Random Waves and Currents (Experiment vs. Theory). *International Journal of Offshore and Polar Engineering, 6*,(1), 27-34.

Ran, Z., Kim, M. H., and Zheng, W. (1999). Coupled Dynamic Analysis of a Moored Spar in Random Waves and Currents (Time-Domain Versus Frequency-Domain Analysis). *Journal of Offshore Mechanics and Arctic Engineering, 121*(3), 194-200.

Rand, R. H. (2005). *Lecture Notes on Nonlinear Vibrations*: Dept. Theoretical & Applied Mechanics, Cornell University, Ithaca NY 14853.

Rapp, D. B. (2008). An Overview of Offshore Concepts, *SPE Expanding Facilities Knowledge Workshop, Session 1: Offshore Concepts Selection, 16 June*. Houston Tx 77079 USA: Mustang Engineering Inc.

Reddy, J. N. (2002). *Energy Principles and Variational Methods in Applied Mechanics*: John Wiley.

Rho, J. B., Choi, H. S., Lee, W. C., Shin, H. S., and Park, I. K. (2002). Heave and pitch motions of a spar platform with damping plate. *Proceedings of the Twelfth (2002) International Offshore and Polar Engineering Conference, Vol 1*, 198-201.

Rodrigues, M. V., Correa, F. N., and Jacob, B. P. (2007). Implicit domain decomposition methods for coupled analysis of offshore platforms. *Communications in Numerical Methods in Engineering, 23*(6), 599-621.

RSI. (2012). Relaible Security Information, Global Security. Retrieved at 29th December, 2012. from http://www.globalsecurity.org/military/systems/ship/platform-spar.htm

Saleh, E., Beliku, J., Aung, T., and Singh, A. (2010). Wave Characteristics in Sabah Waters. *American Journal of Environmental Sciences, 6*(3), 219-223.

Sarpkaya, T. (1986). Force on a circular cylinder in viscous oscillatory flow at low Keulegan—Carpenter numbers. *Journal of Fluid Mechanics, 165*, 61-71.

Sarpkaya, T., and Isaacson, M. (1981). Mechanics of wave forces on offshore structures.

Seebai, T., and Sundaravadivelu, R. (2012). Response analysis of spar platform with wind turbine. *Ships and Offshore Structures*, *8*(1), 94-101.

Siddiqui, N. A., and Ahmad, S. (1996). *Stability and reliability analysis of tension leg platform* Paper presented at the Proceedings, International Conference in Ocean Engineering (ICOE' 96), IIT Madras, India.

Siddiqui, N. A., and Ahmad, S. (2000). Reliability analysis against progressive failure of TLP tethers in extreme tension. *Reliability Engineering & System Safety, 68*(3), 195-205.

Simiu, E., and Leigh, S. D. (1984). Turbulent Wind and Tension Leg Platform Surge. *Journal of Structural Engineering-ASCE, 110*(4), 785-802.

Simos, A. N., and Pesce, C. P. (1997). Mathieu stability in the dynamics of TLP tether considering variable tension along the length. *Transactions on Built Environment 29*, 175–186.

Sun, Z.-c., Wang, X.-g., Liang, S.-x., Liu, S.-X., and Liu, S. (2011). Dynamic response analysis of ddms platform subjected to actions of wave groups and current fources. *Journal of Hydrodynamics, Ser. B, 23*(6), 697-708.

Tahar, A., and Kim, M. H. (2003). Hull/mooring/riser coupled dynamic analysis and sensitivity study of a tanker-based FPSO. *Applied Ocean Research*, *25*(6), 367-382.

Tahar, A., and Kim, M. H. (2008). Coupled-dynamic analysis of floating structures with polyester mooring lines. *Ocean Engineering, 35*(17-18), 1676-1685.

Tahar, A., Ran, Z., and Kim, M. H. (2002). *Hull/Mooring/Riser Coupled Spar Motion Analysis with Buoyancy-Can Effect* Paper presented at the Proceedings of the Twelfth International Offshore and Polar Engineering Conference, May 26-31, Kitakyushu, Japan.

Tao, L. B., Lim, K. Y., and Thiagarajan, K. (2004). Heave response of classic spar with variable geometry. *Journal of Offshore Mechanics and Arctic Engineering-Transactions of the Asme, 126*(1), 90-95.

Tørnes, K., Zeitoun, H., Cumming, G., and Willcocks, J. (2009). *A stability design rationale - A review of present design approaches*.

Triantafyllou, M. S., Yue, D. K. P., and Tein, D. Y. S. (1994). *Damping of moored floating structures.* Paper presented at the Offshore Technology Conference, 2-5 May Houstan, Texax, USA.

Umar, A., Ahmad, S., and Datta, T. K. (2004). Stability analysis of a moored vessel. *Journal of Offshore Mechanics and Arctic Engineering-Transactions of the Asme, 126*(2), 164-174.

Umar, A., and Datta, T. K. (2003). Nonlinear response of a moored buoy. [doi: DOI: 10.1016/S0029-8018(02)00144-0]. *Ocean Engineering, 30*(13), 1625-1646.

Van den Brink, H. W., and Konnen, G. P. (2008). The statistical distribution of meteorological outliers. *Geophysical Research Letters, 35*(23).

Van den Brink, H. W., and Konnen, G. P. (2011). Estimating 10000-year return values from short time series. *International Journal of Climatology, 31*(1), 115-126.

Van den Brink, H. W., Konnen, G. P., Opsteegh, J. D., Van Oldenborgh, G. J., and Burgers, G. (2005). Estimating return periods of extreme events from ECMWF seasonal forecast ensembles. *International Journal of Climatology, 25*(10), 1345-1354.

Vickery, B. J. (1982). *Wind loads on compliant offshore structure.* Paper presented at the Ocean Structural Dynamics Symposium, Oregon State University.

Wagner, D. A., Murff, J. D., Brennodden, H., and Sveggen, O. (1989). Pipe-soil interaction model. *Journal of Waterway, Port, Coastal and Ocean Engineering, 115*(2), 205-220.

Wheeler, J. (1970). Method for calculating forces produced by irregular waves. *Journal of petroleum technology, 22*(3), 359-367.

WorldWaves. (2010). *Fugro OCEANOR, Norway, The European Centre for Medium-Range Weather Forecasts (ECMWF) Wave Model (WAM).*

Yaakob, O., Zainudin, N., Samian, Y., Malik, A. M. A., and Palaraman, R. A. (2004). *Developing Malaysian Ocean Wave Database using Satellite.* Paper presented at the 1st Asian Space Conference November Chiang Mai, Thailand.

Yang, C. K., and Kim, M. H. (2010). Transient effects of tendon disconnection of a TLP by hull-tendon-riser coupled dynamic analysis. *Ocean Engineering, 37*(8-9), 667-677.

Yang, M., Teng, B., Ning, D., and Shi, Z. (2012). Coupled dynamic analysis for wave interaction with a truss spar and its mooring line/riser system in time domain. *Ocean Engineering, 39*(0), 72-87.

Yiu, F., Prislin, I., Beattie, M., Ocker, C., Maroju, S., and Leon, C. (2013). Truss Spar VIM Correlation between Model Test and Field Measurement, *Proceedings of the 45th Offshore Technology Conference (OTC 24251), 6-9 May, Houston, Texas*.

Yu, L., and Tan, J.-h. (2006). Numerical investigation of seabed interaction in time domain analysis of mooring cables. *Journal of Hydrodynamics, Ser. B, 18*(4), 424-430.

Yung, T.-W., Sandstrom, R. E., Slocum, S. T., Ding, Z. J., and Lokken, R. T. (2004). *Advancement of Spar VIV Prediction.* Paper presented at the Offshore Technology Conference, Houston, Texas, USA.

Zaheer, M. M., and Islam, N. (2008a). Aerodynamic response of articulated towers: state-of-the-art. *Wind and Structures, 11*(2), 97-120.

Zaheer, M. M., and Islam, N. (2008b). *Fluctuating wind induced response of double hinged articulated loading platform*.

Zeitoun, H. O., Cumming, G., Tørnes, K., and Brankovié, M. (2008). *Pipeline stability - State of the art*.

Zeitoun, H. O., Tørnes, K., Li, J., Wong, S., Brevet, R., and Willcocks, J. (2009). *Advanced dynamic stability analysis*.

Zhai, G. J., Qi, K., and Kang, H. G. (2008). Overall Structural Strength Analysis of the Cell Spar Platform. *Proceedings of the Chinese-German Joint Symposium on Hydraulic and Ocean Engineering*, 579-583

Zhang, F., Yang, J.-m., Li, R.-p., and Chen, G. (2007a). Numerical investigation on the hydrodynamic performances of a new spar concept. *Journal of Hydrodynamics, Ser. B, 19*(4), 473-481.

Zhang, F., Yang, J.-m., Li, R.-p., and Chen, G. (2008). Coupling effects for cell-truss spar platform: comparison of frequency- and time-domain analyses with model tests. *Journal of Hydrodynamics, Ser. B, 20*(4), 424-432.

Zhang, F., Yang, J. M., Li, R. P., and Chen, G. (2007b). Numerical and experimental research on the global performances of cell-truss spar platform. *China Ocean Engineering, 21*(4), 561-576.

Zhang, F., Yang, J. M., Li, R. P., and Chen, G. (2007c). *Numerical study on the hydrodynamic behavior of a new cell-truss spar platform.* Paper presented at the Proceedings of the 26th International Conference on Offshore Mechanics and Arctic Engineering.

Zhang, L., Zou, J., and E.W., H. (2002). Mathieu instability evaluation for DDCV/SPAR and TLP tendon design *Proceedings of the 11th Offshore Symposium, Society of Naval Architect and Marine Engineer (SNAME), Houston*, 41–49.

Zhang, X., and Zou, J. (2002). *Coupled Effects of Risers/Supporting Guide Frames on Spar Responses.* Paper presented at the Proceedings of the Twelfth International Offshore and Polar Engineering Conference.

Appendices

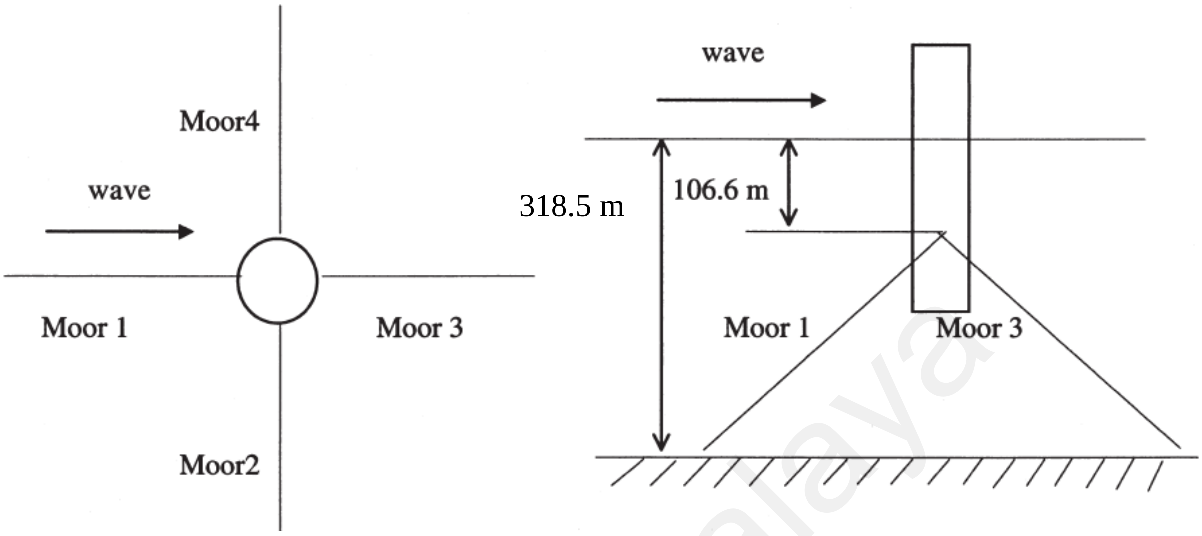

Figure A1: Sketch of the Spar-mooring system arrangement at 1:55 scaled OTRC basin

Table A1: Recognized main particulars of the JIP Spar and mooring system by Ocean Technology and Research Center

Spar hull		Mooring system	
Diameter	40.54 m	Number of mooring lines	4
Draft	198.12 m	Length of mooring line	2000 m
Mass	2.592E+08 kg	Mooring point	-106.6 m
Center of gravity	-105.98 m	Mass per unit length	1100 m
Pitch radius of gyration	62.33 m	Elastic stiffness (EA)	1.5E+09 N
Surge natural period	331.86 s	Representing vertical depth of water in wave basin	318.5 m
Heave natural period	29.03 s		
Pitch natural period	66.77 s		

Publications

ISI Journals

1. Islam, A. B. M. S., Jameel, M., Ahmad S., Jumaat, M. Z. & Kurian V. J. (2013). Structural behaviour of fully coupled spar-mooring system under extreme wave loading. *Journal of Civil Engineering and Management.* DOI:10.3846/13923730.2013.801899. (ISI-Cited Publication-**Q1**)
2. Jameel, M., Ahmad, S., Islam, A. B. M. S., & Jumaat, M. Z. (2013). Nonlinear dynamic analysis of coupled spar platform. *Journal of Civil Engineering and Management. 19(4),* 476-491. (ISI-Cited Publication-**Q1**)
3. Islam, A. B. M. S., Jameel, M., & Jumaat, M. Z. (2012). Oil and gas energy potential at Malaysian sea beds and Spar platform for deep water installation. *International Journal of Green Energy. 9(2),* 111-120. (ISI-Cited Publication-**Q1**)
4. Jameel, M., Ahmad, S., Islam, A. B. M. S., & Jumaat, M. Z. (2013). Erratum. *Journal of Civil Engineering and Management. 19(5),* 772-772. (ISI-Cited Publication-**Q1**)
5. Islam, A. B. M. S., Jameel, M., & Jumaat, M. Z. (2012). Review on offshore energy in Malaysia and floating Spar platform for efficient exploration. *Renewable & Sustainable Energy Reviews. 16*(8), 6268 - 6284. (ISI-Cited Publication-**Q1**)
6. Jameel, M., Islam, A. B. M. S., Khaleel M., & Jumaat, M. Z. (2012). Nonlinear finite element analysis of spar platform. *Advanced Science Letters. 13*: 723-726. (ISI-Cited Publication-**Q2**)
7. Islam, A. B. M. S., Jameel, M., & Jumaat, M. Z. (2011). Effect of time elapse after wave hitting on coupled Spar platform. *International Journal of the Physical Sciences, 6*(11), 2671-2680. (ISI-Cited Publication-**Q2**)
8. Jameel, M., Islam, A. B. M. S., Khaleel M. & How, T. L. T. (2012). Nonlinear analysis of marine riser for energy exploration in shallow and deep water regions. *Energy Education Science and Technology Part A-Energy Science and Research, 30 (Special Issue-1),* 641-660. (ISI-Cited Publication-**Q1**)
9. Islam, A. B. M. S., Jameel, M., Jumaat, M. Z., & Shirazi, S. M. (2011). Spar platform at deep water region in Malaysian sea. *International Journal of the Physical Sciences, 6*(30), 6872 - 6881. (ISI-Cited Publication-**Q2**)
10. Jameel, M., Islam, A. B. M. S., Salman, F. A., Khaleel M. & Jumaat, M. Z. (2012). Wave data for shallow and deep water sedimentary basins of Malaysia. *Advanced Science Letters. 14*: 360-364. (ISI-Cited Publication-**Q2**)

Book chapters

11. Islam, A. B. M. S., Jameel, M., Jumaat, M. Z., & Salam, M. A. (2011). Energy resources at Malaysian sedimentary basins and spar platform as deep sea structure. Edited by: Yi Xie. *ISBN: 9780791859810, ASME Press,* New York, USA.

Conference Proceedings

12. Jameel, M., Ahmad, S., Islam, A. B. M. S., & Jumaat, M. Z. (2011, 19-24 June). Nonlinear analysis of fully coupled integrated Spar-mooring line system. *Proceedings of the 21st International Offshore and Polar Engineering Conference (ISOPE-2011)*, Maui, Hawaii, USA. (**ISI-Cited Publication**)
13. Jumaat, M. Z., Jameel M. & Islam, A. B. M. S. (2011, December 25-27). Nonlinear dynamic coupled behaviour of integrated spar-mooring system in deep water region. IEEC-11-059. *Proceedings of the International Engineering education Conference,* Madina, Kingdom of Saudi Arabia.
14. Jameel, M., Ahmad, S., Khaleel M. & Islam, A. B. M. S. (2012, 17-22 June). Fully coupled nonlinear dynamic response of spar platform under random loads. *Proceedings of the 22nd International Offshore (Ocean) and Polar Engineering Conference (ISOPE-2012)*, Rhodes, Greece. (**ISI-Cited Publication**)
15. Islam, A. B. M. S., Jameel, M., Ahmad, S. and Jumaat, M. Z. (2012, 1-6 July). Nonlinear response of coupled integrated spar platform under severe sea states. *Proceedings of the ASME 31st International Conference on Ocean, Offshore and Arctic Engineering*, (OMAE 2012-83862), Rio de Janeiro, Brazil. (**ISI-Cited Publication**).